Title
Semiclassical Analysis of SU(2) Spin Networks

Author
Yu, Liang

Publication Date
2010

Peer reviewed|Thesis/dissertation

Semiclassical Analysis of $SU(2)$ Spin Networks

by

Liang Yu

A dissertation submitted in partial satisfaction of the

requirements for the degree of

Doctor of Philosophy

in

Physics

in the

Graduate Division

of the

University of California, Berkeley

Committee in charge:

Professor Robert G. Littlejohn, Chair

Professor Ori J. Ganor

Professor Alan D. Weinstein

Fall 2010

Semiclassical Analysis of $SU(2)$ Spin Networks

Abstract

Semiclassical Analysis of $SU(2)$ Spin Networks

by

Liang Yu

Doctor of Philosophy in Physics

University of California, Berkeley

Professor Robert G. Littlejohn, Chair

In the current pursuit of a quantum theory of gravity, the lack of experimental data at the Planck scale has forced physicists to rely on checking the classical limits of their proposed theories to select viable candidates. In loop quantum gravity, the best candidates are the spin foam models in four dimensions, where the vertex amplitudes of a 4-simplex are formulated in terms of the Wigner $15j$-symbols. Historically, the asymptotic expression of the Wigner $6j$-symbol has played an essential role in the classical limit of the spin foam model in three dimensions. Thus, we believe the asymptotic expression of the $15j$-symbol will play an equally important role in the classical limits of the spin foam models in four dimensions. In this thesis, we employ a wide range of techniques, including stationary phase approximation, WKB theory, classical mechanics, symplectic reduction, symbol correspondence, star products, and the Born-Oppenheimer approximation, to derive old and new asymptotic formulas for the Wigner $3j$-, $6j$-, $9j$-, $12j$-, and $15j$-symbols, which are examples of $SU(2)$ spin networks.

To Luyen Pham.

Contents

List of Figures

List of Tables

Acknowledgments

First and foremost, I would like to thank my parents Hang and Jie Xia for their wonderful love and support throughout my life. I am grateful for their courage and sacrifice in giving up a very comfortable life in China to come to America, so that I may obtain an education here. I would also like to thank them for allowing me to choose a study that I love, and for the many encouragements and advices during times of difficulty.

I would like to thank my advisor, Robert Littlejohn, who has taken me on in the first year, and continued his support throughout, despite a few interruptions in my graduate career. I am grateful for the problems he has given me, for patiently explaining the geometry behind semiclassical analysis, and for always pushing me to find the most general results.

I have benefitted from many professors and fellow students at Berkeley. I would like to thank George Smoot, Martin White, Ori Ganor, Raphael Bousso, Hitoshi Murayama, Edgar Knobloch, and Robert Littlejohn from the physics department, and Donald Sarason, John Strain, Jon Wilkening from the math department, for teaching me what they know best. I would also like to thank Peter Shepard, Cindy Keeler, Nadir Jeevanjee, and Boom-Soo Kim from the String Journal Club for many laughs, and for untangling enough of string theory for me to decide not to pursue it. I would like to thank my office mates, Matt Cargo, Hal Haggard, Nadir Jeevanjee, and Austin Hedeman for many interesting discussions. I always enjoy talking to the twins Clement and Gabriel Wong, and to my friend Tommy. I would like to thank Allan Weinstein, Dan Stamper-Kurn, and Ori Ganor for sitting in my qualifying exam. I should not forget to thank my students, who have made me feel productive during the periods when research progress was slow.

The support staffs at the physics department, Claudia, Donna, and Anne, have made it possible for me to come back to physics after two years of absence. During those two years of absence, I have learned a great deal of finance from my supervisors Ben Miller at Moody's Wallstreet Analytics, and from Peter Shepard at MSCI-BARRA.

I am also grateful to my family: Grandpa and Grandma, Cheri, Globey, Cecelia, Wei, Jocelyn, Jonathan, and others, for their support; and to Luyen's phamily: Hue, Ha, Loan, Nam, Trung, and Duc, for the very fun trips we took together; and to our friends for the wonderful dinner gatherings at the house on 58th Street.

Finally, I thank you, Luyen, for your love, understanding, and patience. I hope this thesis will make all your compromises worthwhile.

Chapter 1

Introduction

1.1 Quantum Mechanics, General Relativity, and Loop Quantum Gravity

Ever since quantum mechanics [74] was discovered about 100 years ago, physicists have been trying to quantize the classical theories that describe the four fundamental forces of nature. Three of the forces, the electromagnetic, the strong, and the weak nuclear forces, have been successfully quantized in the unifying language of connections in a Yang-Mills theory [66, 89]. The last classical theory, Einstein's geometrical interpretation of gravity, or general relativity [27, 55, 85], has so far resisted all attempts of quantization by many physicists over the past 75 years. What we have today are two types of candidate theories that embody elements of both quantum mechanics and general relativity. One is string theory [67], which builds on the perturbative formulation of quantum field theory, and the other is loop quantum gravity [73, 81], which builds on general covariance and canonical quantization. They remain candidates because each of them has yet to show that it reduces to the known standard model of matter and general relativity at low energies, which is the basic test that any theory of quantum gravity must pass.

Loop quantum gravity has its origins in the straight-forward canonical approach to quantum gravity, which was originally developed by Dirac, Wheeler, DeWitt, Arnowitt, Deser and Misner. It was briefly abandoned in favor of string theory in the 1980s. Over the last 20 years, it has enjoyed a revitalization after Ashtekar reformulated the theory in terms of connections rather than metrics. It is because connections are naturally described by Wilson loop variables, that the theory is named loop quantum gravity. This brings it much closer to the formulation of the other three forces of nature. More recently, covariant formulations of the theory, the spin foam models, have emerged to become the most promising candidates of quantum gravity.

The spin foam models [64] have their own separate history from the development of three dimensional gravity and topological quantum field theories. A spin foam model is a discrete simplicial model of quantum gravity. In 1968, based on the asymptotic form of the Wigner $6j$-symbol, Ponzano-Regge [68] proposed the first spin foam model for 3D gravity. In 1991, Ooguri [62] sucessfully used a limiting process on the Turaev-Viro models to regularize the infrared divergence, and showed that the Ponzano-Regge model is related

to the simplicial model of a topological quantum field theories [60]. The most promising spin foam models in four dimensions are the Barrett-Crane model [13, 14] and the EPRL model [39]. One of the most pressing open questions for the spin foam models is whether their classical limits will reproduce classical general relativity.

In those spin foam models, the Feynman amplitudes for a single 4-simplex are sums of products of two Wigner $15j$-symbols. In this thesis, we have made significant progress in finding some classical limits of the Wigner $15j$-symbol. In the rest of this introductory chapter, we explain how the Wigner $3nj$-symbols appear in the spin foam models in section 1.2. Then we define the Wigner $3nj$-symbols as $SU(2)$ spin networks in section 1.3. Finally, we give an overview of the methods and results of this thesis in section 1.4.

1.2 The Spin Foam Models

1.2.1 The Ponzano-Regge Model in Three Dimensions

We now describe the Ponzano-Regge model for 3D gravity [68]. Given a three-dimensional manifold M, fix a triangulation by 3-simplices, and assign six representations of $SU(2)$, labeled by half integers $(j_1, j_2, j_3, j_4, j_5, j_6)$, to the six edges of each 3-simplex. The triangulation and the coloring $\{j_e\}$ of the edges together represent a single Feynman diagram of a geometric transition amplitude. The Feynmann rules assign a Wigner $6j$-symbol

$$\left\{ \begin{array}{ccc} j_1(t) & j_2(t) & j_3(t) \\ j_4(t) & j_5(t) & j_6(t) \end{array} \right\} \tag{1.1}$$

to each tetrahedron. The partition function is then a sum of the Feynman amplitudes, where the sum is taken over all edge colorings $\{j_e\}$, given by

$$Z(L) = \sum_{\{j_e\}} \prod_v \frac{1}{\Lambda} \prod_e (-1)^{2j_e}(2j_e+1) \prod_t \exp(-\pi i \sum_i j_i(t)) \left\{ \begin{array}{ccc} j_1(t) & j_2(t) & j_3(t) \\ j_4(t) & j_5(t) & j_6(t) \end{array} \right\}. \tag{1.2}$$

The Feynman amplitude for the edges e and vertices v are chosen to ensure that the partition function is invariant under a refinement of the simplicial decomposition. The choice of the Wigner $6j$-symbol for the amplitude of the 3-simplex is motivated by the remarkable form of its large j asymptotic limit,

$$\exp(-i\pi \sum_i j_i) \left\{ \begin{array}{ccc} j_1 & j_2 & j_3 \\ j_4 & j_5 & j_6 \end{array} \right\} \sim \frac{1}{\sqrt{48\pi V}} \left[(-1)^{\sum_i 2j_i} e^{i(S_R - \pi/4)} + e^{-i(S_R-\pi/4)} \right], \tag{1.3}$$

where

$$S_R = \sum_{i=1}^{6} j_i \, \phi_i \tag{1.4}$$

is the Regge action for a single tetrahedron in Regge's discrete model of classical general relativity [70]. Here ϕ_i is the internal dihedral angle of the tetrahedron at edge i, and V is the volume of the tetrahedron. The product over the tetrahedra in (1.2) produces a term

of the form $e^{i\sum S_R}$. The sum in the exponent is a discrete form of the Euclidean Einstein-Hilbert action $\int d^3x\sqrt{g}R$, where the curvature is modeled by deficit angles on the edges. Assuming that this term dominates the classical limit of the Ponzano-Regge action, then the Ponzano-Regge model is a quantum theory whose classical limit reproduces Euclidean general relativity.

The original Ponzano-Regge model runs into some difficulties with mathematical consistency. The partition function in (1.2) is divergent, and requires regularization. The original regularization employs a simple cutoff $j_e \leq L$, but it fails to put the model on a firm mathematical setting. Decades later, Ooguri [60, 62] used the Turaev-Viro models from topological QFT to regularize the partition function. In that regularization scheme, the Wigner $6j$-symbols are replaced by their q-analogue from the quantum group $SU_q(2)$. In addition to invariance under a refinement of the triangulation, the various identities for the q-deformed $6j$-symbols make the new partition function Z_q invariant under sequences of local Alexander transformations that related any two triangulations of the 3-manifold. In essence, the partition function becomes a topological invariant. In the limit $q \to 1$, and in the continuum limit, the partition function Z_q approaches the functional integral

$$Z = \int [de, dw] \, \exp(i \int e \wedge R) \,, \tag{1.5}$$

where e is a dreibein, ω is a spin connection on M, and $R = d\omega + \omega \wedge \omega$ is the curvature two-form. This action functional is the Einstein-Hilbert action rewritten in a first order formalism. Thus, the Ponzano-Regge spin foam model has well defined regularization based on a topological quantum field theory (TQFT).

1.2.2 Spin Foam Models in Four Dimensions

The Ponzano-Regge model can be generalized to four dimensions. Instead of assigning representations to the edges, we now assign representations to the faces of a 4-simplex. Given a four-dimensional manifold M, fix a triangulation Δ by 4-simplexes. Each 4-simplex has five vertices, ten edges, ten faces, and five tetrahedra. The ten faces of each 4-simplex determines a set of ten bivectors $B = e \wedge e$, where e are the edge vectors. These bivectors satisfy the conditions

1. The bivector changes sign when the orientation of the triangle is reversed.
2. Each bivector is simple: $B \wedge B = 0$.
3. If the two triangles corresponding to B_1 and B_2 share a common edge, then $B_1 + B_2$ is also simple.
4. The sum of 4 bivectors belonging to a single tetrahedron is zero.

These bivectors can be identified with the elements of the Lie algebra $so(4) = su(2) \oplus su(2)$. The quantization of a geometric 4-simplex is then obtained by labeling the triangles with irreducible representations (j, k) of $SU(2) \times SU(2)$. The quantum conditions corresponding to the geometric conditions 1 to 4 above are given by:

1. Reversing the orientation of a triangle maps the representation to its dual.
2. The allowed representations for a triangle consist of the balanced representations (j, j).
3. For each pair of adjacent faces, the Clebsh-Gordan series for the pair of representations has nonzero summands in the balanced representations of $SU(2) \times SU(2)$.
4. The tensor product for the four faces in a tetrahedron is an invariant.

To assign amplitudes to the 4-simplex, we look for topological quantum field theory with similar assignments of representations to the faces of a 4-simplex. It turns out that there exists a spin foam model for a TQFT [32, 61] called the $su(2)$ BF theory in four dimensions. Its partition function is

$$Z_{BF}(\Delta, q) = \sum_{\{j_f, i_t\}} \prod_f dim_q(j_f) \prod_v \phi^{15j}_{q,v}(\mathbf{j}, \mathbf{i}) \,. \tag{1.6}$$

Here q is the deformation parameter for the quantum group, and the sum above is over the coloring j_f of the faces of the triangulation Δ, and over the coloring i_t of the tetrahedra. Taking a leaf from the regularization of the Ponzano-Regge model by topological quantum field theory, we create balanced representations by taking two copies of the $su(2)$ BF theory, and assign the $15j$-symbol to the 4-simplex. After imposing the constraints 1-4 on this TQFT, we obtain the most well-known spin foam model over the last decade, the Barrett-Crane model. Its partition function is given by

$$Z_{BC}(\Delta, q) = \sum_{\{j_f, j'_f, i_t, i'_t\}} \prod_f dim_q(j_f)\, dim_{q^{-1}}(j'_f) \prod_v \phi^{15j}_{q,v}(\mathbf{j}, \mathbf{i})\, \phi^{15j}_{q,v}(\mathbf{j}', \mathbf{i}')\, \delta_{\mathbf{j},\mathbf{j}'} \delta_{\mathbf{i},\mathbf{i}'} \,. \tag{1.7}$$

Here the delta function $\delta_{\mathbf{j},\mathbf{j}'}$ corresponds to the quantum constraint 2, and $\delta_{\mathbf{i},\mathbf{i}'}$ corresponds to the quantum constraint 3. When we take the limit $q \to 1$, corresponding to general relativity with zero cosmological constant, the amplitude for a 4-simplex becomes a product of two Wigner $15j$-symbols. There are problems with the BC model from numerical simulations, so it has been replaced by a more recent model, called the EPRL model [39]. It has a similar expression for the partition function, but the constraints are imposed differently. In other words, the factor $\delta_{\mathbf{j},\mathbf{j}'} \delta_{\mathbf{i},\mathbf{i}'}$ in (1.7) is replaced by a different factor. The amplitude for a 4-simplex in the EPRL model, however, remains a sum over a product of two Wigner $15j$-symbols. Therefore, we believe finding the asymptotic form of the Wigner $15j$-symbol is essential in discovering the classical limit of the vertex-amplitude for the four dimensional spin foam models.

1.3 The Wigner $3nj$-Symbols as $SU(2)$ Spin Networks

The Wigner $3nj$-symbols are examples of spin networks, which are graphical representations for contractions between tensors in the representation of $SU(2)$. The graphical notation for spin networks has been developed by Yutsis et al. [96], El Baz and Castel [37],

Lindgren and Morrison [47], Varshalovich et al. [83], Stedman [79], Wormer and Palnus [95] and others.

Following [96], we will now describe the spin network notation for the first type of the Wigner $3nj$-symbols, for $n = 1, 2, 3, 4, 5$. The Wigner $3j$-symbol,

$$\begin{pmatrix} j_1 & j_2 & j_3 \\ m_1 & m_2 & m_3 \end{pmatrix} = (-1)^{j_1 - j_2 - m_3} (2j_3 + 1)^{-\frac{1}{2}} \ \langle j_1 m_1 j_2 m_2 | j_1 j_2 j_3 - m_3 \rangle \tag{1.8}$$

is a symmetrized version of the Clebsch-Gordan coefficient, describing the addition of two angular momenta to a third. Its spin network notation is an oriented node which links three directed lines, where a counter-clockwise orientation is denoted by a + sign and a clockwise orientation is denoted by a − sign. For example, the $3j$-symbol defined in (1.8) is represented by the spin network in figure 1.1.

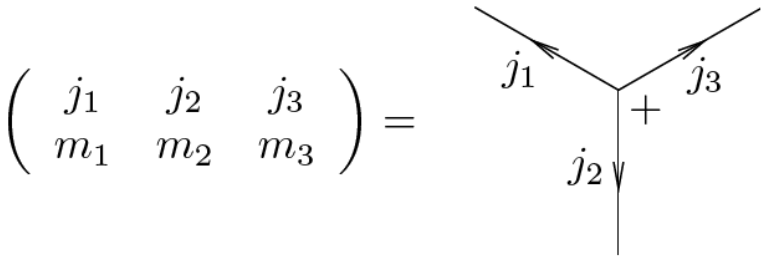

Figure 1.1: The spin network notation for the Wigner $3j$-symbol.

In figure 1.1, the three lines correspond to j_1, j_2, and j_3 and their free ends correspond to the magnetic quantum numbers m_1, m_2, and m_3. By the orientation of the node is meant the cyclic order of the lines j_1, j_2, j_3. The direction of the line j_i indicates the sign of the magnetic quantum number m_i in the Wigner coefficient.

The Wigner $3nj$-symbols for $n > 1$ can be expressed as a sum of products of $3j$-symbols. In spin network notation, a product of two $3j$-symbols is expressed as two disjoint spin networks for these two $3j$-symbols, and a sum over a magnetic quantum number is represented by a connection between two directed lines. For example, a sum over m of a product of two $3j$-symbols is represented by the four legged diagram in figure 1.2.

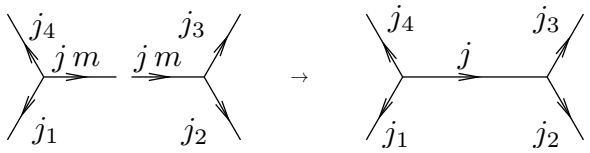

Figure 1.2: A sum over the product of two $3j$-symbols is represented by a concatenation of the line corresponding to the summation indices.

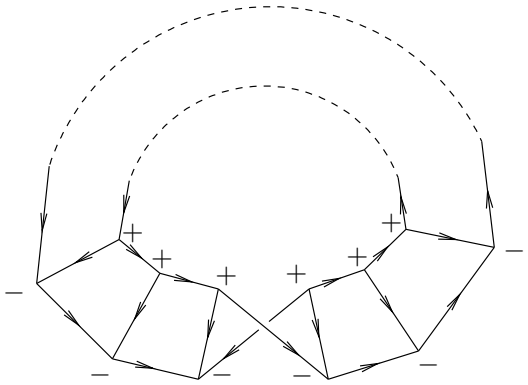

Figure 1.3: The spin network for a general Wigner $3nj$-symbol has the topology of a Möbius strip.

In general, the spin network of a Wigner $3nj$-symbol of the first type has the topology of a Möbius strip, illustrated in figure 1.3. For example, the spin networks for the $6j$-, $9j$-, $12j$-, and $15j$ symbols are displayed in part (a), (b), (c), (d) of figure 1.4, in that order, respectively.

If we cut along the middle of the strip, the $3nj$-symbols can be expressed as a sum of a product of two spin networks. The sum over the magnetic quantum numbers in the middle of the strip is equivalent to taking a scalar product in the angular momentum spaces represented by the lines in the middle of the strip. For example, by cutting the edges j_1, j_2, j_3, j_4 in part (a) of figure 1.4, the $6j$-symbol can be written as a scalar product between a bra and a ket, as illustrated in figure 1.5.

In this thesis, we will often use such a decomposition of the Wigner $3nj$-symbols as a scalar product between two states. Because each $3nj$-symbol has the topology of a Möbius strip, the symmetries of each symbol correspond to the symmetries of the corresponding Möbius strip.

1.4 Overview

We now briefly describe the previous works on the asymptotics of the Wigner $3nj$-symbols. Building on physical intuition and educated guesses, Wigner [93] found the asymptotic amplitudes, and later Ponzano and Regge [68] derived the complete asymptotic formulas for the Wigner $3j$- and $6j$-symbols when all quantum numbers are large. The first rigorous proof of these asymptotic formulas was provided by Schulten and Gordon [76, 77], by approximating recursion relations by differential equations, and applying WKB theory to those equations. They also provided uniform approximations of the Airy type for the transition regions between classical allowed and forbidden regimes. Their line of reasoning was later generalized to the $6j$-symbol from the quantum groups [56, 80]. Along the way, there are also many derivations from other standard asymptotic techniques, such as Stirling's approximation and the stationary phase approximation. For instance, Brussaard

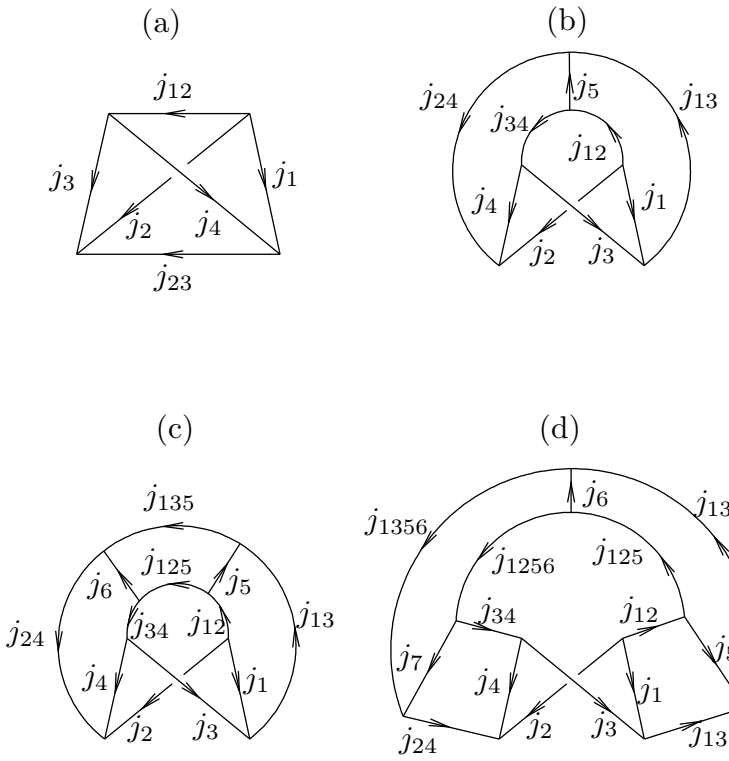

Figure 1.4: The spin networks for the (a) $6j$-symbol, (b) $9j$-symbol, (c) $12j$-symbol, and (d) $15j$-symbol.

$$\left\{ \begin{matrix} j_1 & j_2 & j_{12} \\ j_3 & j_4 & j_{23} \end{matrix} \right\} = (-1)^{2j_2}$$

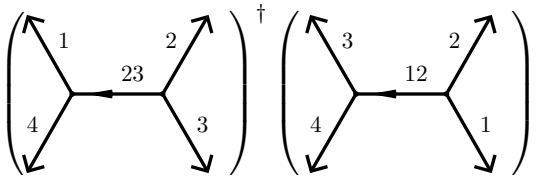

Figure 1.5: Decomposition of the $6j$-symbol spin network into a bra spin network and a ket spin network.

and Tolhoek [24] and Edmond [35] used the Stirling's approximation to find the asymptotic formulas for the $3j$- and $6j$-symbol when some of the quantum numbers are large and others are small. Along a similar line of reasoning, Watson [87, 86] and Anderson [3] found the asymptotic formulas for the $9j$-symbol when some of the quantum numbers are large and others are small. Working with an integral representation for the Clebsch-Gordan coefficients, Reinsch and Morehead [71] used the stationary phase approximation to calculate the higher order terms in the asymptotics for the $3j$-symbol. More recently, because of the connection with loop quantum gravity, there have appeared more geometrical treatments of the asymptotics of the $6j$-symbol. Using methods based on geometric quantization, Roberts [72] and Charles [28] provided new derivations for the asymptotic formula of the $6j$-symbol.

In this thesis, we construct a new geometric method to derive new asymptotic formulas for the $3nj$-symbols. These methods are based on the modern geometric technique of WKB theory, or semiclassical analysis, using Lagrangian manifolds and symbol correspondence. Each chapter in this thesis is a self-contained calculation of the asymptotics of one of the $3nj$-symbols. While chapter 2, 3, and 4 provide new derivations of known results, chapter 5, 6, 7, and 8 contain both new techniques and new results.

In chapter 2, we derive the asymptotic formula of the Wigner $3j$-symbol by a direct application of the stationary phase approximation to the Bargmann wavefunctions, which are related to the wavefunctions in both geometric quantization and in Schwinger's representation. The motivation of this chapter is to show the basic features of the stationary phase calculations in later chapters, without requiring the reader to have any background in semiclassical analysis. In essence, the geometric methods based on geometric quantization and on semiclassical analysis are doing similar stationary phase calculations, but the extra geometric structures in each formalism simplify various parts of the calculation.

In chapter 3, we derive the asymptotic formula of the $3j$-symbol again, but this time using multidimensional WKB theory and the Schwinger model. This introduces the basic setup and technique used in later chapters. By comparison with the calculation in chapter 2, we illustrate the advantages of the semiclassical analysis in the Schwinger representation over a direct stationary phase phase calculation.

In chapter 4, we derive the asymptotic formula of the $6j$-symbol using multidimensional WKB theory and the Schwinger model. This chapter involves novel use of the geometry of a tetrahedron, such as the Gram matrix, the Schläfli identity, and the Hamilton-Rodrigues formula. Moreover, it illustrates novel simplifications that are possible in the presence of symmetries in the problem.

In chapter 5, we use the theory of quantum normal form and the Stratonovich-Weyl symbol correspondence to derive a new uniform approximation of the $6j$-symbol in terms of rotation matrices. In order to derive this uniform approximation, we found that we are required to generalize the theory of uniform approximation to use symplectic transformations that are not induced by a point transformation. Numerically, we found this new uniform approximation to be superior compared to other types of uniform approximations for the $6j$-symbol.

In chapter 6, we generalize the Bohr-Oppenheimer approximation to find new asymptotics of the $9j$-symbol, when some quantum numbers are large and others are small. The generalization involves finding a new gauge-invariant form of multicomponent WKB

wavefunctions, which is achieved through the use of parallel transport of spinors, rotation matrices, and perturbation of Lagrangian manifolds. This chapter uses the results from the analysis of the Lagrangian manifolds associated with the $6j$-symbol from chapter 4.

In chapter 7 and 8, we apply the method developed from chapter 6 to derive new asymptotics of the $12j$- and $15j$-symbol, respectively, when some quantum numbers are large and others are small.

Chapter 2

The Bargmann Representation

2.1 Introduction and Summary

Bargmann constructed a unitary representation of the quantum rotation group $SU(2)$ in a series of papers [10, 11, 12] in the 1960s. This representation is based on the construction for the generators of $SU(2)$ from two sets of commuting boson operators. Thus, by construction, this representation is similar to Schwinger's representation [78] of $SU(2)$ in terms of two sets of harmonic oscillators. The difference is that Bargmann implemented the boson operators in terms of multiplication and differentiation in complex variables, resulting in a Hilbert space consisting entirely of holomorphic functions in the complex variables. Years later, these holomorphic functions are realized to coincide with the wavefunctions resulting from the geometric quantization of the group $SU(2)$ ([94], p177). Therefore, the Bargmann representation is intimately connected with both the Schwinger model and the geometric quantization of the group $SU(2)$. Recently, both the Schwinger's representation and the geometric quantization of $SU(2)$ are used to provide a geometric understanding in the asymptotic analysis of the Wigner $3nj$-symbols. Thus, the Bargmann representation provides a natural connection between these two geometric methods.

Another advantage of the Bargmann representation is that the wavefunctions appearing in the recoupling theory of angular momentum are simply polynomials. Their explicit form allows us to write the recoupling coefficients as elementary integrals, whose asymptotics can be calculated by applying straightforward stationary phase approximations. In this paper, we will perform this stationary phase approximation for the $3j$-symbol, without using any of the geometric methods. Part of the significance of this work is that this elementary calculation can help the non-expert understand the more advanced geometric calculations.

We now provide an outline to the chapter. In section 2.2, we introduce the Bargmann representation of $SU(2)$, and derive the explicit forms of the eigenstates appearing in the recoupling theory of angular momentum. We then relate the Bargmann representation to the Schwinger representation and geometric quantization in section 2.3 and 2.4, respectively. In section 2.5, we write down an exact integral representation of the Wigner $3j$-symbol. We then perform a stationary phase approximation to find the asymptotics of the $3j$-symbol in section 2.6. In the last section, we discuss the simplifications that

the geometric methods could provide to this elementary calculation.

2.2 The Bargmann Representation of $SU(2)$

We now summarize the construction of the Bargmann representation of the quantum rotation group $SU(2)$. Let z_μ, $\mu = 1, 2$, denote the coordinates on $\mathbb{C}^2$. The commutation relations

$$[z_\mu, \frac{\partial}{\partial z_\mu}] = 1 \tag{2.1}$$

allow us to form two independent sets of boson creation operators z_μ and annihilation operators ∂_{z_μ}, $\mu = 1, 2$. Each set of boson operators has a number operator

$$N_\mu = z_\mu \partial_{z_\mu} \,. \tag{2.2}$$

Following Schwinger's construction of the generators of $SU(2)$ in terms of boson creation and annihilation operators, we define

$$\hat{J}_i = z_\mu \sigma^i_{\mu\nu} \frac{\partial}{\partial z_\nu} \,, \tag{2.3}$$

where σ^i are the Pauli matrices. They satisfy the usual commutation relations for the generators of $SU(2)$,

$$[\hat{J}_i, \hat{J}_j] = i\epsilon_{ijk} \hat{J}_k \,. \tag{2.4}$$

The Casimir operator is

$$\hat{J}^2 = \hat{N}(\hat{N} + 1) \,, \tag{2.5}$$

where $\hat{N}$ is half of the total number operator given by

$$\hat{N} = \frac{1}{2}(\hat{N}_1 + \hat{N}_2) \,. \tag{2.6}$$

Since the eigenvalues of $\hat{N}_1, \hat{N}_2$ are integers, the eigenvalues of $\hat{J}^2$ are given by $j(j+1)$, where $j = n/2$ are half integers.

The Hilbert space $\mathcal{F}_2$ consists of entire analytic functions on $\mathbb{C}^2$, that is,

$$\mathcal{F}_2 = \{ f \in \mathcal{C}^\infty(\mathbb{C}^2) \mid \langle f|f\rangle < \infty \} \,. \tag{2.7}$$

The inner product is given by

$$\langle f|g\rangle = \int_{\mathbb{C}^2} \overline{f}(z)\, g(z)\, \frac{e^{-|z|^2}}{\pi^2}\, d^2 z \,, \tag{2.8}$$

where $d^n z$ denotes the usual Euclidean measure on $\mathbb{C}^2 = \mathbb{R}^4$.

In the recoupling theory of three angular momenta, we form the tensor product of three copies of Bargmann spaces. The wavefunctions are analytic functions on $\mathbb{C}^6$. Let

$(z_{11}, z_{12}, z_{21}, z_{22}, z_{31}, z_{32})$ be the coordinates on $\mathbb{C}^6$, then wavefunctions for the basis states $|j_1 m_1 j_2 m_2 j_3 m_3\rangle$ are given by

$$\psi_{jm}(z_1, z_2) = \prod_{r=1}^{3} \frac{1}{\sqrt{(j_r - m_r)!(j_r + m_r)!}} \, z_{r1}^{j_r + m_r} \, z_{r2}^{j_r - m_r} \,. \tag{2.9}$$

We can check that they satisfy

$$\hat{N}\psi_{jm}(z) = j_r \psi_{jm}(z) \,, \tag{2.10}$$

$$\hat{J}_{rz}\psi_{jm}(z) = m_r \psi_{jm}(z) \,, \tag{2.11}$$

$$\langle \psi_{jm} | \psi_{jm} \rangle = 1 \,, \tag{2.12}$$

for $r = 1, 2, 3$, by explicit calculations using (2.3), (2.6), and (2.8).

The diagonal $SU(2)$ action T_U for $U_{\mu\nu} \in SU(2)$ on a wavefunction $f(z)$ is given by

$$T_U(f(z)) = f(U^\dagger_{\mu\nu} z_{1\nu}, U^\dagger_{\mu\nu} z_{2\nu}, U^\dagger_{\mu\nu} z_{3\nu}) \,. \tag{2.13}$$

Since U is unitary, the three determinants

$$\delta_1 = z_{21}z_{32} - z_{31}z_{22} \,, \quad \delta_2 = z_{31}z_{12} - z_{11}z_{32} \,, \quad \delta_3 = z_{11}z_{22} - z_{21}z_{12} \,, \tag{2.14}$$

are invariant under T_U. Let the state $|j_1 j_2 j_3 \mathbf{0}\rangle$ be an eigenstate of $\hat{J}_r^2$, $r = 1, 2, 3$, that is also invariant under T_U.

The normalized wavefunction for $|j_1 j_2 j_3 \mathbf{0}\rangle$ is given by

$$\psi_{j\mathbf{0}}(z) = \frac{\delta_1^{k_1} \delta_2^{k_2} \delta_3^{k_3}}{\sqrt{(j_1 + j_2 + j_3)! k_1! k_2! k_3!}} \,, \tag{2.15}$$

where the non-negative integers k_1, k_2, k_3 are given by

$$k_1 = j_2 + j_3 - j_1 \,, \quad k_2 = j_3 + j_1 - j_2 \,, \quad k_3 = j_1 + j_2 - j_3 \,, \tag{2.16}$$

which is the solution to the equations derived from the eigenvalue equations for $\hat{J}_r^2$, that is, they are solutions to the system of equations

$$k_2 + k_3 = 2j_1 \,, \quad k_3 + k_1 = 2j_2 \,, \quad k_1 + k_2 = 2j_3 \,. \tag{2.17}$$

2.3 Relation to the Schwinger Representation

We now relate the Bargmann representation to the Schwinger representation of $SU(2)$. As explained in [65], this relationship becomes apparent when we write the eigenstates of the harmonic oscillators in the coherent states basis of the Heisenberg-Weyl group [65]. The coherent states basis are given by $|z\rangle = \hat{D}(z)\,|0\rangle$, where $|0\rangle$ is the ground state of

the simple harmonic oscillator, and $\hat{D}(z)$ is an element of the Heisenberg-Weyl group, given by

$$\hat{D}(z) = \exp\left[\frac{i}{\hbar}(x\hat{p} - p\hat{x})\right] = \exp(-|z|^2/2)\exp(z\hat{a}^\dagger)\exp(-\overline{z}\hat{a})\,, \tag{2.18}$$

where $z = x + ip$, and $\hat{a}$ and $\hat{a}^\dagger$ are the usual annihilation and creation operators of the simple harmonic oscillator. The coherent state wavefunction

$$\langle x|z\rangle = (\pi\hbar)^{-1/4}\,\exp\left[-\frac{z^2}{2} + (2/\hbar)^{1/2}zx - \frac{x^2}{2\hbar}\right] \tag{2.19}$$

is the displaced ground state of the simple harmonic oscillator centered at (x, p). Using the exponential generating function for the Hermite polynomials

$$\exp(-z^2 + 2zx) = \sum_{n=0}^{\infty}\frac{z^n}{n!}\,H_n(x)\,, \tag{2.20}$$

we find that the eigenstates $|n\rangle$ of the simple harmonic oscillator written in the coherent state basis is given by

$$\langle z|n\rangle = \sum_{n'}\frac{z^{n'}}{n'!}\int dx(\pi\hbar)^{-1/4}H_{n'}(x)e^{-x^2/2\hbar}\psi_n(x) = \frac{z^n}{n!}\,, \tag{2.21}$$

where we have used the orthonormality of the eigenstates of the simple harmonic oscillator.

Schwinger's representation uses two simple harmonic oscillators. The basis states $|j_1 m\rangle = |n_1 n_2\rangle$ is the product of two eigenstates of the two harmonic oscillators, where $n_1 = j + m$ and $n_2 = j - m$. Thus, the Schwinger wavefunction for $|jm\rangle$ written in the coherent state basis is given by

$$\langle z_1 z_2|n_1 n_2\rangle = \frac{z_1^{j+m}z_2^{j-m}}{(j+m)!(j-m)!}\,, \tag{2.22}$$

which is proportional to the Bargmann wavefunction for $|jm\rangle$.

2.4 Relation to Geometric Quantization

The wavefunctions that result from the geometric quantization of the coadjoint orbits of $SU(2)$ are holomorphic functions on a 2-sphere. We get these functions by restricting the Bargmann wavefunctions to a $\mathbb{C}P^1 = S^2$ subspace of $\mathbf{C}^2$.

Let us start with the Bargmann wavefunctions for the basis states $|jm\rangle$, given by

$$\psi_{jm}(z_1, z_2) = \frac{1}{\sqrt{(j-m)!(j+m)!}}\,z^{j+m}\,z^{j-m}\,. \tag{2.23}$$

The functions $\psi_{jm}(z_1, z_2)$ have the scaling property

$$\psi_{jm}(\lambda z_1, \lambda z_2) = \lambda^{2j}\,\psi_{jm}(z_1, z_2)\,, \tag{2.24}$$

for $\lambda \in \mathbb{C}$. Thus, given this scaling property, the Bargmann wavefunctions are completely determined by its values on a $\mathbb{C}P^1 = S^2$ subspace. Let us choose this subspace to be defined by $|z_1|^2 + |z_2|^2 = 1$, and real z_1. Let $\xi = z_2/z_1$ parametrize the coordinate on this subspace. Then the basis functions $\psi_{jm}(z_1, z_2)$ restricted to the section $\mathbb{C}P^1$ is given by

$$\begin{aligned} \psi(\xi) &= \frac{z_1^{j+m}\, z_2^{j-m}}{[(j+m)!\,(j-m)!\,]^{1/2}} \\ &= \frac{z_1^{2j}(z_2/z_1)^{j-m}}{[(j+m)!\,(j-m)!\,]^{1/2}} \\ &= \frac{1}{[(j+m)!\,(j-m)!\,]^{1/2}} \frac{\xi^{j-m}}{(1+|\xi|^2)^j}\,, \end{aligned} \tag{2.25}$$

where we have used $1 = |z_1|^2 + |z_2|^2 = z_1^2(1+|\xi|^2)$. These basis wavefunctions agree with those used in geometric quantization of $SU(2)$ ([94], p177), as well as the spin coherent state wavefunctions [69].

2.5 An Integral Representation of the $3j$-Symbol

Taking the scalar product between the wavefunction $\psi_{jm}(z)$ from (2.9) and the wavefunction $\psi_{j\mathbf{0}}(z)$ from (2.15), we obtain an exact integral representation of the $3j$-symbol

$$\begin{pmatrix} j_1 & j_2 & j_3 \\ m_1 & m_2 & m_3 \end{pmatrix} = \langle j_1 m_1 j_2 m_2 j_3 m_3 | j_1 j_2 j_3 \mathbf{0}\rangle \tag{2.26}$$

$$\begin{aligned} &= N \int_{\mathbb{C}^6} d^{12}\, z\, \overline{z}_{11}^{j_1+m_1}\, \overline{z}_{12}^{j_1-m_1}\, \overline{z}_{21}^{j_2+m_2}\, \overline{z}_{22}^{j_2-m_2}\, \overline{z}_{31}^{j_3+m_3}\, \overline{z}_{32}^{j_3-m_3}\;\; e^{-|z|^2} \\ &\quad (z_{21}z_{32} - z_{31}z_{22})^{k_1}\, (z_{31}z_{12} - z_{32}z_{11})^{k_2}\, (z_{11}z_{22} - z_{12}z_{21})^{k_3}\,, \end{aligned} \tag{2.27}$$

where the constant in front is

$$N = \frac{1}{\pi^6[(j_1+m_1)!(j_1-m_1)!(j_2+m_2)!(j_2-m_2)!(j_3+m_3)!(j_3-m_3)!]^{1/2}} \tag{2.28}$$

$$\frac{1}{[(j_1+j_2+j_3)!\,k_1!\,k_2!\,k_3!]^{1/2}}\,, \tag{2.29}$$

and where

$$k_1 = j_2 + j_3 - j_1\,, \quad k_2 = j_3 + j_1 - j_2\,, \quad k_3 = j_1 + j_2 - j_3\,. \tag{2.30}$$

2.6 Stationary Phase Approximation

We apply the stationary phase approximation to the above integral expression (2.26) in the limit that j_i for $i = 1, 2, 3$ are large. The basic formula for stationary phase approximation is given by

$$\int e^{f(x)} d^n x = (2\pi)^{n/2} \sum_p \frac{e^{f(p)}}{\sqrt{-\mathrm{Hess}_p(f)}}\,, \tag{2.31}$$

where p stands for the stationary phase points that satisfy the stationary phase conditions

$$\partial_{z_{r\mu}} f(z,\overline{z}) = 0\,, \quad \partial_{\overline{z}_{r\mu}} f(z,\overline{z}) = 0\,. \tag{2.32}$$

2.6.1 Stationary Phase Points

In the integral (2.26), the phase function is

$$f(z,\overline{z}) = \ln \overline{\psi}_{jm}(z) + \ln \psi_{j\mathbf{0}}(z) - \sum_{r\mu} |z_{r\mu}|^2\,, \tag{2.33}$$

where

$$\ln \overline{\psi}_{jm}(z) = \sum_{r=1}^{3} \left[(j_r + m_r) \ln \overline{z}_{r1} + (j_r - m_r) \ln \overline{z}_{r2}\right], \tag{2.34}$$

and

$$\ln \psi_{j\mathbf{0}}(z) = k_1 \ln(z_{21}z_{32} - z_{22}z_{31}) + k_2 \ln(z_{31}z_{12} - z_{32}z_{11}) + k_3 \ln(z_{11}z_{22} - z_{12}z_{21})\,. \tag{2.35}$$

To find the stationary phase points, we note that the twelve conditions (2.32) are equivalent to the following twelve conditions,

$$\hat{I}_r\, f(z,\overline{z}) = 0\,, \tag{2.36}$$
$$\hat{I}^*_r\, f(z,\overline{z}) = 0\,, \tag{2.37}$$
$$\hat{J}^*_{rz}\, f(z,\overline{z}) = 0\,, \tag{2.38}$$
$$\hat{J}_i\, f(z,\overline{z}) = 0\,, \tag{2.39}$$

where the twelve differential operators $\hat{I}_r$, $\hat{I}^*_r$, $\hat{J}_{rz}$, and $\hat{J}_i$, $r = 1,2,3$, $i = 1,2,3$ are given by

$$\hat{I}^*_r = \hat{N}^*_r = \frac{1}{2} \sum_\mu \overline{z}_{r\mu} \frac{\partial}{\partial \overline{z}_{r\mu}}\,, \tag{2.40}$$

$$\hat{J}^*_{rz} = \frac{1}{2} \sum_{\mu\nu} \overline{z}_{r\mu} (\sigma_z)_{\mu\nu} \frac{\partial}{\partial \overline{z}_{r\nu}}\,, \tag{2.41}$$

$$\hat{I}_r = \hat{N}_r = \frac{1}{2} \sum_\mu z_{r\mu} \frac{\partial}{\partial z_{r\mu}}\,, \tag{2.42}$$

$$\hat{J}_i = \frac{1}{2} \sum_{r\mu\nu} z_{r\mu} (\sigma^i)_{\mu\nu} \frac{\partial}{\partial z_{r\nu}}\,. \tag{2.43}$$

From the eigenvalue equations

$$\hat{I}_r^* \overline{\psi}_{jm} = j_r \overline{\psi}_{jm} \,, \tag{2.44}$$

$$\hat{J}_{rz}^* \overline{\psi}_{jm} = m_r \overline{\psi}_{jm} \,, \tag{2.45}$$

$$\hat{I}_r \psi_{j\mathbf{0}} = j_r \psi_{j\mathbf{0}} \,, \tag{2.46}$$

$$\hat{J}_i \psi_{j\mathbf{0}} = 0 \,, \tag{2.47}$$

we find that the result of applying these differential operators on the first two terms of the phase function (2.33) are constants

$$\hat{I}_r^* \ln \overline{\psi}_{jm} = j_r \,, \quad \hat{J}_{rz}^* \ln \overline{\psi}_{jm} = m_r \,, \quad \hat{I}_r \, \ln \psi_{j\mathbf{0}} = j_r \,, \quad \hat{J}_i \ln \psi_{j\mathbf{0}} = 0 \,. \tag{2.48}$$

Applying these twelve operators to the remaining term $\sum_{r\mu} |z_{r\mu}|^2$ generates the functions I_r, J_{rz}, and J_i as follows:

$$\hat{I}_r^* \sum_{r\mu} |z_{r\mu}|^2 = \frac{1}{2} \sum_{\mu} z_{r\mu} \, \overline{z}_{r\mu} \equiv I_r \,, \tag{2.49}$$

$$\hat{J}_{rz}^* \sum_{r\mu} |z_{r\mu}|^2 = \frac{1}{2} \sum_{\mu\nu} \overline{z}_{r\mu} \, (\sigma_z)_{\mu\nu} z_{r\nu} \equiv J_{rz} \,, \tag{2.50}$$

$$\hat{I}_r \sum_{r\mu} |z_{r\mu}|^2 = \frac{1}{2} \sum_{\mu} z_{r\mu} \, \overline{z}_{r\mu} = I_r \,, \tag{2.51}$$

$$\hat{J}_i \sum_{r\mu} |z_{r\mu}|^2 = \frac{1}{2} \sum_{r\mu\nu} z_{r\mu} \, (\sigma^i)_{\mu\nu} \overline{z}_{r\nu} \equiv J_i \,. \tag{2.52}$$

Thus, the stationary conditions (2.36) - (2.39) become the following algebraic equations

$$I_r = j_r \,, \qquad J_{rz} = m_r \,, \qquad J_i = 0 \,. \tag{2.53}$$

We now find the stationary phase points. First we note that the stationary phase conditions are related to the Hopf fibration of the spinor space $\mathbb{C}^6 = \mathbb{R}^{12}$ into a T^3 fiber bundle over an angular momentum space $\mathbb{R}^3 \times \mathbb{R}^3 \times \mathbb{R}^3$. In particular, the projection map $\pi : \mathbb{C}^6 \to \mathbb{R}^3 \times \mathbb{R}^3 \times \mathbb{R}^3$ is expressed in terms of the functions

$$J_{ri} = \sum_{\mu\nu} z_{r\mu} \, (\sigma^i)_{\mu\nu} \overline{z}_{r\nu} \,. \tag{2.54}$$

Explicitly, they are

$$J_{rx} = \frac{1}{2} \left(\overline{z}_{r1} z_{r2} + \overline{z}_{r2} z_{r1} \right) = \mathrm{Re} \left(\overline{z}_{r1} z_{r2} \right) , \tag{2.55}$$

$$J_{ry} = \frac{1}{2} \left(\overline{z}_{r1} z_{r2} - \overline{z}_{r2} z_{r1} \right) = \mathrm{Im} \left(\overline{z}_{r1} z_{r2} \right) , \tag{2.56}$$

$$J_{rz} = \frac{1}{2} \left(|z_{r1}|^2 - |z_{r2}|^2 \right) . \tag{2.57}$$

Since $I_r^2 = \mathbf{J}_r^2$ and $J_i = \sum_r J_{ri}$, the stationary phase conditions (2.53) can be expressed as conditions in the angular momentum space $\mathbb{R}^3 \times \mathbb{R}^3 \times \mathbb{R}^3$. Points of angular momentum space can be visualized as 3 classical angular momentum vectors, each living in its own angular momentum space. The inverse image under π of a set of 3 non-vanishing classical angular momentum vectors is an 3-torus in the large space $\mathbb{C}^6$, parametrized by an overall phase of each spinor.

The stationary phase conditions $I_r = j_r$, $r = 1, 2, 3$, imply each vector $\mathbf{J}_r$ has the length $|\mathbf{J}_r| = j_r$. We now impose the first and last conditions of (2.53), that is, we find three vectors of lengths $J_r = j_r$ that satisfy the triangle condition $\mathbf{J}_1 + \mathbf{J}_2 + \mathbf{J}_3 = \mathbf{0}$.

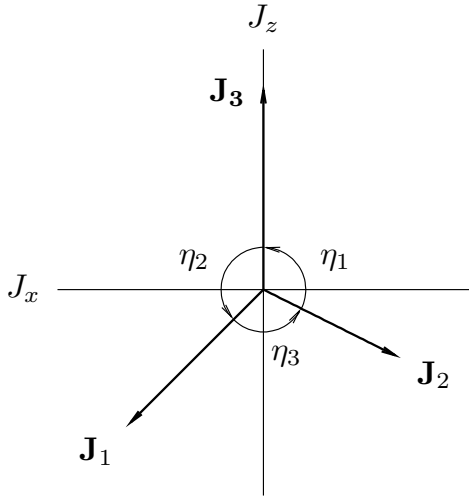

Figure 2.1: Visualization of the stationary phase conditions $|\mathbf{J}_r| = j_r$, $r = 1, 2, 3$, and $\mathbf{J}_i = \mathbf{0}$, $i = x, y, z$, as a triangle with edge lengths j_1, j_2, j_3.

The condition $J_i = 0$, $i = 1, 2, 3$ state the three vectors $\mathbf{J}_1$, $\mathbf{J}_2$, and $\mathbf{J}_3$ form a triangle. This triangle is unique apart from its orientation. Let us start with a standard orientation for the triangle by placing the $\mathbf{J}_3$ along the z-axis, $\mathbf{J}_1$ in the $x - z$ plane with $J_{1x} > 0$, and $\mathbf{J}_2$ in the x-z plane with $J_{2x} < 0$, as illustrated in figure 2.1. These angles η_r lie in the range $0 \leq \eta_r \leq \pi$. and are related to the interior angles of the triangle with lengths J_1, J_2, J_3. From the law of cosine for triangles, we find

$$\cos \eta_r = \frac{J_1^2 - J_2^2 - J_3^2}{2 J_2 J_3} \tag{2.58}$$

and cyclic permutations.

In that orientation, the vectors are

$$\mathbf{J}_1 = J_1 \begin{pmatrix} \sin \eta_2 \\ 0 \\ \cos \eta_2 \end{pmatrix}, \qquad \mathbf{J}_1 = J_2 \begin{pmatrix} -\sin \eta_1 \\ 0 \\ \cos \eta_1 \end{pmatrix}, \qquad \mathbf{J}_1 = J_3 \begin{pmatrix} 0 \\ 0 \\ 1 \end{pmatrix}. \tag{2.59}$$

We choose the spinors to have z_{1r} to be real and positive for all $r = 1, 2, 3$. These uniquely determine the three spinors

$$\begin{pmatrix} z_{11} \\ z_{12} \end{pmatrix} = \sqrt{2J_1} \begin{pmatrix} \cos\eta_2/2 \\ \sin\eta_2/2 \end{pmatrix}, \qquad \begin{pmatrix} z_{21} \\ z_{22} \end{pmatrix} = \sqrt{2J_2} \begin{pmatrix} \cos\eta_1/2 \\ -\sin\eta_1/2 \end{pmatrix}, \quad (2.60)$$
$$\begin{pmatrix} z_{31} \\ z_{32} \end{pmatrix} = \sqrt{2J_3} \begin{pmatrix} 1 \\ 0 \end{pmatrix}.$$

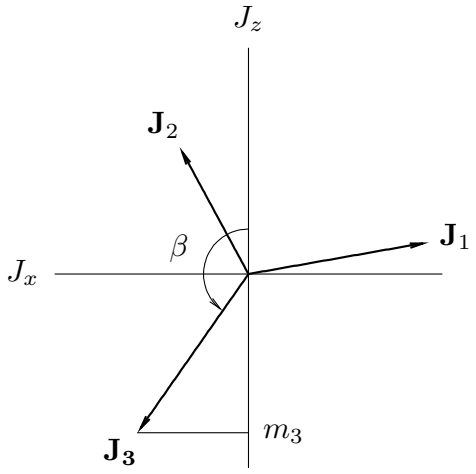

Figure 2.2: The vectors after applying the rotation about the y-axis by an angle β to the triangle in the reference orientation.

The diagonal $SU(2)$ action on the spinor space $\mathbb{C}^6$, in which the $SU(2)$ matrix u is applied to all spinors (z_{r1}, z_{r2}), project to an $SO(3)$ action on angular momentum space. For instance, an $SU(2)$ rotation U generated by $\mathbf{n} \cdot \mathbf{J}$, parametrized by θ, has the following action in angular momentum space,

$$T_U J_{ri} = \sum_j R(\mathbf{n}, \theta)_{ij} J_{rj}(0)\,, \quad (2.61)$$

where $R(\mathbf{n}, \theta)$ is the 3×3 rotation associated with $u(\mathbf{n}, \theta)$. For example, J_z rotates all vectors $\mathbf{J}_r$ about the z-axis.

Once we have $J_i = 0$, we can apply an overall $SU(2)$ rotation u that project to an $SO(3)$ rotation R that rotates the vectors $\mathbf{J}_r$ in (2.59) to a point that satisfies $J_{rz} = m_r$. We do this in two steps. First we rotate the vectors in the x-z plane about the y-axis by an angle β, $0 \le \beta \le \pi$, defined by

$$m_3 = J_3 \cos\beta\,, \quad (2.62)$$

so that $J_{3z} = m_3$. We then rotate the vectors about the vector $\mathbf{J}_3$ by an angle γ to satisfy $J_{2z} = m_2$, $J_{3z} = m_3$. The result of applying the rotations

$$R(\mathbf{j}_3,\gamma)\,R(\mathbf{y},\beta) = R(\mathbf{y},\beta)\,R(\mathbf{j}_3,\gamma) \tag{2.63}$$

to the vectors in (2.59) is

$$\begin{aligned}
\mathbf{J}_1 &= J_1 \begin{pmatrix} \cos\beta\cos\gamma\sin\eta_2 + \sin\beta\cos\eta_2 \\ \sin\gamma\sin\eta_2 \\ -\sin\beta\cos\gamma\sin\eta_2 + \cos\beta\cos\eta_2 \end{pmatrix}, \\
\mathbf{J}_2 &= J_2 \begin{pmatrix} -\cos\beta\cos\gamma\sin\eta_1 + \sin\beta\cos\eta_1 \\ -\sin\gamma\sin\eta_1 \\ \sin\beta\cos\gamma\sin\eta_1 + \cos\beta\cos\eta_1 \end{pmatrix}, \\
\mathbf{J}_3 &= J_3 \begin{pmatrix} \sin\beta \\ 0 \\ \cos\beta \end{pmatrix}.
\end{aligned} \tag{2.64}$$

We may solve for γ by demanding either $J_{1z} = m_1$ or $J_{2z} = m_2$, which imply

$$\cos\gamma = \frac{J_1\cos\beta\cos\eta_2 - m_1}{J_1\sin\beta\sin\eta_2} = \frac{m_2 - J_2\cos\beta\cos\eta_1}{J_2\sin\beta\sin\eta_1}\,. \tag{2.65}$$

These two conditions are equivalent. In general, we find two solutions. Let γ represent the root of (2.65) in the range $[0,\pi]$, and $-\gamma$ the root in the range $[-\pi,0]$.

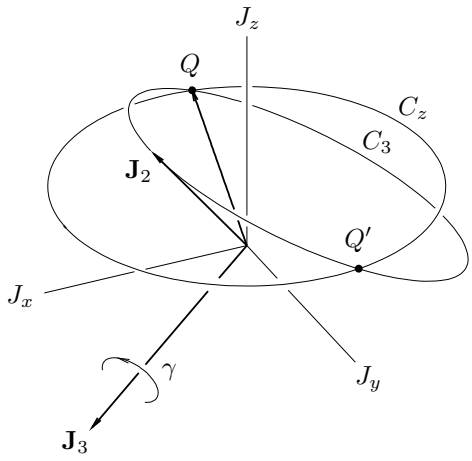

Figure 2.3: Once vector $\mathbf{J}_3$ has the desired projection m_3, we rotate the triangle about the axis $\mathbf{J}_3$ by an angle γ to make $\mathbf{J}_2$ have its desire projection m_2. In general, there are two angles that work, illustrated by the two points Q and Q' in the figure.

We now lift the rotations (2.63) up to an $SU(2)$ rotation

$$u(\mathbf{y},\beta)\,u(\mathbf{z},\gamma) = \begin{pmatrix} e^{-i\gamma/2}\cos\beta/2 & -e^{i\gamma/2}\sin\beta/2 \\ e^{-i\gamma/2}\sin\beta/2 & e^{i\gamma/2}\cos\beta/2 \end{pmatrix}, \tag{2.66}$$

and apply it to the reference spinors (2.60) to obtain a set of spinors

$$\begin{pmatrix} z_{11} \\ z_{12} \end{pmatrix} = \sqrt{2J_1} \begin{pmatrix} e^{-i\gamma/2}\cos\beta/2\cos\eta_2/2 - e^{i\gamma/2}\sin\beta/2\sin\eta_2/2 \\ e^{-i\gamma/2}\sin\beta/2\cos\eta_2/2 + e^{i\gamma/2}\cos\beta/2\sin\eta_2/2 \end{pmatrix}, \quad (2.67)$$

$$\begin{pmatrix} z_{21} \\ z_{22} \end{pmatrix} = \sqrt{2J_2} \begin{pmatrix} e^{-i\gamma/2}\cos\beta/2\cos\eta_1/2 + e^{i\gamma/2}\sin\beta/2\sin\eta_1/2 \\ e^{-i\gamma/2}\sin\beta/2\cos\eta_1/2 - e^{i\gamma/2}\cos\beta/2\sin\eta_1/2 \end{pmatrix}, \quad (2.68)$$

$$\begin{pmatrix} z_{11} \\ z_{12} \end{pmatrix} = e^{-i\gamma/2}\sqrt{2J_3} \begin{pmatrix} \cos\beta/2 \\ \sin\beta/2 \end{pmatrix}. \quad (2.69)$$

These spinors satisfy all the stationary phase conditions (2.53). These two discrete spinor solutions (2.67) - (2.69) for $\pm\gamma$ are not isolated. Any other point in the angular momentum space related to these solutions by an overall rotation about the z axis is also a solution. Moreover, because (2.53) are conditions in angular momentum space, the entire 3-torus fiber in the Hopf fibration containing each of these spinor solutions satisfy the stationary phase conditions. Thus the stationary phase points consist of two disjoint 4-tori.

2.6.2 The Hessian

The stationary phase points consist of two 4-tori, so we have to pick 8 transversal directions to perform the stationary phase approximation. Let $z_{s\mu} = r_{s\mu}e^{i\phi_{s\mu}}$, $s = 1, 2, 3$, $\mu = 1, 2$, and define

$$Z_s = z_{s1}/z_{s2} = R_s e^{i\Phi_s}, \quad (2.70)$$

where $R_s = r_{s1}/r_{s2}$ and $\Phi_s = \phi_{s1} - \phi_{s2}$.

We choose the eight directions transversal to the stationary phase points to be $\partial_{\Phi_1}, \partial_{\Phi_2}, \partial_{R_1}, \partial_{R_2}, \partial_{R_3}, \partial_{r_{12}}, \partial_{r_{22}}, \partial_{r_{32}}$. This is not an orthonormal coordinate system, so the change of coordinates generates a Jacobian factor in the change of the measure.

In terms of the variables Z_s, the original phase function (2.33) becomes

$$\begin{aligned} f &= \sum_s \left[(j_s + m_s)\ln\overline{Z}_s\right] + k_1\ln(Z_2 - Z_3) + k_2\ln(Z_3 - Z_1) + k_3\ln(Z_1 - Z_2) \\ &\quad - \sum_s r_{s2}^2 R_s^2 + \sum_s 4j_s \ln r_{s2} - \sum_s r_{s2}^2. \end{aligned} \quad (2.71)$$

The first derivatives of the phase function f are calculated in (2.72) - (2.79).

derivative	value
$\frac{\partial^2 f}{\partial\Phi_1\,\partial\Phi_1}$	$\frac{k_2 Z_1 Z_3}{(Z_3-Z_1)^2}+\frac{k_3 Z_1 Z_2}{(Z_1-Z_2)^2}$
$\frac{\partial^2 f}{\partial\Phi_1\,\partial\Phi_2}$	$-\frac{k_3 Z_1 Z_2}{(Z_1-Z_2)^2}$
$\frac{\partial^2 f}{\partial\Phi_1\,\partial R_1}$	$-i\left[\frac{k_2 Z_3 e^{i\Phi_1}}{(Z_3-Z_1)^2}+\frac{k_3 Z_2 e^{i\Phi_1}}{(Z_1-Z_2)^2}\right]$
$\frac{\partial^2 f}{\partial\Phi_1\,\partial R_2}$	$\frac{ik_3 Z_1 e^{i\Phi_2}}{(Z_1-Z_2)^2}$
$\frac{\partial^2 f}{\partial\Phi_1\,\partial R_3}$	$\frac{ik_2 Z_1}{(Z_3-Z_1)^2}$
$\frac{\partial^2 f}{\partial\Phi_2\,\partial\Phi_2}$	$\frac{k_1 Z_2 Z_3}{(Z_2-Z_3)^2}+\frac{k_3 Z_1 Z_2}{(Z_1-Z_2)^2}$
$\frac{\partial^2 f}{\partial\Phi_2\,\partial R_1}$	$\frac{ik_3 Z_2 e^{i\Phi_1}}{(Z_1-Z_2)^2}$
$\frac{\partial^2 f}{\partial\Phi_2\,\partial R_2}$	$-i\left[\frac{k_1 Z_3\, e^{i\Phi_2}}{(Z_2-Z_3)^2}+\frac{k_3\, Z_1\, e^{i\Phi_2}}{(Z_1-Z_2)^2}\right]$
$\frac{\partial^2 f}{\partial\Phi_2\,\partial R_3}$	$\frac{ik_1 Z_2}{(Z_2-Z_3)^2}$
$\frac{\partial^2 f}{\partial R_1\partial R_1}$	$-\left[\frac{k_2\, Z_3\, e^{i\Phi_1}}{R_1\,(Z_3-Z_1)^2}+\frac{k_3\, Z_2\, e^{i\Phi_1}}{R_1\,(Z_1-Z_2)^2}+4\,r_{12}^2\right]$
$\frac{\partial^2 f}{\partial R_1\partial R_2}$	$\frac{k_3\, e^{i\Phi_1}\, e^{i\Phi_2}}{(Z_1-Z_2)^2}$
$\frac{\partial^2 f}{\partial R_1\partial R_3}$	$\frac{k_2\, e^{i\Phi_1}}{(Z_3-Z_1)^2}$
$\frac{\partial^2 f}{\partial R_2\partial R_2}$	$-\left[\frac{k_1\, Z_3\, e^{i\Phi_2}}{R_2\,(Z_2-Z_3)^2}+\frac{k_3\, Z_1\, e^{i\Phi_2}}{R_2\,(Z_1-Z_2)^2}+4\,r_{22}^2\right]$
$\frac{\partial^2 f}{\partial R_2\partial R_3}$	$\frac{k_1\, e^{i\Phi_2}}{(Z_2-Z_3)^2}$
$\frac{\partial^2 f}{\partial R_3\partial R_3}$	$-\left[\frac{k_1\, Z_2}{R_3\,(Z_2-Z_3)^2}+\frac{k_2\, Z_1}{R_3\,(Z_3-Z_1)^2}+4\,r_{32}^2\right]$
$\frac{\partial f}{\partial R_1\,\partial r_{12}}$	$-4r_{12}R_1$
$\frac{\partial f}{\partial R_2\,\partial r_{22}}$	$-4r_{22}R_2$
$\frac{\partial f}{\partial R_3\,\partial r_{32}}$	$-4r_{32}R_3$
$\frac{\partial f}{\partial r_{12}\,\partial r_{12}}$	$-2(1+R_1^2+\frac{2J_1}{r_{12}^2})$
$\frac{\partial f}{\partial r_{22}\,\partial r_{22}}$	$-2(1+R_2^2+\frac{2J_2}{r_{22}^2})$
$\frac{\partial f}{\partial r_{32}\,\partial r_{32}}$	$-2(1+R_3^2+\frac{2J_3}{r_{32}^2})$

Table 2.1: The second derivatives of the phase function f.

$$\frac{\partial f}{\partial \Phi_1} = i\left[-(j_1+m_1)+\frac{-k_2Z_1}{Z_3-Z_1}+\frac{k_3Z_1}{Z_1-Z_2}\right], \tag{2.72}$$

$$\frac{\partial f}{\partial \Phi_1} = i\left[-(j_2+m_2)+\frac{k_1Z_2}{Z_2-Z_3}+\frac{-k_3Z_2}{Z_1-Z_2}\right], \tag{2.73}$$

$$\frac{\partial f}{\partial R_1} = \frac{1}{R_1}\left[(j_1+m_1)+\frac{-k_2Z_1}{Z_3-Z_1}+\frac{k_3Z_1}{Z_1-Z_2}-2r_{12}^2R_1^2\right], \tag{2.74}$$

$$\frac{\partial f}{\partial R_2} = \frac{1}{R_2}\left[(j_2+m_2)+\frac{k_1Z_2}{Z_2-Z_3}+\frac{-k_3Z_2}{Z_1-Z_2}-2r_{22}^2R_2^2\right], \tag{2.75}$$

$$\frac{\partial f}{\partial R_3} = \frac{1}{R_3}\left[(j_3+m_3)+\frac{-k_1Z_3}{Z_2-Z_3}+\frac{k_2Z_3}{Z_3-Z_1}-2r_{32}^2R_3^2\right], \tag{2.76}$$

$$\frac{\partial f}{\partial r_{12}} = -2(1+R_1^2)r_{12}+\frac{4j_1}{r_{12}}, \tag{2.77}$$

$$\frac{\partial f}{\partial r_{22}} = -2(1+R_2^2)r_{22}+\frac{4j_2}{r_{22}}, \tag{2.78}$$

$$\frac{\partial f}{\partial r_{32}} = -2(1+R_3^2)r_{32}+\frac{4j_3}{r_{32}}. \tag{2.79}$$

Out of the 36 distinct second derivatives, 21 are nonzero. They are listed in table 2.1.

After simplifying the Hessian matrix through Gaussian eliminations, which keeps the determinant unchanged, we find that the Hessian is the determinant of the matrix

$$H = \begin{pmatrix} H_{11} & H_{12} & 0 & 0 & 0 & 0 & 0 & \\ H_{21} & H_{22} & 0 & 0 & 0 & 0 & 0 & 0 \\ 0 & 0 & H_{33} & 0 & 0 & 0 & 0 & 0 \\ 0 & 0 & 0 & H_{44} & 0 & 0 & 0 & 0 \\ 0 & 0 & 0 & 0 & H_{55} & 0 & 0 & 0 \\ 0 & 0 & 0 & 0 & 0 & H_{66} & 0 & 0 \\ 0 & 0 & 0 & 0 & 0 & 0 & H_{77} & 0 \\ 0 & 0 & 0 & 0 & 0 & 0 & 0 & H_{88} \end{pmatrix}, \tag{2.80}$$

where

$$\begin{aligned}
H_{11} &= \frac{\partial^2 f}{\partial\Phi_1\,\partial\Phi_1}\,,\\
H_{12} &= H_{21} = \frac{\partial^2 f}{\partial\Phi_1\,\partial\Phi_2}\,,\\
H_{22} &= \frac{\partial^2 f}{\partial\Phi_2\,\partial\Phi_2}\,,\\
H_{33} &= -4r_{12}^2\,,\\
H_{44} &= -4r_{22}^2\,,\\
H_{55} &= -4r_{32}^2\\
H_{66} &= -2(1-R_1^2+\frac{2j_1}{r_{12}^2})\,,\\
H_{77} &= -2(1-R_2^2+\frac{2j_2}{r_{22}^2})\,,\\
H_{88} &= -2(1-R_3^2+\frac{2j_3}{r_{32}^2})\,.
\end{aligned}$$

At the stationary points, $r_{s1}=\sqrt{j_s+m_s}$, $r_{s2}=\sqrt{j_s-m_s}$, $s=1,2,3$, so the last three diagonal entries

$$H_{55}=H_{66}=H_{77}=-2(1-R_s^2+2j_s/r_{s2}^2)=-2\left(1-\frac{j_s+m_s}{j_s-m_s}+\frac{2j_s}{j_s-m_s}\right)=-4 \quad (2.81)$$

are constants. Taking the determinant, we find

$$\det H = 4^6\left[\frac{k_1\,k_2\,Z_1\,Z_2\,Z_3^2}{(Z_3-Z_1)^2\,(Z_2-Z_3)^2}+\frac{k_2\,k_3\,Z_1^2\,Z_2\,Z_3}{(Z_3-Z_1)^2\,(Z_1-Z_2)^2}+\frac{k_1\,k_3\,Z_1\,Z_2^2\,Z_3}{(Z_1-Z_2)^2\,(Z_2-Z_3)^2}\right]. \quad (2.82)$$

After factoring out a common factor, this determinant can be put into a more symmetrical form,

$$\begin{aligned}
\det H &= 4^6\frac{Z_1\,Z_2\,Z_3}{(Z_1-Z_2)(Z_2-Z_3)(Z_3-Z_1)}\\
&\qquad\left[\frac{k_1\,k_2\,Z_3\,(Z_1-Z_2)}{(Z_3-Z_1)\,(Z_2-Z_3)}+\frac{k_2\,k_3\,Z_1\,(Z_2-Z_3)}{(Z_3-Z_1)\,(Z_1-Z_2)}+\frac{k_1\,k_3\,Z_2\,(Z_3-Z_1)}{(Z_1-Z_2)\,(Z_2-Z_3)}\right]\\
&= g[\left(\frac{-k_2Z_2}{Z_3-Z_1}+\frac{k_3Z_2}{Z_1-Z_2}\right)\left(\frac{k_1Z_3}{Z_2-Z_3}+\frac{-k_3Z_1}{Z_1-Z_2}\right)\\
&\qquad-\left(\frac{k_2Z_3}{Z_3-Z_1}+\frac{-k_3Z_2}{Z_1-Z_2}\right)\left(\frac{-k_1Z_1}{Z_2-Z_3}+\frac{k_3Z_1}{Z_1-Z_2}\right)]\\
&= g[g_1g_2-g_3g_4]\,,
\end{aligned}$$

where g_1, g_2, g_3, g_4 correspond to the four factors in the four parenthesis. We now express them in terms of the variables $z_{r\mu}$. We find

$$\begin{aligned} g &= 4^6 \frac{Z_1\, Z_2\, Z_3}{(Z_1 - Z_2)(Z_2 - Z_3)(Z_3 - Z_1)} && (2.83) \\ &= 4^6 \frac{z_{11} z_{12} z_{21} z_{22} z_{31} z_{32}}{(z_{11} z_{22} - z_{12} z_{21})(z_{31} z_{12} - z_{32} z_{11})(z_{21} z_{32} - z_{22} z_{31})}\,. && (2.84) \end{aligned}$$

Setting the first derivatives (2.72) and (2.73) to zero at the stationary point, and using $|z_{r1}|^2 = j_r + m_r$, we can rewrite two of the terms in the parenthesis above as

$$g_1 = \frac{-k_2 Z_2}{Z_3 - Z_1} + \frac{k_3 Z_2}{Z_1 - Z_2} = (j_1 + m_1)\frac{Z_2}{Z_1} = z_{11}\overline{z}_{11}\frac{z_{21} z_{12}}{z_{22} z_{11}} = \frac{z_{21} z_{12} \overline{z}_{11}}{z_{22}}\,, \qquad (2.85)$$

$$g_4 = \frac{-k_1 Z_1}{Z_2 - Z_3} + \frac{k_3 Z_1}{Z_1 - Z_2} = (j_2 + m_2)\frac{Z_1}{Z_2} = z_{21}\overline{z}_{21}\frac{z_{11} z_{22}}{z_{12} z_{21}} = \frac{z_{11} z_{22} \overline{z}_{21}}{z_{12}}\,. \qquad (2.86)$$

Using $2j_1 = k_2 + k_3$, $2j_2 = k_1 + k_3$, and $|z_{r2}|^2 = j_r - m_r$, the remaining two terms can be rewritten as

$$\begin{aligned} g_2 = \frac{k_1 Z_3}{Z_2 - Z_3} + \frac{-k_3 Z_1}{Z_1 - Z_2} &= \frac{k_1 Z_2}{Z_2 - Z_3} + \frac{-k_3 Z_2}{Z_1 - Z_2} - (k_1 + k_3) \\ &= (j_2 + m_2) - 2j_2 \\ &= -(j_2 - m_2) \\ &= -z_{22}\overline{z}_{22}\,, && (2.87) \end{aligned}$$

$$\begin{aligned} g_3 = \frac{k_2 Z_3}{Z_3 - Z_1} + \frac{-k_3 Z_2}{Z_1 - Z_2} &= \frac{k_2 Z_1}{Z_3 - Z_1} + \frac{-k_3 Z_1}{Z_1 - Z_2} + (k_2 + k_3) \\ &= -(j_1 + m_1) + 2j_1 \\ &= (j_1 - m_1) \\ &= z_{12}\overline{z}_{12}\,. \end{aligned}$$

Using the values of g_1, g_2, g_3, g_4, and g, we find

$$\begin{aligned} \det H &= g(g_1 g_2 - g_3 g_4) \\ &= g(-z_{21} z_{12} \overline{z}_{11}\overline{z}_{22} + z_{11} z_{22} \overline{z}_{12}\overline{z}_{21}) \\ &= g[-2i(J_{1x} J_{2y} - J_{2x} J_{1y}] \\ &= -4ig\,\Delta_z\,, && (2.88) \end{aligned}$$

where Δ_z is the area of the triangle in the angular momentum space, projected onto the x-y plane.

Since we are using unnormalized coordinates to calculate the second derivatives, the Hessian is equal to $\det H$ times a Jacobian $\prod_{s\mu} r_{s\mu}^{-2}$. Finally, we find

$$\begin{aligned}\text{Hessian} &= (-i)4^7\Delta_z\left[\left(\prod_{s\mu} r_{s\mu}^{-2}\right)\frac{z_{11}z_{12}z_{21}z_{22}z_{31}z_{32}}{(z_{11}z_{22}-z_{12}z_{21})(z_{31}z_{12}-z_{32}z_{11})(z_{21}z_{32}-z_{22}z_{31})}\right]\\ &= \frac{(-i)4^7\,\Delta_z}{\overline{z}_{11}\overline{z}_{12}\overline{z}_{21}\overline{z}_{22}\overline{z}_{31}\overline{z}_{32}(z_{11}z_{22}-z_{12}z_{21})(z_{31}z_{12}-z_{32}z_{11})(z_{21}z_{32}-z_{22}z_{31})}\,. \qquad (2.89)\end{aligned}$$

2.6.3 The Asymptotic Formula

After integrating over the 4-tori stationary phase set, we find

$$\begin{pmatrix} j_1 & j_2 & j_3 \\ m_1 & m_2 & m_3 \end{pmatrix} \approx N\,(2\pi)^8\, e^{\mathrm{Re}\, f(p)}\,\left[\frac{e^{i\,\mathrm{Im}\, f(p)}}{\sqrt{-\mathrm{Hess}_p(f)}}+\frac{e^{i\,\mathrm{Im}\, f(p')}}{\sqrt{\mathrm{Hess}_{p'}(f)}}\right], \qquad (2.90)$$

where p is the stationary point (2.67) - (2.69) with $\gamma > 0$, and p' is the stationary point (2.67) - (2.69) with $\gamma < 0$. Here one factor of $(2\pi)^4$ comes from integrating along the 4 angular directions along the stationary points, another factor of $(2\pi)^4$ comes from doing the stationary phase approximation along 8 transversal directions.

Inserting the Hessian (2.89) into (2.90), we find

$$\begin{pmatrix} j_1 & j_2 & j_3 \\ m_1 & m_2 & m_3 \end{pmatrix} = \frac{(2\pi)^8 N e^{\mathrm{Re} f_1(p)}}{2^7}\,\frac{e^{i\mathrm{Im} f_1(p)}+e^{i\mathrm{Im} f_1(p')}}{\sqrt{\Delta_z}}\,, \qquad (2.91)$$

where f_1 has the same functional form as the phase function f, but with j_r replaced by $j_r + 1/2$. This modification comes from the contribution of the denominator of the Hessian in (2.89). Explicitly, the new phase function f_1 is given by

$$f_1(z,\overline{z}) = \sum_{r=1}^{3}\left[(j_r+1/2+m_r)\ln\overline{z}_{r1}+(j_r+1/2-m_r)\ln\overline{z}_{r2}\right]+\sum(k_i+1/2)\ln\delta_i-\sum_{r\mu}|z_{r\mu}|^2\,. \qquad (2.92)$$

The imaginary part of the phase function f_1 is

$$\begin{aligned}\mathrm{Im}\,(f_1) = &\sum_r[(j_r+1/2+m_r)\arg(\overline{z}_{r1})+(j_r+1/2-m_r)\arg(\overline{z}_{r2})] \qquad (2.93)\\ &+(k_1+1/2)\arg(z_{21}z_{32}-z_{22}z_{31})+(k_2+1/2)\arg(z_{31}z_{12}-z_{32}z_{11})\\ &+(k_3+1/2)\arg(z_{11}z_{22}-z_{12}z_{21})\,.\end{aligned}$$

The last three terms are invariant under overall $SU(2)$ rotations, so they can be evaluated at a point related to the stationary phase points by an overall $SU(2)$ rotation. We choose the reference spinor (2.60). The spinors at this point are all real, so the last three terms vanish. The first three terms evaluated at the stationary point (2.67) - (2.69), is given by

$$
\begin{aligned}
S \equiv \mathrm{Im} f_1(p) \;\; = \;\; & J_3\gamma + J_1 \arg(\cos\beta \sin\eta_2 + \sin\beta\cos\gamma\cos\eta_2 + i\sin\beta\sin\gamma) \\
& + J_2 \arg(-\cos\beta\sin\eta_1 + \sin\beta\cos\gamma\cos\eta_1 + i\sin\beta\sin\gamma) \\
& + m_1 \arg(\sin\beta\cos\eta_2 + \cos\beta\cos\gamma\sin\eta_2 + i\sin\gamma\sin\eta_2) \\
& + m_2 \arg(\sin\beta\cos\eta_1 - \cos\beta\cos\gamma\sin\eta_1 - i\sin\gamma\sin\eta_1) \,, \qquad (2.94)
\end{aligned}
$$

where $J_r = j_r + 1/2$. This phase can be written in terms of $\cos^{-1}$ functions. We note that $\arg(\overline{z}_{11}\overline{z}_{12}) = \cos^{-1}[\mathrm{Re}(\overline{z}_{11}\overline{z}_{12})/|z_{11}z_{12}|]$ and that $|z_{11}z_{12}| = \sqrt{J_1^2 - m_1^2}$, etc. We can also use (2.65) to eliminate $\cos\gamma$. We find

$$
\begin{aligned}
S \;\; = \;\; & J_1 \cos^{-1}\left(\frac{J_1\cos\beta - m_1\cos\eta_2}{\sin\eta_2\, J_{1\perp}}\right) + J_2\cos^{-1}\left(\frac{m_2\cos\eta_1 - J_2\cos\beta}{\sin\eta_1 J_{2\perp}}\right) \\
& + J_3\cos^{-1}\left(\frac{J_1\cos\beta\cos\eta_2 - m_1}{J_1\sin\beta\sin\eta_2}\right) + m_1\cos^{-1}\cos^{-1}\left(\frac{J_1\cos\eta_2 - m_1\cos\beta}{\sin\beta J_{1\perp}}\right) \\
& - m_2\cos^{-1}\left(\frac{J_2\cos\eta_1 - m_2\cos\beta}{\sin\beta\, J_{2\perp}}\right) . \qquad (2.95)
\end{aligned}
$$

Since $S(-\gamma) = -S(\gamma)$ in (2.94), we find that the two terms in parenthesis in (2.91) add up to a cosine. Thus

$$
\begin{pmatrix} j_1 & j_2 & j_3 \\ m_1 & m_2 & m_3 \end{pmatrix} = \frac{(2\pi)^8 N e^{\mathrm{Re}f(p)}}{2^6} \frac{\cos(S+\pi/4)}{\sqrt{\Delta_z}} \,. \qquad (2.96)
$$

we now calculate the constant factor $(2\pi)^8 N e^{\mathrm{Re}f(p)}/2^6$ in front, where

$$
\begin{aligned}
N \;\; = \;\; & \frac{1}{\pi^6\sqrt{(j_1+m_1)!\,(j_1-m_1)!\,(j_2+m_2)!\,(j_2-m_2)!\,(j_3+m_3)!\,(j_3-m_3)!}} \\
& \frac{1}{\sqrt{(j_1+j_2+j_3+1)!\,k_1!\,k_2!\,k_3!}} \,, \qquad (2.97)
\end{aligned}
$$

and

$$
\begin{aligned}
e^{\mathrm{Re}f} \;\; = \;\; & \left(\prod_r |z_{r1}|^{j_r+m_r+1/2}|z_{r2}|^{j_r-m_r+1/2}\right) \; e^{-\sum_{r,\mu}|z_{r\mu}|^2} \qquad (2.98) \\
& |z_{21}z_{32} - z_{31}z_{22}|^{k_1+1/2}\,|z_{31}z_{12} - z_{32}z_{11}|^{k_2+1/2}\,|z_{11}z_{22} - z_{12}z_{21}|^{k_3+1/2} \,.
\end{aligned}
$$

First we evaluate $e^{\mathrm{Re}f}$ at the stationary point p. From the conditions $|z_{r1}| = j_r + m_r$, $|z_{r2}| = j_r - m_r$, and $m_1 + m_2 + m_3 = 0$, we find

$$
\begin{aligned}
& \left(\prod_r |z_{r1}|^{j_r+m_r+1/2}|z_{r2}|^{j_r-m_r+1/2}\right) \; e^{-\sum_{r,\mu}|z_{r\mu}|^2} \\
= \;\; & e^{-2(j_1+j_2+j_3)} \sqrt{\prod_r |j_r+m_r|^{j_r+m_r+1/2}\,|j_r-m_r|^{j_r-m_r+1/2}} \,. \qquad (2.99)
\end{aligned}
$$

The remaining factor,

$$|z_{21}z_{32} - z_{31}z_{22}|^{k_1+1/2}\,|z_{31}z_{12} - z_{32}z_{11}|^{k_2+1/2}\,|z_{11}z_{22} - z_{12}z_{21}|^{k_3+1/2}\,, \tag{2.100}$$

is invariant under diagonal $SU(2)$ actions, so we could evaluate them at the spinors (2.60). The result is

$$\begin{aligned}
|z_{21}z_{32} - z_{31}z_{22}|^{k_1+1/2} &= \left|\sqrt{4j_2j_3}\,\sin(\eta_1/2)\right|^{k_1+1/2} \\
&= \sqrt{|4j_2j_3\,(1-\cos\eta_1)|^{k_1+1/2}} \\
&= \sqrt{\left|2j_2j_3(1-\frac{j_1^2-j_2^2-j_3^2}{2j_2j_3})\right|^{k_1+1/2}} \\
&= \sqrt{(j_1+j_2+j_3)^{k_1+1/2}(j_2+j_3-j_1)^{k_1+1/2}}\,,
\end{aligned} \tag{2.101}$$

$$\begin{aligned}
|z_{31}z_{12} - z_{32}z_{11}|^{k_2+1/2} &= \left|\sqrt{4j_1j_3}\,\sin(\eta_2/2)\right|^{k_2+1/2} \\
&= \sqrt{|4j_1j_3\,(1-\cos\eta_2)|^{k_2+1/2}} \\
&= \sqrt{\left|2j_1j_3(1-\frac{j_2^2-j_1^2-j_3^2}{2j_1j_3})\right|^{k_2+1/2}} \\
&= \sqrt{(j_1+j_2+j_3)^{k_2+1/2}(j_1+j_3-j_2)^{k_2+1/2}}\,,
\end{aligned} \tag{2.102}$$

$$\begin{aligned}
|z_{11}z_{22} - z_{12}z_{21}|^{k_3+1/2} &= \left|\sqrt{4j_1j_2}\,(\sin(\eta_1/2)\,\cos(\eta_2/2) + \sin(\eta_2/2)\,\cos(\eta_1/2))\right|^{k_3+1/2} \\
&= \left|\sqrt{4j_1j_2}\,\sin((\eta_1+\eta_2)/2)\right|^{k_3+1/2} \\
&= \sqrt{|2j_1j_2\,(1-\cos((\eta_1+\eta_2)))|^{k_3+1/2}} \\
&= \sqrt{|2j_1j_2\,(1-\cos(\eta_3))|^{k_3+1/2}} \\
&= \sqrt{\left|2j_1j_2(1-\frac{j_3^2-j_1^2-j_2^2}{2j_1j_2})\right|^{k_3+1/2}} \\
&= \sqrt{(j_1+j_2+j_3)^{k_3+1/2}(j_1+j_2-j_3)^{k_3+1/2}}\,.
\end{aligned} \tag{2.103}$$

Combining the above factors with the factor in (2.99), we find

$$
\begin{aligned}
e^{\mathrm{Re}f(p)} &= e^{-2\,(j_1+j_2+j_3)}\sqrt{\prod_i (j_i+m_i)^{j_i+m_i+1/2}\,(j_i-m_i)^{j_i-m_i+1/2}} \\
&\qquad \times\sqrt{(j_1+j_2+j_3)^{j_1+j_2+j_3+3/2}k_1^{k_1+1/2}k_2^{k_2+1/2}k_3^{k_3+1/2}} \\
&\approx \sqrt{\frac{(j_1+m_1)!(j_1-m_1)!(j_2+m_2)!(j_2-m_2)!(j_3+m_3)!(j_3-m_3)!}{(2\pi)^5}} \\
&\qquad \times\sqrt{(j_1+j_2+j_3)!k_1!k_2!k_3!(j_1+j_2+j_3)}\,, \qquad (2.104)
\end{aligned}
$$

where we have used Stirling's approximation for factorials $n! \approx (2\pi)^{1/2}n^{n+1/2}e^{-n}$. Most of the factorials cancel those that appear in N in (2.97). We find

$$
\frac{(2\pi)^8 N e^{\mathrm{Re}f(p)}}{2^6} = \frac{1}{\sqrt{2\pi}} \qquad (2.105)
$$

in the large j_r limit.

We conclude that the asymptotic formula for the $3j$-symbol is

$$
\begin{pmatrix} j_1 & j_2 & j_3 \\ m_1 & m_2 & m_3 \end{pmatrix} = \pm\frac{\cos(S+\pi/4)}{\sqrt{2\pi|\Delta_z|}}\,. \qquad (2.106)
$$

2.7 Conclusions

In this chapter, the stationary phase calculation of the $3j$-symbol can be grouped roughly into four steps. First we formulate the stationary phase conditions. Second, we find the stationary phase points. Third, we calculate the Hessian, which is part of the amplitude. Last we evaluate the phase function at the stationary phase points to find the relative phase of their contributions. These four steps are in parallel with their more geometrical counterparts in the next two chapters.

In chapter 3 and 4, we apply multidimensional WKB theory to the Schwinger representation of $SU(2)$ to find the asymptotics of the $3j$- and $6j$-symbols. There, the stationary phase conditions are naturally formulated as two sets of Hamilton-Jacobi equations that define two Lagrangian manifolds. In other words, the stationary phase points are the intersection points of these two Lagrangian manifolds. The amplitude determinant is related to the densities on these Lagrangian manifolds at their intersection points, and can be expressed as a determinant of a matrix of Poisson brackets. The relative phase of the phase function, evaluated at two different stationary sets, is formulated as an line integral of $p\,dx$ on these two Lagrangian manifolds. As we will see, the calculation simplifies tremendously in the more geometrical formulation. For example, in the case of the $3j$-symbol, instead of a 8×8 determinant of second derivatives, we only have to evaluate a 2×2 determinant of Poisson brackets to find the amplitude determinant. In the case of the $6j$-symbol, the relative phase, expressed as a line integral, can be reduced to a symplectic area from Stokes's theorem.

The two geometric methods used to calculate asymptotics of the $3nj$-symbols, namely, geometric quantization and the WKB formulation, have strikingly similar structure. It will be interesting to investigate if we could use the Bargmann representation as a bridge to transfer results from one method to the other. Besides acting as a connection between the two methods, the Bargmann wavefunctions themselves are exact. Thus, we could apply straight-forward stationary phase approximation to find higher order terms for the asymptotic formulas of the $3j$-symbols. These are possible avenues of research that we could pursue in the future.

Chapter 3

Semiclassical Analysis of the Wigner $3j$-Symbol

3.1 Introduction and Summary

In this chapter, we will use WKB theory to perform a stationary phase calculation to derive the asymptotics of the Wigner $3j$-symbol. This calculation is similar to the calculations in chapter 2. WKB theory can be formulated using the geometry of Lagrangian manifolds, which are described by classical mechanics of a single particle. Because of this connection to classical mechanics, WKB theory is also called semiclassical analysis. This framework of using classical mechanics to describe quantum mechanics forms the foundation of this thesis.

The outline of this chapter is as follows: in section 3.2, we summarize the results from multidimensional WKB theory, and explain the main formula in terms of the geometry of Lagrangian manifolds. In section 3.3, we introduce the Schwinger representation of the angular momentum algebra $SU(2)$, whose classical mechanics are explained in section 3.4. In section 3.5, we define the $3j$-symbol in the Schwinger model. Next we proceed to analyze the asymptotic limit of the $3j$-symbol. In section 3.6, we describe the two Lagrangian manifolds and calculate their volumes. In section 3.7 we analyze the intersection of these two Lagrangian manifolds, which is analogous to finding the stationary phase points from subsection 2.6.1. Once we have the intersection points, we calculate the amplitude determinant in section 3.8 and the relative phase as an action integral in section 3.9. These calculations are analogous to the calculation of the Hessian in section 2.6.2 and of the relative phase in section 2.6.1. In section 3.10, we put the different parts together to derive the asymptotic formula for the $3j$-symbol.

3.2 Multidimensional WKB Theory

We summarize the relevant results from the semiclassical analysis of quantum mechanics [17, 20, 22, 36, 41, 46].

Consider the quantum mechanics of a point particle moving in $\mathbb{R}^n$. The Hilbert space is $L^2(\mathbb{R}^n)$, so let us denote the wavefunction by $\psi(x_1, \ldots, x_n)$. Given a set of com-

muting observables $\{\hat{A}_1, \ldots, \hat{A}_n\}$, we calculate the WKB formula for their simultaneous eigenstate $\psi(x)$. After substituting the WKB ansatz, $\psi(x) = \Omega(x) \exp[iS(x)/\hbar]$, into the eigenvalue equations, the first order equations are a set of Hamilton-Jacobi equations for $S(x)$, and the second order equations are a set of amplitude transport equations for $\Omega(x)$. The Hamiltonians are the principal Weyl symbols [15, 48, 57, 84, 90, 92] of the observables, which we denote by $\{A_1, \ldots, A_n\}$. The Hamilton-Jacobi equations are of the form

$$A_i\left(x, \frac{\partial S}{\partial x}\right) = a_i\,. \tag{3.1}$$

where a_i, $i = 1, \ldots, n$, denote the eigenvalues.

By introducing the momentum variables $p = \partial S/\partial x$, we can find $S(x)$ in two steps. First we find the level set $A_i(x, p) = a_i$ in the phase space $\mathbb{R}^{2n}$, and solve for $p(x)$ as a function of x on this level set. Then we integrate $p\,dx$ on this level set from some reference point to find $S(x)$. Because the projection of the level set onto the configuration space may not be one-to-one or onto, the action function $S(x)$ may be multi-valued and may only be defined in a classically allowed region in the configuration space.

By assumption, the commutators $[\hat{A}_i, \hat{A}_j] = 0$ vanish. By transcribing to symbols, we find that the corresponding principal symbols Poisson commute to first order in $\hbar$, that is, for our purposes, $\{A_i, A_j\} = 0$. Thus the set of Hamiltonians $\{A_1, \ldots, A_n\}$ define a classically integrable system in the phase space $\mathbb{R}^{2n}$. Moreover, the level sets of $\{A_1, \ldots, A_n\}$ are Lagrangian manifolds, so the function $S(x)$ is well defined, and is independent of paths. The overall phase is determined by the choice of the initial point in the definition of the action S_k, which is arbitrary in the WKB theory. In general, we will not be able to determine the overall phase, so we will rely on other means to fix the phase convention. After normalizing the wavefunction $\psi(x)$, the semiclassical wavefunction in the classically allowed region of the configuration is given by

$$\psi(x) = \langle x|a\rangle = \frac{1}{\sqrt{V}} \sum_k |\Omega_k|^{1/2} \exp[i[S_k(x, a) - \mu_k \pi/2]]\,. \tag{3.2}$$

Here k indexes the set of points in the inverse projection from x onto the the level set. The phase $S_k(x, a)$ is the integral of $p\,dx$ from a given initial point on the Lagrangian manifold to the kth point of the inverse projection, and μ_k is the kth Maslov index. The amplitude determinant Ω_k is given by

$$\Omega_k = \det \frac{\partial^2 S_k(x, a)}{\partial x_i \partial a_j} = [\det\{x_i, A_j\}]^{-1}\,, \tag{3.3}$$

where the Poisson brackets are evaluated on the kth branch of the inverse projection from x to the Lagrangian manifold.

The amplitude Ω_k is a density on the configuration space, which can be lifted up to the Lagrangian manifold. The amplitude transport equations state that this density on the Lagrangian manifold has to be invariant under the Hamiltonian flows generated by A_i. In other words, the density is proportional to the volume n-form $d\alpha_1 \wedge \cdots \wedge d\alpha_n$, where the α_i are conjugate angle variables of the A_i. Finally, the constant V is equal to the volume

of the Lagrangian manifold, measured with respect to this density. For example, if A_i are action variables, we have $V = (2\pi)^n$.

There is a simple formula for the inner product between two WKB wavefunctions. Let $\{\hat{A}_1, \ldots, \hat{A}_n\}$ and $\{\hat{B}_1, \ldots, \hat{B}_n\}$ be two complete sets of commuting observables, with principal symbols A_i and B_i, conjugate angles α_i and β_i, and action functions $S_A(x, a)$ and $S_B(x, b)$. Here a and b denote the eigenvalues. We evaluate $\langle b|a\rangle$ as an integral of the WKB wavefunctions over x, using the stationary phase approximation. The stationary phase points are determined by the phase functions S_A and S_B, and are geometrically the intersections of the two Lagrangian manifolds. Since both Lagrangian manifolds have dimension n in the $2n$-dimensional phase space, they generically intersect at a finite set of isolated points. Let us index these points by k, and denote the corresponding coordinates on the two manifolds by the angle variables α_k and β_k. Then, the result of the stationary phase approximation is

$$\langle b|a\rangle = \frac{(2\pi i)^{n/2}}{\sqrt{V_A V_B}} \sum_k |\Omega_k|^{1/2} \exp[i[S_A(\alpha_k) - S_B(\beta_k) - \mu_k \pi/2]]. \tag{3.4}$$

Here V_A and V_B are the volumes of the respective Lagrangian manifolds, as in (3.2), and the actions S_A and S_B are considered as functions on the respective Lagrangian manifolds. Littlejohn [49] has shown that the amplitude determinant Ω_k can be simplified to a determinant of Poisson brackets between the observables A_i and B_i, that is,

$$\Omega_k = [\det\{A_i, B_j\}]^{-1}. \tag{3.5}$$

The Maslov index μ_k in (3.4) depends on both the Maslov indices for the two WKB wavefunctions, as well as an additional index generated from the stationary phase approximation.

If some of the functions A_i are functionally dependent on B_i, then the two Lagrangian manifolds intersect at some $(n - r)$-dimensional sub-manifolds. Let us assume that the first r of the two sets of variables A and B are functionally independent, and the last $n - r$ are identical, so that we have $A = \{A_1, \ldots, A_r, A_{r+1}, \ldots, A_n\}$ and $B = \{B_1, \ldots, B_r, A_{r+1}, \ldots, A_n\}$. The intersection sets are $(n - r)$-dimensional orbits of the group generated by the Hamiltonian flows associated with $(A_{r+1}, \ldots, A_n)$. In this case, we find

$$\langle b|a\rangle = \frac{(2\pi i)^{r/2}}{\sqrt{V_A V_B}} \sum_k V_k \, |\Omega_k|^{1/2} \exp[i[S_A(\alpha_k) - S_B(\beta_k) - \mu_k \pi/2]], \tag{3.6}$$

where V_k is the volume of the kth intersection, and where Ω_k is still given by (3.5), but it is understood that only the first r of A's and B's enter into the determinant. The phase difference $S_A - S_B$ for branch k can be evaluated at any point on the $n - r$-intersection, since the integral of $p\,dx$ along the intersection cancels out between S_A and S_B.

3.3 The Schwinger Model

The Schwinger model for angular momenta was introduced in Schwinger's original paper, which is reprinted in Biedenharn and van Dam [78]. Other references include

Bargmann [11], Biedenharn and Louck [18], and Sakurai [74]. Here we introduce the Schwinger model for a single angular momentum, as well as for several angular momenta.

In the Schwinger model, each angular momentum vector is associated with two quantum harmonic oscillators. Let us start with one angular momentum, and index the two harmonic oscillators by Greek indices $\mu, \nu, \cdots = 1, 2$. The Hilbert space is $\mathcal{H} = L^2(\mathbb{R}^2)$, so we can write the wavefunctions as $\psi(x_1, x_2)$.

Let $\hat{H}_\mu = (1/2)(\hat{x}_\mu + \hat{p}_\mu)$ be the Hamiltonian for the individual oscillators, and let $\hat{H} = \sum_\mu \hat{H}_\mu$ be the total Hamiltonian. The eigenvalues of $\hat{H}$ are $n + 1$, with $n = 0, 1, \ldots$. Let $a_\mu = (\hat{x}_\mu + i\hat{p}_\mu)/\sqrt{2}$ and $a_\mu^\dagger = (\hat{x}_\mu - \hat{p}_\mu)/\sqrt{2}$ be the usual annihilation and creation operators. We define the operators

$$\hat{I} = \frac{1}{2} \sum_\mu a_\mu^\dagger a_\mu = \frac{1}{2}(\hat{H} - 1)\,, \tag{3.7}$$

and

$$\hat{J}_i = \frac{1}{2} \sum_{\mu\nu} a_\mu^\dagger \sigma_{\mu\nu}^i \, a_\nu\,, \tag{3.8}$$

where σ^i is the ith Pauli matrix. Here we use the indices $i, j, \cdots = 1, 2, 3$ to denote the x, y, z Cartesian components of a 3-vector. Define $\hat{\mathbf{J}}^2 = \sum_i \hat{J}_i^2$. These operators satisfy the usual commutation relations of the quantum rotation group $SU(2)$,

$$[\hat{J}_i,\ \hat{J}_j] = i \sum_k \epsilon_{ijk} \hat{J}_k\,, \tag{3.9}$$

and

$$[\hat{\mathbf{J}}^2, \hat{J}_i] = 0\,, \qquad [\hat{I}, \hat{J}_i] = 0\,. \tag{3.10}$$

From the operator identity $\hat{\mathbf{J}}^2 = \hat{I}(\hat{I} + 1)$ and (3.7), we see that the eigenvalues of $\hat{H}$, which are integers $n = 1, 2, \ldots$, are related to the label j for the $SU(2)$ representations through the relation $j = (n-1)/2$. The eigenspace of $\hat{H}$, or $\hat{I}$, is $(2j+1)$-dimensional, so it consist of a single copy of the jth irrep of $SU(2)$. The simultaneous eigenstates of $\hat{\mathbf{J}}^2$ and $\hat{J}_z$ are $|j\, m\rangle = |n_1\, n_2\rangle$, where $n_1 = j + m, n_2 = j - m$.

We now generalize the Schwinger model to N angular momenta. We index them by the indices $r, s, \cdots = 1, \ldots, N$. The oscillator Hamiltonian, coordinates and momenta, annihilation and creation operators become $\hat{H}_{r\mu}$, $\hat{x}_{r\mu}$ and $\hat{p}_{r\mu}$, $a_{r\mu}$ and $a_{r\mu}^\dagger$, respectively. The Hilbert space is $L^2(\mathbb{R}^{2N})$, so the wavefunctions are now $\psi(x_{11}, x_{12}, x_{21}, \ldots, x_{N2})$. We define the operators

$$\hat{I}_r = \frac{1}{2}\sum_\mu a^\dagger_{r\mu} a_{r\mu}\,, \tag{3.11}$$

$$\hat{J}_{r\mu} = \frac{1}{2}\, a^\dagger_{r\mu}\sigma^i_{\mu\nu}\, a_{r\nu}\,, \tag{3.12}$$

$$\hat{\mathbf{J}}^2_r = \sum_i \hat{J}^2_{ri}, \tag{3.13}$$

$$\hat{J}_i = \sum_r \hat{J}_{ri} \qquad \text{or} \qquad \hat{\mathbf{J}} = \sum_r \hat{\mathbf{J}}_r\,, \tag{3.14}$$

$$\hat{\mathbf{J}}^2 = \sum_i \hat{J}^2_i\,. \tag{3.15}$$

These satisfy the identities

$$\hat{\mathbf{J}}^2_r = \hat{I}_r(\hat{I}_r + 1), \tag{3.16}$$

and the commutation relations $[\hat{I}_r, \hat{J}_{si}] = [\hat{I}_r, \hat{\mathbf{J}}^2_s] = 0$. Moreover, each angular momentum vector $\hat{\mathbf{J}}_r$, and each partial or total sum of these angular momenta, obeys the standard $SU(2)$ commutation relations among its components.

The N angular momenta operators generate an action of $[SU(2)]^N$ on the Hilbert space. For instance, let us look at the simultaneous rotation of all angular momenta by the same element of $SU(2)$. The commutation relations

$$[\hat{J}_i,\, a_{r\mu}] = -\frac{1}{2}\sum_\nu \sigma^i_{\mu\nu}\, a_{r\nu}\,, \tag{3.17}$$

$$[\hat{J}_i,\, a^\dagger_{r\mu}] = +\frac{1}{2}\sum_\nu a^\dagger_{r\nu}\, \sigma^i_{\nu\mu}\,, \tag{3.18}$$

express the transformation of the oscillators under infinitesimal quantum rotations. We define a finite rotation operator in the axis-angle or Euler angle form, respectively, by

$$U(\mathbf{n}, \theta) = \exp(-i\theta\, \mathbf{n}\cdot\mathbf{J})\,, \tag{3.19}$$

$$U(\alpha, \beta, \gamma) = U(\mathbf{z}, \alpha)\, U(\mathbf{y}, \beta)\, U(\mathbf{z}, \gamma)\,, \tag{3.20}$$

where $\mathbf{n}$ is a unit vector defining an axis of rotation, and θ is an angle of rotation about that axis. The U operators form a faithful representation of $SU(2)$. The exponentiated version of (3.17) and (3.18) are

$$U^\dagger a_{r\mu} U = \sum_\nu u_{\mu\nu} a_{r\nu}\,, \qquad U^\dagger a^\dagger_{r\mu} U = \sum_\nu a^\dagger_{r\nu}\,(u^{-1})_{\nu\mu}\,, \tag{3.21}$$

where $u = u(\mathbf{n}, \theta)$ or $u = u(\alpha, \beta, \gamma)$ are 2×2 matrices given by

$$u(\mathbf{n}, \theta) = \exp(-i\theta\, \mathbf{n}\cdot\sigma/2) = cos\theta/2 - i\,\mathbf{n}\cdot\sigma \sin\theta/2. \tag{3.22}$$

Similarly, the vector operators satisfy the conjugate relations

$$U^\dagger \hat{J}_{ri} U = \sum_j R_{ij} \hat{J}_{rj} \,, \tag{3.23}$$

where R is the 3×3 orthogonal rotation matrix with the same axis and angle as U. The relation between R and u is

$$R_{ij} = \frac{1}{2} \operatorname{tr}(u^\dagger \sigma_i u \sigma_j). \tag{3.24}$$

This is the usual projection from $SU(2)$ to $SO(3)$, in which the inverse image of a given $R \in SO(3)$ is a pair $(u, -u)$ in $SU(2)$.

3.4 The Classical Mechanics of the Schwinger Model

Before we investigate the Lagrangian manifolds associated with the operators defined in the quantum Schwinger model, we must understand the classical mechanics of the Schwinger model, since the flows on the Lagrangian manifolds are Hamiltonian flows of these symbols.

We start with a single angular momentum. The symbol of the quantum oscillators are the classical oscillators $H_\mu = (1/2)(x_\mu^2 + p_\mu^2)$ and $H = \sum_\mu H_\mu$. The classical configuration space is $\mathbb{R}^2$ and the phase space is $\mathbb{R}^4$. We introduce complex coordinates on phase space $z_\mu = (x_\mu + ip_\mu)/\sqrt{2}$ and $\overline{z}_\mu = (x_\mu - ip_\mu)/\sqrt{2}$, where we use an overbar for complex conjugation. These are simply the symbols of the creation and annihilation operators. The variables z_μ and $i\overline{z}_\mu$ are canonically conjugate, so the Poisson bracket of two functions f and g on phase space can be written as

$$\{f, g\} = \sum_\mu \left(\frac{\partial f}{\partial x_\mu} \frac{\partial g}{\partial p_\mu} - \frac{\partial f}{\partial p_\mu} \frac{\partial g}{\partial x_\mu} \right) \tag{3.25}$$

$$= \sum_\mu \left(\frac{\partial f}{\partial z_\mu} \frac{\partial g}{\partial (i\overline{z}_\mu)} - \frac{\partial f}{\partial (i\overline{z}_\mu)} \frac{\partial g}{\partial z_\mu} \right) . \tag{3.26}$$

Let us denote the Weyl symbol of an operator $\hat{A}$ by $\operatorname{sym}(\hat{A})$. Then we have

$$\operatorname{sym}(\hat{I}) = I - \frac{1}{2} \,, \qquad \operatorname{sym}(\hat{J}_i) = J_i \,, \tag{3.27}$$

where

$$I = \frac{1}{2} \sum_\mu \overline{z}_\mu z_\mu = \frac{1}{2} \sum_\mu |z_\mu|^2 \,, \tag{3.28}$$

and

$$J_i = \frac{1}{2} \sum_{\mu\nu} \overline{z}_\mu \sigma^i_{\mu\nu} \, z_\nu \,, \tag{3.29}$$

for $i = 1, 2, 3$. We define the total angular momentum $\mathbf{J}^2 = \sum_i J_i^2$, which satisfies the identity $\mathbf{J}^2 = I^2$. Moreover, we have the Poisson bracket relations $\{I, J_i\} = 0$, $\{J_i, J_j\} = \sum_k \epsilon_{ijk} J_k$, $\{J_i, \mathbf{J}^2\} = 0$.

The Hamiltonian I generates a $U(1)$ action on the phase space $\mathbb{R}^4$ or $\mathbb{C}^2$. The Hamilton's equations for I are

$$\frac{dz_\mu}{d\psi} = \frac{dI}{\partial(i\overline{z}_\mu)} = -\frac{i}{2} z_\mu \,, \qquad \frac{d(i\overline{z}_\mu)}{d\psi} = -\frac{dI}{\partial z_\mu} = -\frac{i}{2} \overline{z}_\mu \,, \tag{3.30}$$

where ψ is the parameter of the orbits. These have the solutions

$$z_\mu(\psi) = \exp(-i\psi/2) z_\mu(0) \,, \qquad \overline{z}_\mu(\psi) = \exp(i\psi/2)\, \overline{z}_\mu(0) \,. \tag{3.31}$$

A level set of $I = j$ for $j > 0$ is S^3, which is foliated into circles by the Hamiltonian flows of I in (3.31). This foliation of S^3 into circles is precisely the Hopf fibration [40, 58]. The quotient space is $S^2 = S^3/S^1$.

The Hamiltonians J_i generate an $SU(2)$ group action on the phase space $\mathbb{C}^2$. Let $\mathbf{n}$ be a unit vector and θ an angle. The solution of Hamilton's equation for the Hamiltonian $\mathbf{n} \cdot \mathbf{J}$ is

$$\frac{dz_\mu}{d\theta} = \frac{\partial(\mathbf{n} \cdot \mathbf{J})}{\partial(i\overline{z}_\mu)} = -\frac{i}{2} \sum_\nu (\mathbf{n} \cdot \sigma)_{\mu\nu}\, z_\nu \,, \tag{3.32}$$

and its complex conjugate is

$$z_\mu(\theta) = \sum_\nu u(\mathbf{n}, \theta)_{\mu\nu}\, z_\nu(0) \,. \tag{3.33}$$

The functions J_i define a map $\pi : \mathbb{R}^4 \to \mathbb{R}^3$, where $\mathbb{R}^3$ is the 'angular momentum space,' the space with coordinates (J_1, J_2, J_3). The map π is not one-to-one. Because the definitions of the functions J_i in (3.29) do not depend on the overall phase of the spinors, the inverse image of a point in the angular momentum space is a circle, the Hopf fiber. These circles are precisely the orbits of the Hamiltonian flow of I (3.31).

The coordinates J_i provide a reduced Lie-Poisson bracket for functions f, g that are constant on these circles. We write such a function as $f(z_1, z_2, \overline{z}_1, \overline{z}_2) \equiv f(\mathbf{J})$. If f and g are any two such functions, then their Poisson bracket can be computed directly in angular momentum space via

$$\{f,\, g\} = \mathbf{J} \cdot \left(\frac{\partial f}{\partial \mathbf{J}} \times \frac{\partial g}{\partial \mathbf{J}} \right) . \tag{3.34}$$

The complex coordinates $(z_\mu, i\overline{z}_\mu)$ transform as a spinor under the Hamiltonian flows generated by J_i. These Hamiltonian flows are the classical analog of (3.21). The classical analog of (3.23) is that the values of the functions J_i under the Hamiltonian flows is $J_i = \sum_j R_{ij} J_j$, where R is the usual projection of $U(\mathbf{n}, \theta)$ from $SU(2)$ to $SO(3)$.

We now have two spaces, the original 'large phase space' $\mathbb{R}^4$ or $\mathbb{C}^2$, and the 'angular momentum space' $\mathbb{R}^3$. As we will see, the angular momentum space is useful for visualizing the intersection of Lagrangian manifolds in terms of angular momentum vectors.

The classical mechanic of N angular momenta is a simple generalization of the one angular momentum case. We have $2N$ classical oscillators $H_{r\mu} = (1/2)(x_{r\mu}^2 + p_{r\mu}^2)$. The configuration space is $(\mathbb{R}^2)^N = \mathbb{R}^{2N}$, the large phase space is $(\mathbb{R}^4)^N = \mathbb{R}^{4N}$ or $(\mathbb{C}^2)^N = \mathbb{C}^{2N}$. We define $z_{r\mu} = (x_{r\mu} + ip_{r\mu})/\sqrt{2}$, $\overline{z}_{r\mu} = (x_{r\mu} - ip_{r\mu})/\sqrt{2}$,

$$I_r = \frac{1}{2} \sum_{\mu} |z_{r\mu}|^2 \,, \tag{3.35}$$

$$J_{ri} = \frac{1}{2} \sum_{\mu\nu} \overline{z}_{r\mu}\, \sigma^i_{\mu\nu}\, z_{r\nu} \,, \tag{3.36}$$

as well as $\mathbf{J}_r^2 = \sum_i J_{ri}^2$, $J_i = \sum_r J_{ri}$, and $\mathbf{J}^2 = \sum_i J_i^2$.

The flow generated by I_r for a specific value of r is just a multiplication of the rth spinor (z_{r1}, z_{r2}) by a phase factor $\exp(-i\psi_r/2)$, leaving the other spinors unaffected. The N commuting flows generated by all I_r's constitute a $U(1)^N = T^N$ action on the large phase space.

As in the single angular momentum case, the Poisson bracket reduces to a Lie-Poisson bracket,

$$\{f,\, g\} = \sum_r \mathbf{J}_r \cdot \left(\frac{\partial f}{\partial \mathbf{J}_r} \times \frac{\partial g}{\partial \mathbf{J}_r} \right) \,, \tag{3.37}$$

for functions f and g that are invariant along all the I_r flows.

Any partial or total sum of the angular momenta $\mathbf{J}_r$ generates an $SU(2)$ action on the large phase space, in that the $SU(2)$ matrix u is applied to all spinors (z_{r1}, z_{r2}) whose r values lie in the sum. For example, the total angular momentum $\mathbf{J}$ rotates all spinors by the same rotation matrix u. These $SU(2)$ actions on the large phase space project to $SO(3)$ actions on the angular momentum space. For instance, the flow generated by $\mathbf{n} \cdot \mathbf{J}$, parametrized by θ, has the following orbits in the angular momentum space:

$$J_{ri}(\theta) = \sum_j R(\mathbf{n}, \theta)_{ij}\, J_{rj}(0) \,, \tag{3.38}$$

where $R(\mathbf{n}, \theta)$ is the 3×3 rotation associated with $u(\mathbf{n}, \theta)$. For example, J_z rotates all vectors $\mathbf{J}_r$ about the z-axis.

For reference, we write out the components of J_r explicitly:

$$J_{rx} = \frac{1}{2} \left(\overline{z}_{r1} z_{r2} + \overline{z}_{r2} z_{r1} \right) = \mathrm{Re} \left(\overline{z}_{r1} z_{r2} \right) , \tag{3.39}$$

$$J_{ry} = \frac{1}{2} \left(\overline{z}_{r1} z_{r2} - \overline{z}_{r2} z_{r1} \right) = \mathrm{Im} \left(\overline{z}_{r1} z_{r2} \right) , \tag{3.40}$$

$$J_{rz} = \frac{1}{2} \left(|z_{r1}|^2 - |z_{r2}|^2 \right) . \tag{3.41}$$

Thus the phase space of the Schwinger model has a fiber bundle structure, where the fiber consists of the overall phases of the spinors, and the base space consists of the angular momentum space. A point in the angular momentum space is represented by N

classical angular momentum vectors. The fiber above a point in the angular momentum space is an N-torus in the large phase space. The flow along the fiber is generated by the flows of I_r. If we denote the angle variable conjugate to I_r by ψ_r, $r = 1, \ldots, N$, then their periods are 4π.

3.5 The $3j$-Symbol in the Schwinger Model

We now define the $3j$-symbol

$$\begin{pmatrix} j_1 & j_2 & j_3 \\ m_1 & m_2 & m_3 \end{pmatrix} \tag{3.42}$$

as a scalar product of two quantum states in the Schwinger model of three angular momenta $\mathcal{H} \otimes \mathcal{H} \otimes \mathcal{H}$. The first state $|j_1 j_2 j_3 m_1 m_2 m_3\rangle = |j_1 m_1\rangle\,|j_2 m_2\rangle\,|j_3 m_3\rangle$ is a simultaneous eigenstate of one complete set of commuting observables $(\hat{I}_1, \hat{I}_2, \hat{I}_3, \hat{J}_{1z}, \hat{J}_{2z}, \hat{J}_{3z})$. The second state $|j_1 j_2 j_3 \mathbf{0}\rangle$ is the normalized state of the simultaneous eigenstate of another set of observables $(\hat{I}_1, \hat{I}_2, \hat{I}_3, \hat{J}_x, \hat{J}_y, \hat{J}_z)$, with eigenvalues $(j_1, j_2, j_3, \mathbf{0})$. Although the observables in the second set do not all commute, the second state exists and is unique from the usual rules for the addition of angular momenta. Disregarding the phase convention, we have

$$\begin{pmatrix} j_1 & j_2 & j_3 \\ m_1 & m_2 & m_3 \end{pmatrix} = \langle j_1 j_2 j_3 m_1 m_2 m_3 | j_1 j_2 j_3 \mathbf{0}\rangle \ . \tag{3.43}$$

Thus, we have expressed the $3j$-symbol as an inner product between two eigenstates, associated with two sets of observables, $(\hat{I}_1, \hat{I}_2, \hat{I}_3, \hat{J}_{1z}, \hat{J}_{2z}, \hat{J}_{3z})$ on the left and $(\hat{I}_1, \hat{I}_2, \hat{I}_3, \hat{J}_x, \hat{J}_y, \hat{J}_z)$ on the right.

We will apply the multidimensional WKB theory to find this scalar product, and thereby find the asymptotic form of the $3j$-symbol. From the symbols of the operators in (3.27), we find the Hamilton-Jacobi equations for the operators $\hat{I}_r$ and $\hat{J}_{rz}$ are respectively

$$I_r = J_r \,, \qquad J_{rz} = m_r \,, \tag{3.44}$$

where we have defined the classical magnitude of the angular momentum vectors to be

$$J_r = j_r + 1/2 \,. \tag{3.45}$$

These define a Lagrangian manifold corresponding to the wavefunction of the eigenstate on the left. We will call this manifold the jm-torus, for reasons that will become clear below. The Hamilton-Jacobi equations for the observables $\hat{I}_r$ and $\hat{J}_i$ are respectively

$$I_r = J_r \,, \qquad J_i = 0 \,, \tag{3.46}$$

which define a Lagrangian manifold corresponding to the wavefunction of the eigenstate on the right. We will call this manifold the Wigner manifold. To prove that this level set is a Lagrangian manifold, note that the differentials dA_i are linearly independent, so the vector fields X_i are too, and span a 6-dimensional tangent space to the manifold at each point. Evaluating the symplectic form on these vector fields, we have $w(X_i, X_j) = -\{A_i, A_j\}$.

These Poisson brackets all vanish in general, except for $\{J_i, J_j\}$, which happen to vanish on the level set where $\mathbf{J} = \mathbf{0}$. Thus the symplectic form restricted to the level set vanishes, so the level set is Lagrangian, and (3.46) are Hamilton-Jacobi equations.

3.6 The Lagrangian Manifolds

Let us look at the jm-torus associated with the jm-state $|j_1 j_2 j_3 m_1 m_2 m_3\rangle$. It is the level set defined by $I_r = J_r$, $J_{rz} = m_r$ for $r = 1, 2, 3$. Since $I_r = I_{r1} - I_{r2}$ and $J_{rz} = I_{r1} - I_{r2}$, the level set is also defined by the equivalent conditions

$$I_{r1} = \frac{1}{2}\left(J_r + m_r\right), \qquad I_{r2} = \frac{1}{2}\left(J_r - m_r\right). \tag{3.47}$$

Since each of the six $I_{r\mu}$ is a harmonic oscillator Hamiltonian times $1/2$, a level set of $I_{r\mu}$'s is a 6-torus. We may choose the coordinates to be the variables of evolution of $I_{r\mu}$, which we will denote by $\theta_{r\mu}$. The Hamiltonian flow generated by $I_{r\mu}$ multiplies $z_{r\mu}$ by $\exp(-i\theta_{r\mu}/2)$, while leaving all other z's unaffected, as illustrated in figure 3.1. The period of the angles $\theta_{r\mu}$ is 4π, so the volume of the jm-torus with respect to the measure $d\theta_{11} \wedge \cdots \wedge d\theta_{32}$ is $(4\pi)^6$.

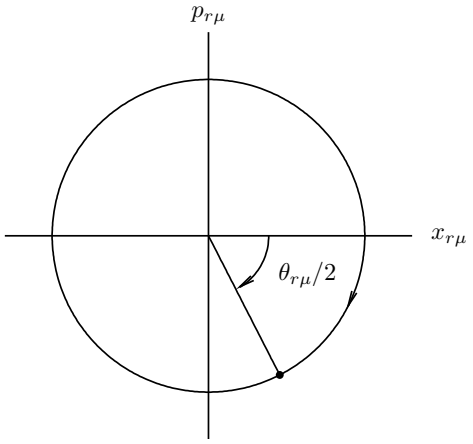

Figure 3.1: The flow generated by $I_{r\mu}$ as seen in the $x_{r\mu}$-$p_{r\mu}$ plane.

These tori are also the orbits of the flows generated by the observable I_r and J_{rz}. We denote the evolution variables of I_r and J_{rz} by ψ_r and ϕ_r, respectively. While canonical coordinates $(\theta_{r\mu}; I_{r\mu})$ are convenient for calculating the action, $(\psi_r, \phi_r; I_r, J_{rz})$ are more convenient in visualizing the angular momentum vectors that correspond to the Lagrangian manifold. Using a canonical transformation generated by

$$F_2(\theta_{r1}, \theta_{r2}, I_r, J_{rz}) = \frac{1}{2}\left[\theta_{r1}(I_r + J_{rz}) + \theta_{r2}(I_r - J_{rz})\right], \tag{3.48}$$

that implies $I_r = I_{r1} + I_{r2}$, $J_{rz} = I_{r1} - I_{r2}$, we find the relationship between the two coordinates are

$$\psi_r = \frac{1}{2}(\theta_{r1} + \theta_{r2})\,, \qquad \phi_r = \frac{1}{2}\,(\theta_{r1} - \theta_{r2})\,. \tag{3.49}$$

The Jacobian in this coordinate transformation is $(1/2)^3 = 1/8$. Since the period for ϕ_r is 2π, we find the volume of the torus with respect to $d\psi_1 \wedge d\psi_2 \wedge d\psi_3 \wedge d\phi_1 \wedge d\phi_2 \wedge d\phi_3$ is

$$V_{jm} = (2\pi)^3(4\pi)^3\,. \tag{3.50}$$

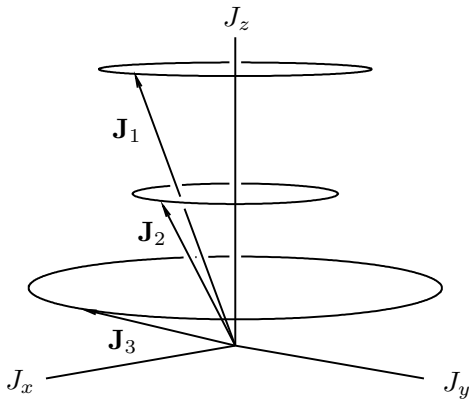

Figure 3.2: Visualization of the jm-torus in the angular momentum space.

We will use the J_{rz}'s to evaluate the amplitude determinant, so the volume we will use in the final formula is V_{jm}. The jm-torus can be projected to the angular momentum space. Its image in angular momentum space is a 3-torus. The 3-torus can be visualized as three classical vectors $\mathbf{J}_r$ in a single angular momentum space, with specified values of $m = J_{rz}$, 'precessing' about the z-axis. See figure 3.2. Each point of this 3-torus is associated with a 3-torus fiber, which consists of independently changing the overall phases of the three spinors. The six-dimensional jm-torus is thus the Cartesian product $T^3 \times T^3$.

Now let us turn our attention to the level set associated with the state $|j_1 j_2 j_3 \mathbf{0}\rangle$. This is the level set of $I_r = J_r$ and $\mathbf{J} = 0$. For convenience, we denote the classical observables $(I_1, I_2, I_3, J_x, J_y, J_z)$ collectively by A_i, $i = 1, \ldots, 6$.

In the angular momentum space, the condition $\mathbf{J} = \mathbf{0}$ put the three vectors $\mathbf{J}_1$, $\mathbf{J}_2$, and $\mathbf{J}_3$ into three sides of a triangle. Up to orientation, this triangle is unique. For instance, one such set of vectors is illustrated in figure 3.3, where we put $\mathbf{J}_3$ along the z-axis, with $\mathbf{J}_1$ in the $x - z$ plane with $J_{1x} > 0$. The directions of the vectors are given by the angles η_r, which lie in the range $0 \le \eta_r \le \pi$. These angles are related to the interior angles of the triangle. From the law of coine, we find the angles η_r are given by

$$\cos\eta_1 = \frac{J_1^2 - J_2^2 - J_3^2}{2J_2J_3}\,, \tag{3.51}$$

and cyclic permutations.

Given any two triangles with the same sides, there exists a unique rotation that maps one into the other. Thus the Wigner manifold projected onto the angular momentum

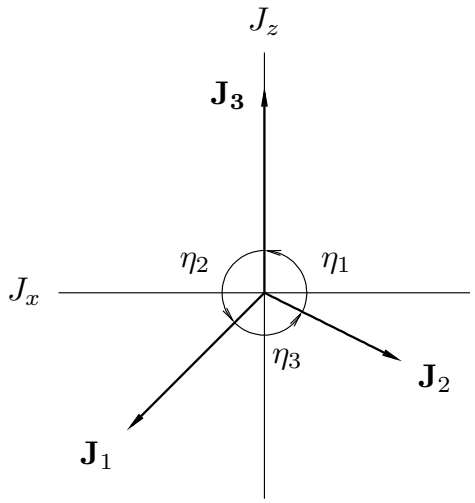

Figure 3.3: Visualization of the reference orientation for a point in the Wigner manifold in the angular momentum space.

space $\mathbb{R}^3 \times \mathbb{R}^3 \times \mathbb{R}^3$ is diffeomorphic to $SO(3)$. Since the inverse image of any given point of angular momentum space is a 3-torus in the large phase space, the Wigner manifold is a 3-torus bundle over $SO(3)$. However, this bundle is not a trivial bundle, because the $SU(2)$ lift of a closed path in $SO(3)$ in the base manifold is not necessarily close in the large phase space. For example, even though the $SU(2)$ rotation $u = -1$ projects to the identity in $SO(3)$, it maps a point in the large phase space to a different point.

The bundle structure is illustrated in figure 3.4. The lower part of this figure refers to the $SO(3)$ manifold in the angular momentum space, and the vertical lines refer to the T^3 fibers. Pick a point A in this manifold, and let a be a point in the fiber above A. The $SU(2)$ rotation $u = -1$ moves a to a different point a' in the same fiber above A. The same is true for any other point b. If we follow the flows generated by the three I_r, parametrized by the angles ψ_r, to range from 0 to 4π, and the flows generated by J_i to range over all of $SU(2)$, we cover the Wigner manifold exactly twice. In this way, we have a coordinate system for the Wigner manifold, given by $(\alpha, \beta, \gamma, \psi_1, \psi_2, \psi_3)$, the first three of which are Euler angles on $SU(2)$. With respect to the Haar measure on $SU(2)$ and the obvious measure on the 3-tori, namely,

$$\sin\beta \, d\alpha \wedge d\beta \wedge d\psi_1 \wedge \psi_2 \wedge \psi_3 \,, \tag{3.52}$$

the integral of this measure over the Wigner manifold is

$$V_W = \frac{1}{2}(16\pi^2)(4\pi)^3 = 2^9\pi^5 \,, \tag{3.53}$$

where the factor $1/2$ compensates for the fact that the Wigner manifold is covered twice in this coordinate system.

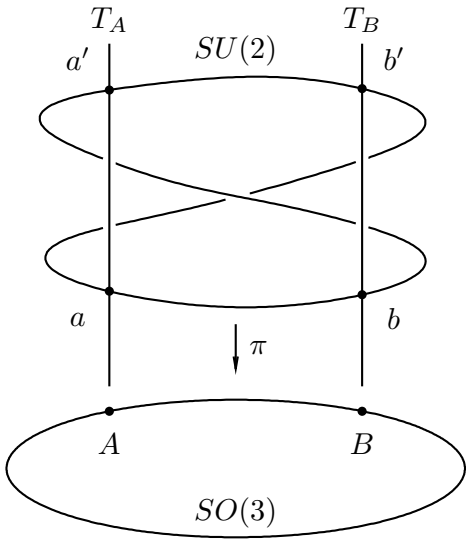

Figure 3.4: The 3-torus bundle structure of the Wigner manifold.

3.7 Intersection of Manifolds

The intersection of the two Lagrangian manifolds are defined by the conditions

$$I_r = J_r\,, \qquad J_{rz} = m_r\,, \qquad J_i = 0\,. \tag{3.54}$$

These conditions are almost the same as (2.53), except J_r is equal to $j_r + 1/2$ here, instead of j_r. Therefore we can find the intersections by following the procedure in section 2.6.1. We start with a point in the Wigner manifold that projects to the point A in figure 3.3. To intersect with the jm-torus, we first rotate this reference orientation about the y-axis by a unique angle β, $0 \le \beta \le \pi$, defined by

$$m_3 = J_3 \cos\beta\,, \tag{3.55}$$

to obtain $J_{3z} = m_3$. The result of this rotation is shown in figure 3.5, for a certain negative value of m_3.

Next we rotate the triangle about $\mathbf{J}_3$ by an angle γ, which does not change $\mathbf{J}_3$ or its projection, but rotates $\mathbf{J}_1$ and $\mathbf{J}_2$ in a cone, as illutrated in figure 3.6.

The result of applying the rotation

$$R(\mathbf{j}_3,\gamma)\,R(\mathbf{y},\beta) = R(\mathbf{y},\beta)\,R(\mathbf{j}_3,\gamma) \tag{3.56}$$

to the vectors

$$\mathbf{J}_1 = J_1 \begin{pmatrix} \sin\eta_2 \\ 0 \\ \cos\eta_2 \end{pmatrix}\,, \qquad \mathbf{J}_1 = J_2 \begin{pmatrix} -\sin\eta_1 \\ 0 \\ \cos\eta_1 \end{pmatrix}\,, \qquad \mathbf{J}_1 = J_3 \begin{pmatrix} 0 \\ 0 \\ 1 \end{pmatrix}\,, \tag{3.57}$$

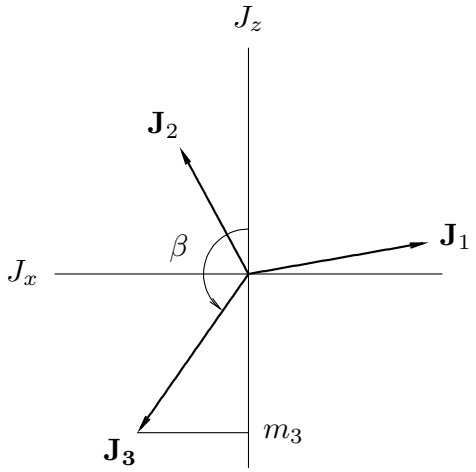

Figure 3.5: The angular momentum vectors after applying the rotation about the y-axis by an angle β to the point in the Wigner manifold in the reference orientation.

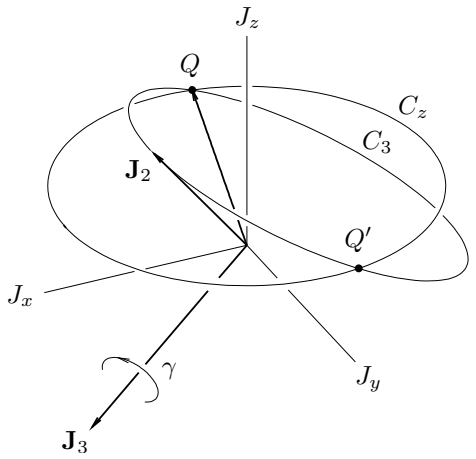

Figure 3.6: Once vector $\mathbf{J}_3$ has the desired projection m_3, we rotate the triangle by angle γ about the axis $\mathbf{J}_3$ to make $\mathbf{J}_2$ have its desired projection m_2. This cannot always be done for real angles γ, but when it can be done there are generically two angles that work, illustrated by points Q and Q' in the figure.

in the reference orientation in figure 3.3 is given by

$$\begin{aligned}
\mathbf{J}_1 &= J_1 \begin{pmatrix} \cos\beta\cos\gamma\sin\eta_2 + \sin\beta\cos\eta_2 \\ \sin\gamma\sin\eta_2 \\ -\sin\beta\cos\gamma\sin\eta_2 + \cos\beta\cos\eta_2 \end{pmatrix}, \\
\mathbf{J}_2 &= J_2 \begin{pmatrix} -\cos\beta\cos\gamma\sin\eta_1 + \sin\beta\cos\eta_1 \\ -\sin\gamma\sin\eta_1 \\ \sin\beta\cos\gamma\sin\eta_1 + \cos\beta\cos\eta_1 \end{pmatrix}, \\
\mathbf{J}_3 &= J_3 \begin{pmatrix} \sin\beta \\ 0 \\ \cos\beta \end{pmatrix}.
\end{aligned} \tag{3.58}$$

We choose the angle γ so that either $J_{1z} = m_1$ or $J_{2z} = m_2$, which leads to

$$\cos\gamma = \frac{J_1\cos\beta\cos\eta_2 - m_1}{J_1\sin\beta\sin\eta_2} = \frac{m_2 - J_2\cos\beta\cos\eta_1}{J_2\sin\beta\sin\eta_1}. \tag{3.59}$$

If the common value of the two expressions on the right-hand side of (3.59) lies in the range $(-1,+1)$, then there are two real angles γ satisfying (3.59), corresponding to the two points Q and Q' in figure 3.6. Otherwise, we are in the classically forbidden region of the $3j$-symbol. For simplicity, we will assume that we are in the classically allowed region. We denote the root in the range $[0,\pi]$ by γ, and the other root in $[-\pi,0]$ by $-\gamma$.

In this way, we obtain two points, P and P', that lie in the projection of the intersection of the two Lagrangian manifolds in the angular momentum space. Since the conditions (3.54) are invariant under overall rotations about the z-axis, we get a pair of circles as solutions to (3.54) in the angular momentum space by applying such rotations to P and P'. Thus, the projection of the intersection of the jm-manifold and the Wigner manifold is generically a pair of circles.

In the large phase space, the inverse image of this pair of circles under π is generically a pair of 3-torus bundles over a circle. Since the I_r-flows and the J_z-flow commute, these bundles are trivial. Thus each intersection set is a 4-torus, on which coordinates are $(\psi_1,\psi_2,\psi_3,\phi)$, where ϕ is the angle of evolution along the J_z-flow. The volume of either one of the 4-tori with respect to the measure $d\psi_1\wedge d\psi_2\wedge d\psi_3\wedge d\phi$ is

$$V_I = \frac{1}{2}(4\pi)^4. \tag{3.60}$$

The reason why the jm-torus and the Wigner manifold intersect in a 4-torus is because the lists of functions defining the two manifolds, $(I_1,I_2,I_3,J_{1z},J_{2z},J_{3z})$, $(I_1,I_2,I_3,J_x,J_y,J_z)$, have three functions in common, and J_z in the second list is a function of (J_{1z},J_{2z},J_{3z}) in the first list.

We can replace the second list by another list to show explicitly the four variables in common. We perform a canonical transformation

$$(\phi_1,\phi_2,\phi_3,J_{1z},J_{2z},J_{3z}) \to (\tilde\phi_1,\tilde\phi_2,\tilde\phi_3,\tilde J_{1z},\tilde J_{2z},\tilde J_{3z}) \tag{3.61}$$

on the functions in the second list, generated by

$$F_2(\phi_1,\phi_2,\phi_3,\tilde{J}_{1z},\tilde{J}_{2z},\tilde{J}_{3z}) = \phi_1\tilde{J}_{1z} + \phi_2\tilde{J}_{2z} + \phi_3(J_1 - \tilde{J}_{1z} - \tilde{J}_{2z})\,. \tag{3.62}$$

This gives $\tilde{J}_{1z} = J_{1z}$, $\tilde{J}_{2z} = J_{2z}$, and $\tilde{J}_z = J_{1z} + J_{2z} + J_{3z}$ and $\tilde{\phi}_1 = \phi_1 - \phi_3$, $\tilde{\phi}_2 = \phi_2 - \phi_3$, and $\tilde{\phi}_3 = \phi_3$. This transformation has unit determinant, so the volume of the jm-torus is still given by (3.50). Dropping the tildes, the second list is now $(I_1, I_2, I_3, J_{1z}, J_{2z}, J_z)$, which has four functions in common with the first list.

3.8 The Amplitude Determinant

The amplitude determinant in the WKB theory is given by the determinant of Poisson brackets between the distinct subsets of the two lists of observables. These subsets are $E = (J_{1z}, J_{2z})$ in the A-list, and $D = (J_x, J_y)$ in the B-list. Calculating this determinant explicitly, we find

$$\begin{aligned} |\det\{E,D\}| &= \begin{vmatrix} \{J_{1z},J_x\} & \{J_{1z},J_y\} \\ \{J_{2z},J_x\} & \{J_{2z},J_y\} \end{vmatrix} = \begin{vmatrix} J_{y1} & -J_{x1} \\ J_{y2} & -J_{x2} \end{vmatrix} \\ &= |J_{x1}J_{y2} - J_{x2}J_{y1}| = |\mathbf{z}\cdot(\mathbf{J_1}\times\mathbf{J_2})| = 2\Delta_z \end{aligned} \tag{3.63}$$

where Δ_z is the projection of the area of the 1-2-3 triangle at an intersection point onto the x-y plane. This quantity is invariant under rotations about the z-axis, so it is constant on the intersection of the two Lagrangian manifolds.

3.9 The Action Integrals

The action functions S_A and S_B are defined relative to some reference point on each manifold. For the jm-torus, we pick the point b where each $z_{r\mu}$ is real and nonnegative. According to (3.47), the spinors at this reference point are given explicitly by

$$\begin{pmatrix} z_{r1} \\ z_{r2} \end{pmatrix} = \begin{pmatrix} \sqrt{J_r + m_r} \\ \sqrt{J_r - m_r} \end{pmatrix}. \tag{3.64}$$

The projection of b onto angular momentum space is a set of vectors $\mathbf{J}_r$ $r = 1,2,3$, of given lengths J_r, that lie in the x-z plane, with $J_{rz} = m_r$ and $J_x \geq 0$. This is illustrated in figure 3.2.

As for the Wigner manifold, we take the reference point to be a point a in figure 3.4. The spinors at this point is given by

$$\begin{aligned} &\begin{pmatrix} z_{11} \\ z_{12} \end{pmatrix} = \sqrt{2J_1}\begin{pmatrix} \cos\eta_2/2 \\ \sin\eta_2/2 \end{pmatrix}, \qquad \begin{pmatrix} z_{21} \\ z_{22} \end{pmatrix} = \sqrt{2J_2}\begin{pmatrix} \cos\eta_1/2 \\ -\sin\eta_1/2 \end{pmatrix}, \\ &\begin{pmatrix} z_{31} \\ z_{32} \end{pmatrix} = \sqrt{2J_3}\begin{pmatrix} 1 \\ 0 \end{pmatrix}, \end{aligned} \tag{3.65}$$

where we have chosen z_{r1} to be real and positive for all r. This point projects onto the standard orientation of the triangle, point A in figure 3.4, where the angular momentum vectors have the values shown in (3.57).

Now to obtain a point c common to both the jm-torus and the Wigner manifold, we lift the rotation (3.56) to an $SU(2)$ rotation

$$u(\mathbf{y},\beta)\,u(\mathbf{z},\gamma) = \begin{pmatrix} e^{-i\gamma/2}\cos\beta/2 & -e^{i\gamma/2}\sin\beta/2 \\ e^{-i\gamma/2}\sin\beta/2 & e^{i\gamma/2}\cos\beta/2 \end{pmatrix}, \tag{3.66}$$

and apply it to the reference spinors (z_{r1}, z_{r2}), $r = 1, 2, 3$, in (3.65). Here the angles β and γ are defined by (3.55) and (3.59). Thus we obtain the spinors at the common point c, corresponding to γ, or c', corresponding to $-\gamma$, in the intersection between the jm-torus and the Wigner manifold,

$$\begin{pmatrix} z_{11} \\ z_{12} \end{pmatrix} = \sqrt{2J_1}\begin{pmatrix} e^{-i\gamma/2}\cos\beta/2\cos\eta_2/2 - e^{i\gamma/2}\sin\beta/2\sin\eta_2/2 \\ e^{-i\gamma/2}\sin\beta/2\cos\eta_2/2 + e^{i\gamma/2}\cos\beta/2\sin\eta_2/2 \end{pmatrix}, \tag{3.67}$$

$$\begin{pmatrix} z_{21} \\ z_{22} \end{pmatrix} = \sqrt{2J_2}\begin{pmatrix} e^{-i\gamma/2}\cos\beta/2\cos\eta_1/2 + e^{i\gamma/2}\sin\beta/2\sin\eta_1/2 \\ e^{-i\gamma/2}\sin\beta/2\cos\eta_1/2 - e^{i\gamma/2}\cos\beta/2\sin\eta_1/2 \end{pmatrix}, \tag{3.68}$$

$$\begin{pmatrix} z_{11} \\ z_{12} \end{pmatrix} = e^{-i\gamma/2}\sqrt{2J_3}\begin{pmatrix} \cos\beta/2 \\ \sin\beta/2 \end{pmatrix}. \tag{3.69}$$

The basic strategy in computing the action integrals for the WKB formula is illustrated in figure 3.7. In computing the action S_{jm} on the jm-torus, we start at the reference point b and follow the flows generated by $I_{r\mu}$, $r = 1, 2, 3$, $\mu = 1, 2$ to reach the common point c or c'. For the action S_W on the Wigner manifold, we start at the reference point a and follow the flows generated by the rotations (3.56) to reach the common points c or c'.

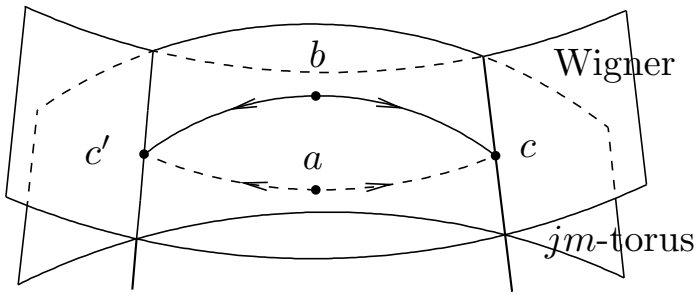

Figure 3.7: The action integral S_{jm} is defined relative to a reference point a on the Wigner manifold, and the action integral S_W is defined relative to a reference point b on the jm-torus.

In computing action integrals we use the identity

$$\sum_{r\mu} p_{r\mu}dx_{r\mu} = \frac{i}{2}\sum_{r\mu}(\overline{z}_{r\mu}\,dz_{r\mu} - z_{r\mu}\,d\overline{z}_{r\mu}) + \frac{1}{2}\,d\sum_{r\mu} x_{r\mu}p_{r\mu}\,. \tag{3.70}$$

The integral of the left-hand side is the usual action one would need for wavefunctions $\psi(x_{11},\ldots,x_{32})$, but it can be replaced by the integral of the first differential form on the right, for the following reasons. First, the integral of the exact differential on the right contributes the difference in the function $(1/2)\sum_{r\mu} x_{r\mu}p_{r\mu}$ between the initial and final points. But the final point is the common point of intersection between the jm-torus and the Wigner manifold, so this contribution cancels when we subtract actions as in (3.6). As for the initial points on the two manifolds, these have been chosen, in (3.64) and (3.65), so that all $z_{r\mu}$ are purely real, so $p_{r\mu}=0$. Thus the function in question vanishes at the initial points. As for the integral of the first term on the right-hand side of (3.70), it can be written as

$$S = \mathrm{Im}\int \sum_{r\mu} z_{r\mu}\, d\overline{z}_{r\mu}\,. \tag{3.71}$$

For the action on the jm-torus, between initial point (3.64) and final point (3.67)-(3.69), we follow a path consisting of flows of the functions $I_{r\mu}=(1/2)|z_{r\mu}|^2$ taken one at a time by angles $\theta_{r\mu}$. Along the $I_{r\mu}$-flow we have $d\overline{z}_{r\mu}/d\theta_{r\mu}=(i/2)\overline{z}_{r\mu}$, so the contribution to S_{jm} is

$$\mathrm{Im}\int_0^{\theta_{r\mu}} \frac{i}{2}|z_{r\mu}|^2\, d\theta_{r\mu} = I_{r\mu}\theta_{r\mu}\,, \tag{3.72}$$

since $I_{r\mu}$ is constant along its own flow and since $\theta_{r\mu}=0$ at the reference point. Thus the total action between initial and final points on the jm-torus is

$$S_{jm} = \sum_{r\mu} I_{r\mu}\theta_{r\mu}\,. \tag{3.73}$$

Since $\theta_{r\mu}=2\arg\overline{z}_{r\mu}$, where the spinors are those in (3.67)-(3.69), we can write the action on the jm-torus as

$$S_{jm} = 2\sum_{r\mu} I_{r\mu}\arg\overline{z}_{r\mu} = \sum_r J_r \arg(\overline{z}_{r1}\overline{z}_{r2}) + \sum_r m_r \arg(\overline{z}_{r1}z_{r2})\,. \tag{3.74}$$

Using equations (3.67)-(3.69), this can be written as

$$\begin{aligned} S_{jm} \;=\; & J_3\gamma + J_1\arg(\cos\beta\sin\eta_2+\sin\beta\cos\gamma\cos\eta_2+i\sin\beta\sin\gamma) \\ & +J_2\arg(-\cos\beta\sin\eta_1+\sin\beta\cos\gamma\cos\eta_1+i\sin\beta\sin\gamma) \\ & +m_1\arg(\sin\beta\cos\eta_2+\cos\beta\cos\gamma\sin\eta_2+i\sin\gamma\sin\eta_2) \\ & +m_2\arg(\sin\beta\cos\eta_1-\cos\beta\cos\gamma\sin\eta_1-i\sin\gamma\sin\eta_1)\,. \end{aligned} \tag{3.75}$$

Here the range of the arg function is taken to be $[-\pi,0)$. The values of S_{jm} on the two branches differ by a sign. We shall write S_{jm} and $-S_{jm}$ for γ and $-\gamma$, respectively.

Equation (3.75) can be rewritten in terms of $\cos^{-1}$ functions. We note that $\arg(\overline{z}_{11}\overline{z}_{12}) = \cos^{-1}[\mathrm{Re}(\overline{z}_{11}\overline{z}_{12})/|z_{11}z_{12}|]$ and that $|z_{11}z_{12}|=\sqrt{J_1^2-m_1^2}$, etc. We can also use (3.59) to eliminate $\cos\gamma$. This gives

$$
\begin{aligned}
S_{jm} \;=\; & J_1 \cos^{-1}\left(\frac{J_1\cos\beta - m_1\cos\eta_2}{\sin\eta_2\, J_{1\perp}}\right) + J_2\cos^{-1}\left(\frac{m_2\cos\eta_1 - J_2\cos\beta}{\sin\eta_1 J_{2\perp}}\right) \\
& + J_3\cos^{-1}\left(\frac{J_1\cos\beta\cos\eta_2 - m_1}{J_1\sin\beta\sin\eta_2}\right) + m_1\cos^{-1}\cos^{-1}\left(\frac{J_1\cos\eta_2 - m_1\cos\beta}{\sin\beta J_{1\perp}}\right) \\
& - m_2\cos^{-1}\left(\frac{J_2\cos\eta_1 - m_2\cos\beta}{\sin\beta\, J_{2\perp}}\right). \qquad (3.76)
\end{aligned}
$$

where

$$
J_{r\perp} = \sqrt{J_r^2 - m_r^2}\,, \qquad (3.77)
$$

and where the range of the $\cos^{-1}$ function is $[0,\pi]$.

Now we consider the action on the Wigner manifold between the initial point (3.65) and the final point (3.67)-(3.69). The path between these points is generated by the product of rotations (3.66), so we consider the action integral (3.71) along a rotation by angle θ generated by $\mathbf{n}\cdot\mathbf{J}$. The Hamilton's equations are $d\overline{z}_{r\mu}/d\theta = (i/2)\sum_\nu \overline{z}_{r\nu}(\mathbf{n}\cdot\sigma)_{\nu\mu}$, so we have

$$
S_W = \mathrm{Im}\int_0^\theta \frac{1}{2}\sum_{r\mu\nu}\overline{z}_{r\nu}(\mathbf{n}\cdot\sigma)_{\nu\mu}\, z_{r\mu}\, d\theta = \int_0^\theta (\mathbf{n}\cdot\mathbf{J})\, d\theta = (\mathbf{n}\cdot\mathbf{J})\,\theta = 0\,, \qquad (3.78)
$$

where we have used (3.36), the fact that $\mathbf{n}\cdot\mathbf{J}$ is constant along its own flow, and the fact that $\mathbf{J}=0$ on the Wigner manifold. The action vanishes. Thus, the phase of the matrix element (3.43) is determined entirely by the action integral along the jm-torus. This is the same relative phase function (2.95) in section 2.6.3, and it agrees with the result obtained by Ponzano and Regge, Miller, and others.

3.10 The Asymptotic Formula

We now have the amplitude determinants and the action integrals, as well as the the volume V_I, $V_A = V_{jm}$, $V_B = V_W$, from the general formula

$$
\langle b|a\rangle = \frac{2\pi}{\sqrt{V_A V_B}}\sum_{\mathrm{br}} V_I \frac{e^{i(S-\mu\pi/2)}}{|\det\{E,D\}|}\,, \qquad (3.79)
$$

we obtain to within an overall phase the result of Ponzano and Regge,

$$
\begin{pmatrix} j_1 & j_2 & j_3 \\ m_1 & m_2 & m_3 \end{pmatrix} = (\text{phase}) \times \frac{\cos(S_{jm}+\pi/4)}{\sqrt{2\pi\Delta_z}}\,. \qquad (3.80)
$$

Here we have used the known result that the relative Maslov index is 1, without deriving it.

3.11 Conclusions

By comparing the semiclassical calculation in this chapter with the calculation in the Bargmann representation in chapter 2, we see that the calculations in this chapter are more geometrical in the semiclassical analysis. Moreover, many of the tedious calculations from chapter 2 are reduced to problems in classical mechanics, where powerful techniques from symplectic geometry become available.

In this chapter, we have carefully chosen the reference points on the two Lagrangian manifolds, in order to use the one-form (3.71) to calculate the action integral for S_A and S_B at the two intersection points. If all we wanted was the difference between the relative actions $S_A - S_B$, evaluated at the two intersection points, then such careful choices are not necessary, as we will see in the semiclassical analysis of the $6j$-symbol in chapter 4. In fact, the relative phase for the $6j$-symbol becomes a symplectic area on a 2-sphere through the classical technique of symplectic reduction, and is therefore independent of the reference points.

An obvious generalization of the basic methods in this chapter is to extend our analysis from $SU(2)$ to $SU(3)$, which is the gauge group in quantum chromodynamics (QCD). This is a promising avenue for future research, since there exists a Schwinger type model for $SU(3)$ [29] in terms of quantum harmonic oscillators, and spin networks are known to be useful for lattice gauge theory of QCD [31, 30].

Chapter 4

Semiclassical Analysis of the Wigner $6j$-Symbol

4.1 Introduction and Summary

We apply multidimensional WKB theory to the Schwinger model of four angular momenta to find the asymptotic formula for the Wigner $6j$-symbol. We pay special attention to the action integral, which we will calculate using two independent methods. The first method relies on symplectic reduction, where the reduced phase space of the $6j$-symbol is the 2-sphere of Kapovich and Millson [45]. The second method is a more direct calculation that can be generalized to higher $3nj$-symbols.

The Wigner $6j$-symbol, or Racah W-coefficient, is the simplest, nontrivial, closed spin network. It has many applications in atomic, molecular and nuclear physics. Such applications are described in the book by Edmonds [35]. More recently the $6j$-symbol and other $3nj$-symbols have found applications in quantum computing [54] and in algorithms for molecular scattering calculations [2, 34, 6, 5, 7]. In general, spin networks are important in lattice QCD and in loop quantum gravity, where they provide a gauge-invariant basis.

There have been geometric derivations of the Wigner $6j$-symbol based on the technique of geometric quantization by Roberts [72] and Charles [28]. See chapter 2 for how those geometric method and the WKB method in this chapter are related to the Bargmann representation. The model used in this chapter bear the closest relation to the four angular momenta model used in the paper by Charles [28], where the 2-sphere reduced space also appears. In addition, there has been some work on the q-deformed $6j$-symbol, important for the regularization of the Ponzano-Regge spin-foam model [82, 62, 60] and for its possible connection to quantum gravity with cosmological constant. In particular, Mizoguchi and Tada [56], and later Taylor and Woodward [80], applied the discrete WKB method of Schulten and Gordon to the q-deformed $6j$-symbol, and obtain its asymptotic formula. The results are geometrically interesting, but it seems that at present there is no geometrical treatment of the asymptotics of the q-deformed $6j$-symbol.

Our calculation of the $6j$-symbol in this chapter serves to illustrate the simplifications offered by our semiclassical techniques to the calculation of the relative phase. In addition, it lays the foundation for developments of new results. These new results include a

new uniform approximations for the $6j$-symbol in chapter 5, and a new asymptotic formula for the $9j$-symbol in chapter 6.

The outline of this chapter is as follows: in section 4.2, we define the $6j$-symbol as a scalar product of two wavefunctions in the Schwinger space of four angular momenta. We then perform semiclassical analysis to derive the WKB formula for this scalar product. First, we analyze the Lagrangian manifolds and derive their volumes in section 4.3. Then we find the intersections of the Lagrangian manifolds and derive their volumes. Finally, we calculate the amplitude determinant in section 4.5 and the action integral using a reduced phase space in section 4.6. We then put the results together and derive the asymptotic formula for the $6j$-symbol in section 4.7. In section 4.8, we provide an independent derivation of the action integral in the large phase space. The last section contains conclusions and discussions.

4.2 The $6j$-Symbol in the Schwinger Model

The $6j$-symbol is a recoupling coefficient in the addition of four angular momenta. The Hilbert space is $\mathcal{K} = \mathcal{H}_{j_1} \otimes \mathcal{H}_{j_2} \otimes \mathcal{H}_{j_3} \otimes \mathcal{H}_{j_4}$, where each $\mathcal{H}_{j_r}$ is a Schwinger angular momemtum space. See chapter 3 for more details on the Schwinger space. In the invariant subspace $\mathcal{Z}$ of the total angular momentum, standard recoupling theory gives three ways of constructing an orthonormal basis. One way is to couple angular momenta according to the scheme $1+2=12$, $12+3=123$, $123+4=0$, giving normalized states $|A\rangle = |j_{12}\rangle$. Another way couples according to the scheme $2+3=23$, $1+23=123$, $123+4=0$, giving us normalized states $|B\rangle = |j_{23}\rangle$. A third way gives $|j_{13}\rangle$, which we will not make use here.

The Wigner $6j$-symbol is proportional to the scalar product between the two states $|A\rangle$ and $|B\rangle$ in $\mathcal{Z}$, that is,

$$\left\{ \begin{array}{ccc} j_1 & j_2 & j_{12} \\ j_3 & j_4 & j_{23} \end{array} \right\} = \frac{(-1)^{j_1+j_2+j_3+j_4}}{\sqrt{(2j_{12}+1)(2j_{23}+1)}} \, \langle B|A\rangle \ , \tag{4.1}$$

where the states $|A\rangle$ and $|B\rangle$ above can be expressed as eigenstates of complete sets of operators,

$$|A\rangle = \left| \begin{array}{cccccc} \hat{I}_1 & \hat{I}_2 & I_3 & \hat{I}_4 & \hat{\mathbf{J}}_{12}^2 & \hat{\mathbf{J}}_{\rm tot} \\ j_1 & j_2 & j_3 & j_4 & j_{12} & \mathbf{0} \end{array} \right\rangle \ , \tag{4.2}$$

$$|B\rangle = \left| \begin{array}{cccccc} \hat{I}_1 & \hat{I}_2 & I_3 & \hat{I}_4 & \hat{\mathbf{J}}_{23}^2 & \hat{\mathbf{J}}_{\rm tot} \\ j_1 & j_2 & j_3 & j_4 & j_{23} & \mathbf{0} \end{array} \right\rangle \ , \tag{4.3}$$

in a notation that we will use to list the operators and their associated quantum numbers for a particular state. The operators $\hat{I}_r$ and $\hat{J}_{ri}$, $r = 1,2,3,4$, $i = 1,2,3$, are defined by Schwinger's representation, as follows:

$$\hat{I}_r = \frac{1}{2} \sum_{r\mu} \hat{a}_{r\mu}^\dagger \hat{a}_\mu \ , \qquad \hat{J}_{ri} = \frac{1}{2} \sum_{\mu\nu} \hat{a}_{r\mu}^\dagger (\sigma)_{\mu\nu}^i \hat{a}_{r\nu} \ , \tag{4.4}$$

where $\hat{a}_{r\mu}$ and $\hat{a}_{r\mu}^\dagger$ are the usual annihilation and creation operators for the μth quantum oscillator in the rth Schwinger angular momentum space. The intermediate and total angular momentum operators are sums of the vector operators $\mathbf{J}_r$, defined as follows:

operator	Weyl symbol
$\hat{I}_r$	$I_r - 1/2$
$\hat{\mathbf{J}}_r$	$\mathbf{J}_r$
$\hat{\mathbf{J}}_{\rm tot}$	$\mathbf{J}_{\rm tot}$
$\hat{\mathbf{J}}_{12}$	$\mathbf{J}_{12}$
$\hat{\mathbf{J}}_{23}$	$\mathbf{J}_{23}$
$\hat{\mathbf{J}}_r^2$	$\mathbf{J}_r^2 - 3/8$
$\hat{\mathbf{J}}_{12}^2$	$\mathbf{J}_{12}^2 - 3/4$
$\hat{\mathbf{J}}_{23}^2$	$\mathbf{J}_{23}^2 - 3/4$

Table 4.1: Weyl symbols of selected operators. In rows containing operators $\hat{I}_r$, $\hat{\mathbf{J}}_r$ and $\hat{\mathbf{J}}_r^2$, $r = 1, \ldots, 4$.

$$\hat{\mathbf{J}}_{12} = \hat{\mathbf{J}}_1 + \hat{\mathbf{J}}_2\,, \tag{4.5}$$
$$\hat{\mathbf{J}}_{23} = \hat{\mathbf{J}}_2 + \hat{\mathbf{J}}_3\,, \tag{4.6}$$
$$\hat{\mathbf{J}}_{\rm tot} = \hat{\mathbf{J}}_1 + \hat{\mathbf{J}}_2 + \hat{\mathbf{J}}_3 + \hat{\mathbf{J}}_4\,. \tag{4.7}$$

4.3 The Lagrangian Manifolds

The eigenvalue equations for the A- and B-lists of operators in (4.2) - (4.3) lead to Hamilton-Jacobi equations that correspond to two lists of classical observables,

$$A = (I_1, I_2, I_3, I_4, \mathbf{J}_{12}^2, \mathbf{J}_{\rm tot}), \tag{4.8}$$
$$B = (I_1, I_2, I_3, I_4, \mathbf{J}_{23}^2, \mathbf{J}_{\rm tot}), \tag{4.9}$$

where the functions I_r and J_{ri}, $r = 1, 2, 3, 4$, are defined as follows:

$$I_r = \frac{1}{2}\sum_{\mu=1}^{2} \overline{z}_{r\mu} z_{r\mu}\,, \qquad J_{ri} = \frac{1}{2}\sum_{\mu=1}^{2} \overline{z}_{r\mu} (\sigma^i)_{\mu\nu} z_{r\nu}\,. \tag{4.10}$$

These functions are the Weyl symbols of the corresponding operators. The correspondences between operators and their symbols are listed in table 4.1.

As discussed in chapter 3, the Lagrangian manifolds that support the semiclassical approximations to the states $|A\rangle$ and $|B\rangle$ are the level sets of these lists of classical observables in the phase space $\Phi_{4j} = (\mathbb{C}^2)^4 = \mathbb{C}^8$. We will call the level sets of the A- and B-lists the A- and B-manifolds, respectively.

We denote the lists of contour values, which are related to the eigenvalues in the asymptotic limit, by a and b. We have

$$a = (J_1, J_2, J_3, J_4, J_{12}^2, \mathbf{0}), \tag{4.11}$$
$$b = (J_1, J_2, J_3, J_4, J_{23}^2, \mathbf{0}), \tag{4.12}$$

where $J_r = j_r + 1/2$, $r = 1, 2, 3, 4, 12, 23$. Let us work with the A-manifold first, since the analysis for the B-manifold is completely analogous.

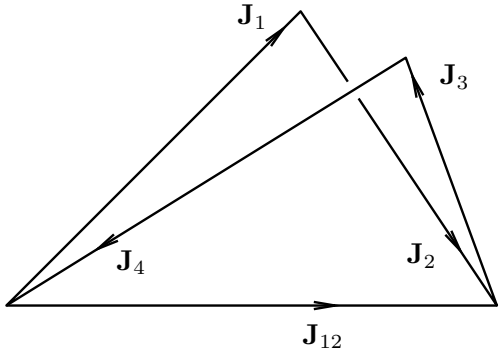

Figure 4.1: Visualizing the A-manifold in angular momentum space

Let us pick a point on the A-manifold, and evaluate the vector functions $\mathbf{J}_r$, $r = 1, \ldots, 4$ to find its projection in the angular momentum space. These vectors can be arranged into a geometric figure in $\mathbb{R}^3$, as follows. We compute the vector $\mathbf{J}_{12} = \mathbf{J}_1 + \mathbf{J}_2$, and arrange the vectors $(\mathbf{J}_1, \mathbf{J}_2, -\mathbf{J}_{12})$ to create a triangle with sides (J_1, J_2, J_{12}). Also, since $\mathbf{J}_{\text{tot}} = \mathbf{0}$, we can arrange the vectors $(\mathbf{J}_3, \mathbf{J}_4, \mathbf{J}_{12})$ into a second triangle, creating a figure like figure 4.1. The condition $A = a$ does not fix the dihedral angle between the two triangles at the edge $\mathbf{J}_{12}$, nor does it specify the orientation of the tetrahedron having these two triangles as two of its faces. Thus, using an action of the group $SO(2) \times SO(3)$ generated by $\mathbf{J}_{12}^2$ and $\mathbf{J}_{\text{tot}}$, regarded as observables on the angular momentum space, we can find all the other vectors that satisfy the conditions $A = a$. Thus we see that the projection of the A-manifold onto the angular momentum space is topologically $SO(2) \times SO(3)$. The $SO(2)$ action generated by $\mathbf{J}_{12}^2$ projects to a "butterfly" motion illustrated in figure 4.2, in which the butterfly flaps one of its wings. As the triangle 1-2-12 rotates around the edge 12, the length $|\mathbf{J}_{23}|$ varies between a maximum and minimum value. The minimum value is reached when triangles 1-2-12 and 3-4-12 lie in the same plane on the same side of line 12, and the maximum is reached on the opposite sides of line 12.

At each point in this projection, there is a 4-torus fiber, where I_r, $r = 1, \ldots, 4$, generate the flows along the fiber. Thus we have an action of $U(1)^5 \times SU(2)$ on the A-manifold the large phase space, which projects onto an action of $SO(2) \times SO(3)$ in the angular momentum space.

To find the topology of the A-manifold, we first find the isotropy subgroup of the $U(1)^5 \times SU(2)$ action on a point x_0 on this manifold. If we denote coordinates on $U(1)^5 \times SU(2)$ by $(\psi_1, \psi_2, \psi_3, \psi_4, \theta, u)$, where $u \in SU(2)$ and where the five angles are

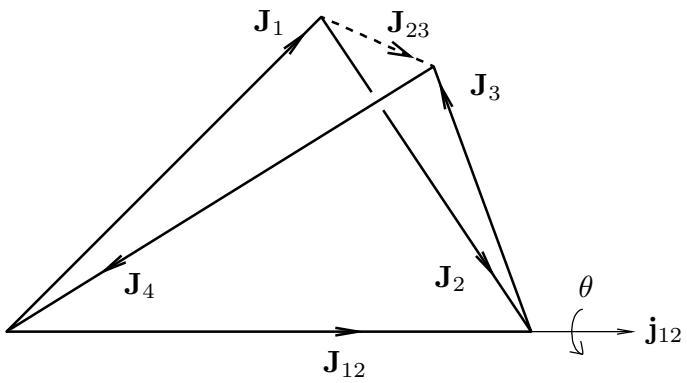

Figure 4.2: The function $\mathbf{J}_{12}^2$ generates a rotation about axis $\mathbf{j}_{12}$ of vectors $\mathbf{J}_1$ and $\mathbf{J}_2$, rotating triangle 1-2-12 by an angle θ while leaving triangle 3-4-12 fixed. The result is a family of tetrahedra with different values of J_{23}, which is a function of θ.

the 4π-periodic evolution variables corresponding to $(I_1, I_2, I_3, I_4, \mathbf{J}_{12}^2)$, respectively, then the isotropy subgroup is generated by two elements, say, $x = (2\pi, 2\pi, 2\pi, 2\pi, 0, -1)$ and $y = (0, 0, 2\pi, 2\pi, 2\pi, -1)$. The isotropy subgroup itself is the group with four elements $e, x, y, xy = (\mathbb{Z}_2)^2$. Thus the A-manifold is topologically $U(1)^5 \times SU(2)/(\mathbb{Z}_2)^2$. The analysis is the same for the B-manifold.

Now it is easy to find the invariant measure on the A- and B-manifolds. It is $d\psi_1 \wedge d\psi_2 \wedge d\psi_3 \wedge d\psi_4 \wedge d\theta \wedge du$, where du is the Haar measure on $SU(2)$. Thus, the volume of the A- or B-manifold with respect to this measure is

$$V_A = V_B = \frac{1}{4}(4\pi)^5 \times 16\pi^2 = 2^{12}\pi^7 \,, \tag{4.13}$$

where the 1/4 compensates for the 4-element isotropy subgroup.

4.4 Intersections of Manifolds

The intersections of the projections of the two Lagrangian manifolds in the angular momentum space are the solutions to the following equations:

$$\begin{aligned} |\mathbf{J}_r| &= J_r \,, & \sum_{r=1}^{4} \mathbf{J}_r &= \mathbf{0} \,, \\ |\mathbf{J}_1 + \mathbf{J}_2| &= J_{12} \,, & |\mathbf{J}_2 + \mathbf{J}_3| &= J_{23} \,, \end{aligned} \tag{4.14}$$

where $J_r = j_r + 1/2$, $r = 1, \ldots, 4$, $J_{12} = j_{12} + 1/2$ and $J_{23} = j_{23} + 1/2$.

A nice way of constructing these vectors uses the singular value decomposition of the Gram matrix of dot products. We define three auxiliary vectors

$$\begin{aligned}
\mathbf{A}_1 &= \mathbf{J}_1\,, && (4.15)\\
\mathbf{A}_2 &= \mathbf{J}_1 + \mathbf{J}_2 = \mathbf{J}_{12}\,, && (4.16)\\
\mathbf{A}_3 &= \mathbf{J}_1 + \mathbf{J}_2 + \mathbf{J}_3 = -\mathbf{J}_4\,, && (4.17)
\end{aligned}$$

which are the three vectors running along the edges emanating from the lower left vertex in figure 4.3. We arrange these vectors as columns of a 3×3 matrix F, and we let $G = F^T F$, where T means transpose. Then G is the symmetric, nonnegative definite Gram matrix of dot products, that is,

$$G_{ij} = \mathbf{A}_i \cdot \mathbf{A}_j\,. \tag{4.18}$$

The components of G can be found in terms of the six lengths $\mathbf{J}_r$, $r = 1, 2, 3, 4, 12, 23$, as follows:

$$\begin{aligned}
G_{11} &= A_1^2 = J_1^2\,, \qquad G_{22} = A_2^2 = J_{12}^2\,, \qquad G_{33} = A_3^2 = J_4^2\,,\\
G_{12} &= G_{21} = \mathbf{A}_1 \cdot \mathbf{A}_2 = \frac{1}{2}\,(J_{12}^2 + J_1^2 - J_2^2)\,,\\
G_{13} &= G_{31} = \mathbf{A}_1 \cdot \mathbf{A}_3 = \frac{1}{2}\,(J_1^2 + J_4^2 - J_{23}^2)\,, && (4.19)\\
G_{23} &= G_{32} = \mathbf{A}_2 \cdot \mathbf{A}_3 = \frac{1}{2}\,(J_{12}^2 + J_4^2 - J_3^2)\,.
\end{aligned}$$

Suppose the singular decomposition of F is $F = UDV^T$, where U and V are real orthogonal matrices and D is a real diagonal matrix, containing the real singular values d_i on the diagonal. Then $G = VD^2V^T$, so V is the orthogonal matrix that diagonalizes G and the eigenvalues of G are d_i^2. In order to find F, we first construct G by (4.19) and diagonalize it to obtain V and the eigenvalues d_i^2 of G. If these eigenvalues are nonnegative, then their square roots are the singular values d_i of F, and the matrix D is determined. This does not determine U, but that matrix amounts to an overall rotation of the tetrahedron which is arbitrary anyway. So we can set U to anything convenient, such as the identity matrix. Then we have $F = DV^T$, and the vectors $\mathbf{A}_i$ can be obtained as the columns of F. From these we can find the $\mathbf{J}$'s by inverting (4.19) and using $\mathbf{J}_{12} = \mathbf{J}_1 + \mathbf{J}_2$ and $\mathbf{J}_{23} = \mathbf{J}_2 + \mathbf{J}_3$. The resulting vectors $\mathbf{J}_r$, $r = 1, 2, 3, 4$, $\mathbf{J}_{12}$, $\mathbf{J}_{23}$ in the angular momentum space form a tetrahedron, which is illustrated in figure 4.3.

This method not only gives an explicit solution to (4.14) for these vectors, it also shows that they are unique to within an overall action of $O(3)$. The group $O(3)$ can be conveniently decomposed into proper rotations in $SO(3)$ and spatial inversion. It is a basic fact of geometrical figures in $\mathbb{R}^3$ that spatial inversion is not equivalent to any proper rotation unless the figure is planar. Therefore, the solution set of (4.14) in the angular momentum space in general consists of two disconnected subsets, each diffeomorphic to $SO(3)$, related by spatial inversion. Each subset consists of tetrahedra of nonzero volume related by proper rotations. At values where the tetrahedron is flat but still 2-dimensional, the two subsets merge into one, which is still diffeomorphic to $SO(3)$.

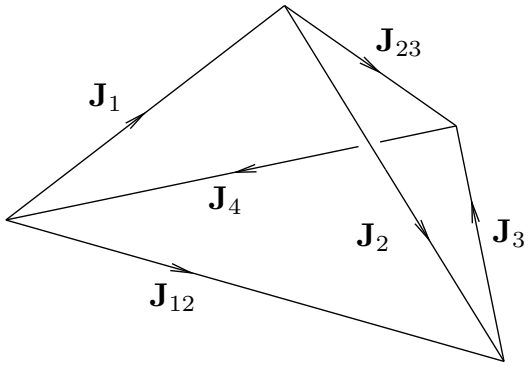

Figure 4.3: One of the two intersections is represented by a tetrahedron with the six lengths J_r, $r = 1, \ldots, 4$, J_{12}, and J_{23}. The other intersection is represented by its mirror image.

The inverse image of π at each point of the intersection set in the angular momentum space is a 4-torus fiber in the large phase space. Any point in this fiber satisfies the conditions (4.14). Thus, in general, the intersection of the A- and B-manifolds in the large phase space consists of two disconnected subsets, where each subset is a 4-torus bundle over $SO(3)$. These subsets are 7-dimensional, so the A- and B-manifolds, which are 8-dimensional, intersect in two 7-dimensional submanifolds. The situation can be visualized as in figure 4.4, where $A \cap B = I_1 \cup I_2$, and where I_1 and I_2 are the connected intersection sets. Each intersection set is an orbit of the group $U(1)^4 \times SU(2)$. The $U(1)^4$ action is generated by I_r, $r = 1, \ldots, 4$, and represents the phases of the four spinors. The $SU(2)$ action is generated by the total angular momentum $\mathbf{J}_{\rm tot}$.

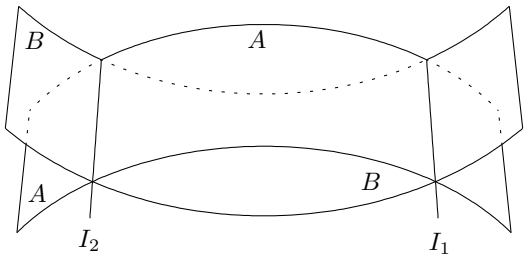

Figure 4.4: An illustration of the intersection of the two 8-dimensional A- and B-manifolds in the large phase space. The two intersections I_1 and I_2 are 7-dimensional.

The isotropy subgroup of this group is $\mathbb{Z}_2$, generated by element $(2\pi, 2\pi, 2\pi, 2\pi, -1)$ in the coordinates $(\psi_1, \psi_2, \psi_3, \psi_4, u)$ for the group actions of $U(1)^4 \times SU(2)$, where $u \in SU(2)$. The volume of the intersection manifold I_1 or I_2 with respect to the measure $d\psi_1 \wedge d\psi_2 \wedge d\psi_3 \wedge d\psi_4 \wedge du$ is

$$V_I = \frac{1}{2}\,(4\pi)^4 \times 16\pi^2 = 2^{11}\,\pi^6\,, \tag{4.20}$$

where the 1/2 compensates for the two element isotropy subgroup.

4.5 Amplitude Determinant

The amplitude determinant in the WKB theory is given by the determinant of Poisson brackets between the two distinct subsets of the lists of observables. These subsets are $D = \mathbf{J}_{12}^2$ in the A-list, and $E = \mathbf{J}_{23}^2$ in the B-list. However, since we have used $d\theta$ in the volume form on the A- and B-manifolds when computing the volumes V_A and V_B in (4.13), we should use instead $D = J_{12} = \mathbf{j}_{12} \cdot \mathbf{J}_{12}$ in the A-list, and $E = J_{23}^2 = \mathbf{j}_{23} \cdot \mathbf{J}_{23}$ in the B-list. The Poisson bracket for the amplitude evaluated at the intersection manifold I_1 is then given by

$$\{E,\, D\} = \{J_{12},\, J_{23}\} = \frac{\mathbf{J}_2 \cdot [(\mathbf{J}_2 + \mathbf{J}_3) \times (\mathbf{J}_1 + \mathbf{J}_2)]}{|\mathbf{J}_{12}|\, |\mathbf{J}_{23}|} = \frac{6V}{J_{12} J_{23}}\,, \tag{4.21}$$

where V is the signed volume of the tetrahedron, $6V = \mathbf{J}_1 \times (\mathbf{J}_2 \times \mathbf{J}_3)$, and where we have used (3.34) to evaluate the Poisson bracket. Thus the two stationary phase sets have the same amplitude.

Note that the amplitude $|\Omega|^{1/2}$ contains the factor

$$\sqrt{J_{12} J_{23}} = \frac{1}{2} \sqrt{(2j_{12}+1)(2j_{23}+1)}\,, \tag{4.22}$$

which cancels the square roots seen in the definition of the $6j$-symbol in (4.1).

4.6 The Action Integral in the Reduced Phase Space

Since the A- and B-manifold intersect at two subsets I_1 and I_2, the WKB formula for the inner product $\langle A|B\rangle$ has two terms, that is,

$$\langle B|A\rangle = \frac{(2\pi i)^{1/2}}{\sqrt{V_A V_B}}\; V_I\, |\Omega|^{1/2}\; \left(\exp[i[S_{A1} - S_{B1} - \mu_1 \pi/2]] + \exp[i[S_{A2} - S_{B2} - \mu_2 \pi/2]]\right)\,, \tag{4.23}$$

where S_{Ai} and S_{Bi} are the actions $S_A(x)$ and $S_B(x)$, respectively, evaluated on the two intersection I_i, $i = 1, 2$. Figure 4.5 illustrates two points p_1 and p_2 on the intersection manifolds I_1 and I_2, respectively, as well as paths that may be used to compute the actions S_A and S_B.

Let us define

$$S_1 = S_{A1} - S_{B1}\,, \qquad S_2 = S_{A2} - S_{B2}\,. \tag{4.24}$$

Since we are not fixing the overall phase, we can factor out a common phase factor to find

$$\begin{aligned} & e^{i(S_1 - \mu_1\pi/2)} + e^{i(S_2 - \mu_2 \pi/2)} \\ = \;& e^{i(S_1+S_2)/2 - i(\mu_1+\mu_2)\pi/4} \left(e^{i(S_1 - S_2)/2 + i(\mu_2 - \mu_1)\pi/4} + e^{i(S_2 - S_1)/2 + i(\mu_1 - \mu_2)\pi/4)} \right) \\ = \;& e^{i(S_1+S_2)/2 - i(\mu_1+\mu_2)\pi/4} \cos\left[(S_2 - S_1)/2 - (\mu_2 - \mu_1)\pi/4\right]\,. \end{aligned}$$

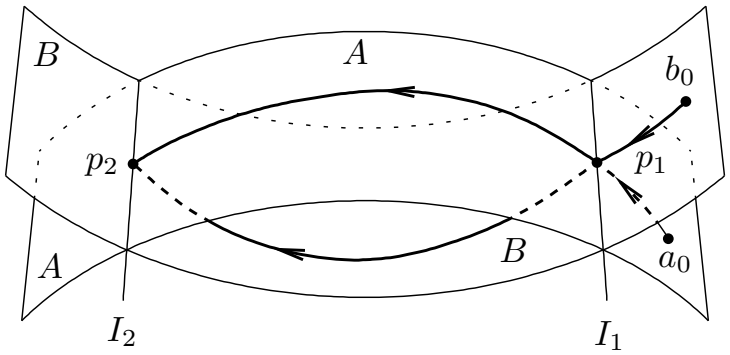

Figure 4.5: Paths for computing action functions S_A and S_B relative to initial points a_0 and b_0 on the two manifolds are shown.

Thus, disregarding an overall phase, we only need to calculate the relative phase $S = S_2 - S_1$ to compute the WKB formula. Moreover, S can be expressed as a line integral along the path that goes from p_1 to p_2 along the A-manifold and then back to p_1 along the B-manifold, as illustrated in figure 4.4. That is,

$$S = S_2 - S_1 = \int_{a_0}^{p_2} - \int_{b_i}^{p_2} - \int_{a_0}^{p_1} + \int_{b_0}^{p_1} p\, dx = \oint p\, dx\,. \tag{4.25}$$

The loop integral can also be rewritten by Stokes' theorem as an integral of the symplectic two form over an enclosed area, since on $\Phi_{4j} = \mathbb{C}^8$ all cycles are boundaries. By carefully choosing the path, we can assume that the winding numbers around the 4-torus in the intersection sets I_1 and I_2 are all zero, so the loop is also a boundary in the level set of $(I_1, I_2, I_3, I_4, \mathbf{J}_{\rm tot})$. We calculate the loop integral by projecting the symplectic area enclosed onto an area in a reduced phase space, through a symplectic reduction by the symmetries generated by $(I_1, I_2, I_3, I_4, \mathbf{J}_{\rm tot})$.

We carry out the symplectic reduction [1, 53] in two steps. In the first step, we start with the level set $I_r = J_r$ in the large phase space $(\mathbb{C}^2)^4$, which is the product of 3-spheres $(S^3)^4$. The I_r, $r = 1, \ldots, 4$, generate the action of the group $U(1)^4$, corresponding to the phases of the four spinors. After dividing this level set by the $U(1)^4$ action, we obtain the space of orbits Σ_{4j}, which is topologically $(S^2)^4$, consisting of the set of four vectors $\mathbf{J}_r$ in $\mathbb{R}^3$, $r = 1, \ldots, 4$, with fixed lengths $|\mathbf{J}_r| = J_r$. The space Σ_{4j} is 8-dimensional. In the second step, we consider the level set of the momentum map of the action of $SO(3)$ on Σ_{4j}, given by $\mathbf{J}_{\rm tot} = \mathbf{0}$. This manifold consists of the set of four vectors $\mathbf{J}_r$ in $\mathbb{R}^3$ of fixed lengths J_r such that $\sum_r \mathbf{J}_r = \mathbf{0}$. The vectors can be placed end-to-end to form a closed link, that is, a four-sided polygon in $\mathbb{R}^3$. After dividing by the $SO(3)$ action, which changes the orientation of the four-sided polygon, we obtain the shape space of the four-sided polygon. This is the reduced phase space, which we denote by Γ.

A point in this space specifies a quadrilateral in $\mathbb{R}^3$, modulo overall proper rotations. We can draw in the two remaining edges, of lengths J_{12} and J_{23} to fill in a tetrahedron. The lengths J_{12} and J_{23} are variable functions on this reduced space. In fact, any rota-

tionally invariant quantity associated with the tetrahedron, such as the dihedral angles, the areas of the faces, the signed volume, etc, is also a function on Γ.

It is easy to find two independent functions on Γ as coordinates on it. We may take one coordinate to be J_{12}. For a fixed value of J_{12}, the allowed set of shapes is generated by executing the butterfly motion about the axis $\mathbf{J}_{12}$, that is, rotating the triangle 1-2-12 about this axis, relative to the 3-4-12 triangle, so the remaining coordinate can be taken to be the dihedral angle ϕ_{12} at the edge 12. Thus, coordinates on Γ can be taken to be (J_{12}, ϕ_{12}).

For each value of J_{12}, a circle of shapes is generated as ϕ_{12} goes from 0 to 2π. However, at the endpoints where J_{12} reaches its maximum or minimum values, and one of the 1-2-12 or 3-4-12 triangles degenerates into a line, there is only a single shape. For example, the case $J_{12} = J_{12,\min} = |J_1 - J_2|$ is illustrated in part (a) of figure 4.6. In this case the rotation of vectors $\mathbf{J}_1$ and $\mathbf{J}_2$ about the axis $\mathbf{J}_{12}$ does not change the shape. Similarly, part (b) illustrates the case $J_{12} = J_{12,\min} = |J_3 - J_4|$. In both cases, the $\mathbf{J}_{12}^2$-action rotates the 1-2-12 triangle, but does not change the shape since the new configurations that result are related to the original ones by an overall $SO(3)$ transformation. A similar analysis applies for the case $J_{12} = J_{12,\max}$.

Figure 4.6: When J_{12} is at its lower limit for given (J_1, J_2, J_3, J_4), the shape of the tetrahedron degenerates into the shape of a flag, which is not changed under the $\mathbf{J}_{12}^2$-action. Thus the lower limit corresponds to only one point of the reduced phase space.

We see that the set of shapes generated in this manner for all allowed values of J_{12} is a cylinder with two endpoints pinched to two points, creating a topological sphere. We conclude that $\Gamma = S^2$ topologically.

The symplectic form on Γ may be obtained by projecting $\omega = dp \wedge dx$ on $\Phi_{4j} = \mathbb{C}^8$ to $\Gamma = S^2$, but it is easier just to notice that ϕ_{12} is the parameter of evolution along the flow generated by J_{12}, so (ϕ_{12}, J_{12}) form a canonically conjugate (q, p) pair on the sphere. The same obviously applies to J_{23} and its conjugate dihedral angle ϕ_{23}, so we have

$$dJ_{12} \wedge d\phi_{12} = dJ_{23} \wedge d\phi_{23}\,, \tag{4.26}$$

indicating two sets of canonical coordinates on Γ, related by canonical transformations. These are examples of the action-angle variables discovered by Kapovich and Millson [44, 45]. The area of the sphere Γ with respect to the form $dJ_{12} \wedge d\phi_{12}$ is obviously just $2\pi(J_{12,\max} - J_{12,\min})$. The area is $2\pi D$, where $D = \dim \mathcal{Z}$.

The A-manifold projects to a level set of J_12 in Γ. To plot these level sets of J_12, we map Γ into a unit 2-sphere in $\mathbb{R}^3$ with standard coordinates (x, y, z) by associating

(ϕ_{12}, J_{12}) with a standard set of spherical angles (θ, ϕ), where $\phi = \phi_{12}$ and θ is defined by

$$J_{12} = J_{12,\min} + \frac{D}{2}\,(1 + \cos\theta)\,. \tag{4.27}$$

Then the symplectic form on the sphere is $(-1/2)D \sin\theta d\theta \wedge d\phi$.

The quantized orbits of J_{12} on the space Γ are illustrated in part (a) of figure 4.7, for $D = 4$. The orbits are just small circles. The minimum and maximum values of J_{12} are at the south and north poles, respectively.

The length J_{23} as a function of $J_1, J_2, J_3, J_4, J_{12}$ and ϕ_{12} can be derived from the geometry of the tetrahedron. It is given by [76]

$$\begin{aligned} J_{23}^2 &= \frac{1}{2J_{12}^2}\left[(J_{12}^2(-J_{12}^2 + J_1^2 + J_2^2) + J_3^2(J_{12}^2 + J_1^2 - J_2^2) + J_4^2(J_{12}^2 - J_1^2 + J_2^2)\right] \\ &+ \frac{8}{J_{12}^2}\,F(J_{12}, J_1, J_2)\,F(J_{12}, J_3, J_4)\,\cos\phi_{12}\,, \end{aligned} \tag{4.28}$$

where $F(a, b, c)$ is the area of a triangle with sides a, b, c, that is,

$$F(a, b, c) = \frac{1}{4}[(a + b + c)(-a + b + c)(a - b + c)(a + b - c)]^{1/2}\,. \tag{4.29}$$

The B-manifold projects onto a level set of J_{23}. Some of these J_{23} level sets are illustrated in parts (b) and (c) of that figure. The function J_{23} has a minimum on the x-z plane with $x > 0$, and increases monotonically toward a maximum on the same plane with $x < 0$. The orbits are symmetric across the plane $\theta_{12} = 0$.

The intersection sets I_1 and I_2 of the A- and B-manifolds project onto the intersection points of the level sets of J_{12} and J_{23} on Γ, which are labelled P and Q in part (d) of figure 4.8, respectively. We associate P with I_1. Since the point P lies in the region $y < 0$, which satisfies $V < 0$, we take I_1 as the intersection manifold upon which $V < 0$.

Consider a path on Γ that starts at P, and follow the level set of J_{12} to Q, and then back to P along the level set of J_{23}. This path is the projection of the loop for the integral (4.25) in the large phase space Φ_{4j}. We note that the space Φ_{4j} and Γ are related by symplectic reduction, so the symplectic area of the shaded region in Γ, as shown in part (f) of figure 4.7, is equal to the symplectic area of the region bounded by the closed loop for the action integral in the level set of $(I_1, I_2, I_3, I_4, \mathbf{J}_{\rm tot})$. Thus

$$S = 2\int_{J_{12,\,\rm lower}}^{J_{12}} \phi_{12}\, dJ_{12}\,, \tag{4.30}$$

where $J_{12,\,\rm lower}$ is the minimum value of J_{12} on the level set of J_{23}.

Using the Schläfli identity [76], which states

$$d\left(\sum_i J_i\phi_i\right) = \sum_i \phi_i dJ_i\,, \tag{4.31}$$

we have

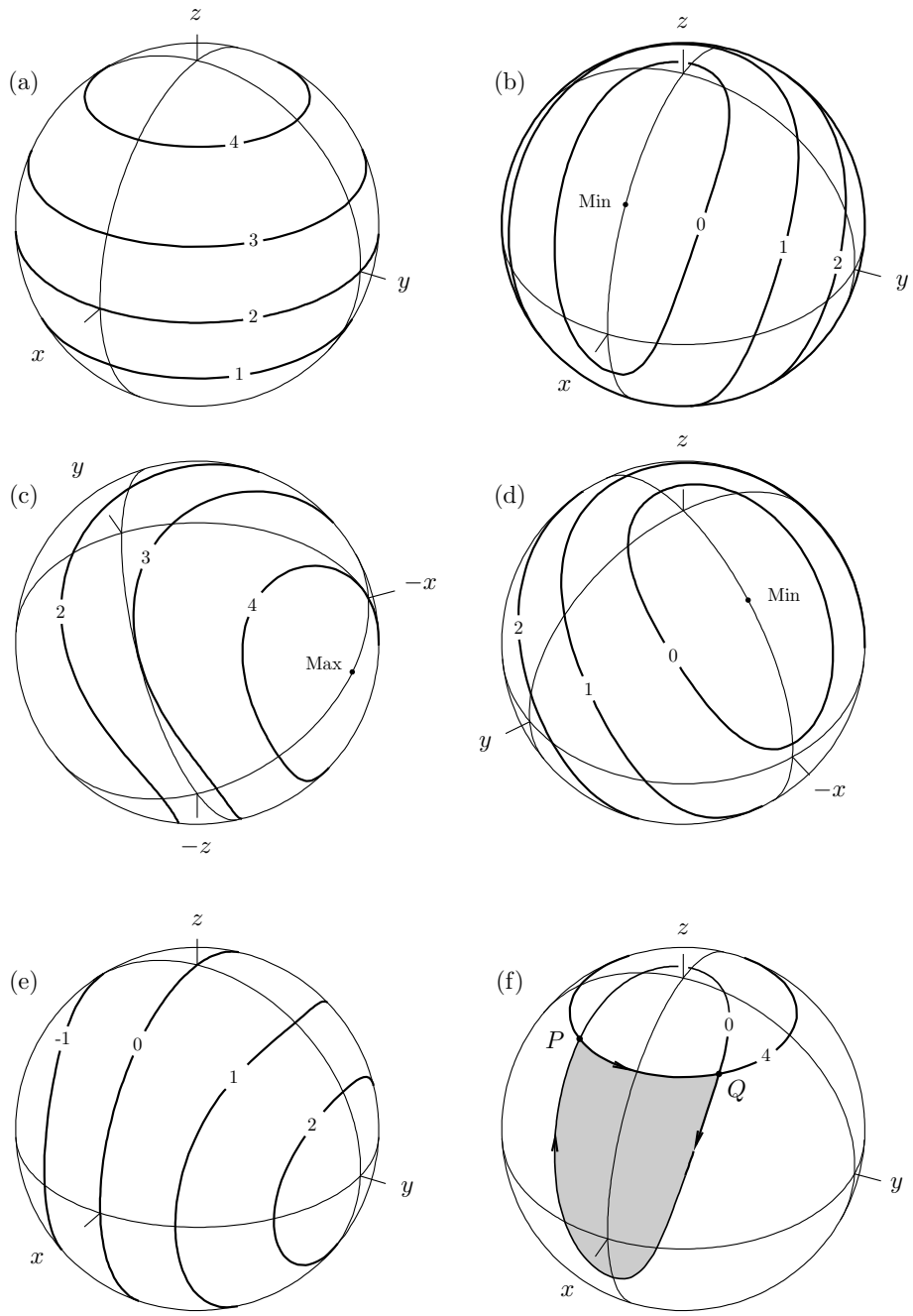

Figure 4.7: Orbits on the reduced phase space. In (a), orbits of J_{12}; in (b) and (c), of J_{23}; in (d), of J_{13}; in (e), of the volume V. Part (f) shows the orbits relevant to the $6j$-symbol.

$$\frac{\partial}{\partial J_{12}}\left(\sum_i J_i\phi_i\right) = \phi_{12}\,, \tag{4.32}$$

where $i = 1, 2, 3, 4, 12, 23$, and ϕ_i are the internal dihedral angles expressed as functions of the six J_i. Thus the anti-derivative of ϕ_{12} is $\sum_i J_i\phi_i$, and we find

$$S = 2\sum_i J_i\phi_i + S_0\,, \tag{4.33}$$

where S_0 is an integration constant. This constant can be found by evaluating S at $J_{12,\,\mathrm{lower}}$. The result is that S_0 is a half-integer multiple of π. See (5.92) in chapter 5 for more details. Thus, we conclude that

$$S = 2\sum_i J_i\phi_i + S_0 = -2\sum_i J_i\psi_i + \frac{n\pi}{2}\,, \tag{4.34}$$

where the constant term contributes to the overall phase and the Maslov index.

4.7 The Asymptotic Formula

Thus, based on the pieces of the formula (4.23) we have determined so far, we find the asymptotic formula for the $6j$-symbol,

$$\left\{\begin{array}{ccc} j_1 & j_2 & j_{12} \\ j_3 & j_4 & j_{23} \end{array}\right\} = (\text{phase}) \times \frac{1}{\sqrt{12\pi|V|}}\,\cos\left[\sum_i J_i\psi_i + \pi/4\right]\,, \tag{4.35}$$

where we have guessed the Maslov index.

4.8 The Action Integral in the Large Phase Space

Let us find an explicit loop in the large phase space Φ_{4j}, and calculate the relative phase S more directly from an action integral on this loop. This provides an independent verification of the result for the relative phase in (4.34).

In computing the relative phase, we note that the loop integral in (4.25) can be evaluated with respect to the complex one-form

$$\oint \sum_{r\mu} p_{r\mu}\,dx_{r\mu} = \mathrm{Im}\oint \sum z_{r\mu}d\overline{z}_{r\mu}\,, \tag{4.36}$$

which differ from the symplectic form by an exact form. See (3.71) for more information on this complex one-form.

We shall construct the loop by following the Hamiltonian flows of the observables $(I_1, I_2, I_3, I_4, \mathbf{J}, J_{12}^2, J_{23}^2)$. Let us start at a point p at the intersection I_1 that has $V < 0$. Since the flows generated by $(I_1, I_2, I_3, I_4, \mathbf{J})$ confine us to I_1, we follow the J_{12}^2-flow, and trace out a path on the A-manifold that takes us to a point q on I_2. Similarly, to go back to another point p' in I_1, we follow the J_{23}^2-flow, and trace out a path on the B-manifold.

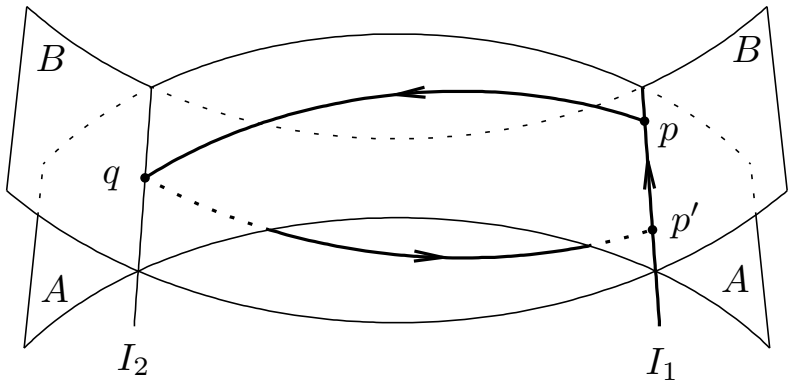

Figure 4.8: The $\mathbf{J}^2_{12}$-flow takes us from a point p of intersection manifold I_1 along the A-manifold to a point q of maniofld I_2; and then the $\mathbf{J}^2_{23}$-flow takes us back to point p' of I_1. To close the loop it is necessary to connect p' to p inside I_1.

Finally, we follow the flows generated by $(I_1, I_2, I_3, I_4, \mathbf{J})$ to trace out a path from p' back to p along I_1.

The J^2_{12}-flow rotates triangle 1-2-12 about the axis $\mathbf{j}_{12} = \mathbf{J}_{12}/J_{12}$, while leaving triangle 3-4-12 fixed. By choosing the angle of rotation to be twice the interior dihedral angle along edge 12, that is, $2\phi_{12}$, as illustrated in part (a) of figure 4.9, we get another tetrahedron with the same edge lengths, but with an inverted volume, as illustrated in part (b) of that figure. Thus, $2\phi_{12}$ is the correct angle to reach a point in I_2. Similarly, the J^2_{23}-flow rotates triangle 2-3-23 about the axis $\mathbf{j}_{23}$, while leaving 1-4-23 triangle fixed. To get back to a point p' in I_1, we choose the angle of rotation to be twice the interior dihedral angle along edge 23, that is, $2\phi_{23}$, as illustrated in part (c) of figure 4.9. The result is part (d) of that figure, a tetrahedron in which the volume has been inverted a second time, taking us back to the original, negative, volume in part (a).

To close the loop, we must get back to the starting point p from p' in I_1, by following the flows generated by $(I_1, I_2, I_3, I_4, \mathbf{J})$. We first apply an $SU(2)$ action generated by $\mathbf{J}$ to the point p' to reach another point p'' in I_1, whose projection onto the angular momentum space is an $SO(3)$ transformation of the tetrahedron in part (d) of figure 4.9, returning it to the original orientation in part (a) of that figure. Then we follow the flows of I_r, $r = 1, \ldots, 4$ to transform the overall phases of the four spinors back to their original values at p.

The necessary $SO(3)$ rotation is uniquely determined by its transformation on one of the triangle faces of the tetrahedron. Notice that the vector $\mathbf{J}_4$ is fixed by both the J^2_{12}-flow and the J^2_{23}-flow. Thus, the $SO(3)$ rotation must be a rotation about $\mathbf{J}_4$. Let us look at the transformation of the triangle 1-4-23 from part (a) to part (d) of figure 4.9. The effect of the J^2_{12}-flow on $\mathbf{J}_1$ is the same as that of a rotation about $\mathbf{J}_4$ by an angle $2\phi_4$, twice the internal dihedral angle along edge 4, since both rotations effectively reflect $\mathbf{J}_1$ across the triangle 1-4-23. To undo its effect on $\mathbf{J}_1$, we apply a rotation about $-\mathbf{j}_4$ by the angle $2\phi_4$. Since the J^2_{23}-flow does not change $\mathbf{J}_1$, this rotation about $-\mathbf{j}_4$ is the necessary

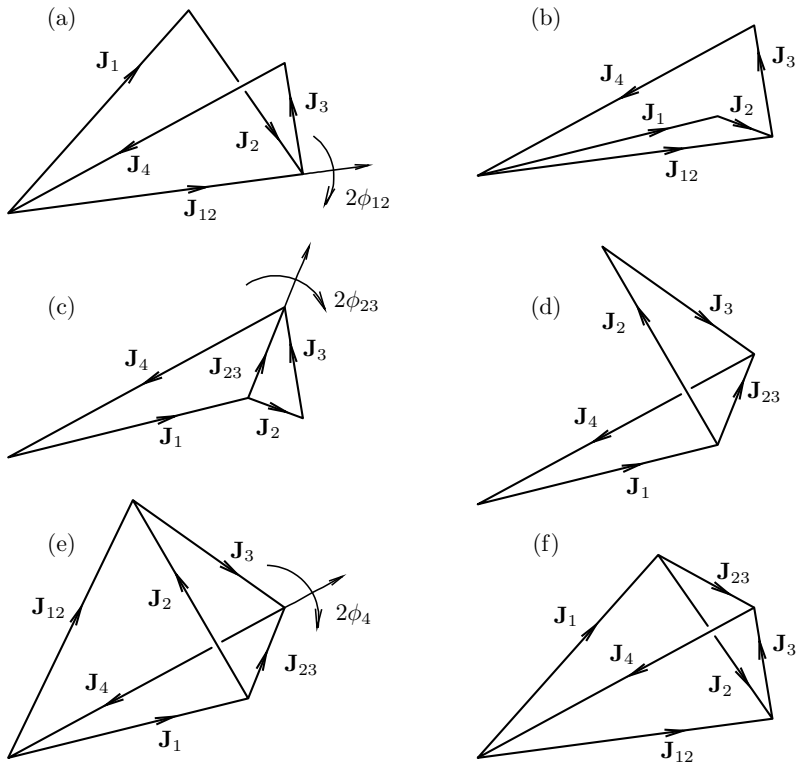

Figure 4.9: A cycle of rotational transformations that takes a tetrahedron in $\mathbb{R}^3$ back into itself.

$SO(3)$ rotation that returns the tetrahedron back to its original orientation. This rotation is illustrated in part (e) of figure 4.9, which is the same as part (d) except that all vectors are drawn. The effect of the final rotation is illustrated in part (f), which is the same as part (a) except that all vectors are drawn.

To summarize the rotational history in the angular momentum space, we have applied the rotations

$$R(-\mathbf{j}_4, 2\phi_4) R_{23}(\mathbf{j}'_{23}, 2\phi_{23}) R_{12}(\mathbf{j}_{12}, 2\phi_{12}) \,, \tag{4.37}$$

where R_{12} acts only on $\mathbf{J}_1$ and $\mathbf{J}_2$, and R_{23} acts only on $\mathbf{J}_2$ and $\mathbf{J}_3$, and $R(-\mathbf{j}_4, 2\phi_4)$ acts on all four vectors. The corresponding $SU(2)$ rotations, with the same axes and angles, take us from point p in figure 4.8 to another point p'' along the sequence $p \to q \to p' \to p''$. The point p'', which is not shown in figure 4.8, has the same projection onto angular momentum space as p. Thus p and p'' differ by the phases of the four spinors. We close the loop and move from p'' to p along the Hamiltonian flows generated by (I_1, I_2, I_3, I_4).

Let us find the four phases for the four spinors. We start with the first spinor, by looking at the actions of the rotations (4.37) on the vector $\mathbf{J}_1$,

$$R(-\mathbf{j}_4, 2\phi_4)\, R_{12}(\mathbf{j}_{12}, 2\phi_{12})\, \mathbf{J}_1 = \mathbf{J}_1 \,, \tag{4.38}$$

where we omit the subscripts on the R's because it is understood that only vector $\mathbf{J}_1$ is being acted upon, and where we omit the middle rotation in (4.37) since it does not act on $\mathbf{J}_1$. The product of the two rotations in (4.38) is not the identity, but it is a rotation about axis $\mathbf{j}_1$ since it leaves $\mathbf{J}_1$ invariant.

To find the angle of this rotation, we use the Rodrigues-Hamilton formula [91], which states that the product of three rotations about three axis meeting at a point, with the three rotation angles being twice the interior dihedral angles, is the identity rotation. For instance, applying the Rodrigues-Hamilton formula to the three axis $\mathbf{j}_{12}$, $-\mathbf{j}_4$, and $\mathbf{j}_1$ meeting at a vertex of the tetrahedron in part (f) of figure 4.9, we have

$$R(\mathbf{j}_1, 2\phi_1)\, R(-\mathbf{j}_4, 2\phi_4)\, R(\mathbf{j}_{12}, 2\phi_{12}) = I \,. \tag{4.39}$$

Thus, the product of the two rotations in (4.38) is $R(\mathbf{j}_1, -2\phi_1)$.

We now lift the rotations in (4.39) up to rotations in $SU(2)$, by replacing each $SO(3)$ rotation by an $SU(2)$ rotation with the same axis and angle. From (4.39), the product $u(\mathbf{j}_1, 2\phi_1) u(-\mathbf{j}_4, 2\phi_4) u(\mathbf{j}_{12}, 2\phi_{12})$ is either $+1$ or -1, depending on the homotopy class of the closed loop in $SO(3)$. To find this class, we continuously deform the tetrahedron, bringing dihedral angles ϕ_{12} to zero, so that the tetrahedron becomes flat. At the end of this deformation, $\phi_{12} = 0$ and one of ϕ_1 and ϕ_4 is 0 and the other is π. Thus, the closed loop in $SO(3)$ becomes an element of the non-contractible homotopy class of the homotopy group $\mathbb{Z}_2$ of $SO(3)$, so the product of the three $SU(2)$ matrices is -1, which is equivalent to a rotation about $\mathbf{j}_1$ by an angle 2π. Moving the factor $u(\mathbf{j}_1, 2\phi_1)$ to the other side, we find

$$u(-\mathbf{j}_4, 2\phi_4)\, u(\mathbf{j}_{12}, 2\phi_{12}) = u(\mathbf{j}_1, -2\phi_1)\, u(\mathbf{j}_1, 2\pi) \,. \tag{4.40}$$

The action of the two $SU(2)$ rotations on the right hand side of (4.40) on the first spinor at the point p is a pure phase. To undo this pure phase, we follow the Hamiltonian flow of I_1 by an angle $2\phi_1 - 2\pi$, which can be read off from (4.40).

Next we turn to the vector $\mathbf{J}_3$. The action of the rotations from (4.37) on $\mathbf{J}_3$ is given by

$$R(-\mathbf{j}_4, 2\phi_4)R(\mathbf{j}'_{23}, 2\phi_{23})\,\mathbf{J}_3 = \mathbf{J}_3\,, \tag{4.41}$$

where we omit the first rotation in (4.37), since it does not act on $\mathbf{J}_3$. Using the Rodrigues-Hamilton formula again at the 3-4-23 vertex of part (c) of figure 4.9, we find

$$R(-\mathbf{j}'_{23}, 2\phi_{23})\,R(\mathbf{j}_4, 2\phi_4)\,R(-\mathbf{j}_3, 2\phi_3) = I\,. \tag{4.42}$$

Now using $R(-\mathbf{a}, \alpha) = R(\mathbf{a}, \alpha)^{-1}$ and taking the inverse of (4.42), we obtain

$$R(\mathbf{j}_3, 2\phi_3)\,R(-\mathbf{j}_4, 2\phi_4)\,R(\mathbf{j}'_{23}, 2\phi_{23}) = I\,. \tag{4.43}$$

We now lift the rotations in (4.43) up to the rotations $u(\mathbf{j}_3, 2\phi_3)\,u(-\mathbf{j}_4, 2\phi_4)\,u(\mathbf{j}'_{23}, 2\phi_{23})$ in $SU(2)$. We find the homotopy class of this loop by taking $\phi_{23} \to 0$, which makes one of ϕ_4 and ϕ_3 zero and the other π, so the loop in $SO(3)$ belongs to the noncontractible class. Thus, the lift into $SU(2)$ is -1, which is equivalent to a rotation about $\mathbf{j}_3$ by angle -2π. Thus we find

$$u(-\mathbf{j}_4, 2\phi_4)\,u(\mathbf{j}'_{23}, 2\phi_{23}) = u(\mathbf{j}_3, -2\phi_3)\,u(\mathbf{j}_3, 2\pi)\,, \tag{4.44}$$

which when applied to the third spinor at point p in figure 4.8 generates an pure phase. To undo this pure phase, we follow the I_3-flow by the angle $2\phi_3 - 2\pi$.

As for $\mathbf{J}_2$, the rotations from (4.37) acting on it are given by

$$R(-\mathbf{j}_4, 2\phi_4)R(\mathbf{j}'_{23}, 2\phi_{23})R(\mathbf{j}_{12}, 2\phi_{12})\,\mathbf{J}_2 = \mathbf{J}_2\,. \tag{4.45}$$

We first use (4.43) to obtain

$$R(-\mathbf{j}_4, 2\phi_4)R(\mathbf{j}'_{23}, 2\phi_{23}) = R(-\mathbf{j}_3, 2\phi_3)\,. \tag{4.46}$$

Substituting this into (4.45) we obtain the product

$$R(-\mathbf{j}_3, 2\phi_3)\,R(\mathbf{j}_{12}, 2\phi_{12})\,. \tag{4.47}$$

The Rodrigues-Hamilton formula with reference to the 2-3-12 vertex of the original tetrahedron in part (a) of figure 4.9 gives

$$R(\mathbf{j}_2, 2\phi_2)R(-\mathbf{j}_3, 2\phi_3)R(\mathbf{j}_{12}, 2\phi_{12})\,\mathbf{J}_2 = I\,. \tag{4.48}$$

Thus, we find

$$R(\mathbf{j}_2, 2\phi_2)R(-\mathbf{j}_4, 2\phi_4)R(\mathbf{j}'_{23}, 2\phi_{23})R(\mathbf{j}_{12}, 2\phi_{12}) = I\,. \tag{4.49}$$

To find the homotopy class of this loop we deform the tetrahedron into a planar shape as before, and find that two of the four angles $(\phi_2, \phi_4, \phi_{23}, \phi_{12})$ are 0 and two are π. The loop

in $SO(3)$ thus becomes the product of two rotations with angles 2π, which belongs to the contractible homotopy class. Therefore the lift into $SU(2)$ is closed. We find

$$u(-\mathbf{j}_4, 2\phi_4)u(\mathbf{j}'_{23}, 2\phi_{23})u(\mathbf{j}_{12}, 2\phi_{12}) = u(\mathbf{j}_2, -2\phi_2)\,, \tag{4.50}$$

which when applied to the second spinor at point p in figure 4.8, generates an pure phase. To undo this pure phase, we follow the I_2-flow by the angle $2\phi_2$.

Finally, we treat vector $\mathbf{J}_4$. The effect of (4.37) on $\mathbf{J}_4$ is simply

$$R(-\mathbf{j}_4, 2\phi_4)\,\mathbf{J}_4 = \mathbf{J}_4\,, \tag{4.51}$$

since the first two rotations do not act on $\mathbf{J}_4$. When the lift of this rotation to $u(\mathbf{j}_4, 2\phi_4)$ in $SU(2)$ is applied to the fourth spinor at point p in figure 4.8, it generates an pure phase. To undo this pure phase, we follow the I_4-flow by the angle $2\phi_4$.

The actions associated with these spin rotations are easily computed, using the complex 1-form (3.71) and the methods of section 3.9. To summarize the results, let $\mathbf{J}_p$ be a partial or total sum of the four angular momentum vectors, with magnitude $|\mathbf{J}_p| = J_p$. Then the action along the path generated by $\mathbf{n}\cdot\mathbf{J}_p$ with elapsed angle θ is simply $(\mathbf{n}\cdot\mathbf{J}_p)\theta$. In particular, the third rotation in (4.37), the overall rotation of the tetrahedron, does not contribute to the action since in this case $\mathbf{J}_p = \mathbf{J}_{\rm tot}$ vanishes on the A- and B-manifolds. The first and second spin rotations specified by (4.37) contribute $J_{12}(2\phi_{12}) + J_{23}(2\phi_{23})$ to the total action. The action of the last four flows generated by I_r are given by $J_1(2\phi_1 - 2\pi) + J_2(2\phi_2) + J_3(2\phi_3 - 2\pi) + J_4(2\phi_4)$. Altogether, we have

$$S = \oint p dx = 2\sum_{r=1}^{6} J_r\phi_r - 2\pi(J_1 + J_3)\,, \tag{4.52}$$

where index $r = 5$ means $r = 12$ and $r = 6$ means $r = 23$. This can be written as

$$S = -2\sum_{r=1}^{6} J_r(\pi - \phi_r) + 2\pi(J_2 + J_4 + J_{12} + J_{23})\,, \tag{4.53}$$

where from quantization conditions the final term is an integer multiple of 2π. We recognize the first term is the phase of Ponzano and Regge.

4.9 Conclusions

In this chapter, we have used semiclassical analysis to derive the asymptotic formula of the Wigner $6j$-symbol. The derivation in this chapter is in parallel with those for the Wigner $3j$-symbol in chapter 3. Powerful techniques from classical mechanics, such as symmetries and symplectic reduction, have played a major role in our derivation. These techniques simplify the calculations of both the amplitude determinant and the action integral to a few simple lines.

The semiclassical analysis we have employed so far rely on the Weyl-symbol correspondence between operators on $L^2(\mathbb{R}^2)$ and functions on $\mathbb{C}^2$. For example, see table 4.1. There is another more direct route to the reduced phase space of the $6j$-symbol, through

the use of another symbol correspondence, called the Stratonovich-Weyl symbol correspondence. This symbol correspondence relate operators on $\mathbb{C}^{2j+1}$, the usual carrier space of the representations of $SU(2)$, to functions on a symplectic 2-sphere. The emergence of the 2-sphere as a phase space for the $6j$-symbol and its applications to uniform approximations of the $6j$-symbol will be the subject of the next chapter.

The moduli space of tetrahedra in $\mathbb{R}^3$ and the Schläfli identity in Euclidean space have played a major role in the derivation of the relative phase of the $6j$-symbol. It will be interesting to turn this derivation around, and use the symplectic geometry of the Schwinger model to derive the Schläfli identity. Such a proof will be the first symplectic proof of this identity that has so far been based on metrical geometry.

Chapter 5

A Uniform Approximation for the Wigner $6j$-Symbol

5.1 Introduction and Summary

The Wigner $6j$-symbol has an asymptotic formula, first obtained by Ponzano and Regge [68], and later proved by Schulten and Gordon [77]. The formula has the usual problems of primitive WKB approximations. For example, it diverges at the classical turning points, which are called caustics. Although the quantum numbers in the $6j$-symbol are discrete, they can come very close, or even fall exactly on a caustic, as shown by the theory of Brahmagupta quadrilaterals [75]. For these values near the caustic, the WKB formula is a poor approximation. To illustrate this situation, a plot of the WKB formula and the exact $6j$-symbols are displayed in figure 5.1 below. Thus there is interest in uniform approximations that are accurate near the caustics and are valid over as wide a range of quantum numbers as possible.

When one of the j's is varied and the others held fixed, the $6j$-symbol has two caustics, as illustrated in figure 5.1. In addition to proving the asymptotic formula for the $6j$-symbol, Schulten and Gordon [77] has provided uniform asymptotic approximations of the Airy function type. This uniform approximation can only cover one of the two caustics at a time. If two such uniform approximations are used, then they do not match smoothly in the middle. In order to cover both caustics at the same time, we would expect to find a uniform approximation of the Weber function type, which is based on the eigenfunctions of the harmonic oscillator.

It turns out, however, that a Weber function type uniform approximation for the $6j$-symbol does not exist in general. The reason for this is topological. Uniform approximations are based on a smooth, area preserving map between the phase space of the given problem and the standard problem. The phase space of the $6j$-symbol is a sphere, as we have seen in chapter 4. The Lagrangian manifolds for the $6j$-symbol are two circles. whereas the Lagrangian manifolds for the harmonic oscillator consist of a vertical line and a circle. In some cases, as those intersections of the two circles illustrated in figure 5.4, there are topological obstructions for the existence of a continuous map from one set of Lagrangian manifolds to the other. This obstruction manifests in the fact that the area between the two

caustic points for the $6j$-symbol is not in general of the form $(n + 1/2)\pi$ for some integer n. For the harmonic oscillator, the area between the two caustics is always of the form $(n + 1/2)\pi$, a condition that is equivalent to the Bohr-Sommerfeld quantization condition. Thus, there are no area preserving map between the Lagrangian manifolds of the $6j$-symbol and those of the simple harmonic oscillator.

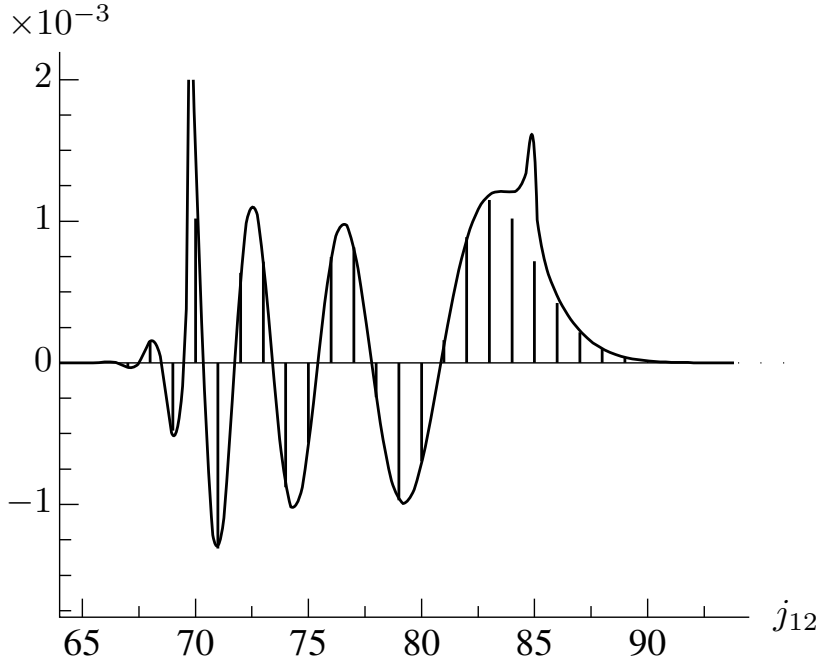

Figure 5.1: The $6j$-symbol as a function of j_{12} for $j_1 = 16$, $j_2 = 80$, $j_3 = 208$, $j_4 = 272$, and $j_{23} = 276$. Sticks are the values of the $6j$-symbol, and the curve is the Ponzano-Regge approximation.

We have noticed, however, that the Wigner d-matrices, or rotation matrices, also has a spherical phase space that arises in its semiclassical analysis. Moreover, the Lagrangian manifolds for the d-matrices are also topological circles, and the intersections capture the intersection structure of the $6j$-symbol. Inspired by these similarities, we have worked out the details of an area preserving map between the Lagrangian manifolds of the $6j$-symbol and those of the d-matrices, and derived a uniform approximation based on this map. The resulting approximation is uniform over the entire range of both j_{12} and j_{23}, for fixed j_1, j_2, j_3, and j_4.

Now we give an outline of this chapter. In section 5.2, we describe the traditional method of constructing a uniform semiclassical approximation through the "method of comparison equation," and point out the necessary generalizations for our problem. We also display the main uniform formula for the $6j$-symbol here. In section 5.3, we review the basic result of quantum normal form theory, and recast the method of comparison equation using the language of a quantum normal forms. We re-derive the Airy approximation as an example. In section 5.4, we find the symbols for the matrix operators that define the

Wigner $6j$-symbol, and look at the intersections of their associated Lagrangian manifolds on the 2-sphere. In section 5.6, we explain the choice of the rotation matrices as a normal form for the $6j$-symbol, and describe the symplectic map used to construct the unitary transformation. Finally, in section 5.9, we derive a new uniform approximation for the $6j$-symbol, up to an overall phase. In the last section, we determine the overall phase and provide details on the implementation and numerical results of the uniform formula.

5.2 Traditional Method of Uniform Semiclassical Approximations

The traditional method of constructing uniform semiclassical approximations, the "method of comparison equations", is reviewed by Berry and Mount [16]. In this method one takes a one-dimensional Schrödinger equation (a second-order differential equation in x) and performs a coordinate transformation $X = X(x)$ to create a new Schrödinger equation in X which, after the neglect of terms of order $\hbar^2$, becomes a standard, solvable equation. The most common standard or "comparison" equations in practice are differential equations for Airy or Weber (parabolic cylinder) functions.

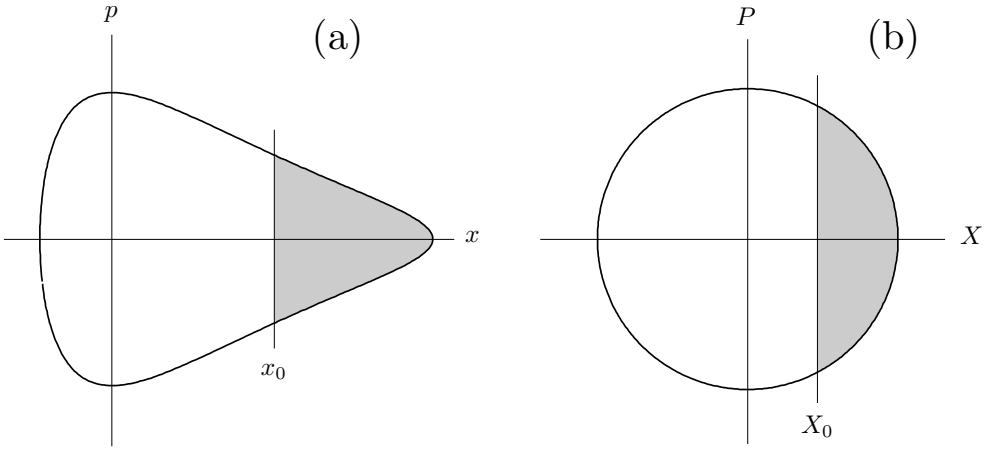

Figure 5.2: In the method of comparison equations, the phase space of a nonlinear oscillator (a) is mapped into the phase space of the harmonic oscillator (b). The function $X(x)$ is determined by the equality of areas; for example, in the figure the shaded areas are equal, and $X_0 = X(x_0)$.

Underlying the change of variable used in the method of comparison equations is a transformation between the phase spaces of the original problem and the standard problem. If the change of variable is given by $X = X(x)$, then it induces a "point transformation", given by $X = X(x)$ and $P = (dx/dX)\,p$, where the second part is the usual lift of a point transformation into a canonical transformation. The second equation can also be written $p dx = P dX$, which can be integrated to derive the condition

$$s(x) = S(X)\,, \tag{5.1}$$

where s and S are the actions of the original problem and the standard problem, respectively. The geometry of this map between phase spaces is illustrated in figure 5.2, in which the method of comparison equations is used to map a quantized curve of a nonlinear oscillator, the Morse oscillator, part (a) of the figure, into a quantized curve of a standard problem, the harmonic oscillator, part (b) of the figure. Equation (5.1) implies the equality of the shaded areas in the figure. The meaning of the equation $s(x) = S(X)$ is clear: areas are preserved by this phase space transformation. In other words, the transformation is canonical. The condition (5.1) can be analytically continued into the classically forbidden regions, where p, P, s, and S all become complex, but the resulting change of variable $X = X(x)$ remains real and smooth throughout.

A natural extension to the theory of uniform approximation is to extend the class of canonical transformations used from the class of point transformations to the more general canonical transformations. Treating differential equations in phase space suggests that we use the symbols of the differential operators, which are functions on phase space. Through the symbol correspondence, classical normal form theory are carried over to a "quantum normal form" theory for the differential operators, where the standard problem is sometimes referred to as a quantum normal form. Examples of quantum normal form calculations and an interesting perspective on Bohr-Sommerfeld or torus quantization may be found in [26, 25]. In those references, only the problem of determining eigenvalues is considered, but in the present application we are interested in the transformation of the wave-functions, a problem that involves extra features. As it turns out, it is necessary to carry out not only a unitary transformation, which at the classical level maps a pair of orbits into another pair that are in standard form, but also a certain non-unitary transformation, to make the densities of probability on the orbits come out in standard form.

Another advantage of recasting the method of comparison equations into the language of normal form calculations is that it allows us to consider more general operators besides those found in Schödinger equations. For example, in our derivation, we will use the Stratonovich-Weyl symbol correspondence, which maps matrix operators to functions on a 2-sphere. The necessary unitary transformation is a unitary matrix constructed based on a canonical map on the 2-sphere. See section 5.12 for more details on the general construction of a unitary transformation from a canonical map.

In the usual method of comparison equations, the uniform approximation for the exact solution $\psi(x)$ is given by

$$\psi(x) \approx \frac{a(x)}{A(X)}\,\Psi(X)\,, \tag{5.2}$$

where $\Psi(X)$ is the standard solution of the standard problem and $a(x)$ and $A(X)$ are the amplitudes of the two semiclassical approximations, $a(x)$ for the original problem and $A(X)$ for the standard problem. Both amplitudes diverge at the caustics, but their ratio has a definite limit and in fact is smooth everywhere across both classically allowed and forbidden regions.

Similarly, it turns out that the uniform approximation for the $6j$-symbol in terms of d-matrices is given by

$$\left\{ \begin{array}{ccc} j_1 & j_2 & j_{12} \\ j_3 & j_4 & j_{23} \end{array} \right\} = (\text{phase}) \, \frac{A_{\text{PR}}}{A_d} \, d^j_{mm'}(\beta) \,, \tag{5.3}$$

where A_{PR} is the the amplitude for the $6j$-symbol and A_d is the amplitude for the d-matrices. In other words, the uniform approximation for the $6j$-symbol is of the same form (5.2) that emerges from the method of comparison equations.

5.3 Normal Form Theory for Uniform Approximations

The quantum normal form theory is based on an $\hbar$-expansion of a symbol correspondence. An example of a symbol correspondence is the Weyl symbol in earlier chapters, that relate operators on the Hilbert space $\mathcal{H} = L^2(\mathbb{R}^2)$ of two harmonic oscillators to functions on the phase space $\mathbb{R}^4$. In general, because of the Dirac quantization scheme of replacing Poisson brackets by commutators, a symbol correspondence satisfies the following basic property:

$$[\hat{A}, \hat{B}] \quad \leftrightarrow \quad i\hbar\{A, B\} + O(\hbar^2) \,, \tag{5.4}$$

where in the above, a right arrow indicates taking the symbol of an operator, and a left arrow indicates taking the inverse symbol of a function. In general we will denote operators with a hat on top, and its symbol by the same letter without the hat. In (5.4), if we take $\hat{B}$ to be a Hamiltonian $\hat{H}$, and take $\hat{A}$ to be a generator $\hat{G}$ for a unitary operator $\hat{U}$, then we can deduce an integral form of (5.4),

$$\hat{K} = \hat{U}\hat{H}\hat{U}^\dagger \quad \leftrightarrow \quad K = H \circ Z^{-1} \,, \tag{5.5}$$

where on the left, $\hat{K}$ is a new, usually solvable, Hamiltonian, called a normal form of $\hat{H}$, and on the right, Z is a canonical transformation generated by the symbol A. Thus we can choose Z so that K, and therefore $\hat{K}$, is simple. This is the idea behind the theory of quantum normal forms. For more details on the construction of the unitary operator $\hat{U}$, see section 5.12 and the original papers [25, 26].

We now apply (5.5) to find the eigenstate $|\psi\rangle$ with eigenvalue E_0 for a Hamiltonian $\hat{H}$. To be concrete, we assume $\hat{H}$ is a differential operator in the x variable and use the Weyl symbol correspondence. By definition, $|\psi\rangle$ satisfies the eigenvalue equation

$$(\hat{H} - E_0)\,|\psi\rangle = 0 \,. \tag{5.6}$$

Its semiclassical wavefunction is represented by the Lagrangian manifold defined by the level set $H(x,p) - E_0 = 0$, where H is the symbol of $\hat{H}$. Suppose there exist a canonical transformation $Z : (x,p) \to (X(x,p), P(x,p))$ such that a vertical line $x = x_0$ is mapped to another vertical line $X = X_0$, and the level set $H - E_0 = 0$ is mapped to a another level set $N(X,P) - N_0 = 0$, where $N(X,P)$ is the symbol of a normal form operator $\hat{N}$ with known eigenstates. Such a canonical transformation is illustrated in figure 5.2 above, where

H is the Morse oscillator and N is the harmonic oscillator. We assume the canonical map Z satisfies

$$H \circ Z^{-1} - E_0 = A(N - N_0)\,, \tag{5.7}$$
$$x \circ Z^{-1} - x_0 = B(x - X_0)\,, \tag{5.8}$$

for some functions $A = A(x,p)$ and $B = B(x,p)$. We construct a unitary operator $\hat{U}$ based on the symplectic transformation Z, and define

$$\hat{K}_1 = \hat{U}\hat{H}\hat{U}^\dagger\,, \qquad \hat{K}_2 = \hat{U}\hat{x}\hat{U}^\dagger\,. \tag{5.9}$$

From (5.5), the symbols of $\hat{K}_1$ and $\hat{K}_2$ are the canonical transformations of H and x, respectively, which are given by the right hand side of (5.7) and (5.8), that is,

$$K_1 = A(N - N_0)\,, \qquad K_2 = B(x - X_0)\,. \tag{5.10}$$

To relate the operators $\hat{H}$ and $\hat{N}$, insert $\hat{U}$ on the left and the identity operator $\hat{I} = \hat{U}^\dagger\hat{U}$ on the right of $(\hat{H} - E_0)$ in (5.6). We find

$$\hat{U}(\hat{H} - E_0)\hat{U}^\dagger\hat{U}\ |\psi\rangle = \hat{K}_1\hat{U}\ |\psi\rangle = 0\,. \tag{5.11}$$

Again we insert $\sqrt{\hat{A}}$ on the left and the identity operator $\hat{I} = \frac{1}{\sqrt{\hat{A}}}\sqrt{\hat{A}}$ on the right of $(\hat{H} - E_0)$ in (5.11). We find

$$\sqrt{\hat{A}}\,(\hat{K}_1)\frac{1}{\sqrt{\hat{A}}}\sqrt{\hat{A}}\,\hat{U}\ |\psi\rangle = \hat{A}\,(\hat{N} - N_0)(\sqrt{\hat{A}}\,\hat{U}\ |\psi\rangle) = 0\,, \tag{5.12}$$

where we have used an operator identity

$$\sqrt{\hat{A}}\,(\hat{K}_1)\frac{1}{\sqrt{\hat{A}}} = \hat{A}\,(\hat{N} - N_0)\,, \tag{5.13}$$

which is based on the following star product identity to first order in $\hbar$,

$$\sqrt{A} * (A(N - N_0)) * \frac{1}{\sqrt{A}} = A * (N - N_0)\,, \tag{5.14}$$

From (5.12), we conclude that the eigenstate of $\hat{N}$ with eigenvalue N_0 is given by

$$|N_0\rangle = \sqrt{\hat{A}}\,\hat{U}\ |\psi\rangle\ . \tag{5.15}$$

Inverting the relationship between $|\psi\rangle$ and $|N_0\rangle$ in (5.15), we obtain

$$|\psi\rangle = \hat{U}^\dagger\frac{1}{\sqrt{\hat{A}}}\,|N_0\rangle\ . \tag{5.16}$$

An analogous calculation for the operator $\hat{x}$ leads to

$$|x_0\rangle = \hat{U}^\dagger \frac{1}{\sqrt{\hat{B}}} |X_0\rangle \,, \tag{5.17}$$

where $|X_0\rangle$ is an eigenstate of $\hat{x}$ with eigenvalue X_0.

Taking the scalar product between the states in (5.16) and (5.17), we find

$$\begin{aligned} \langle x_0 \,|\, \psi \rangle &= \left\langle X_0 \left| \frac{1}{\sqrt{\hat{B}}} \hat{U} \hat{U}^\dagger \frac{1}{\sqrt{\hat{A}}} \right| N_0 \right\rangle \\ &= \left\langle X_0 \left| \frac{1}{\sqrt{\hat{B}}} \frac{1}{\sqrt{\hat{A}}} \right| N_0 \right\rangle , \end{aligned} \tag{5.18}$$

where in the second equality, we have used the unitary property of $\hat{U}$ to cancel $\hat{U}$ and $\hat{U}^\dagger$.

Let us demonstrate the formula (5.18) by deriving the Airy type uniform approximation for the Schródinger equation,

$$(\hat{p}^2 - p^2(\hat{x}))\,|\psi\rangle = 0\,, \tag{5.19}$$

where $p(\hat{x}) = \sqrt{E_0 - V(\hat{x})}$, and where $V(x)$ is the potential. We will assume that there is a canonical map Z induced by a point transformation, given by $(X = F(x),\, P = p/F'(x))$, and that it maps the Schrödinger equation into the Airy equation in the sense of their symbols. That is,

$$(p^2 - p^2(x)) \circ Z^{-1} = (F'(x))^2 \left(P^2 - \frac{p^2(x)}{(F'(x))^2} \right) = A(X)(P^2 - X)\,, \tag{5.20}$$

where $P^2 + X$ is the symbol of the operator for the Airy equation. We find that $A(X) = (F'(x))^2$, and $F'(x) = p(x)/\sqrt{X}$, where $x = F^{-1}(X)$. From the relation $dX/dx = F'(x) = p(x)/\sqrt{X}$, we see that $\sqrt{X}dX = p(x)dx$, which leads to the map

$$\frac{2}{3} X^{3/2} = \int p dx\,, \tag{5.21}$$

which is used in the Airy type uniform approximation.

Since we are using a point transformation, the explicit form of the unitary transformation is known, and it is given by $\hat{U}\,|x_0\rangle = \sqrt{F'(x_0)}\,|X_0\rangle$. Thus we have $|x_0\rangle = \hat{U}^\dagger\,(1/\sqrt{F'(\hat{x})})\,|X_0\rangle$, and $\hat{B} = 1/\sqrt{F'(\hat{x})}$, where again, $x = F^{-1}(X)$.

Using (5.18), we find

$$\psi(x_0) = \left\langle X_0 \left| \frac{1}{\sqrt{\hat{B}}} \frac{1}{\sqrt{\hat{A}}} \right| N_0 \right\rangle \tag{5.22}$$

$$= \left\langle X_0 \left| \frac{1}{\sqrt{p(F^{-1}(\hat{x}))/\sqrt{\hat{x}}}} \right| N_0 \right\rangle \tag{5.23}$$

$$= \frac{X_0^{1/4}}{(p(x_0))^{1/2}} \,\mathrm{Ai}(X_0)\,, \tag{5.24}$$

which is the usual expression for the Airy type uniform approximation for the Schrödinger equation. We now apply the theory of quantum normal form to the $6j$-symbol.

5.4 The $6j$-Symbol: Matrix Operators and Their Symbols

We set $\hbar = 1$, so all angular momenta are dimensionless. We label the j's in the $6j$-symbol by

$$\left\{ \begin{array}{ccc} j_1 & j_2 & j_{12} \\ j_3 & j_4 & j_{23} \end{array} \right\}, \tag{5.25}$$

which is how it would be used in the recoupling of three angular momenta.

The quantum numbers j_i, $i = 1, 2, 3, 4, 12, 23$ give the magnitudes of the angular momenta and do not specify the sign of the operator. For example, instead of coupling three angular momenta to obtain a fourth, that is, setting $\hat{\mathbf{J}}_4 = \hat{\mathbf{J}}_1 + \hat{\mathbf{J}}_2 + \hat{\mathbf{J}}_3$, we can couple four angular momenta with a sum of zero,

$$\hat{\mathbf{J}}_1 + \hat{\mathbf{J}}_2 + \hat{\mathbf{J}}_3 + \hat{\mathbf{J}}_4 = \mathbf{0}\,, \tag{5.26}$$

by effectively changing the sign of $\mathbf{J}_4$. This is how we shall regard the recoupling problem in this chapter. Usually we will think of j_i, $i = 1, 2, 3, 4$ as given, while j_{12} and j_{23} are variable intermediate angular momenta that result from the coupling of the first three angular momenta. The intermediate angular momenta j_{12} and j_{23} are the quantum numbers of the squares of the operators

$$\hat{\mathbf{J}}_{12} = \hat{\mathbf{J}}_1 + \hat{\mathbf{J}}_2\,, \qquad \hat{\mathbf{J}}_{23} = \hat{\mathbf{J}}_2 + \hat{\mathbf{J}}_3\,. \tag{5.27}$$

Using this definition from the re-coupling of four angular momenta, the $6j$-symbol (5.25) is proportional to the unitary matrix element $\langle j_{12}|j_{23}\rangle$ that takes one from the eigenbasis of one intermediate angular momentum (j_{12}) to the eigenbasis of the other (j_{23}). These bases span the subspace of the product space of four angular momenta in which (5.26) holds as an operator equation. We shall denote this subspace by Z. According to (5.26), the total angular momentum vanishes on Z. The orthonormality relations satisfied by the $6j$-symbol are essentially a statement of the unitarity of the matrix $\langle j_{12}|j_{23}\rangle$. The exact $6j$-symbol is given by

$$\left\{ \begin{array}{ccc} j_1 & j_2 & j_{12} \\ j_3 & j_4 & j_{23} \end{array} \right\} = \frac{1}{\sqrt{(2j_{12}+1)(2j_{23}+1)}} \, \langle j_{12}|j_{23}\rangle \ . \tag{5.28}$$

Given the values of j_1, j_2, j_3, j_4, let us now determine the size of the matrix $\langle j_{12}|j_{23}\rangle$. To be defined, the $6j$-symbol must satisfy four triangle inequalities associated with the four triples, (j_1, j_2, j_{12}), (j_2, j_3, j_{23}), (j_3, j_4, j_{12}), and (j_1, j_4, j_{23}). For example, j_{12} must lie between the bounds

$$|j_1 - j_2| \le j_{12} \le j_1 + j_2\,, \tag{5.29}$$

in integer steps. These imply that j_{12} and j_{23} vary between the limits

$$j_{12,\min} \leq j_{12} \leq j_{12,\max}\,, \tag{5.30}$$
$$j_{23,\min} \leq j_{23} \leq j_{23,\max}\,, \tag{5.31}$$

where

$$j_{12,\min} = \max(|j_1 - j_2|, |j_3 - j_4|)\,, \tag{5.32}$$
$$j_{23,\min} = \max(|j_2 - j_3|, |j_1 - j_4|)\,, \tag{5.33}$$
$$j_{12,\max} = \min(j_1 + j_2, j_3 + j_4)\,, \tag{5.34}$$
$$j_{23,\max} = \min(j_2 + j_3, j_1 + j_4)\,. \tag{5.35}$$

We shall reserve lower case j_i for quantum numbers. For semiclassical purposes, we shall set

$$J_i = j_i + \frac{1}{2}\,, \tag{5.36}$$

for $i = 1, 2, 3, 4, 12, 23$. It is useful to rewrite (5.30) for these variables. We have

$$J_{12,\min} \leq J_{12} \leq J_{12,\max}\,, \tag{5.37}$$
$$J_{23,\min} \leq J_{23} \leq J_{23,\max}\,, \tag{5.38}$$

where

$$J_{12,\min} = \max(|J_1 - J_2|, |J_3 - J_4|)\,, \tag{5.39}$$
$$J_{23,\min} = \max(|J_2 - J_3|, |J_1 - J_4|)\,, \tag{5.40}$$
$$J_{12,\max} = \min(J_1 + J_2, J_3 + J_4)\,, \tag{5.41}$$
$$J_{23,\max} = \min(J_2 + J_3, J_1 + J_4)\,. \tag{5.42}$$

The number of allowed j_{12} or j_{23} values is the same, and it is the dimension D of the subspace Z as well as the size of the matrix $\langle j_{12}|j_{23}\rangle$. It is given by

$$D = \dim Z = j_{12,\max} - j_{12,\min} + 1 = j_{23,\max} - j_{23,\min} + 1\,. \tag{5.43}$$

The dimension of Z can be written as $D = 2j + 1$ for some integer or half integer j. The Stratonovich-Weyl symbol correspondence provides a mapping between $2j + 1$ dimensional matrices and functions on a 2-sphere of radius $J = j + 1/2$. This mapping depends on the basis we choose in Z. To proceed, we shall choose the $|j_{12}\rangle$ basis, which we relabel by

$$|j, m\rangle = |j_{12}\rangle\ , \tag{5.44}$$

where

$$j = (D-1)/2\,, \tag{5.45}$$

and

$$m = j_{12} - 1/2(j_{12,\min} + j_{12,\min}) = -j, \ldots, j \tag{5.46}$$

is the deviation of j_{12} from its average value. Using this basis, we can define the basic coordinate operators that satisfy the commutation relations of the $SU(2)$ algebra. Let $\hat{K}_+$ and $\hat{K}_-$ be the usual raising the lower operators in the $|j,m\rangle = |j_{12}\rangle$ basis. Define

$$\hat{K}_x = \frac{1}{2}\left(\hat{K}_+ + \hat{K}_-\right), \tag{5.47}$$

$$\hat{K}_y = \frac{1}{2i}\left(\hat{K}_+ - \hat{K}_-\right), \tag{5.48}$$

$$\hat{K}_z = \hat{J}_{12} - J_{12,\text{avg}}\,, \tag{5.49}$$

where $\hat{J}_{12} = \sqrt{\hat{\mathbf{J}}_{12}^2}$, and

$$J_{12,\text{avg}} = \frac{1}{2}\left(J_{12,\min} + J_{12,\max}\right). \tag{5.50}$$

The Stratonovich Weyl symbol of the operators $(\hat{K}_x, \hat{K}_y, \hat{K}_z)$ are simply the Cartesian coordinate functions (K_x, K_y, K_z) of a 2-sphere of radius $J = D/2$, with spherical angles (θ_{12}, ϕ_{12}). Explicitly,

$$K_x = (D/2)\sin\theta_{12}\,\cos\phi_{12}\,, \tag{5.51}$$

$$K_x = (D/2)\sin\theta_{12}\,\cos\phi_{12}\,, \tag{5.52}$$

$$K_z = (D/2)\cos\theta_{12}\,. \tag{5.53}$$

We have labeled the azimuthal angle by ϕ_{12}, because it is conjugate to J_z and J_{12}.

This is the $6j$-sphere, on which the north pole is $K_z = D/2$ or $J_{12} = J_{12,\max}$, the south pole is $K_z = -D/2$ or $J_{12} = J_{12,\min}$, and curves of constant J_{12} in general are small circles $K_z = \text{const}$. These small circles are illustrated in figure 5.3, which shows several curves of constant J_{12}.

The states $|j_{12}\rangle$ and $|j_{23}\rangle$ are defined by the eigenvalue equations,

$$\left(\hat{J}_{12} - \sqrt{j_{12}(j_{12}+1)}\right)|j_{12}\rangle = 0\,, \tag{5.54}$$

$$\left(\hat{J}_{23} - \sqrt{j_{23}(j_{23}+1)}\right)|j_{23}\rangle = 0\,, \tag{5.55}$$

where $\hat{J}_{23} = \sqrt{\hat{\mathbf{J}}_{23}^2}$. In the asymptotic limit of large j's, we can replace $\sqrt{j_{12}(j_{12}+1)}$ and $\sqrt{j_{23}(j_{23}+1)}$ by $J_{12} = j_{12} + 1/2$ and $J_{23} = j_{23} + 1/2$, respectively. Then (5.54) and (5.55) become

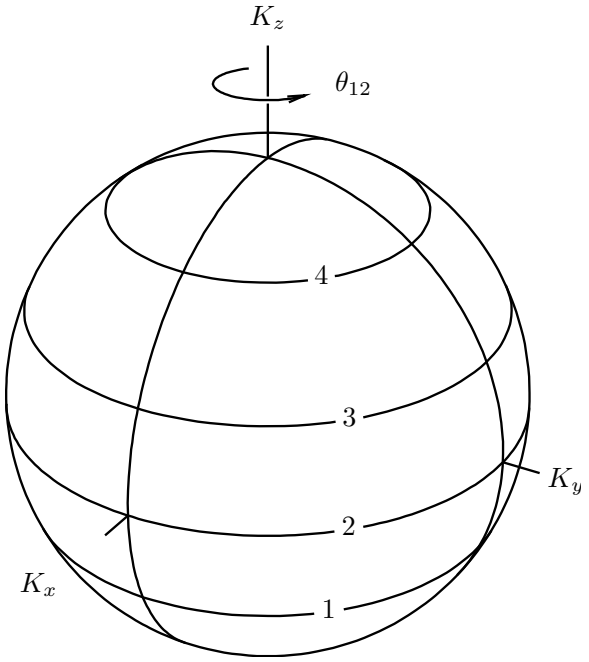

Figure 5.3: The phase space of the $6j$-symbol is a sphere of radius $D/2$ in a space in which (K_x, K_y, K_z) are Cartesian coordinates. To within an additive constant, K_z is J_{12}. Several curves of constant J_{12}, which are small circles, are shown.

$$\left(\hat{J}_{12} - (j_{12} + 1/2)\right) |j_{12}\rangle = \left(\hat{K}_z - m\right) |j_{12}\rangle = 0\,, \tag{5.56}$$

$$\left(\hat{J}_{23} - (j_{23} + 1/2)\right) |j_{23}\rangle = 0\,, \tag{5.57}$$

where we have used the definitions of $\hat{K}_z$ from (5.46) and m from (5.49) in the first equation. The symbol K_z of $\hat{K}_z$ is given by (5.53) above. The exact matrix elements of the operator $\hat{J}_{23}^2$ in the $|j_{12}\rangle$ basis can be found in the appendix of [76]. It is a symmetric tridiagonal matrix, and it has the form

$$\hat{J_{23}^2} = \hat{A} + \frac{1}{2}(\hat{J}_- \hat{B} + \hat{B}\hat{J}_+)\,, \tag{5.58}$$

where $\hat{A}$ and $\hat{B}$ are diagonal, and their diagonal matrix elements can be read off from the following matrix elements of $\hat{J}_{23}^2$:

$$\begin{aligned}\left\langle j_{12} \,\middle|\, \hat{J}_{23}^2 \,\middle|\, j_{12} \right\rangle \quad &= \frac{1}{2j_{12}(j_{12}+1)}\{j_{12}(j_{12}+1)[-j_{12}(j_{12}+1) + j_1(j_1+1) + j_2(j_2+1)] \\ &\quad + j_3(j_3+1)[j_{12}(j_{12}+1) + j_1(j_1+1) - j_2(j_2+1)] \\ &\quad + j_4(j_4+1)[j_{12}(j_{12}+1) - j_1(j_1+1) + j_2(j_2+1)]\}\,, \end{aligned} \tag{5.59}$$

$$\begin{aligned}&\left\langle j_{12} - 1 \,\middle|\, \hat{J}_{23}^2 \,\middle|\, j_{12} \right\rangle \\ = \;& \frac{\left\{[j_{12}^2 - (j1-j2)^2][(j1+j2+1)^2 - j_{12}^2][j_{12}^2 - (j3-j4)^2][(j3+j4+1)^2 - j_{12}^2]\right\}^{1/2}}{2j_{12}[(2j_{12}-1)(2j_{12}+1)]^{1/2}}\,. \end{aligned} \tag{5.60}$$

Making the approximation $(2j_{12}+1)(2j_{12}-1) = 4(j_{12}+1)^2$ in the denominator of (5.60), and noting that the symbol of $\hat{K}_x = (\hat{J}_+ + \hat{J}_-)/2$ is K_x, we have the symbol of $\hat{J}_{23}$ to first order

$$\begin{aligned} J_{23}^2(K_z, \phi_{12}) \;&=\; \frac{1}{2J_{12}^2}\left[(J_{12}^2(-J_{12}^2 + J_1^2 + J_2^2) + J_3^2(J_{12}^2 + J_1^2 - J_2^2) + J_4^2(J_{12}^2 - J_1^2 + J_2^2)\right] \\ &+\; \frac{8}{J_{12}^2}\, F(J_{12}, J_1, J_2)\, F(J_{12}, J_3, J_4)\, \cos\phi_{12}\,, \end{aligned} \tag{5.61}$$

where the symbol J_{12} is equal to K_z up to an additive constant, and $F(a,b,c)$ is the area of a triangle with sides a, b, c,

$$F(a,b,c) = \frac{1}{4}[(a+b+c)(-a+b+c)(a-b+c)(a+b-c)]^{1/2}\,. \tag{5.62}$$

The level set $J_{23}(K_z, \phi_{12}) = j_{23} + 1/2$ is illustrated in figure 5.4. It turns out that the function J_{23} in (5.61), when viewed as a function of $J_1, J_2, J_3, J_4, J_{12}$, and ϕ_{12}, is identical to the sixth edge length J_{23} as a function of the other five edge lengths $J_1, J_2, J_3, J_4, J_{12}$

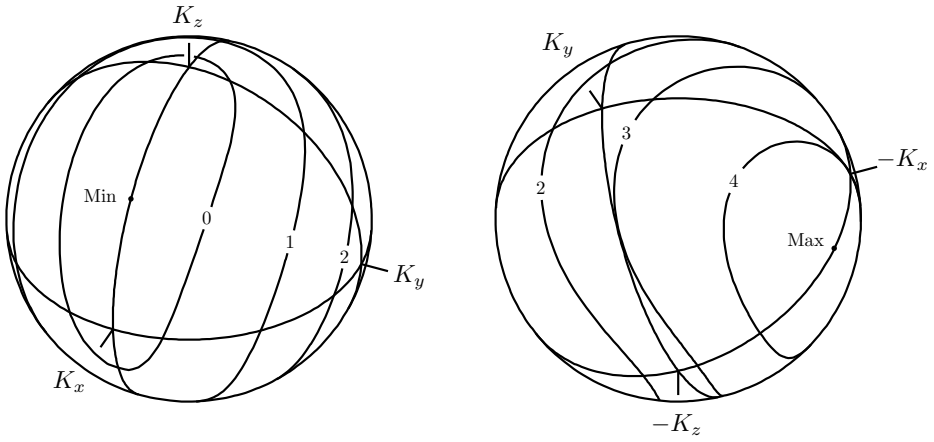

Figure 5.4: Curves of constant J_{23} on the $6j$-sphere. The first view shows the north pole and the point $J_{23} = J_{23,\min}$ and the second shows the south pole and the point $J_{23} = J_{23,\min}$.

and the dihedral angle ϕ_{12}. See (4.28) in section 4.6. This function was used to describe the shape space of tetrahedra [45] and in the WKB analysis of the $6j$-symbol using the Schwinger model in chapter 4. This identification of the function J_{23} with the edge of a tetrahedron allows us to use the Schläfli identity from section 4.6 to evaluate the area of the lune between the two curves $J_{12} = \text{const}$ and $J_{23} = \text{const}$ in terms of the Ponzano Regge phase.

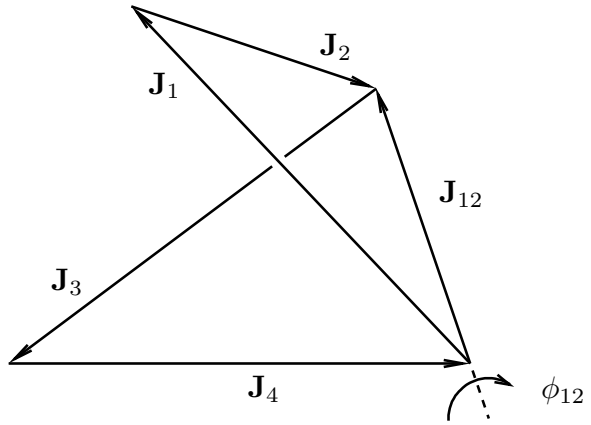

Figure 5.5: Definition of the interior dihedral angle ϕ_{12}. The function J_{23} is the edge length, not shown, as a function of the five edge lengths shown and the dihedral angle ϕ_{12}.

5.5 The Intersection of Orbits for the $6j$-Symbol

The level sets $J_{12} = j_{12} + 1/2$ and $J_{23} = j_{23} + 1/2$ are topological circles. If these two circles intersect, as illustrated in part (a) of figure 5.6, then we are in the classically allowed region. If these two circles do not intersect, as illustrated in part (b) of figure 5.6, then we are in the classically forbidden region. The intersection points, P and Q in part (a) of the figure, represent stationary phase points. From chapter 4, these points represent real tetrahedra with the six lengths $J_1, J_2, J_3, J_4, J_{12}$, and J_{23}. Thus, the constructibility of such a tetrahedra distinguishes the classically allowed region from the classically forbidden region.

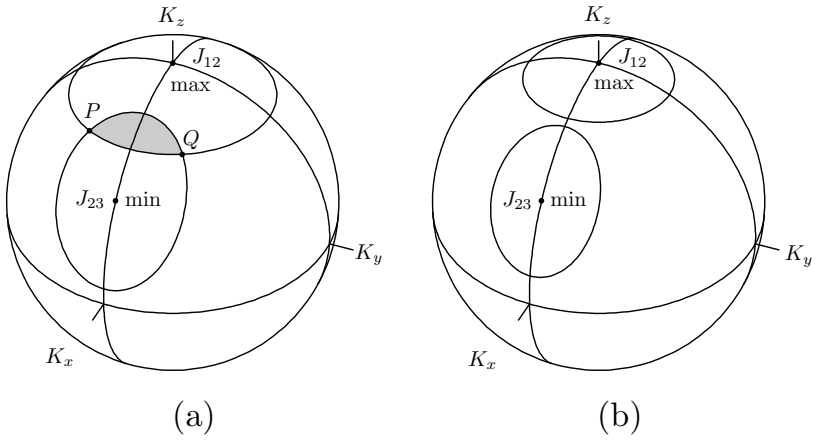

Figure 5.6: In part (a), the classically allowed region, an orbit of constant J_{12} intersects an orbits of constant J_{23}. In part (b), the classically forbidden region, the orbits do not intersect.

It turns out that the volume function V^2 of a tetrahedron with the six edge lengths $J_1, J_2, J_3, J_4, J_{12}, J_{23}$ provides a constructibility condition that tells us whether we are in the classically allowed region, in which $V^2 > 0$, or the classically forbidden region, in which $V^2 < 0$. This function is related to the nonnegative definite Gram matrix G from chapter 4, in the following way:

$$36V^2 = \det G\,. \tag{5.63}$$

An example of the curve $V^2 = 0$ is plotted in figure 5.7, inside the square region of the J_{12}-J_{23} plane bounded by the classical limits (5.37) - (5.38) for certain fixed values of j_i, $i = 1, 2, 3, 4$. This curve divides the square region in figure 5.7 into one classically allowed region and four classically forbidden regions, which are labeled $ABCD$ in the figure. Points on the curve $V^2 = 0$ represent the caustics of the $6j$-symbol.

We now make the correspondence between the regions $ABCD$ and the way the two circles intersect on the sphere. First we look at the caustic curve $V^2 = 0$. On this caustic curve, the two curves $J_{12} = \text{const}$ and $J_{23} = \text{const}$ are tangent. Because both J_{12} and J_{23} are even functions of ϕ_{12}, such tangency can occur only in the plane $K_y = 0$, where

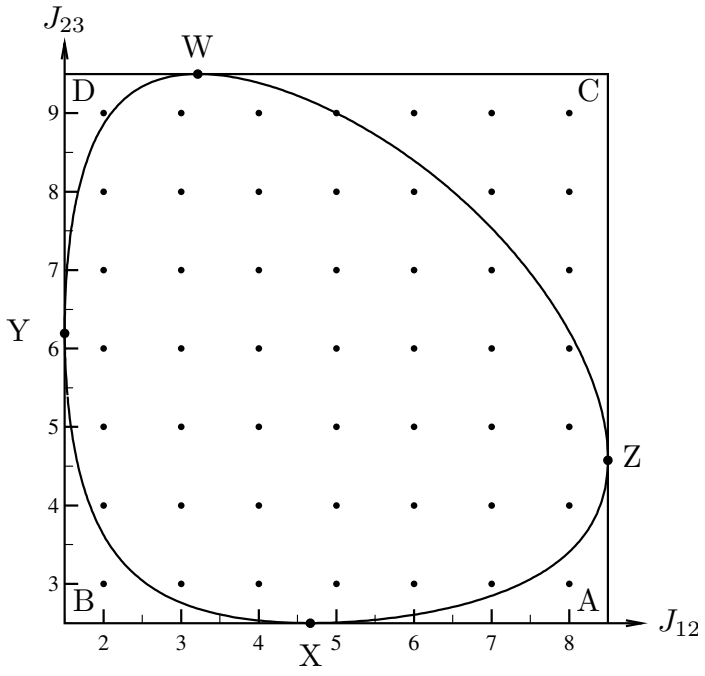

Figure 5.7: Caustics occur when the curve $J_{12} = \text{const}$ is tangent to the curve $J_{23} = \text{const}$. The four types of such tangency are illustrated.

$\phi_{12} = 0$. In figure 5.8, we illustrate the different types of tangency, which correspond to the four segments of the caustic curve $V^2 = 0$ in figure 5.7. We deduce the correspondence from the direction in which we move from the classically forbidden region into the classically allowed region.

From part A of figure 5.8 we move into the classically allowed region if we either decrease J_{12} or increase J_{23}. Thus we see that it corresponds to region A of figure 5.7. Next we look at part B of figure 5.8. From this caustic, we pass back into the classically allowed region if either J_{12} increases or J_{23} increases, so we are in region B of figure 5.7. Similarly, from the caustic in part C of figure 5.8, we pass back into the classically allowed region if we let either J_{12} or J_{23} decrease, so this corresponds to region C of figure 5.7. Finally, from the configuration in part D in figure 5.8, we pass back into a classically allowed region if either J_{23} decreases or J_{12} increases, so we are in region D in figure 5.7.

In the case of an ordinary oscillator with a flat phase space, the difference in the actions between the two turning points is one-half the area of the orbit, and has the form $(n+1/2)\pi$, where n is an integer. As explained in the introduction of this chapter, this is a requirement for the existence of a uniform approximation of the Weber function type. The analogous statement for the $6j$-symbol with the spherical phase space is sometimes true, and sometimes not. A case where it is true is obtained from diagrams A and B of figure 5.8, in which we regard j_{23} fixed and j_{12} variable. As J_{12} decreases from the north pole (its maximum value), we first encounter a caustic of the type A, where the area of the lune is zero. Continuing to decrease J_{12}, we pass through the classically allowed region, finally

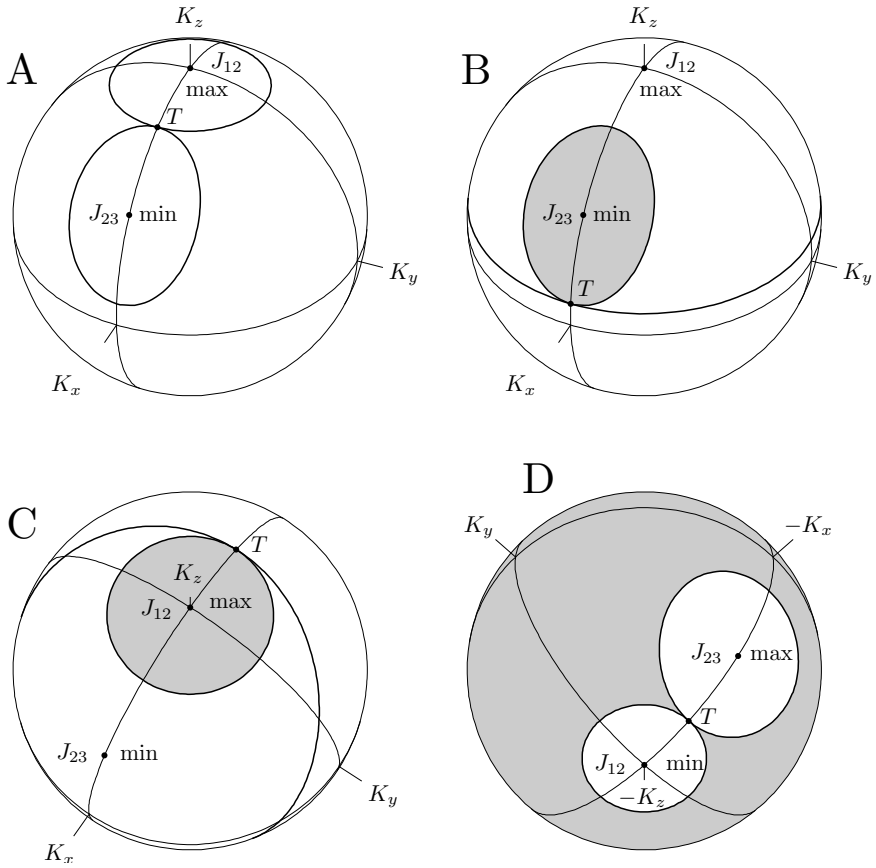

Figure 5.8: Caustics occur when the curve $J_{12} = \text{const}$ is tangent to the curve $J_{23} = \text{const}$. The four types of such tangency are illustrated.

encountering a caustic of the type B at the lower turning point, where the area of the lune is the quantized area of the oval $j_{23} = const.$ This area has the form $(n + 1/2)2\pi$, so a uniform approximation of the Weber function type is possible.

A case where the area between caustics is not quantized and a uniform approximation of the Weber function type does not exist is obtained when j_{23} has a value such as that illustrated in part C of figure 5.8. In this case, as we let J_{12} decrease from its maximum value at the north pole the first caustic we encounter is of type C, where the area of the lune is the area of the curve $J_{12} = \text{const}$. This area is not quantized, since the value of J_{12} at the caustic is not quantized. As J_{12} decreases, we eventually reach the lower caustic of type B, where the area of the lune is the quantized area of the orbit $j_{23} = \text{const}$. Thus, the difference between the areas, one quantized and the other not, is not quantized.

We will now show that the d-matrices have a phase space, an orbit and caustic structure that are identical, from a topological standpoint, to those of the $6j$-symbol.

5.6 Rotation Matrices

We now summarize the result of a semiclassical analysis of the d-matrices. The d-matrices are defined by

$$d^j_{mm'}(\beta) = \langle m|U_y(\beta)|m'\rangle \ , \tag{5.64}$$

where $U_y(\beta) = \exp(-i\beta J_y)$ is a rotation operator with Euler angle β about the y-axis, and $|m\rangle$ and $|m'\rangle$ are standard rotation basis states, that is, eigenstates of J_z. To indicate both the operator and the quantum number, we will write these states as $|J_z \,:\, m\rangle$ and $|J_z \,:\, m'\rangle$. By conjugation the rotation operator $U_y(\beta)$ rotates the angular momentum vector,

$$U_y(\beta)^\dagger \mathbf{J} U_y(\beta) = R_y(\beta)\mathbf{J} \, , \tag{5.65}$$

where $R_y(\beta)$ is the 3×3 rotation matrix for an active rotation about the y-axis. We define

$$\hat{\mathbf{n}} = R_y(\beta)\hat{\mathbf{z}} = \begin{pmatrix} \cos\beta & 0 & \sin\beta \\ 0 & 1 & 0 \\ -\sin\beta & 0 & \cos\beta \end{pmatrix} \begin{pmatrix} 0 \\ 0 \\ 1 \end{pmatrix} = \begin{pmatrix} \sin\beta \\ 0 \\ \cos\beta \end{pmatrix} \ , \tag{5.66}$$

which is illustrated in figure 5.9. This implies

$$(\mathbf{n}\cdot\mathbf{J})\, U_y(\beta)\, |J_z \,:\, m'\rangle = U_y(\beta)\, (\mathbf{z}\cdot\mathbf{J})\ |J_z \,:\, m'\rangle = m'\, U_y(\beta)\ |J_z \,:\, m'\rangle \ , \tag{5.67}$$

where we have used (5.65) and

$$\hat{\mathbf{n}} \cdot [R_y(\beta)\mathbf{J}] = [R_y(\beta)^{-1}\, \hat{\mathbf{n}}] \cdot \mathbf{J} = \hat{\mathbf{z}} \cdot \mathbf{J} = J_z \, . \tag{5.68}$$

Therefore $U_y(\beta)\ |J_z \,:\, m'\rangle$ is an eigenstate of

$$J_n \equiv \hat{\mathbf{n}} \cdot \mathbf{J} = J_z \cos\beta + J_x \sin\beta \, , \tag{5.69}$$

with eigenvalue m'. We will write

$$U_y(\beta)\,|J_z\,:\,m'\rangle = |J_n\,:\,m'\rangle\ , \tag{5.70}$$

so that

$$d^j_{mm'}(\beta) = \langle J_z\,:\,m|J_n\,:\,m'\rangle\ . \tag{5.71}$$

In this way the d-matrix is written as a unitary matrix element connecting the eigenstates of two different operators.

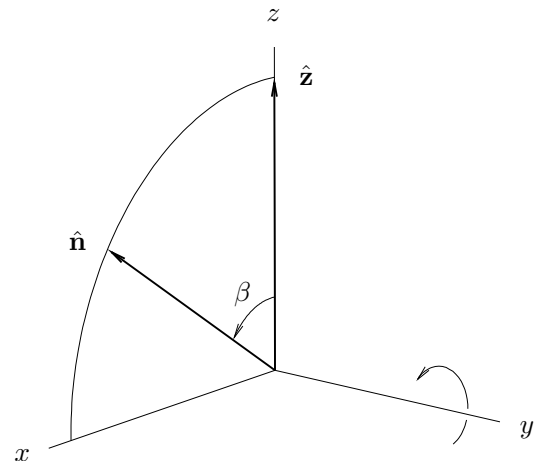

Figure 5.9: Definition of the Euler angle β and unit vector $\hat{\mathbf{n}}$.

Similar to the $6j$-symbol, the Stratonovich-Weyl symbol correspondence suggests that the classical phase space for $d^j_{mm'}(\beta)$ is a sphere, the "d-sphere," of radius

$$J = j + \frac{1}{2}\,. \tag{5.72}$$

The area of a loop on the surface of the sphere is given by

$$\text{area} = \oint J_z\,d\phi\,, \tag{5.73}$$

where ϕ is the azimuthal angle. The total area of the sphere is therefore $4\pi J = (2j+1)(2\pi)$, that is, the sphere consists of $2j+1$ Planck cells, corresponding to the $2j+1$ basis states $|J_z\,:\,m\rangle$ or $|J_n\,:\,m'\rangle$. Curves of constant $\hat{\mathbf{z}}\cdot\mathbf{J} = J_z$ and $\hat{\mathbf{n}}\cdot\mathbf{J} = J_n$ are small circles centered on the axes $\hat{\mathbf{z}}$ and $\hat{\mathbf{n}}$, respectively, as illustrated in figure 5.10.

The classical observables J_z and J_n are functions on the d-sphere that vary continuously between the limits

$$-J \le J_z\,,\ J_n \le +J\,. \tag{5.74}$$

The quantized orbits of J_z and J_n are those enclosing $n+1/2$ Planck cells where n is an integer. This implies $J_z = m$ and $J_n = m'$ with the usual rules for quantum numbers m and m'

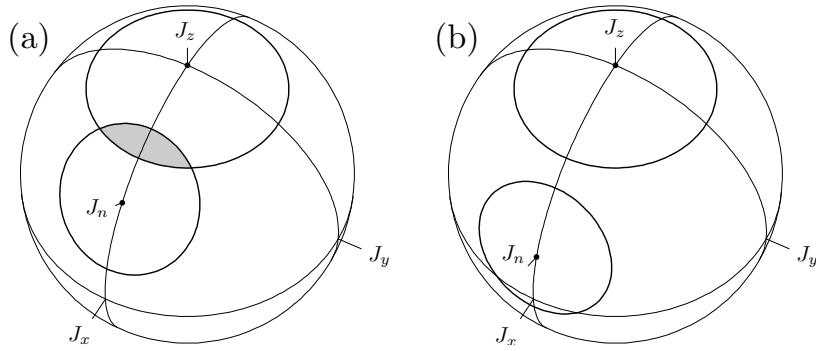

Figure 5.10: Curves of constant J_z and J_n may intersect in the classically allowed region (a) or not intersect in the classically forbidden region (b).

$$-j \leq m\,,\, m' \leq +j\,, \tag{5.75}$$

in integer steps. Thus the maximum and minimum values of m and m' lie one-half unit away from the maximum and minimum values of the classical observables J_z and J_n, as illustrated in figure 5.11. This figure may be compared to figure 5.7 for the $6j$-symbol.

When the J_z-orbit and the J_n-orbit intersect on another as in part (a) of figure 5.10, then we are in the classically allowed region of the d-matrices. There are generically two intersection points related by a reflection in the plane $J_y = 0$, marked by unit vectors from the origin $\hat{\mathbf{a}}$ and $\hat{\mathbf{a}}'$ in figure 5.12. We concentrate on the intersection $\hat{\mathbf{a}}$, for which $J_y > 0$; at the other intersection $\hat{\mathbf{a}}'$ we have $J_y < 0$.

We now find the intersection points of these two circles. Let (θ, ϕ) be the usual spherical coordinates referred to the axis $\hat{\mathbf{z}}$, and let (θ', ϕ') be an alternative set referred to the axis $\hat{\mathbf{n}}$. That is, the Cartesian coordinates (x, y, z) as a function of the (θ', ϕ') coordinates is given by $R_y(\beta)(x', y', z')$. Thus the coordinate transformation $(\theta, \phi) \to (\theta', \phi')$ is specified by

$$\begin{aligned} \sin\theta\cos\phi &= \cos\beta\sin\theta'\cos\phi' + \sin\beta\cos\theta'\,, \\ \sin\theta\sin\phi &= \sin\theta'\sin\phi'\,, \\ \cos\theta &= -\sin\beta\sin\theta'\cos\phi' + \cos\beta\cos\theta'\,, \end{aligned} \tag{5.76}$$

The azimuthal angle ϕ' is conjugate to J_n, so both (ϕ, J_z) and (ϕ', J_n) are canonical coordinates on the sphere.

In the coordinate systems $(\theta, \phi), (\theta', \phi')$, the θ and θ' coordinates of intersection $\hat{\mathbf{a}}$ are given by

$$\cos\theta = \frac{J_z}{J} = \frac{m}{j+\frac{1}{2}}\,, \qquad \cos\theta' = \frac{J_n}{J} = \frac{m'}{j+\frac{1}{2}}\,, \tag{5.77}$$

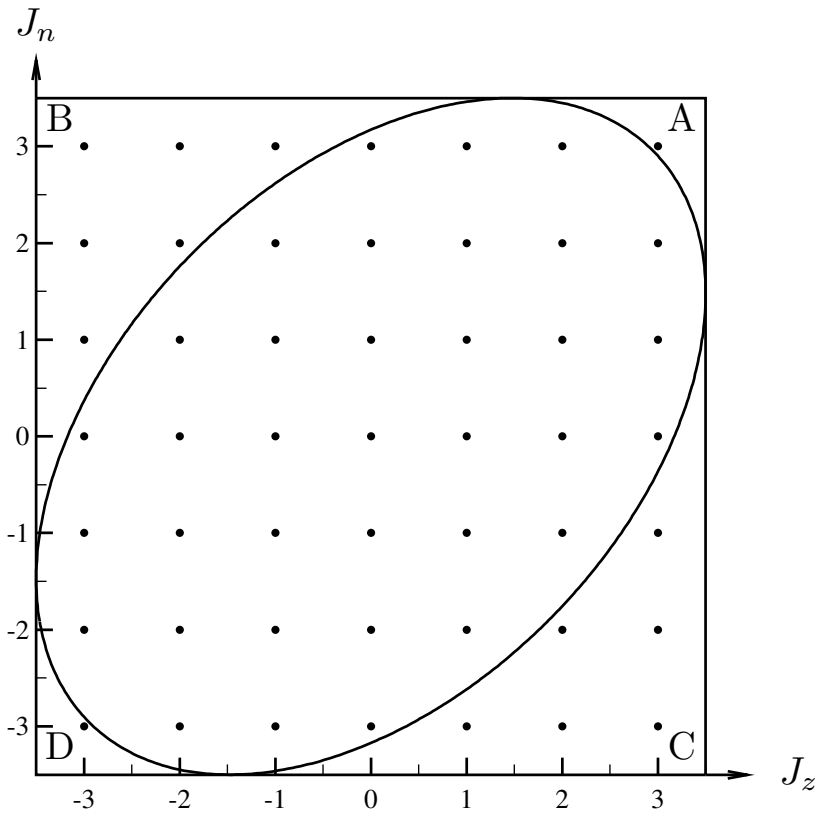

Figure 5.11: The square identifies the bounds on the classical observables J_z and J_n, while the spots indicate the quantized values $J_z = m$, $J_n = m'$. The ellipse is the caustic curve.

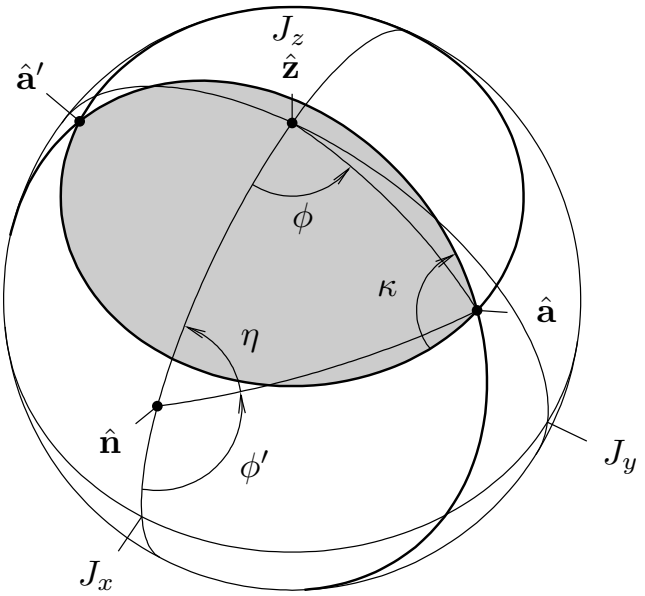

Figure 5.12: Definitions of the angles ϕ, η, and κ. Vector $\hat{\mathbf{a}}$ points to the intersection of the J_z orbit with the J_n orbit, with $J_y > 0$.

where J_z and J_n take on their quantized values. As for the ϕ and ϕ' coordinates of intersection point $\hat{\mathbf{a}}$, they can be obtained by solving (5.76), assuming θ, θ', and β are given. This gives

$$\cos\phi = \frac{\cos\theta' - \cos\beta\cos\theta}{\sin\beta\sin\theta}\,, \tag{5.78}$$

$$\cos\eta = \frac{\cos\theta - \cos\beta\cos\theta'}{\sin\beta\sin\theta'}\,, \tag{5.79}$$

where we write $\eta = \pi - \phi'$ as illustrated in figure 5.12. Equation (5.78) and (5.79) uniquely determine ϕ and η in the interval $[0, \pi]$.

We define κ as the opening angle of the lune, as illustrated in the figure. It is given by

$$\cos\kappa = \frac{\cos\theta\cos\theta' - \cos\beta}{\sin\theta\sin\theta'}\,. \tag{5.80}$$

We define Φ_d as one-half of the area of the shaded lune seen in figure 5.12, then from [21],

$$\Phi_d = J\kappa - J_z\phi - J_n\eta = \left(j + \frac{1}{2}\right)\kappa - m\phi - m'\eta\,. \tag{5.81}$$

The caustics of the d-matrices occur when the small circles $J_z = \text{const}$ and $J_n = \text{const}$ are tangent or, equivalently, when the vectors $(\hat{\mathbf{z}}, \hat{\mathbf{n}}, \hat{\mathbf{a}})$ all lie in the plane $J_y = 0$, and so are linearly dependent. This condition can be expressed as $V_d = 0$, where

$$V_d = (\hat{\mathbf{z}} \times \hat{\mathbf{n}}) \cdot \hat{\mathbf{a}} = \sin\beta \sin\theta \sin\phi \,. \tag{5.82}$$

Multiplying

$$V_d^2 = \sin^2\beta \sin^2\theta \left(1 - \left(\frac{\cos\theta' - \cos\beta\cos\theta}{\sin\beta\sin\theta}\right)^2\right) \tag{5.83}$$

$$= 2\cos\beta\cos\theta\cos\theta' + \sin^2\beta - \cos^2\theta - \cos^2\theta' \tag{5.84}$$

by J^2, and setting the result to zero gives us an equation of the caustic in J_z-J_n space,

$$J_z^2 + J_n^2 - 2J_zJ_n\cos\beta - J^2\sin^2\beta = 0\,, \tag{5.85}$$

where we have used (5.77). The caustic curve is an ellipse whose axes are oriented 45° to the J_z-J_n axes, and whose semimajor and semiminor axes are $2^{1/2}\cos(\beta/2)$, $2^{1/2}\sin(\beta/2)$. An example is illustrated in figure 5.11. The ellipse touches the boundary defined by the classical limits (5.74) at four points, creating four classically forbidden regions labeled ABCD in figure 5.11.

Another point of view on the caustics is to hold J_z and J_n fixed, thereby fixing the sizes of the two small circles, and to vary β, which moves the position of the small circle $J_n = \text{const}$. Then the small circles are tangent at the turning points $\beta = \beta_1$ or β_2, where $0 \le \beta_1 \le \beta_2 \le \pi$, and where

$$\beta_1 = |\theta - \theta'|\,, \qquad \beta_2 = \min(\theta + \theta', 2\pi - \theta - \theta')\,. \tag{5.86}$$

The classically allowed region is $\beta_1 \le \beta \le \beta_2$, while the two classically forbidden regions are $0 \le \beta \le \beta_1$ and $\beta_2 \le \beta \le \pi$.

The four types of tangencies of the two small circles are illustrated in figure 5.13. In all four parts of the figure, T is the caustic point. In part A we are at the upper turning point $\beta = \beta_2$, because if β decreases we obtain two intersection points and are in the classically allowed region. In fact, this is the case $\beta_2 = \theta + \theta' \le \pi$. Or if we hold β fixed but decrease either J_z or J_n, again we enter the classically allowed region, since one or the other of the two small circles expands and the tangency develops into two intersection points. Thus part A of figure 5.13 corresponds to the corner A of figure 5.11. In part B of figure 5.13 we are at the lower turning point $\beta = \beta_1 = \theta - \theta' > 0$, since if β increases we move into the classically allowed region. The same happens if we hold β fixed and either increase J_z or decrease J_n, so this corresponds to corner B of figure 5.11. In part C of figure 5.13 we are at the lower turning point $\beta = \beta_1 = \theta' - \theta > 0$, which corresponds to corner C of figure 5.11, since we enter the classically allowed region if either J_n increases or J_z decreases. Finally, in part D of figure 5.13 we are at the upper turning point $\beta_2 = 2\pi - \theta - \theta' < \pi$, which corresponds to corner D of figure 5.11, since we enter the classically allowed region if either J_z or J_n increases.

The four types of tangencies of orbits for the $6j$-symbol, illustrated in figure 5.8, are topologically identical to the four types for the d-matrices, illustrated in figure 5.13. Similarly, the four classically forbidden regions of the $6j$-symbol, illustrated in figure 5.7, are

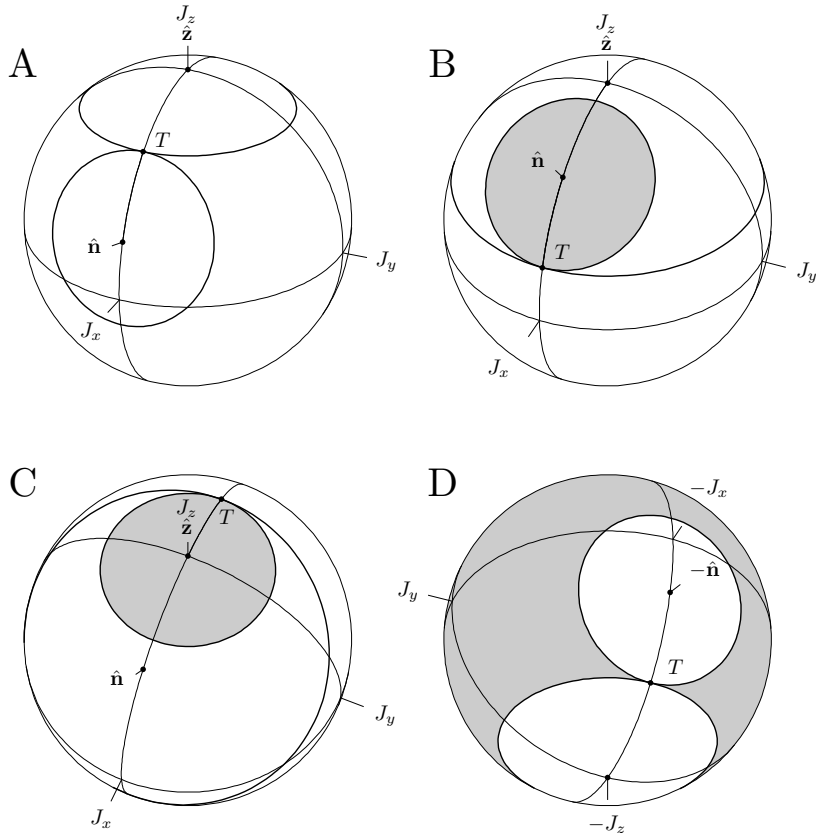

Figure 5.13: Caustics of the d-matrices occur when the two small circles $J_z = \text{const}$ and $J_n = \text{const}$ are tangent. There are four possible types of tangency.

in one-to-one correspondence with the four classically forbidden regions of the d-matrices, illustrated in figure 5.11. Comparing figures 5.7 and 5.11, we see that the labelings of the corners by ABCD are not the same; but this is because the point on the d-sphere of maximum j_n, namely, the point in the direction $\mathbf{n}$, corresponds to the point on the $6j$-sphere of minimum J_{23}. If the J_{23} axis in figure 5.7 had been drawn increasing downward instead of upward, the labels on all four corners of both figure 5.7 and figure 5.11 would coincide.

The similarity of the caustic structures of the $6j$-symbol and the d-matrices suggest that we use the d-matrices as a quantum normal form. Note that the choice of the quantum normal form is not fixed yet, since it depends on the value of β.

5.7 Fixing the Normal Form

The total area of the $6j$-sphere and that of the d-sphere must be equal, which implies

$$2j + 1 = D\,, \tag{5.87}$$

where D is given by (5.43), and j is the parameter of the d-matrix $d^j_{mm'}(\beta)$. This relation agrees with the choice (5.45) used in the Stratonovich Weyl symbol correspondence.

The quantum numbers j_{12} and j_{23} determine a specific pair of orbits on the $6j$-sphere, the small circle $J_{12} = j_{12} + 1/2$, and the oval $J_{23} = j_{23} + 1/2$. The canonical map is required to map the small circle $J_{12} = j_{12} + 1/2$, a quantized orbit, onto small circle $J_z = \text{const}$ on the d-sphere . Because area is preserved, the small circle on the d-sphere must also be quantized and contain the same area about the north pole as the original small circle on the $6j$-sphere. That is, we must have $j_{12,\max} - j_{12} = j - m$ and $j_{12} - j_{12,\min} = j + m$, or

$$m = j_{12} - j_{12,\text{avg}}\,, \tag{5.88}$$

where $j_{12,\text{avg}} = (j_{12,\min} + j_{12,\max})/2$. This determines the quantum number m in $d^j_{mm'}(\beta)$, which agrees with the choice (5.46) used in the symbol correspondence. Note that we are only required to map this specific small circle of constant J_{12} on the $6j$-sphere onto the corresponding small circle on the d-sphere; other small circles of constant J_{12} on the $6j$-sphere, for other values of J_{12}, are *not* mapped to small circles of constant J_z on the d-sphere.

Similarly, we are required to map the quantized oval $J_{23} = j_{23} + 1/2$ on the $6j$-sphere onto a small circle on the d-sphere that is centered about some direction$\hat{\mathbf{n}}$ that lies on the semicircle $J_y = 0, J_x > 0$ on the d-sphere. The direction $\hat{\mathbf{n}}$ is a function of the angle β, which will be specified momentarily. Because area is preserved, the new small circle on the d-sphere will be a quantized orbit $J_n = m'$, enclosing the same area about the axis $\hat{\mathbf{n}}$ as the oval $J_{23} = j_{23} + 1/2$ encloses about the point $J_{23,\min}$. Since the minimum of J_{23} corresponds to the maximum of J_n, the quantum number m' satisfies $j_{23} - j_{23,\min} = j - m'$, and $j_{23,\max} - j_{23} = j + m'$, or

$$m' = j_{23,\text{avg}} - j_{23}\,. \tag{5.89}$$

i	A	A	B	B	C	D	D
1	π	0	π	0	π	π	0
2	π	0	0	π	π	0	π
3	0	π	π	0	π	0	π
4	0	π	0	π	π	π	0
12	π	π	π	π	0	0	0
23	0	0	π	π	0	π	π

Table 5.1: The dihedral angles ψ_i on the segments of the caustic curve bounding classically forbidden regions ABCD. There are two possibilities for segments B and D, and one for segments A and C.

The parameter β is determined by requiring that the area of the lune on the $6j$-sphere should equal to the area of the lune on the d-sphere. Effectively, we rotate the small circle $J_n = m'$ until the two areas are equal. This is in the classically allowed region; in the classically forbidden region, the analytic continuations of the areas on the two spheres are set equal. In this way, if the $6j$-symbol is in the classically allowed region, then so is the d-matrix, and vice versa. This condition is the analogue of (5.1) in the standard method of comparison equations.

According to (4.33), which was derived using the Schläfli identity, the area on the $6j$-sphere enclosed by the curves $J_{12} = \text{const}$ and $J_{23} = \text{const}$ is equal to twice the Ponzano-Regge action plus a constant. That is,

$$\Phi_{\rm PR} = \frac{1}{2}(\text{area of the lune}) + \Phi_0\,, \tag{5.90}$$

where Φ_0 is an extra phase, and the Ponzano-Regge phase is given by

$$\Phi_{\rm PR} = \sum_i J_i \psi_i\,, \tag{5.91}$$

where $\psi_i \in [0, \pi]$, $i = 1, 2, 3, 4, 12, 23$ are the exterior dihedral angles of the tetrahedron associated with edges J_i. The possible values of the ψ_i on the caustic curve are summarized in table 5.1. The four segments of the caustic curve are identified by the classically forbidden region (ABCD) to which they are adjacent. In segment A, B, and D there are two possibilities, while in segment C there is only one. In segment A, the first column applies if $J_{12,\max} = J_3 + J_4$ and the second column otherwise; in segment B, the first column applies if $J_{23,\min} = J_2 - J_3$ or $J_4 - J_1$ and the second column otherwise; and in segment D, the first column applies if $J_{23,\max} = J_2 + J_3$, and the second column otherwise. The dihedral angles in a flat tetrahedron such as the ones labeled $Y \to X$ and $X \to Z$ are 0 for interior segments and π for segments bounding the outside of the plane figure.

Although some angles ψ_i are discontinuous at points $XYZW$, the Ponzano-Regge phase $\Phi_{\rm PR}$ is continuous everywhere on the caustic boundary, hence everywhere inside and on the caustic boundary.

We can determine Φ_0 by evaluating both the area of the lune and $\Phi_{\rm PR}$ at any point in the classically allowed region or on the caustic curve, as in figure 5.7, since $\Phi_{\rm PR}$ is

a continuous function of position inside and on that curve. A point on segment A of the caustic boundary is convenient, since the area of the lune vanishes there, as shown by part A of figure 5.8. In this way, using the values of the angles in table 5.1, and (5.41), we find

$$\Phi_0 = (J_1 + J_2 + J_3 + J_4 + J_{12} - J_{12,\max})\pi = (\nu_{\rm ex} + \frac{3}{2})\pi\,, \tag{5.92}$$

where

$$\nu_{\rm ex} = j_1 + j_2 + j_3 + j_4 + j_{12} - j_{12,\max}\,. \tag{5.93}$$

Note that $\nu_{\rm ex}$ is an integer. As a check one can evaluate $\Phi_{\rm PR}$ and the area of the lune at other points on the caustic boundary (segments BCD) and see that the answer for Φ_0 agrees with (5.92). Thus β is determined by the equation

$$\Phi_{\rm PR} = \Phi_d(\beta) + \Phi_0\,. \tag{5.94}$$

Despite the complications arising from the extra term Φ_0, the geometrical meaning of (5.94) is simple: the areas of the lunes on the two spheres are equal.

In the classically forbidden region, the analytic continuations of the areas of the two lunes become complex, but their real parts are constant in any given region (ABCD).

The value of ψ_i should agree as we approach the caustic curve from the classically allowed and forbidden regions. The angle ψ_i is either 0 or π, depending on the index i and the region ABCD, as shown in table 5.1. If $\psi = 0$, $\cos\psi_i = 1$ on the caustic curve, then $\cos\psi_i$ is real and > 1 in the classically forbidden region. In this case we choose $\psi_i = i\overline{\psi}_i$, where $\overline{\psi}_i = \cosh^{-1}(\cos\psi_i)$ is real and positive. If $\psi_i = \pi$, $\cos\psi_i = -1$ on the caustic curve, then $\cos\psi_i$ is real and < -1 in the classically forbidden region. In this case we choose $\psi_i = \pi + i\overline{\psi}_i$, where $\overline{\psi}_i = -\cosh^{-1}(-\cos\psi_i)$ is real and negative. We can summarize these two cases by

$$\overline{\psi}_i = \mathrm{sign}(\cos\psi_i)\cosh^{-1}(|\cos\psi_i|)\,. \tag{5.95}$$

Despite the sign and absolute value functions, ψ_i is a smooth function of position in any of the four classically forbidden regions. With these definitions, the imaginary part of the analytic continuation of $\Phi_{\rm PR}$ is

$$\overline{\Phi}_{\rm PR} = \sum_i J_i\overline{\psi}_i\,, \tag{5.96}$$

where the sum runs over all six i. The quantity $\overline{\Phi}_{\rm PR}$ vanishes on the caustic curve and becomes real and negative as we move into the classically forbidden region A or D, or real and positive as we move into regions B or C.

We now define a quantity related to the analytic continuation of Φ_d into the classically forbidden regions. If we hold β fixed and vary J_z or J_n, moving from the interior of the ellipse to the boundary, then all the angles ϕ, η, and κ approach either 0 or π, depending on which segment ABCD of the boundary we approach. The values of these angles on the caustics are summarized in table 5.2. For uniformity of notation, we write α_i, $i = 1, 2, 3$, for κ, ϕ, and η, as indicated in the table, and similarly we write k_i, $i = 1, 2, 3$ for

i	α_i	k_i	A	B	C	D
1	κ	j	0	π	π	0
2	ϕ	$-m$	0	0	π	π
3	η	$-m'$	0	π	0	π
		ν_d	0	$j-m'$	$j-m$	$-m-m'$

Table 5.2: Values of the angles κ, ϕ and η on caustics of type ABCD, also integer ν_d for four caustic types.

$j, -m, -m'$, where the signs are the same as in the three terms of the expression (5.81) for Φ_d.

The angles α_i are extended into the classically forbidden region in a manner exactly like that used for the ψ_i in the case of the $6j$-symbol, as explained above. That is, if $\alpha_i = 0$ on the segment of the caustic curve adjacent to a given classically forbidden region, then we define $\alpha_i = i\overline{\alpha}_i$, where $\overline{\alpha}_i = \cosh^{-1}(\cos\alpha_i)$ is real and positive; while if $\alpha_i = \pi$ on the caustic curve, then we define $\alpha_i = \pi + i\overline{\alpha}_i$, so that $\overline{\alpha}_i = -\cosh^{-1}(-\cos\alpha_i)$ is real and negative. In the classically forbidden regions, the quantities $\cos\alpha_i$, given by (5.78) - (5.80), lie outside the interval $[-1, +1]$.

We now define a quantity related to the analytic continuation of Φ_d into the classically forbidden regions

$$\overline{\Phi}_d = \sum_{i=1}^{3} k_i\overline{\alpha}_i = \sum_{i=1}^{3} k_i \mathrm{sign}(\cos\alpha_i)\cosh^{-1}|\cos\alpha_i| \,. \tag{5.97}$$

Despite the absolute value and sign functions, $\overline{\Phi}_d$ is smooth over any given classically forbidden region. This is important for root finders that rely on smoothness, such as the Newton-Raphson method. The quantity $\overline{\Phi}_d$ is zero on the caustic boundary and real and negative as we move into the classically forbidden regions B and C, and real and positive as we move into the classically forbidden regions A and D. These are the same rules as for $\overline{\Phi}_{\mathrm{PR}}$.

To find β in the classically forbidden region, the imaginary parts need to be equated, that is,

$$\overline{\Phi}_{\mathrm{PR}} = \overline{\Phi}_d(\beta) \,. \tag{5.98}$$

The root of (5.94) and (5.98) can be found by the Newton-Raphson method, where the derivatives $d\Phi_d/d\beta$ and $d\overline{\Phi}_d/d\beta$ can be found from (5.81) and (5.97), respectively.

5.8 The Canonical Map on the Sphere

After we have fixed the value of β, we show the existence of the required canonical map by construction. This canonical map must map the two curves $J_{12} = \text{const}$ and $J_{23} = \text{const}$ on the $6j$-sphere, to the two curves $J_z = \text{const}$ and $J_n = \text{const}$ on the d-sphere, as illustrated in figure 5.14. If the phase space is a plane instead of a sphere, and if the level

sets of $J_{12} = \text{const}$ are straight lines instead of small circles, we can squeeze or stretch the curve $J_{23} = \text{const}$ into any desired shape by moving the small circles $J_{12} = c$, such as the circle 2 on the left of figure 5.14, vertically towards or away from the small circle 1 on the left. That would result in a usual point transformation as illustrated in figure 5.2. However, in this problem, the phase space is a sphere of finite area, moving the circle 2 on the left of figure 5.14 up and down while preserving the area between the circles 1 and 2 would be impossible. Thus we can rule out point transformations. This is the reason why we must generalize our theory to handle general canonical transformations that are not point transformations in section 5.3.

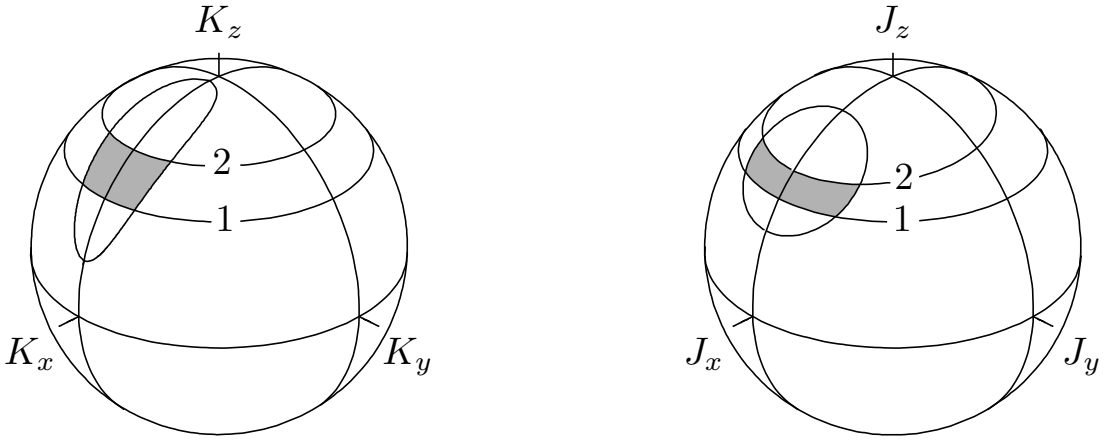

Figure 5.14: The canonical map that maps a small circle $K_z = z$ to a small circle $J_\alpha = \text{const}$ that is tilted by some angle $\alpha(z)$ around the y-axis. This tilt of the circle 2 effectively squeezes the shaded area in the $6j$-sphere, and pushes the curve $J_{23} = \text{const}$ outward toward the curve $J_n = \text{const}$ in the d-sphere.

Instead of moving the circle 2 up and down vertically, we can effectively squeeze or stretch the shaded area in figure 5.14 by tilting circle 2 by some angle $\alpha(c)$ about the y axis, as illustrated on the right side of figure 5.14. The angle $\alpha(c)$ is determined by equating the area of the two shaded regions in figure 5.14. The shaded area on the left can be viewed as the difference of two Ponzano Regge actions for two different values of J_{12}. The area on the right can also be viewed as the difference between two d actions for different values of m. However, since the circles 1 and 2 do not have the same axis, we must take into account the modification of the angle from β to $\beta - \alpha$ for one of the actions. By equating the two shaded areas, the resulting equation for $\alpha(c)$ is given by

$$\Phi_{\text{PR}}(c) - \Phi_{\text{PR}}(j_{12} + 1/2) = \Phi_{\text{d}}(\beta - \alpha(c), K_z(c)) - \Phi_{\text{d}}(\beta, K_z(j_{12} + 1/2))\,, \tag{5.99}$$

where the argument in Φ_{PR} is the value of J_{12}, and the second argument in Φ_{d} is the value of m. Solving for $\alpha(c)$, we find a map that maps the small circles $J_{12} = c$ to tilted small circles $J_\alpha = \alpha(c) \cdot \mathbf{J} = K_z(c)$. This way, we have shown the existence of a canonical map that maps the curves $J_{12} = \text{const}$ and $J_{23} = \text{const}$ to the curves $J_z = \text{const}$ and $J_n = \text{const}$.

This canonical map allows us to construct a unitary operator that transforms a $6j$-symbol into a rotational matrix.

5.9 A Uniform Approximation for the $6j$-Symbol

We now derive the uniform approximation for the $6j$-symbol using formula (5.18) and the canonical map $Z : (K_x, K_y, K_z) \to (J_x, J_y, J_z)$ on the sphere. The Hamiltonian H is J_{23}, and the normal form is J_n. The coordinates K_z and J_z replace the coordinates x and X, respectively. From the construction of Z, we have

$$(J_{23}(K_z, \phi_{12}) - J_{23}) \circ Z^{-1} = A(J_n - m')\,, \tag{5.100}$$

$$(J_{12}(K_z, \phi_{12}) - J_{12}) \circ Z^{-1} = B(J_z - m)\,, \tag{5.101}$$

for some functions $A(J_z, \phi)$ and $B(J_z, \phi)$. The formula (5.18) gives

$$\langle j_{12}|j_{23}\rangle = \langle J_z : m|\frac{1}{\sqrt{\hat{A}\hat{B}}}|J_n : m'\rangle\ . \tag{5.102}$$

Because $\hat{A}$ and $\hat{B}$ are part of the amplitude, we only need to evaluate them to zeroth order. We assume that $A = f(J_z, J_n)$ and $B = g(J_z, J_n)$ can be expressed, respectively, as some functions f, g of the variables J_z and J_n, so to zeroth order, $\hat{A} = f(\hat{J}_z, \hat{J}_n)$ and $\hat{B} = g(\hat{J}_z, \hat{J}_n)$. Acting $\hat{J}_z$ on $|J_z : m\rangle$ on the left replaces the operator $\hat{J}_z$ by the eigenvalue m. Similarly, acting $\hat{J}_n$ on $|J_n : m'\rangle$ on the right replaces the operator $\hat{J}_n$ by m'. Here we have ignored the ordering of $\hat{J}_z$ and $\hat{J}_n$, since we are evaluating $\hat{A}$ and $\hat{B}$ to zeroth order. Thus (5.102) becomes

$$\langle j_{12}|j_{23}\rangle = \frac{1}{\sqrt{f(m,m')g(m,m')}}\,\langle J_z : m|J_n : m'\rangle \tag{5.103}$$

$$= \frac{1}{\sqrt{A(m,\phi_0)B(m,\phi)}}\,d^j_{mm'}(\beta)\,, \tag{5.104}$$

where the point $(J_z, \phi) = (m, \phi_0)$ is the intersection point of the level sets $J_z = m$ and $J_n = m'$, and $\phi = \phi_0$ is given by (5.78).

From the definitions of A in (5.100), we evaluate A at the point (m, ϕ_0) as a limit $\phi \to \phi_0$ on the curve $K_z = m$. We find

$$A(m,\phi_0) = \lim_{\phi\to\phi_0}\frac{J_{23}\circ Z^{-1} - J_{23}}{J_n(m,\phi) - m'} \tag{5.105}$$

$$= \frac{\partial J_{23}(K_z(m,\phi), \phi_{12}(m,\phi))/\partial\phi}{\partial J_n(m,\phi)/\partial\phi} \tag{5.106}$$

$$= \frac{(\partial J_{23}/\partial\phi_{12})\,(\partial\phi_{12}/\phi)}{\partial J_n(m,\phi)/\partial\phi} \tag{5.107}$$

$$= \frac{\{J_{12}, J_{23}\}\,(\partial\phi_{12}/\phi)}{\{J_z, J_n\}}\,, \tag{5.108}$$

where we have used L'Hôptal rule in the second equality, and the chain rule and the fact $\partial K_z(m,\phi)/\partial\phi = 0$ in the third equality. In the fourth equality, we have used the fact that (J_{12}, ϕ_{12}) are canonical coordinates in the numerator, and (K_z, ϕ) are canonical coordinates in the denominator, so the derivatives can be replaced by Poisson brackets.

Similarly, we can evaluate B from its definition in (5.101) as a limit $J_z \to m$ on the curve $\phi = \phi_0$. We find

$$B(m,\phi_0) = \lim_{J_z\to m} \frac{K_z \circ Z^{-1} - m}{J_z - m} = \frac{\partial K_z/\partial J_z}{\partial J_z/\partial J_z} = \frac{\partial K_z}{\partial J_z}\,. \tag{5.109}$$

It turns out the product of the two derivatives is equal to the Jacobian of the canonical transformation at the intersection point (m, ϕ_0), which is equal to unity by the area preserving property of the map. To see this, note that $K_z(J_z = m, \phi) = m$ implies that $\partial K_z/\partial\phi = 0$ at (m, ϕ_0). So the Jacabian simplifies, and we have

$$1 = \det\begin{pmatrix} \partial K_z/\partial J_z & \partial K_z/\partial\phi \\ \partial\phi_{12}/\partial J_z & \partial\phi_{12}/\partial\phi \end{pmatrix} = \left(\frac{\partial K_z}{\partial J_z}\right)\left(\frac{\partial\phi_{12}}{\partial\phi}\right)\,. \tag{5.110}$$

Thus

$$A(m,\phi_0)\,B(m,\phi_0) = \frac{\{J_{12}, J_{23}\}}{\{J_z, J_n\}}\,. \tag{5.111}$$

Putting (5.111) back into (5.104), we find

$$\langle j_{12}|j_{23}\rangle = \left(\frac{\{J_z, J_n\}}{\{J_{12},\, J_{23}\}}\right)^{1/2} d^j_{mm'}(\beta)\,. \tag{5.112}$$

Using the expression of J_n from (5.69), we find

$$|\{J_z, J_n\}| = \sin\beta\sqrt{J^2 - J_z^2}\sin\phi_0 = \sin\beta J_y\,, \tag{5.113}$$

where $J_y = \sqrt{J^2 - J_z^2}\sin\phi_0$. Either through a direct calculation using the expression of J_{23} from (5.61), or from (4.21), we have

$$|\{J_{12}, J_{23}\}| = \frac{\{J_{12}^2, J_{23}^2\}}{J_{12}\,J_{23}} = \frac{6V}{J_{12}\,J_{23}}\,. \tag{5.114}$$

Finally, putting the Poisson brackets back into (5.112) and using the definition of the $6j$-symbol (5.28), we arrive at the uniform approximation of the $6j$-symbol in terms of the d-matrices,

$$\begin{Bmatrix} j_1 & j_2 & j_{12} \\ j_3 & j_4 & j_{23} \end{Bmatrix} = (-1)^\gamma \frac{1}{\sqrt{4J_{12}\,J_{23}}}\left(\frac{|\{J_z, J_n\}|}{|\{J_{12},\, J_{23}\}|}\right)^{1/2} d^j_{mm'}(\beta) \tag{5.115}$$

$$= (-1)^\gamma \left(\frac{|\sin\beta\, J_y|}{|24V|}\right)^{1/2} d^j_{mm'}(\beta)\,, \tag{5.116}$$

where we have put back an arbitrary phase $(-1)^\gamma$ that we have ignored up to now.

5.10 The Overall Phase and Numerical Analysis

We will determine the phase by comparing the known WKB approximation for the $6j$-symbol and the d-matrices in the classically allowed and forbidden regions. In the classically allowed region, the Ponzano-Regge formula is

$$\left\{ \begin{array}{ccc} j_1 & j_2 & j_{12} \\ j_3 & j_4 & j_{23} \end{array} \right\} = \frac{1}{\sqrt{12\pi|V|}} \cos\left(\Phi_{\rm PR} + \frac{\pi}{4}\right) . \tag{5.117}$$

The asymptotic expression for the d-matrices is

$$d^j_{mm'} = \frac{(-1)^{j-m'}}{\sqrt{(\pi/2)|\sin\beta J_y|}} \cos\left(\Phi_d - \frac{\pi}{4}\right) . \tag{5.118}$$

We have chosen β so that

$$\Phi_{\rm PR} = \Phi_d(\beta) + \Phi_0 \,, \tag{5.119}$$

where

$$\Phi_0 = (J_1 + J_2 + J_3 + J_4 + J_{12} - J_{12,\max})\pi = (\nu_{\rm ex} + \frac{3}{2})\pi \,, \tag{5.120}$$

and where

$$\nu_{\rm ex} = j_1 + j + 2 + j_3 + j_4 + j_{12} - j_{12,\max} \,. \tag{5.121}$$

Taking cosines,

$$\cos\left(\Phi_{\rm PR} + \frac{\pi}{4}\right) = \cos\left(\Phi_d + \nu_{\rm ex}\pi + \frac{3\pi}{2} + \frac{\pi}{4}\right) = (-1)^{\nu_{\rm ex}} \cos\left(\Phi_d - \frac{\pi}{4}\right) . \tag{5.122}$$

Comparing (5.117) and (5.118) in (5.116), and using (5.122), we can read off the phase

$$(-1)^\gamma = (-1)^{\nu_{\rm ex}+m'-j} \,. \tag{5.123}$$

in the classically allowed region.

We can do a similar comparison in the four classically forbidden regions (ABCD) to find the overall phases in those regions. Finally, we obtain the uniform approximation of the $6j$-symbol in terms of the rotation matrices, complete with phases,

$$\left\{ \begin{array}{ccc} j_1 & j_2 & j_{12} \\ j_3 & j_4 & j_{23} \end{array} \right\} = (-1)^{\nu_{\rm ex}+m'-j+\nu_{6j}-\nu_d} \left(\frac{|\sin\beta\, J_y|}{|24V|}\right)^{1/2} d^j_{mm'}(\beta) \,, \tag{5.124}$$

where $\nu_{6j} = 0$ and $\nu_d = 0$ in the classically allowed region, and

$$\nu_{6j} = {\sum_i}' j_i \,, \qquad \nu_d = {\sum_i}' k_i \,, \tag{5.125}$$

in the classically forbidden regions. Here the prime in the sum for ν_{6j} means to sum only over i such that ψ_i on a segment of the caustic curve has the value π in table 5.1, and the prime in the sum for ν_d means to sum only over i such that α_i on a segment of the caustic curve has the value π in table 5.2.

We now discuss the how the errors in the formula (5.124) compare to those for the Ponzano Regge approximation. Figure 5.15 shows the results of numerical tests of the new uniform approximation, with comparison with the Ponzano-Regge approximation. In the figure, errors are plotted as a function of j_{12} for the $6j$-symbols

$$\left\{ \begin{array}{ccc} 39/2 & 23 & j_{12} \\ 17/2 & 20 & 47/2 \end{array} \right\} \quad \text{and} \quad \left\{ \begin{array}{ccc} 156 & 184 & j_{12} \\ 68 & 160 & 188 \end{array} \right\} \tag{5.126}$$

in part (a) and part (b) of the figure, respectively. The values of the five fixed j's in part (b) are 8 times those in part (a). The plots show the absolute value of the difference between the exact $6j$-symbol and the approximate value. In both parts of the figure, the curve labeled PR is the error of the Ponzano-Regge approximation, while that labeled U is the error of the uniform approximation. The error of the Ponzano-Regge approximation is large near the caustics, as expected, while the error of the uniform approximation is fairly flat throughout the classically allowed region and up to the caustics. The error of both approximations falls rapidly to zero in the classically forbidden regions, as of course does the exact $6j$-symbol.

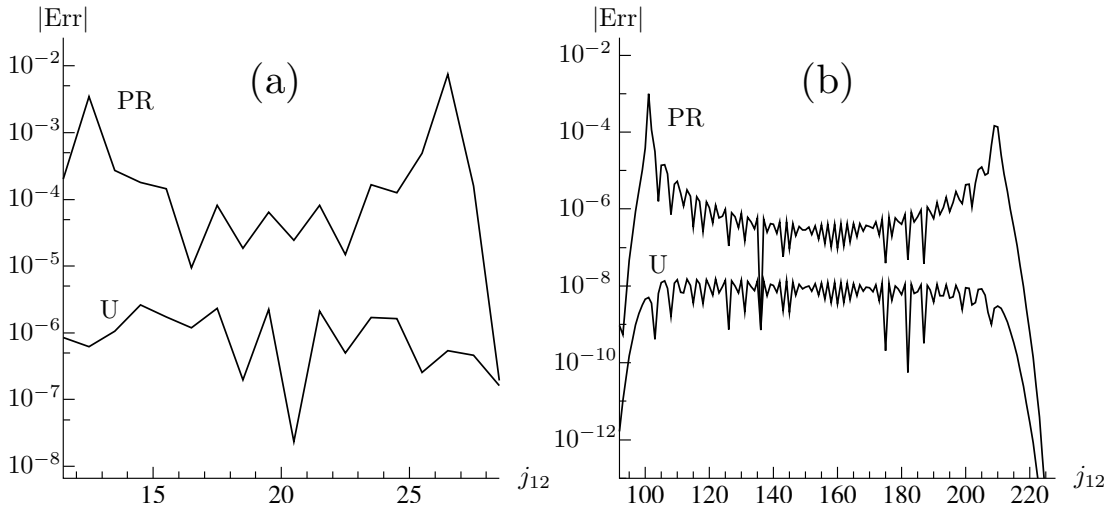

Figure 5.15: Absolute value of the error of the Ponzano-Regge approximation (PR) and of the uniform approximation (U) as a function of j_{12} for values of the other five j's shown in (5.126). The error is defined as the difference between the approximate value and the exact value.

In the classically allowed region the error is oscillatory, and it is possible for the Ponzano-Regge error to be less than that of the uniform approximation simply because it accidentally happens to fall near a zero of the cosine function. One such descending spike near $j_{12} = 140$ can be seen in part (b) of the figure. It is clear, however, that a fair

comparison of the errors in the classically allowed region must use the amplitude of the oscillatory function and ignore the oscillations. By this measure the error of the uniform approximation in figure 5.15 is approximately 30 times smaller than that of the Ponzano-Regge approximation in the center of the classically allowed region and gets better as we approach the caustics. This ratio is nearly the same in parts (a) and (b), indicating that both errors scale in the same way with j. In the classically forbidden region the errors can be compared directly, without removing any oscillatory factor, and again for the values used the figure shows that the error in the uniform approximation is smaller than that in the Ponzano-Regge approximation.

The error term for the Ponzano-Regge approximation is unknown, as is that for the uniform approximation, so there is no theory by which the errors can be compared. We would expect, however, on general grounds that the two error terms should scale the same with j, a conclusion that is supported by the numerical evidence. That the ratio between the errors should be as small as seen in figure 5.15 was a surprise to us, and we have no explanation for it. The values of the j's chosen in that example were essentially random, but when we try other "randomly chosen" values of the j's we get similar plots. If we systematically search for j values such that the error of the uniform approximation is as unfavorable as possible relative to that of the Ponzano-Regge approximation in the classically allowed region, we find cases such as

$$\left\{ \begin{array}{ccc} 44 & 40 & j_{12} \\ 20 & 24 & 28 \end{array} \right\}, \tag{5.127}$$

which gives the error plots in figure 5.16. In this case the two errors are comparable for an extended range of j_{12}. We have found no cases in which the uniform approximation is much worse than the Ponzano-Regge approximation in the classically allowed region.

5.11 Conclusions

By connecting the Wigner $6j$-symbol with the rotational d-matrices, which has known asymptotics, we have not only derived a new uniform approximation, but also provided an independent derivation for the asymptotics of the $6j$-symbol. The geometric meaning of the phase function of the $6j$-symbol is clear. It is the area enclosed by the two level sets corresponding to the $\hat{J}_{12}$ and $\hat{J}_{23}$ operators. This area can be evaluated using the Schläfli identity for Euclidean tetrahedra. However, the identification of the J_{23} level set with the edge length J_{23} of a tetrahedron is not as natural as in the semiclassical analysis of the $6j$-symbol in chapter 4, where we started with a tetrahedron from the beginning. This identification may seem accidental here, but we believe there are deeper reasons, and it warrants further investigation. For now, we simply note that the eigenvalue equation of the tri-diagonal operator $\hat{J}_{23}^2$ leads directly to the three-term recursion relation for the $6j$-symbol [76].

For future consideration, there is a natural extension of the present work to the q-deformed $6j$-symbol, where q is a root of unity. In this case, the level set for the symbol J_{23} of the operator $\hat{J}_{23}$ can be read off from another three-term recursion relation for the q-deformed $6j$-symbol. It turns out that this level set can be identified with the edge length

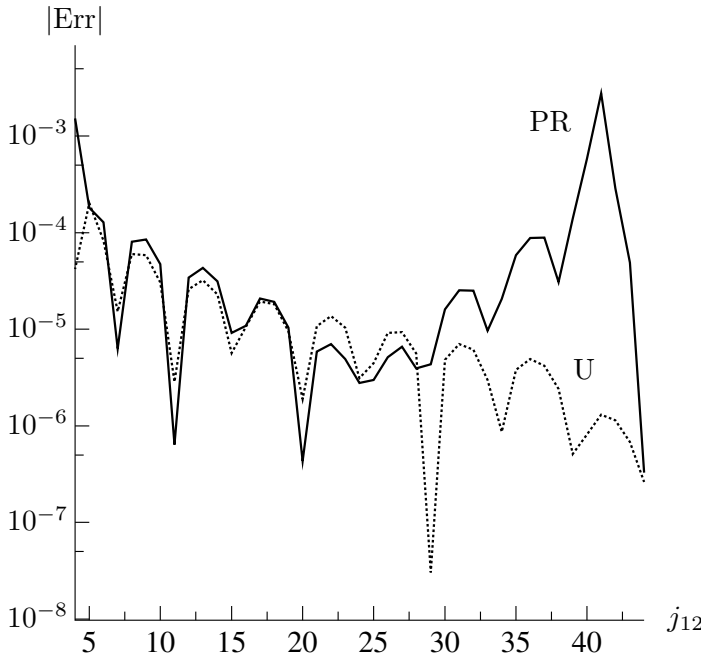

Figure 5.16: Comparison of Ponzano-Regge (PR) and uniform (U) errors as a function of j_{12} for the $6j$-symbol (5.127). The dotted curve is the error in the uniform approximation.

function $J_{23}(J_{12}, \phi_{12})$ of a spherical tetrahedron with the edge lengths $J_1, J_2, J_3, J_4, J_{12}, J_{23}$ and dihedral angle ϕ_{12}, in a constant positive curvature space. The area enclosed by the J_{23} and J_{12} level sets can again be evaluated from the Schläfli identity for spherical tetrahedra. In fact, this area is evaluated in the context of discrete WKB approximation to the q-deformed recursion relations by Mizoguchi and Tada [56]. It consists of the Ponzano-Regge phase, plus an additional term proportional to the curvature and the volume V of this tetrahedron. Unfortunately, the identification of the J_{23} level set with the edge length function $J_{23}(J_{12}, \phi_{12})$ depends on a series of algebraic manipulation and approximations. Thus, we conclude that the missing link for a geometric derivation for the asymptotic limits of the q-deformed $6j$-symbol is a natural identification for the J_{23} function. One possible way to supply this missing link is finding a $4J$ model for the q-deformed case, similar to the one used for the regular $6j$-symbol in chapter 4. This may be possible through the deforming maps that relate the q-deformed $SU(2)_q$ angular momentum operators and the regular $SU(2)$ angular momentum operators [33]. This will be the subject of future research.

The spherical phase space of the Stratonovich Weyl symbol correspondence has attracted the attention of string theorists who want to understand how geometry emerges from algebra. They call it the fuzzy sphere, and is an intriguing geometric object in its own right. In the next chapter, we investigate another interesting geometrical structure, that of a spinor fiber bundle, which emerges from the semiclassical analysis of the Wigner $9j$-symbol, when we represent some angular momenta exactly by linear algebra, and treat others semiclassically.

5.12 Appendix: Construction of the Normal Form Unitary Operator

Now we give more details on the construction of $\hat{U}$ from Z. Although we do not actually need to construct $\hat{U}$ in our calculation, for completeness, and to make it clear that Z^{-1}, not Z, should be used in (5.5), we present the following discussion.

Given the Hamiltonian $\hat{H}$, its zeroth order symbol H_0, and a desired normal form K_0, we assume there exist a symplectic map Z of the phase space that transforms H_0 to K_0, in other words, $K_0 = H_0 \circ Z^{-1}$. We imbed Z into a smooth one parameter family of symplectic maps Z_ϵ, $\epsilon \in [0,1]$, with the boundary condition $Z_0 = I$ and $Z_1 = Z$. We set the symbol of the generators of the unitary transformation G_ϵ to be the solution of the differential equation

$$\frac{dZ_\epsilon^\mu}{d\epsilon} = \{Z_\epsilon^\mu, G_\epsilon\}\,. \tag{5.128}$$

Once we have G_ϵ, we use the inverse symbol map to find $\hat{G}_\epsilon$, and construct $\hat{U}_\epsilon$ as the solution of the operator equation

$$\frac{d\hat{U}_\epsilon}{d\epsilon} = -\frac{i}{\hbar}\,\hat{U}_\epsilon \hat{G}_\epsilon\,, \tag{5.129}$$

with boundary condition $\hat{U}_0 = \hat{I}$. We finally set $\hat{U} = \hat{U}_1$.

To show that $K_0 = H_0 \circ Z^{-1}$ is indeed the principal symbol of $\hat{K} = \hat{U}\hat{H}\hat{U}^\dagger$. We will trace the evolution of ϵ backwards from $\hat{K}$ to $\hat{H}$. Suppose $\hat{K}$ is known. Denote the symbol of $\hat{K}$ up to order $\hbar$ by K_0'. We want to show that $K_0' = K_0$. Define $\hat{H}_\epsilon = \hat{U}_\epsilon^\dagger \hat{K} \hat{U}_\epsilon$, so that $\hat{H}_0 = \hat{K}$, $\hat{H}_1 = \hat{H}$. Differentiate $\hat{H}_\epsilon$ and use (5.129) to get

$$\frac{d\hat{H}_\epsilon}{d\epsilon} = \frac{i}{\hbar}[\hat{G}_\epsilon, \hat{H}_\epsilon]\,. \tag{5.130}$$

Transcribing to symbols using (5.4), and keeping terms up to first order in $\hbar$, we find

$$\frac{dH_\epsilon}{d\epsilon} = -\{G_\epsilon, H_\epsilon\}\,. \tag{5.131}$$

Then $K_0' \circ Z_\epsilon$ is the solution to the above equation, as a result of the following calculation:

$$\begin{aligned}
\frac{d}{d\epsilon}(K_0' \circ Z_\epsilon) &= \frac{dK_0'}{d\epsilon} \circ Z_\epsilon + (K_{0,\mu}' \circ Z_\epsilon)\,\frac{dZ_\epsilon^\mu}{d\epsilon} \\
&= (K_{0,\mu}' \circ Z_\epsilon)\{Z_\epsilon^\mu, G_\epsilon\} \\
&= \{K_0' \circ Z_\epsilon, G_\epsilon\}\,,
\end{aligned} \tag{5.132}$$

where we have used (5.128) in the second equality, and the chain rule in the third equality. Thus, we find $H_\epsilon = K_0' \circ Z_\epsilon$.

The boundary condition $H_0 = K_0' \circ Z_\epsilon$ at $\epsilon = 1$ then requires $K_0' = H_0 \circ Z^{-1}$, which is equal to the normal form K_0 by our choice of the symplectic map Z. This shows the symbol of $\hat{K} = \hat{U}\hat{H}\hat{U}^\dagger$ up to order $\hbar$ is in the required normal form K_0.

Chapter 6

The Wigner $9j$-Symbol with Small and Large Quantum Numbers

6.1 Introduction and Summary

This chapter contains new asymptotic formulas for the $9j$-symbol when some quantum numbers are large and others small. In particular, we derive in full detail an asymptotic formula for the $9j$-symbol in the limit of one small and eight large angular momenta, as well as several in the limit of two small angular momenta. The main theoretical tool we use is a generalization of the Born-Oppenheimer approximation, in which the small angular momenta are the fast degrees of freedom and the large angular momenta are the slow degrees of freedom.

In standard applications in molecular physics, the Born-Oppenheimer approximation couples a set of electronic modes by means of a potential energy matrix, in which the matrix elements are all functions of position and so commute with one another. In our applications the modes of the fast degrees of freedom are coupled by a matrix of noncommuting operators. The required generalization of the Born-Oppenheimer approximation in this case was presented by Littlejohn and Flynn [50] and applied by those authors to a semiclassical treatment of spin-orbit coupling [51]. The method involves diagonalizing the matrix of operators by means of the Moyal star product, in a perturbation expansion in powers of $\hbar$. The results are interesting geometrically, in that there appears a bundle whose base space is the classical phase space of the slow degrees of freedom, with a fiber that is the Hilbert space for the fast degrees of freedom. The fiber bundle carries a Berry's connection, whose curvature contributes to the symplectic form on the base space. This paper makes extensive use of the techniques developed in [50, 51], and assumes a familiarity with them. In addition we note the work of Emmrich and Weinstein [38]. which reinterpreted the transformations of Littlejohn and Flynn as a deformation of the Weyl symbol correspondence and placed the whole procedure in a more mathematical setting.

In this chapter, as in the spin-orbit problem [51], the small angular momentum is represented by exact linear algebra, and the states are represented by multicomponent wave-functions. We use Schwinger's model [78] from chapter 4 to represent the large angular momenta. Some of the issues we face in this chapter are non-Abelian symmetry groups in

the presence of the Born-Oppenheimer approximation and the problem of constructing gauge-invariant expressions for wave-functions and matrix elements.

Part of the significance of this work is a new asymptotic formula for the Wigner $9j$-symbol in terms of a modified form of the well-known Ponzano-Regge formula [68] for the $6j$-symbol. The other part is the demonstration of a new technique that is generally applicable to the studies of higher $3nj$-symbols.

We will briefly review some of the previous works on the asymptotics of the $3nj$-symbol, when some of the angular momenta are small and others are large. Basic references for the definitions and properties of the $3nj$-symbols include Edmonds [35], Biedenharn and Louck [19], Brink and Satchle [23], and Varshalovich [83]. Let us use the notation (s, l) to classify the various asymptotic limits of the $3nj$-symbols, where s and l denote the number of small and large angular momenta, respectively. For a given $3nj$-symbol, not all possibilities $l + s = 3nj$ are allowed, since the sum of two small angular momenta must be small. For the $3j$-symbol, in 1957, Brussaard and Tolhoek [24] used the Stirling's approximation in a sum formula for the Clebsch-Gordan coefficient to derive the $(1, 2)$ case. In 1968, Ponzano and Regge [68] used intuitive methods to guess the $(0, 3)$ case for the $3j$-symbol, as well as the $(0, 6)$ case for the $6j$-symbol. in 1960, Edmonds [35] found the $(1, 5)$ case, which trivially leads to the $(2, 4)$ case [59]. In 1999, Watson [86, 87] derived the $(3, 3)$ case for the $6j$-symbol, as well as the $(4, 5)$ case for the $9j$-symbol. More recently, Anderson et. al. [3, 4] extended Watson's result of the $9j$-symbol to the $(6, 3)$ case where all the small angular momenta are in different rows. The other $(6, 3)$ case where all three small angular momenta are in the same row is still an open problem. Later Haggard and Littlejohn [8] found the formula for $(0, 9)$ case. Our results in this paper will fill in most of the gap for the $9j$-symbol by deriving asymptotic formulas of the $(1, 8)$ case and the $(2, 7)$ case.

Now we give a brief overview of our derivation. After we apply the techniques from [51] to the $9j$-symbol, each multicomponent wave-function consists of a spinor factor and a factor in the form of a scalar WKB solution. The action in the scalar WKB solution is the integral of $p\,dx$ on a Lagrangian manifold. We introduce a nearby Lagrangian manifold, the "$6j$ manifold," which is just the A- or B-manifold from chapter 4. This Lagrangian manifold appears in the semiclassical analysis of the $6j$-symbol, and its action is analyzed in chapter 4. We perturb the unknown action around the action on the $6j$ manifold, through a two steps process. First we introduce an intermediate manifold using the coordinate transformation that gives rise to the gauge invariant coordinates from [51]. By writing the initial gauge-dependent action as a line integral, and perturbing the path for the line integral from the initial Lagrangian manifold to a path on the intermediate manifold, we can write the original line integral as a sum of a gauge-invariant line integral and a geometric phase. Then we perturb the gauge-invariant line integral again by following nearby Hamiltonian flows on the intermediate manifold and on the $6j$ manifold, respectively. This second perturbation further splits the gauge-invariant line integral into a known action on the $6j$ manifold, and a perturbation. When we combine the geometric phase and the perturbation with the spinor field on the Lagrangian manifold, we obtain a field of quantum rotations acting on a fixed spinor. As a result, we obtain a factorization of the multicomponent wave function into a known scalar WKB factor, namely, those for the $6j$-symbol from chapter 4, and a field of

quantum rotations of a reference spinor. Although the quantum rotations are difficult to handle by themselves, they partially cancel out when we take an inner product between two multicomponent wave functions. In the case of the two $6j$ manifolds, there are two components in the intersection set, and only one rotation is required for each Lagrangian manifold. It turns out that the spinor inner product generates a factor of a Wigner d-matrix, and an additional relative phase between the two terms of the WKB approximation. In the end, we find an asymptotic formula for the $9j$-symbol in terms of a Wigner d-matrix and a modified Ponzano-Regge formula.

Now we give an outline of the chapter. In section 6.2, we display the main result of this paper, namely, a new asymptotic formula for the $9j$-symbol where one of the angular momenta is small. In section 6.3, we describe the representation we use for the $9j$-symbol, and express it as an inner product between two multicomponent wave-functions. In section 6.4, we derive a gauge invariant factorization of the wave function. In section 6.5, we use this factorization to derive the asymptotic formula for the $9j$-symbol. Some plots of our formula are presented in section 6.6. The last section contains comments and conclusions. The appendices contain some generalizations to higher $3nj$-symbols.

6.2 An Asymptotic Formula for the $9j$-Symbol

We quote the main result of this paper, namely, a new asymptotic formula for the $9j$-symbol, where one angular momentum, $j_3 = s$, is small compared to the others. We have chosen j_3 to be the small quantum number in the main formula below, but any other choice can be reduced to this case by the symmetries of the $9j$-symbol. The formula is

$$\left\{ \begin{array}{ccc} j_1 & j_2 & j_{12} \\ s & j_4 & j_{34} \\ j_{13} & j_{24} & j_5 \end{array} \right\} = \frac{(-1)^{j_1+j_2+j_4+j_5+2s+\nu}}{\sqrt{(2j_{13}+1)(2j_{34}+1)\,(12\pi V)}} \cos\left(\sum_i (j_i + \frac{1}{2})\,\psi_i + \frac{\pi}{4} - s\pi + \mu\phi_1 + \nu\phi_4 \right) d^s_{\nu\,\mu}(\theta)\,. \tag{6.1}$$

Here the indices on the d-matrix are given by $\mu = j_{13} - j_1$ and $\nu = j_{34} - j_4$. They are of the same order of magnitude as the small parameter s. The sum in the argument of the cosine runs over the six large angular momenta $i = 1, 2, 4, 5, 12, 24$. Out of the eight large angular momenta, these are the ones that do not involve the index $i = 3$. The geometric quantities V, ψ_i, ϕ_1, ϕ_4, and θ are functions of the vector configuration of the tetrahedron in Figure 6.1, the construction of which we will describe shortly. In exactly the same way as they appear in the Ponzano Regge formula [68], V is the volume of the tetrahedron, and each ψ_i is the external dihedral angle at the edge J_i, where $\psi \in [0, \pi]$. The angle $\phi_1 \in [0, \pi]$ is an interior dihedral angle of a tetrahedron containing the edge J_1, but the tetrahedron in question is not the one in figure 6.1, but rather a related, second tetrahedron in figure 6.2. Similarly, the angle $\phi_4 \in [0, \pi]$ is the internal dihedral angle at J_4 in a third tetrahedron in figure 6.3. The angle $\theta \in [0, \pi]$ is not a dihedral angle, but it is the angle between $\mathbf{J}_1$ and $\mathbf{J}_4$, which is adjacent in figure 6.2 and 6.3. Explicitly, the angles ϕ_1, ϕ_4, and θ are defined in terms of the vectors $\mathbf{J}_i$ as follows:

$$\phi_1 = \pi - \cos^{-1}\left(\frac{(\mathbf{J}_1 \times \mathbf{J}_4)\cdot(\mathbf{J}_1 \times \mathbf{J}_5)}{|\mathbf{J}_1 \times \mathbf{J}_4|\,|\mathbf{J}_1 \times \mathbf{J}_5|}\right), \tag{6.2}$$

$$\phi_4 = \pi - \cos^{-1}\left(\frac{(\mathbf{J}_4 \times \mathbf{J}_1)\cdot(\mathbf{J}_4 \times \mathbf{J}_5)}{|\mathbf{J}_4 \times \mathbf{J}_1|\,|\mathbf{J}_4 \times \mathbf{J}_5|}\right), \tag{6.3}$$

$$\theta = \cos^{-1}\left(\frac{\mathbf{J}_1 \cdot \mathbf{J}_4}{J_1\,J_4}\right) = \cos^{-1}\left(\frac{\mathbf{J}_{12}\cdot\mathbf{J}_4 - \mathbf{J}_2\cdot\mathbf{J}_4}{J_1\,J_4}\right). \tag{6.4}$$

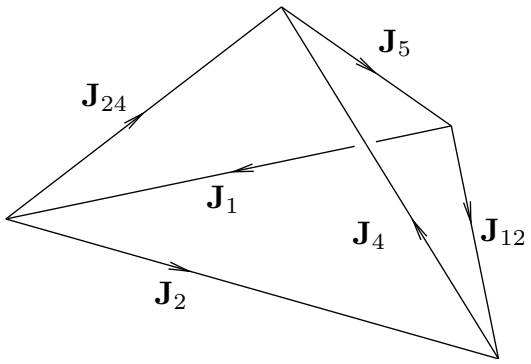

Figure 6.1: The tetrahedron constructed from the six edge lengths J_r, $r = 1, 2, 4, 5, 12, 24$.

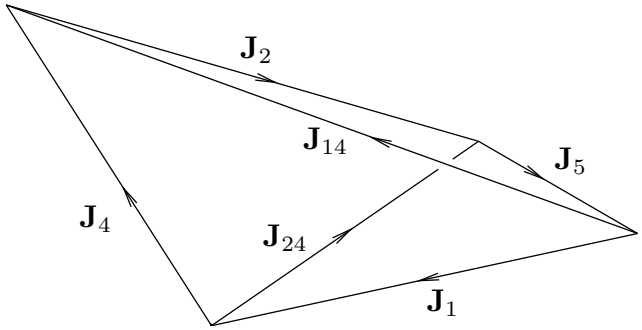

Figure 6.2: The vectors from figure 6.1 are rearranged from $\mathbf{J}_1 + \mathbf{J}_2 + \mathbf{J}_4 + \mathbf{J}_5 = \mathbf{0}$ to $\mathbf{J}_1 + \mathbf{J}_4 + \mathbf{J}_2 + \mathbf{J}_5 = \mathbf{0}$ to form a different polygon. The intermediate vector $\mathbf{J}_{12}$ no longer appears. Instead, we have $\mathbf{J}_{14} = \mathbf{J}_1 + \mathbf{J}_4$.

To use formula (6.1), we construct the vector configurations of the tetrahedron in figure 6.1, given the six edge lengths J_r, $r = 1, 2, 4, 5, 12, 24$, according to the procedure in section 4.4 of chapter 4. There, a Gram matrix G, which consists of dot products between three vectors at a vertex of the tetrahedron in figure 6.1, say $\mathbf{J}_1$, $\mathbf{J}_{12}$, $-\mathbf{J}_5$, are expressed in terms of the six edge lengths $J_r = j_r + 1/2$, $r = 1, 2, 4, 5, 12, 24$. Then a singular decomposition of G gives a vector configuration of the three vectors, and the

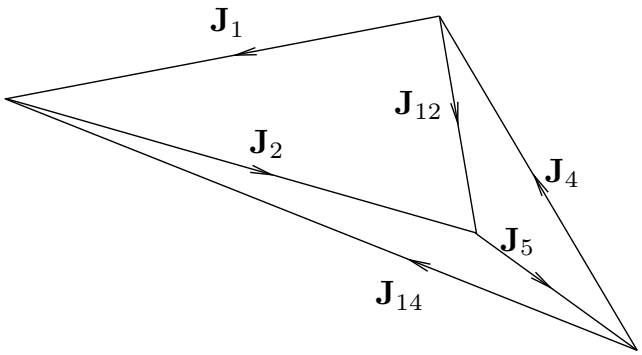

Figure 6.3: The vectors from figure 6.1 are rearranged from $\mathbf{J}_1 + \mathbf{J}_2 + \mathbf{J}_4 + \mathbf{J}_5 = \mathbf{0}$ to $\mathbf{J}_4 + \mathbf{J}_1 + \mathbf{J}_2 + \mathbf{J}_5 = \mathbf{0}$ to form a different polygon. The intermediate vector $\mathbf{J}_{24}$ no longer appears. Instead, we have $\mathbf{J}_{14} = \mathbf{J}_1 + \mathbf{J}_4$.

remaining three vectors are constructed from the different pairs of those three vectors. For instance, the resulting vector configuration for the values $(J_1, J_2, J_4, J_5, J_{12}, J_{24}) = (101, 123, 88, 64.5, 68.5, 92.5)$ is illustrated in figure 6.1. Notice the tetrahedra from figure 6.2 and figure 6.3 contain the edge length J_{14}, which is not related to any of the nine quantum numbers of the $9j$-symbol in (6.1), so we cannot use the same procedure above to directly construct their vector configurations. However, the vectors $\mathbf{J}_r$, $r = 1, 2, 4, 5$ in the tetrahedra in figure 6.2 and figure 6.3 are related to those in figure 6.1 by parallel translations, and $\mathbf{J}_{14} = \mathbf{J}_1 + \mathbf{J}_4$, so we can find the vector configurations in figure 6.2 and figure 6.3 once we have those in figure 6.1. Thus, the quantities $V, \psi_i, \phi_1, \phi_4, \theta$ are all functions of the six edge lengths J_r, $r = 1, 2, 4, 5, 12, 24$.

6.3 A Representation for the $9J$-Symbol

6.3.1 Defining the $9J$-Symbol

We define the $9j$-symbol as an inner product of two multicomponent wave-functions, using a variation of Edmond's definition, (6.4.2) in [35]. It is

$$\left\{ \begin{array}{ccc} j_1 & j_2 & j_{12} \\ s & j_4 & j_{34} \\ j_{13} & j_{24} & j_5 \end{array} \right\} = \frac{\langle b|a\rangle}{[(2j_{12}+1)(2j_{34}+1)(2j_{13}+1)(2j_{24}+1)]^{\frac{1}{2}}}\,, \tag{6.5}$$

where $|a\rangle$ and $|b\rangle$ are normalized simultaneous eigenstates of lists of operators with certain eigenvalues. We will ignore the phase conventions of $|a\rangle$ and $|b\rangle$ for now, since we did not use them to derive our formula. In our notation, the two states are

$$|a\rangle = \left| \begin{array}{cccccccc} \hat{I}_1 & \hat{I}_2 & \mathbf{S}^2 & \hat{I}_4 & \hat{I}_5 & \hat{\mathbf{J}}_{13}^2 & \hat{\mathbf{J}}_{24}^2 & \hat{\mathbf{J}}_{\rm tot} \\ j_1 & j_2 & s & j_4 & j_5 & j_{13} & j_{24} & \mathbf{0} \end{array} \right\rangle\,, \tag{6.6}$$

$$|b\rangle = \left| \begin{array}{cccccccc} \hat{I}_1 & \hat{I}_2 & \mathbf{S}^2 & \hat{I}_4 & \hat{I}_5 & \hat{\mathbf{J}}_{12}^2 & \hat{\mathbf{J}}_{34}^2 & \hat{\mathbf{J}}_{\rm tot} \\ j_1 & j_2 & s & j_4 & j_5 & j_{12} & j_{34} & \mathbf{0} \end{array} \right\rangle . \tag{6.7}$$

In the above notation, the large ket lists the operators on the top row, where a hat is used to distinguish an operator from its classical symbol function, and the corresponding quantum numbers are listed on the bottom row.

We now specify the Hilbert space where the two states $|a\rangle$ and $|b\rangle$ live. The states belong to a total Hilbert space of five angular momenta $\mathcal{H}_1 \otimes \mathcal{H}_2 \otimes \mathcal{H}_4 \otimes \mathcal{H}_5 \otimes \mathcal{H}_s$. Each large angular momentum $\hat{\mathbf{J}}_r$, $r = 1, 2, 4, 5$, acts on its own copy of the Schwinger space of two harmonic oscillators, namely, $\mathcal{H}_r = L^2(\mathbb{R}^2)$. The small angular momentum $\mathbf{S}$ is represented by the usual $2s + 1$ dimensional representation of $SU(2)$, that is to say, it acts on $\mathcal{H}_s = \mathbb{C}^{2s+1}$.

We now define the lists of operators in (6.6) and (6.7). First we look at the operators $\hat{I}_r$, $r = 1, 2, 4, 5$, $\hat{\mathbf{J}}_{12}^2$, and $\hat{\mathbf{J}}_{24}^2$, which act only on the large angular momentum spaces, $\mathcal{H}_r = L^2(\mathbb{R}^2)$, $r = 1, 2, 4, 5$, each of which can be viewed as a space of wave functions $\psi(x_{r1}, x_{r2})$ for two harmonic oscillators of unit frequency and mass. Let $\hat{a}_{r\mu} = (\hat{x}_{r\mu} + i\hat{p}_{r\mu})/\sqrt{2}$, and $\hat{a}_{r\mu}^\dagger = (\hat{x}_{r\mu} - i\hat{p}_{r\mu})/\sqrt{2}$, $\mu = 1, 2$, be the usual annihilation and creation operators. The operators $\hat{I}_r$ and $\hat{J}_{ri}$ are constructed from $\hat{a}$ and $\hat{a}^\dagger$ as follows,

$$\hat{I}_r = \frac{1}{2} \sum_\mu \hat{a}_{r\mu}^\dagger \hat{a}_{r\mu} , \qquad \hat{J}_{ri} = \frac{1}{2} \sum_{\mu\nu} \hat{a}_{r\mu}^\dagger (\sigma_i)_{\mu\nu} \hat{a}_{r\nu} , \tag{6.8}$$

where $i = 1, 2, 3$, and σ_i are the Pauli matrices. The quantum numbers j_r, $r = 1, 2, 4, 5$ specify the eigenvalues of both $\hat{I}_r$ and $\hat{\mathbf{J}}_r^2$, that is, j_r and $j_r(j_r + 1)$, respectively.

The operators $\hat{\mathbf{J}}_{12}^2$ and $\hat{\mathbf{J}}_{24}^2$ that define the intermediate couplings of the large angular momenta are defined as partial sums of the $\hat{\mathbf{J}}_r$,

$$\hat{\mathbf{J}}_{12} = \hat{\mathbf{J}}_1 + \hat{\mathbf{J}}_2 , \qquad \hat{\mathbf{J}}_{24} = \hat{\mathbf{J}}_2 + \hat{\mathbf{J}}_4 . \tag{6.9}$$

The quantum numbers j_{12} and j_{24} specify the eigenvalues of the operators $\hat{\mathbf{J}}_{12}^2$ and $\hat{\mathbf{J}}_{24}^2$, that is, $j_{12}(j_{12}+1)$ and $j_{24}(j_{24}+1)$, respectively. See chapter 3 for more detail on the Schwinger model.

Now we turn our attention to the operator S^2 that acts only on the small angular momentum space $\mathbb{C}^{2s+1}$. Let $\mathbf{S}$ be the vector of dimensionless spin operators represented by $(2s + 1) \times (2s + 1)$ matrices that satisfy the $SU(2)$ commutation relations,

$$[S_i, S_j] = i \sum_k \epsilon_{ijk} S_k . \tag{6.10}$$

The Casimir operator, $\mathbf{S}^2 = s(s + 1)$, is proportional to the identity operator, so its eigenvalue equation is trivially satisfied.

The remaining operators, $\hat{\mathbf{J}}_{13}^2$, $\hat{\mathbf{J}}_{34}^2$, and $\hat{\mathbf{J}}_{\rm tot}$, act on both $\mathcal{H}_r$ and $\mathcal{H}_s$. As in the spin-orbit problem [51], these are represented by non-diagonal matrices of differential operators. Even for the operators $\hat{I}_r$, $\hat{J}_{12}^2$, $\hat{J}_{24}$, above, they should be viewed as differential operators times the identity matrix. Similarly, the operators $\mathbf{S}$, S^2 should be viewed as

matrices times the identity operator on all $\mathcal{H}_r$. The following equations define $\hat{\mathbf{J}}_{13}^2$, $\hat{\mathbf{J}}_{34}^2$, and $\hat{\mathbf{J}}_{\rm tot}$:

$$
\begin{aligned}
(\hat{J}_{13}^2)_{\alpha\beta} &= [\hat{I}_1(\hat{I}_1+1)+\hbar^2 s(s+1)]\delta_{\alpha\beta}+2\hbar\,\hat{\mathbf{J}}_1\cdot\mathbf{S}_{\alpha\beta}, &(6.11)\\
(\hat{J}_{34}^2)_{\alpha\beta} &= [\hat{I}_4(\hat{I}_4+1)+\hbar^2 s(s+1)]\delta_{\alpha\beta}+2\hbar\,\hat{\mathbf{J}}_4\cdot\mathbf{S}_{\alpha\beta}, &(6.12)\\
(\hat{\mathbf{J}}_{\rm tot})_{\alpha\beta} &= (\hat{\mathbf{J}}_1+\hat{\mathbf{J}}_2+\hat{\mathbf{J}}_4+\hat{\mathbf{J}}_5)\delta_{\alpha\beta}+\hbar\,\mathbf{S}_{\alpha\beta}. &(6.13)
\end{aligned}
$$

6.3.2 The Multicomponent Wave-Functions

We follow the approach used in [50, 51] to find the WKB form of the multicomponent wave-functions $\psi_\alpha^a(x)=\langle x,\alpha|a\rangle$ and $\psi_\alpha^b(x)=\langle x,\alpha|b\rangle$. Let us focus on $\psi_\alpha^a(x)$, since the treatment of ψ^b is analogous. Temporarily, we will drop the index a in the following.

Let $\hat{D}_i$, $i=1,\ldots,10$, denote the the operators listed in the definition of $|a\rangle$ in (6.6). We seek a unitary operator $\hat{U}$, such that $\hat{D}_i$ for all $i=1,\ldots,10$ are diagonalized when conjugated by $\hat{U}$, that is,

$$
\sum_{\alpha\beta}\hat{U}^\dagger_{\alpha\,\mu}(\hat{D}_i)_{\alpha\,\beta}\,\hat{U}_{\beta\,\nu}=(\hat{\Lambda}_i)_{\mu\,\nu}\,. \tag{6.14}
$$

Here $\hat{\Lambda}_i$, $i=1,\ldots,10$ is a list of diagonal matrix operators, and we have employed the index summation notation in (6.14). Let $\phi^{(\mu)}$ be the simultaneous eigenfunction for the $\mu^{\rm th}$ diagonal entries $\hat{\lambda}_i$ of the operators $\hat{\Lambda}_i$, then we obtain a simultaneous eigenfunction $\psi_\alpha^{(\mu)}$ of the original list of operators $\hat{D}_i$ from

$$
\psi_\alpha^{(\mu)}=\hat{U}_{\alpha\,\mu}\,\phi^{(\mu)}\,. \tag{6.15}
$$

Here the index μ is called the polarization index, in the same sense used in [51]. There is no summation over the polarization index in (6.15). Since we are interested in ψ_α only to first order in $\hbar$, all we need are the zeroth order term U of the Weyl symbol matrix of $\hat{U}$ and the first order symbol matrix Λ_i of $\hat{\Lambda}_i$. The resulting asymptotic form of the wavefunction $\psi(x)$ is a product of a scalar WKB part Be^{iS} and a spinor part τ, that is,

$$
\psi_\alpha^{(\mu)}(x)=B(x)\,e^{i\,S(x)/\hbar}\,\tau_\alpha^{(\mu)}(x,p)\,. \tag{6.16}
$$

Here the action $S(x)$ and the amplitude $B(x)$ are simultaneous solutions to the Hamilton-Jacobi and the transport equations, respectively, that are associated with the Hamiltonians $\lambda_i^{(\mu)}$. The spinor τ^μ is the $\mu^{\rm th}$ column of the matrix U,

$$
\tau_\alpha^{(\mu)}(x,p)=U_{\alpha\mu}(x,p)\,, \tag{6.17}
$$

and where $p=\partial S(x)/\partial x$.

Now let us apply the above strategy to the $9j$-symbol. The Weyl symbols of the operators $\hat{I}_r$ and $\hat{J}_{ri}$ are $I_r-1/2$ and J_{ri}, respectively, where

$$
I_r=\frac{1}{2}\sum_\mu \overline{z}_{r\mu}z_{r\mu}\,,\qquad J_{ri}=\frac{1}{2}\sum_{\mu\nu}\overline{z}_{r\mu}(\sigma_i)_{\mu\nu}z_{r\nu}\,, \tag{6.18}
$$

and where $z_{r\mu} = x_{r\mu} + ip_{r\mu}$ and $\overline{z}_{r\mu} = x_{r\mu} - ip_{r\mu}$ are the symbols of $\hat{a}$ and $\hat{a}^\dagger$, respectively. The symbols of the remaining operators have the same expressions as (6.9), (6.11)-(6.13), but without the hats.

Among the operators $\hat{D}_i$, $\hat{J}_{13}^2$ and the vector of the three operators $\hat{\mathbf{J}}_{\rm tot}$ are non-diagonal. By looking at (6.11), the expression for $\hat{J}_{13}^2$, we see that the zeroth order term of the symbol matrix J_{13}^2 is already proportional to the identity matrix, so the spinor τ must be an eigenvector for the first order term $\mathbf{J}_1 \cdot \mathbf{S}$. Let $\tau^{(\mu)}(\mathbf{J}_1)$ be the eigenvector of the matrix $\mathbf{J}_1 \cdot \mathbf{S}$ with eigenvalue μI_1, that is,

$$(\mathbf{J}_1 \cdot \mathbf{S})_{\alpha\beta}\, \tau_\beta^{(\mu)} = \mu I_1\, \tau_\beta^{(\mu)}\,, \tag{6.19}$$

where $\mu = -s, \ldots, +s$. In order to preserve the diagonal symbol matrices I_r through the unitary transformation, we must choose the spinor $\tau^{(\mu)}$ to depend only on the direction of $\mathbf{J}_1$. One possible choice of $\tau^{(\mu)}$ is the "north standard gauge," (see Appendix A of [51]), in which the spinor $\delta_{\alpha\,\mu}$ is rotated along a great circle from the z-axis to the direction of $\mathbf{J}_1$. Explicitly,

$$\tau_\alpha^{(\mu)}(\mathbf{J}_1) = e^{i(\mu-\alpha)\phi_1}\, d_{\alpha\,\mu}^{(s)}(\theta_1)\,, \tag{6.20}$$

where (θ_1, ϕ_1) are the spherical coordinates that specify the direction of $\mathbf{J}_1$. Note that this is not the only choice, since (6.19) is invariant under a local $U(1)$ gauge transformation. In other words, any other spinor $\tau' = e^{ig(\mathbf{J}_1)}\,\tau$ that is related to τ by a $U(1)$ gauge transformation satisfies (6.19). This local gauge freedom is parametrized by the vector potential

$$\mathbf{A}_1^{(\mu)} = i(\tau^{(\mu)})^\dagger\, \frac{\partial \tau^{(\mu)}}{\partial \mathbf{J}_1}\,, \tag{6.21}$$

which transforms as $\mathbf{A}^{(\mu)'} = \mathbf{A}^{(\mu)} - \nabla_{\mathbf{J}_1}(g)$ under a local gauge transformation. Moreover, the gradient of the spinor can be expressed in terms of the vector potential, (see (A.22) in [51]), as follows,

$$\frac{\partial \tau^{(\mu)}}{\partial \mathbf{J}_1} = i\left(-\mathbf{A}_1^{(\mu)} + \frac{\mathbf{J}_1 \times \mathbf{S}}{I_1^2}\right)\, \tau^{(\mu)}\,. \tag{6.22}$$

Once we obtain the complete set of spinors $\tau^{(\mu)}$, $\mu = -s, \ldots, s$, we can construct the zeroth order symbol matrix U of the unitary transformation from (6.17).

Now let us show that all the transformed symbol matrices of the operators in (6.6), namely, the Λ_i, are diagonal to first order. Let us write $\hat{\Lambda}[\hat{D}]$ to denote the operator $\hat{U}^\dagger \hat{D} \hat{U}$, and write $\Lambda[\hat{D}]$ for its Weyl symbol matrix. First, consider the operators $\hat{I}_r$, $r = 1, \ldots, 4$, which are proportional to the identity matrix. Using the operator identity

$$[\hat{\Lambda}(\hat{I}_r)]_{\mu\nu} = \hat{U}_{\alpha\mu}^\dagger(\hat{I}_r \delta_{\alpha\beta})\hat{U}_{\beta\nu} = \hat{I}_r \delta_{\mu\nu} - \hat{U}_{\alpha\mu}^\dagger[\hat{U}_{\alpha\nu},\, \hat{I}_r]\,, \tag{6.23}$$

we find

$$[\Lambda(\hat{I}_r)]_{\mu\nu} = (I_r - 1/2)\delta_{\mu\nu} - i\hbar U_{0\alpha\mu}^* \{U_{0\alpha\nu},\, I_r\}\,, \tag{6.24}$$

where we have used the fact that the symbol of a commutator is a Poisson bracket. Since $U_{\alpha\mu} = \tau_\alpha^{(\mu)}$ is a function only of $\mathbf{J}_1$, and since the Poisson brackets $\{\mathbf{J}_1, I_r\} = 0$ vanish for $r = 1, 2, 4, 5$, the second term in (6.24) vanishes. We have

$$[\Lambda(\hat{I}_r)]_{\mu\nu} = (I_r - 1/2)\,\delta_{\mu\nu}\,. \tag{6.25}$$

Similarly, we find

$$[\Lambda(\hat{J}_{24}^2)]_{\mu\nu} = J_{24}^2\,\delta_{\mu\nu}\,. \tag{6.26}$$

Now we find the symbol matrices $\Lambda(\hat{\mathbf{J}}_{13})$ for the vector of operators $\hat{\mathbf{J}}_{13}$, where

$$[\hat{\Lambda}(\hat{\mathbf{J}}_{13})]_{\mu\nu} = \hat{U}_{\alpha\mu}^\dagger(\hat{\mathbf{J}}_1\delta_{\alpha\beta})\hat{U}_{\beta\nu} + \hbar\,\hat{U}_{\alpha\mu}^\dagger\mathbf{S}_{\alpha\beta}\hat{U}_{\beta\nu}\,. \tag{6.27}$$

After converting the above to Weyl symbols, we find

$$\begin{aligned}
[\Lambda(\hat{\mathbf{J}}_{13})]_{\mu\nu} &= \mathbf{J}_1\delta_{\mu\nu} - i\hbar U_{\alpha\mu}^*\{U_{\alpha\mu},\,\mathbf{J}_1\} + \hbar\,U_{\alpha\mu}^*\mathbf{S}_{\alpha\beta}U_{\beta\nu} \\
&= \mathbf{J}_1\delta_{\mu\nu} - i\hbar\tau_\alpha^{(\mu)*}\{\tau_\alpha^{(\nu)},\,\mathbf{J}_1\} + \hbar\,\tau_\alpha^{(\mu)*}\mathbf{S}_{\alpha\beta}\tau_\beta^{(\nu)}\,.
\end{aligned}$$

Let us denote the ith component of the second term above by $T_{\mu\nu}^i$, and use (6.22), the orthogonality of τ,

$$\tau_\alpha^{(\mu)*}\,\tau_\alpha^{(\nu)} = \delta_{\mu\nu}\,, \tag{6.28}$$

to get

$$\begin{aligned}
T_{\mu\nu}^i &= -i\hbar\tau_\alpha^{(\mu)*}\{\tau_\alpha^{(\nu)},\,J_{1i}\} \\
&= -i\hbar\tau_\alpha^{(\mu)*}\epsilon_{kji}J_{1k}\frac{\partial\tau_\alpha^{(\nu)}}{\partial J_{1j}} \\
&= \hbar(\mathbf{A}_1^{(\mu)}\times\mathbf{J}_1)_i\,\delta_{\mu\nu} + \hbar\frac{\mu J_{1i}}{I_1}\delta_{\mu\nu} - \hbar\,\tau_\alpha^{(\mu)*}S_{\alpha\beta}^i\tau_\beta^{(\nu)}\,,
\end{aligned}$$

where in the second equality, we have used the reduced Lie-Poisson bracket from (3.34) to evaluate the Poisson bracket $\{\tau, \mathbf{J}_1\}$, and where in the third equality, we have used (6.22) for $\partial\tau/\partial\mathbf{J}_1$. Notice the term involving $\mathbf{S}$ in $T_{\mu\nu}^i$ cancels out the same term in $\Lambda(\hat{\mathbf{J}}_{13})$, leaving us with a diagonal symbol matrix,

$$[\Lambda(\hat{\mathbf{J}}_{13})]_{\mu\nu} = \mathbf{J}_1\left[1 + \frac{\mu\hbar}{I_1}\right] + \hbar\,\mathbf{A}_1^{(\mu)}\times\mathbf{J}_1\,. \tag{6.29}$$

See (4.12) in [51]. Taking the square, we obtain

$$[\Lambda(\hat{\mathbf{J}}_{13}^2)]_{\mu\nu} = (I_1 + \mu\hbar)^2\delta_{\mu\nu}\,, \tag{6.30}$$

Thus we see that $\Lambda(\hat{\mathbf{J}}_{13}^2)$ is diagonal.

Finally, let us look at the last three remaining operators $\hat{\mathbf{J}}_{\rm tot}$ in (6.13). Since the symbols $\mathbf{J}_r$ for $r = 2, 4, 5$ Poisson commutes with $\mathbf{J}_1$, we find $\Lambda(\hat{\mathbf{J}}_r) = \mathbf{J}_r$. Using $\Lambda(\hat{\mathbf{J}}_{13})$ from (6.29), we obtain

$$[\Lambda(\hat{\mathbf{J}}_{\rm tot})]_{\mu\nu} = \left[\mathbf{J}_1\left(1+\frac{\mu\hbar}{I_1}\right) + \hbar\,\mathbf{A}_1^{(\mu)}\times\mathbf{J}_1 + (\mathbf{J}_2+\mathbf{J}_4+\mathbf{J}_5)\right]\delta_{\mu\nu}\,. \tag{6.31}$$

Therefore all Λ_i, $i = 1, \ldots, 10$ are diagonal.

For a single polarization μ, disregarding the eigenvalue equation for S^2, we have 9 Hamilton-Jacobi equations associated with the Λ_i in the 16 dimensional phase space $\mathbb{C}^8$. It turns out that not all of them are functionally independent. In particular, the Hamilton-Jacobi equations $\Lambda(\hat{I}_1) = I_1 - 1/2\hbar = j_1\hbar$ and $\Lambda(\hat{J}_{13}^2) = (I_1 + \mu\hbar)^2 = (j_{13} + 1/2)^2\hbar^2$ are functionally dependent. The two equations are consistent only when we choose the polarization $\mu = j_{13} - j_1$. This reduces the number of independent Hamilton-Jacobi equations for $S(x)$ from 9 to 8, half of dimension of the phase space $\mathbb{C}^8$. These 8 equations define the Lagrangian manifold associated with the action $S(x)$ seen in (6.16).

Now let us restore the index a. We express the multicomponent wave-function $\psi_\alpha^a(x)$ in the form of (6.16),

$$\psi_\alpha^a(x) = B_a(x)\,e^{iS_a(x)/\hbar}\,\tau_\alpha^a(x,p) \tag{6.32}$$

Here the action $S_a(x)$ is the solution to the eight Hamilton-Jacobi equations associated with the $\mu^{\rm th}$ entries λ_i^a of 8 of the symbol matrices Λ_i^a.

$$\begin{aligned}
I_1 &= (j_1+1/2)\hbar\,, \\
I_2 &= (j_2+1/2)\hbar\,, \\
I_4 &= (j_4+1/2)\hbar\,, \\
I_5 &= (j_5+1/2)\hbar\,, \\
J_{24}^2 &= (j_{24}+1/2)^2\hbar^2\,, \\
\mathbf{J}_{\rm tot}^{(a)} &= \mathbf{J}_1\left[1+\frac{\mu\hbar}{I_1}\right] + \hbar\,\mathbf{A}_1\times\mathbf{J}_1 + (\mathbf{J}_2+\mathbf{J}_4+\mathbf{J}_5) = \mathbf{0}\,,
\end{aligned} \tag{6.33}$$

and $\tau^a = \tau^{(\mu)}$ with $\mu = j_{13} - j_1$. Note that both τ^a and S_a involve the vector potential $\mathbf{A}_1$, so they are gauge dependent quantities.

We carry out an analogous analysis for $\psi^b(x)$. The result is

$$\psi_\alpha^b(x) = B_b(x)\,e^{iS_b(x)/\hbar}\,\tau_\alpha^b(x,p)\,, \tag{6.34}$$

where $S_b(x)$ is the solution to the following 8 Hamilton-Jacobi equations,

$$
\begin{aligned}
I_1 &= (j_1 + 1/2)\hbar\,, \\
I_2 &= (j_2 + 1/2)\hbar\,, \\
I_4 &= (j_4 + 1/2)\hbar\,, \\
I_5 &= (j_5 + 1/2)\hbar\,, \\
J_{12}^2 &= (j_{12} + 1/2)^2\hbar^2\,, \\
\mathbf{J}_{\rm tot}^{(b)} &= \mathbf{J}_4\left[1 + \frac{\nu\hbar}{I_4}\right] + \hbar\,\mathbf{A}_4 \times \mathbf{J}_4 + (\mathbf{J}_1 + \mathbf{J}_2 + \mathbf{J}_5) = \mathbf{0}\,.
\end{aligned}
\tag{6.35}
$$

Here the spinor $\tau^b = \tau_b^{(\nu)}$ satisfies

$$
(\mathbf{J}_4 \cdot \mathbf{S})_{\alpha\beta}\,(\tau_b^{(\nu)})_\beta = \nu I_4\,(\tau_b^{(\nu)})_\beta\,, \tag{6.36}
$$

where $\nu = j_{34} - j_4$. The vector potential $\mathbf{A}_4$ is defined by

$$
\mathbf{A}_4 = i(\tau^b)^\dagger\,\frac{\partial \tau^b}{\partial \mathbf{J}_4}\,. \tag{6.37}
$$

Again, both τ^b and S_b involve the vector potential $\mathbf{A}_4$, so they are gauge dependent quantities.

6.4 A Gauge-Invariant Form of the Multicomponent Wave-Functions

In this section, we derive a gauge-invariant factorization for $\psi^a(x)$. In general, an action $S(x)$ is defined by the integral of pdx on a Lagrangian manifold. The action $S_a(x)$ is associated with the Lagrangian manifold $\mathcal{L}_a$, the level set defined by (6.33). We will express $S_a(x)$ in terms of an action on a nearby gauge-invariant Lagrangian manifold. First, we pick a reference point z_0 on $\mathcal{L}_a$ and let x_0 be the x coordinates of z_0, and write $S_a(x) = \int_\gamma p dx$ as a line integral along a path γ that connects x_0 to x. Because $\mathcal{L}_a$ is Lagrangian, $S_a(x)$ is independent of the path γ chosen. Then we define an intermediate nearby gauge-invariant manifold $\mathcal{L}'_a$ using a set of gauge invariant coordinates z', which we will define in the next paragraph. We then express the line integral $S_a(x)$ on $\mathcal{L}_a$ as a perturbation of a line integral $S'_a(x) = \int_\gamma p'(x)dx$, where $p'(x)$ is the coordinate representation of $\mathcal{L}'_a$. Because $\mathcal{L}'_a$ is not Lagrangian, $S'_a(x)$ will depend on the path γ. Finally, we express the line integral $S'_a(x)$ on $\mathcal{L}'_a$ as a perturbation of a known action $S_a^{6j}(x)$, which is supported on another nearby gauge-invariant Lagrangian manifold $\mathcal{L}_a^{6j}$, the so called A-manifold in chapter 4. This manifold appears in the analysis of the Ponzano-Regge action of the $6j$-symbol. We then show that the sum of the perturbations are independent of the path γ chosen, by combining the extra phases generated from these perturbations with the spinor field, and show that the result becomes a field of quantum rotations of a fixed reference spinor on the Lagrangian manifold $S_a^{6j}(x)$. We show the advantages of our factorization by deriving a simple expression for the inner products between two multicomponent wave-functions.

6.4.1 The Intermediate Manifold

The gauge invariant coordinates z' were introduced in [50, 51] to formulate gauge invariant quantization conditions, and to show the overall wave function $\psi(x)$ in (6.16) is invariant under a local $U(1)$ gauge transformation. We use the coordinate map from z to z' here to define a gauge invariant intermediate manifold $\mathcal{L}'_a$. Note the notation z' in [51] denote vectors of real (x, p) coordinates, here z' refer to complex coordinates. We define a near-identity map Z as follows,

$$z'_{r\mu} = Z_{r\mu}(z_{r\mu}) = z_{r\mu} - i\hbar(\tau^a)^\dagger \left(\frac{\partial \tau^a}{\partial z_{r\mu}}\right) , \tag{6.38}$$

where $Z_{r\mu}$ are the functions, and $z'_{r\mu}$ are the values of the functions evaluated at $z_{r\mu}$. Since τ^a only depends on $\mathbf{J}_1$, the derivatives $\partial\tau^a/\partial z_{r\mu}$ for $r = 2, 4, 5$ vanish, and we have

$$z'_{r\mu} = Z_{r\mu}(z_{r\mu}) = z_{r\mu} , \qquad r = 2, 4, 5. \tag{6.39}$$

For $r = 1$, we use the chain rule, (6.18), and (6.21) to find

$$\begin{aligned} z'_{1\mu} = Z_{1\mu}(z_{r\mu}) &= z_{1\mu} - i\hbar\tau^\dagger \left(\frac{\partial \tau}{\partial \mathbf{J}_1}\right) \cdot \frac{\partial \mathbf{J}_1}{z_{1\mu}} \\ &= z_{1\mu} - i\hbar \mathbf{A}_1 \cdot \left(\frac{1}{2}\sum_\nu \boldsymbol{\sigma}_{\mu\nu}\, z_{1\nu}\right) . \end{aligned}$$

Using the identity

$$\sigma_i\, \sigma_j = \delta_{ij} + i\epsilon_{ijk}\sigma_k , \tag{6.40}$$

we obtain to first order

$$\begin{aligned} J_{1j} \circ Z &= \frac{1}{2}\,\overline{z}'\sigma_i z' , \\ &= \left[\overline{z}_1 + \frac{i\hbar}{2} A_{1i}\overline{z}_1\, \sigma_i\right] \sigma_j \left[z_1 - \frac{i\hbar}{2} A_{1k}\sigma_k\, z_1\right] \\ &= \frac{1}{2}\overline{z}_1\sigma_j z_1 - \frac{1}{2}\hbar\epsilon_{ijk}A_{1i}J_{1k} + \frac{1}{2}\hbar\epsilon_{ijk}A_{1k}J_{1i} \\ &= J_{1j} + \hbar(\mathbf{A}_1 \times \mathbf{J}_1)_j . \end{aligned} \tag{6.41}$$

To follow these manipulations, one must pay close attention to the difference between the functions and the values of the functions.

Looking at the last Hamilton-Jacobi equation from (6.33), we see that the gauge dependence of $\mathbf{J}_{\rm tot}$ is captured by the coordinate transformation Z, that is,

$$\mathbf{J}^{(a)}_{\rm tot} = \left[1 + \frac{\mu\hbar}{I_1}\right] \mathbf{J}_1 \circ Z + (\mathbf{J}_2 + \mathbf{J}_4 + \mathbf{J}_5) = \mathbf{0} . \tag{6.42}$$

Therefore, it is tempting define a new gauge-invariant manifold by dropping Z from (6.42). This is equivalent to treating Z as an active map that maps points on $\mathcal{L}_a$ to a new gauge-invariant manifold $\mathcal{L}'_a$ that is the level set of the following equations,

$$\begin{aligned} I_1 &= (j_1 + 1/2)\hbar\,, \\ I_2 &= (j_2 + 1/2)\hbar\,, \\ I_4 &= (j_4 + 1/2)\hbar\,, \\ I_5 &= (j_5 + 1/2)\hbar\,, \\ J_{24}^2 &= (j_{24} + 1/2)^2\hbar^2\,, \\ \mathbf{J}_{\rm tot}^{(a)\prime} &= \mathbf{J}_1\left[1 + \frac{\mu\hbar}{I_1}\right] + (\mathbf{J}_2 + \mathbf{J}_4 + \mathbf{J}_5) = \mathbf{0}\,. \end{aligned} \tag{6.43}$$

It is easy to check that $I_1 \circ Z = I_1$ to first order, and the remaining four equations are not affected by Z.

In this way, we have defined a gauge-invariant manifold $\mathcal{L}'_a$ through the map Z. In other words, if $(x, p(x)) \in \mathcal{L}_a$, then $(x', p') = Z(x, p(x)) \in \mathcal{L}'_a$ and vice versa. Here $(x, p(x))$ is the coordinate representation of the Lagrangian manifold $\mathcal{L}_a$, and $(x, p'(x))$ denotes the coordinate representation of $\mathcal{L}'_a$.

6.4.2 First Perturbation of the Action

Now let us relate the line integral $S_a(x)$ to the line integral $S'_a(x) = \int_\gamma p'(x)\,dx$. We express the map Z from (6.38) in terms of the x, p coordinates,

$$p'_{1\mu} = p_{1\mu} - i\hbar(\tau^a)^\dagger \frac{\partial \tau^a}{\partial x_{1\mu}}\,, \tag{6.44}$$

$$x'_{1\mu} = x_{1\mu} + i\hbar(\tau^a)^\dagger \frac{\partial \tau^a}{\partial p_{1\mu}}\,. \tag{6.45}$$

To find the value of $p'(x)$ in terms of x, $p(x)$, use the relations $p' = p'(x')$ and $(x', p'(x')) = Z(x, p(x))$, as follows,

$$p(x) - i\hbar(\tau^a)^\dagger \frac{\partial \tau^a}{\partial x} = p' = p'(x') = p'\left(x + i\hbar(\tau^a)^\dagger \frac{\partial \tau^a}{\partial p}\right)\,. \tag{6.46}$$

Expanding in powers of $\hbar$, we find

$$\begin{aligned} p'_{1\mu}(x) &= p_{1\mu}(x) - i\hbar(\tau^a)^\dagger \left[\frac{\partial \tau^a}{\partial x_{1\mu}} + \frac{\partial \tau^a}{\partial p_{1\nu}}\frac{\partial p_{1\nu}}{\partial x_{1\mu}}\right] \\ &= p_{1\mu}(x) - i\hbar(\tau^a)^\dagger \frac{d\tau^a}{dx_{1\mu}}\,, \end{aligned} \tag{6.47}$$

and $p'_{r\mu}(x) = p_{r\mu}(x)$ for $r = 2, 4, 5$. Integrating along the path γ, we obtain the relation

$$\begin{aligned} S_a(x) &= S'_a(x) + i\hbar \int_\gamma (\tau^a)^\dagger \frac{d\tau^a}{d\mathbf{x}_1} \cdot d\mathbf{x}_1 \\ &= S'_a(x) + \hbar \int_\gamma \mathbf{A}_1 \cdot d\mathbf{J}_1 \,, \end{aligned} \tag{6.48}$$

where we have used the definition of $\mathbf{A}_1$ in (6.21) in the second equality.

6.4.3 Second Perturbation of the Action

We now express the line integral $S'(x)$ as a perturbation of a known action $S_a^{6j}(x)$ on a nearby gauge-invariant Lagrangian manifold $\mathcal{L}_a^{6j}$. The Lagrangian manifold $\mathcal{L}_a^{6j}$ is defined by the following Hamilton-Jacobi equations:

$$\begin{aligned} I_1 &= (j_1 + 1/2)\hbar \,, \\ I_2 &= (j_2 + 1/2)\hbar \,, \\ I_4 &= (j_4 + 1/2)\hbar \,, \\ I_5 &= (j_5 + 1/2)\hbar \,, \\ J_{24}^2 &= (j_{24} + 1/2)^2\hbar^2 \,, \\ \mathbf{J}_{\rm tot} &= \mathbf{J}_1 + \mathbf{J}_2 + \mathbf{J}_4 + \mathbf{J}_5 = \mathbf{0} \,, \end{aligned} \tag{6.49}$$

in analogy with the Hamilton-Jacobi equations for the A- or B-manifold in chapter 4.

Now we find the difference between $S'_a(x)$ and $S_a^{6j}(x)$. We lift γ to two nearby paths γ_1 and γ'_1 on $\mathcal{L}_a^{6j}$ and $\mathcal{L}'_a$, respectively, which follow the Hamiltonian flows generated by the Hamiltonians in (6.49) and (6.43), respectively. Since the first five Hamiltonians $(I_1, I_2, I_4, I_5, J_{24}^2)$ are identical in (6.49) and (6.43), we will focus on the segments of γ_1 and γ'_1 that are generated by $\mathbf{n} \cdot \mathbf{J}_{\rm tot}$ and $\mathbf{n} \cdot \mathbf{J}_{\rm tot}^{(a)'}$. Here $\mathbf{n}$ is some fixed unit vector, and θ is the parameter along the flows of the two segments. Let us denote the projection of the two segments onto the x space by $x(\theta)$ and $x'(\theta)$, respectively. We assume $S'_a(x'(\theta)) = S'_a(x(\theta))$ holds to first order.

The equations of motion for the Hamiltonian $\mathbf{n} \cdot \mathbf{J}_{\rm tot}$ are

$$\frac{d\overline{z}_{r\mu}}{d\theta} = \frac{\partial(\mathbf{n} \cdot \mathbf{J}_{\rm tot})}{\partial(-iz_{r\mu})} = \frac{i}{2} \sum_\nu \overline{z}_{r\nu} (\mathbf{n} \cdot \boldsymbol{\sigma})_{\nu\mu} \,, \tag{6.50}$$

so the line integral is

$$S^{6j}(\theta) = \mathrm{Im} \int_0^\theta \sum_{r\nu} z_{r\nu} d\overline{z}_{r\nu} = \int_0^\theta (\mathbf{n} \cdot \mathbf{J}_{\rm tot})\, d\theta = 0 \,, \tag{6.51}$$

where we have used (6.50) for $d\overline{z}$ and the definitions for $\mathbf{J}_r$ in (6.18) in the second equality, and where we have used $\mathbf{J}_{\rm tot} = \mathbf{0}$ on $\mathcal{L}_a^{6j}$ in the last equality. Thus the action generated by part of the flow in γ_1 vanishes.

The equation of motion for the Hamiltonian $\mathbf{n} \cdot \mathbf{J}_{\rm tot}^{(a)'}$ is

$$\frac{d\overline{z}_{r\nu}}{d\theta} = \frac{i}{2}\sum_{\rho}\overline{z}_{r\rho}(\mathbf{n}\cdot\boldsymbol{\sigma})_{\rho\nu}\left(1+\frac{\mu\hbar}{I_1}\right) - \frac{i\mu\hbar}{2I_1^2}(\mathbf{n}\cdot\hat{\mathbf{J}}_1)\overline{z}_{1\nu}\,, \tag{6.52}$$

so the line integral is

$$\begin{aligned} S_a'(\theta) &= \int_0^\theta (\mathbf{n}\cdot\mathbf{J}_{\rm tot}^{(a)'})\,d\theta - \frac{\mu\hbar}{I_1}\int_0^\theta (\mathbf{n}\cdot\mathbf{J}_1)\,d\theta \\ &= -\frac{\mu\hbar}{I_1}\int_0^\theta (\mathbf{n}\cdot\mathbf{J}_1)\,d\theta\,, \end{aligned} \tag{6.53}$$

where we have used (6.52), (6.18) in the first equality, and the last equation of (6.43) in the second equality. Thus the part of line integral along γ_1' does not vanish.

From the difference of the line integrals in (6.51) and (6.53), we obtain

$$S_a'(x) = S_a^{6j}(x) - \sum_i \frac{\mu\hbar}{I_1}\int_{\gamma_1^i}\mathbf{n}_i\cdot\mathbf{J}_1\,d\theta\,, \tag{6.54}$$

where the sum in the last term is over the segments in γ_1^i of γ_1 that are generated by Hamiltonians of the type $\mathbf{n}_i\cdot\mathbf{J}_{\rm tot}$.

Combining the two perturbations (6.48) and (6.54), we can express the action $S_a(x)$ on the gauge-dependent Lagrangian manifold $\mathcal{L}_a$ as a perturbation of a known action $S_a^{6j}(x)$ on the gauge-invariant Lagrangian manifold $\mathcal{L}_a^{6j}$,

$$S_a(x) = S_a^{6j}(x) + \hbar\int_\gamma \mathbf{A}_1\cdot d\mathbf{J}_1 - \sum_i \frac{\mu\hbar}{I_1}\int_{\gamma_1^i}\mathbf{n}_i\cdot\mathbf{J}_1\,d\theta\,. \tag{6.55}$$

We note that the second perturbation in (6.55) vanishes unless γ_1 contains flows generated by the total angular momentum. Moreover, since the only Hamiltonian in (6.49) that generates flows that change the values of $\mathbf{J}_1$ or $\mathbf{J}_5$ is the total angular momentum, the first perturbation in (6.55) also vanishes unless γ contains flows generated by the total angular momentum. In other words, only the flows of the Hamiltonians $\mathbf{n}\cdot\mathbf{J}_{\rm tot}$ generate the two perturbations in (6.55).

Since both $S_a(x)$ and $S_a^{6j}(x)$ are actions on Lagrangian manifolds, their values are independent of the path γ we choose to perform this perturbation. Thus, the last two terms in (6.55) together should also be independent of the path γ_1. We show this is indeed the case by rewriting the spinor field on the Lagrangian manifold $\mathcal{L}_a^{6j}$, which is independent of γ_1, in terms of these two terms and a field of rotational matrices on $\mathcal{L}_a^{6j}$, which is also independent of γ_1.

6.4.4 Rewriting the Spinor Field

We now turn our attention to the spinor $\tau^a(z)$ in the multicomponent wavefunction in (6.16). Let z_0 be the reference point and let γ_1 be the path from z_0 to z on $\mathcal{L}_a^{6j}$, as defined above. If γ_1 is generated by the Hamiltonian flows of $(I_1, I_2, I_4, I_5, J_{24}^2)$,

which do not change the value of $\mathbf{J}_1$, we have $d\mathbf{J}_1 = 0$ along γ_1. Since the spinor $\tau^a(z)$ only depend on $\mathbf{J}_1$, we find

$$\tau^a(z) = \tau^a(z_0)\,. \tag{6.56}$$

If γ_1 is generated by the Hamiltonian flows of $\mathbf{n}\cdot\mathbf{J}_{\rm tot}$ by an angle θ, then $d\mathbf{J}_1$ is nonzero, and is given by

$$d\mathbf{J}_1 = \mathbf{n}\times\mathbf{J}_1 d\theta\,. \tag{6.57}$$

so the spinor $\tau^a(z)$ will change. We analyze how a spinor section $\tau^a(z)$, such as the one from (6.20), changes as we follow γ_1. To express the gauge dependence of $\tau^a(z)$ on the gauge potential $\mathbf{A}_1$, we find it convenient to express $\tau^a(z)$ in terms of the parallel transport of the spinor along γ_1, that is,

$$\tau^a(z) = \exp\left\{-i\int_{\gamma_1}\mathbf{A}_1\cdot d\mathbf{J}_1\right\}\,\tilde\tau^a(z)\,. \tag{6.58}$$

Here $\tilde\tau^a$ is the solution to the parallel transport equation along γ,

$$\frac{d\tilde\tau^a}{d\theta} = \frac{i}{\mathbf{J}_1^2}\left[\left(\frac{d\mathbf{J}_1}{d\theta}\times\mathbf{J}_1\right)\cdot\mathbf{S}\right]\tilde\tau^a(\theta)\,, \tag{6.59}$$

with the initial condition $\tilde\tau^a(0) = \tau^a(z_0)$. We see that the phase in (6.58) cancels the first term in (6.55).

To generate a phase that will cancel the second perturbation in (6.55), we rewrite the parallel transported spinor $\tilde\tau^a$ in terms of quantum rotation matrices. Let us define

$$U(\mathbf{n}, d\theta) = e^{-i(\mathbf{n}\cdot\mathbf{S})d\theta}\,, \tag{6.60}$$

which has the same axis and angle as those in γ_1. We decompose the axis $\mathbf{n}$ into components parallel and perpendicular to $\mathbf{J}_1$, and get

$$\mathbf{n} = \frac{\mathbf{n}\cdot\mathbf{J}_1}{J_1^2}\,\mathbf{J}_1 + \frac{\mathbf{J}_1\times(\mathbf{n}\times\mathbf{J}_1)}{J_1^2}\,. \tag{6.61}$$

Using the fact that $\tilde\tau^a(\mathbf{J}_1)$ is an eigenvector of $\mathbf{J}_1\cdot\mathbf{S}$ from (6.19), and the parallel transport equation from (6.59), with $d\mathbf{J}_1$ defined in (6.57), we find

$$\begin{aligned}
& U(\mathbf{n}, d\theta)\,\tilde\tau^a(z) \\
= \;& \exp\left\{-i\frac{\mathbf{J}_1\times(\mathbf{n}\times\mathbf{J}_1)}{J_1^2}\cdot\mathbf{S}\,d\theta\right\}\left[e^{-i\frac{\mathbf{n}\cdot\mathbf{J}_1}{J_1^2}\,\mathbf{J}_1\cdot\mathbf{S}\,d\theta}\,\tilde\tau^a(z)\right] \\
= \;& e^{-i\mu\frac{\mathbf{n}\cdot\mathbf{J}_1}{J_1}\,d\theta}\left[\exp\left\{-i\frac{\mathbf{J}_1\times d\mathbf{J}_1}{J_1^2}\cdot\mathbf{S}\right\}\tilde\tau^a(z)\right] \\
= \;& e^{-i\mu\frac{\mathbf{n}\cdot\mathbf{J}_1}{J_1}\,d\theta}\,\tilde\tau^a(z+dz)\,.
\end{aligned} \tag{6.62}$$

Moving the exponential to the other side, and integrating with respect to $d\theta$ along γ_1 from z_0 to z, we find an expression for the parallel transport of the spinor in terms of the rotation matrix, as follows,

$$\tilde{\tau}^a(z) = \exp\left\{ i\mu \int_\gamma \frac{\mathbf{n}\cdot\mathbf{J}_1}{J_1}\, d\theta \right\} U(\mathbf{n},\, \theta)\, \tau^a(z_0)\,. \tag{6.63}$$

In general, if γ_1 consists of segments generated by overall rotations, say $\gamma = \prod_i \gamma_1^i$, then by applying the above formula sequentially, we have

$$\tilde{\tau}^a(z) = \exp\left\{ i\mu \int_\gamma \frac{\mathbf{n}(\gamma)\cdot\mathbf{J}_1}{J_1}\, d\theta_\gamma \right\} \prod_{\gamma_1^i} U(\mathbf{n}_i,\, \theta_i)\, \tau^a(z_0)\,. \tag{6.64}$$

Putting (6.64) back into (6.58), we have

$$\tau^a(z) = \exp\left\{ -i\int_\gamma \mathbf{A}_1\cdot d\mathbf{J}_1 + i\frac{\mu}{J_1}\int_\gamma \frac{\mathbf{n}(\gamma)\cdot\mathbf{J}_1}{J_1}\, d\theta_\gamma \right\} \left[\prod_{\gamma_1^i} U(\mathbf{n}_i,\, \theta_i) \right] \tau^a(z_0)\,. \tag{6.65}$$

We note that the product of rotation matrices are almost uniquely defined by the two end points z_0 and z. To see this, project this series of rotations onto a series of classical rotations R_i in $SO(3)$. Because both $\mathbf{J}_1$ and $\mathbf{J}_5$ are invariant under the other Hamiltonian flows of $(I_1, I_2, I_4, I_5, J_{24}^2)$, the triangle 1-5-24 can only change orientation under the flows of the total angular momentum. Thus, this series of rotations R_i must take the triangle 1-5-24 at z_0 to the triangle 1-5-24 at z. There is a unique rotation R that does this. Thus the product of the rotation matrices $U(\mathbf{n}_i,\, \theta_i)$ is equal to a lift U of the $SO(3)$ rotation matrix R. We can now write

$$U_a(x) = \prod_{\gamma_1^i} U(\mathbf{n}_i,\, \theta_i)\,. \tag{6.66}$$

We conclude that both the spinor field $\tau^a(z)$ and the field of rotation matrices $U(z)$ are independent of the path γ_1. As a result, the phase factors in (6.65), and the perturbations in (6.55) are independent of the path γ_1.

When we put (6.55) and (6.65) together into the multicomponent wave-function $\psi^a(x) = B(x)e^{iS_a(x)/\hbar}\,\tau^a(x)$, the phase factors exactly cancel out. In the end, we obtain a gauge-invariant representation of the wave-function,

$$\psi^a(x) = B_a(x)\, e^{iS_a^{6j}(x)/\hbar}\, U_a(x)\, \tau^a(x_0)\,. \tag{6.67}$$

Similarly, the multicomponent wave-function for the state $|b\rangle$ has the following form,

$$\psi^b(x) = B_b(x)\, e^{iS_b^{6j}(x)/\hbar}\, U_b(x)\, \tau^b(x_0)\,, \tag{6.68}$$

where for convenience, we have chosen the same reference point z_0. This is possible, because the reference points are arbitrary on both manifolds, and we can choose z_0 to lie in the intersection of $\mathcal{L}_a^{6j}$ and $\mathcal{L}_b^{6j}$.

6.4.5 The Inner Products of Multicomponent Wave-Functions

We now take the inner product between the two multicomponent wave-functions $\psi^a(x)$ and $\psi^b(x)$, and perform a stationary phase approximation. From Eqs (6.67) and (6.68), we find

$$\langle b|a\rangle = \int dx B_a(x) B_b(x)\, e^{i(S_a^{6j}(x) - S_b^{6j}(x))/\hbar} (\tau^b(x_0))^\dagger [U_b(x)]^\dagger\, U_a(x)\, \tau^a(x_0)\,. \tag{6.69}$$

Let $\mathcal{M}_k$ denote the $k^{\rm th}$ component of the intersection set of the two Lagrangian manifolds $\mathcal{L}_a^{6j}$ and $\mathcal{L}_b^{6j}$. Choose the reference point $z_0 \in \mathcal{M}_0$. We know the difference of the two actions $S_b(x_k) - S_a(x_k)$ is constant in each component $\mathcal{M}_k$, since the integrals of $p\,dx$ cancel along flows in the intersection. In particular, since $S_b(x_0) = S_a(x_0) = 0$, it vanishes on $\mathcal{M}_0$. Similarly, by their unitary property, the product of the rotation matrices cancel out along flows in the intersections, and is constant in each $\mathcal{M}_k$. In particular, it is the identity matrix in $\mathcal{M}_0$.

Suppose we know the result of the stationary phase approximation to the integral in (6.69), when the spinors and rotation matrices are absent. In other words, suppose we know

$$\int dx B_a(x) B_b(x)\, e^{i(S_a^{6j}(x) - S_b^{6j}(x))/\hbar} = e^{i\kappa} \sum_k \Omega_k \exp\{i[S_a^{6j}(x_k) - S_b^{6j}(x_k) - \mu_k \pi/2]/\hbar\}\,. \tag{6.70}$$

Then by treating the spinors as slowly varying and evaluating them at the stationary points in (6.69), we find

$$\langle b|a\rangle = e^{i\kappa} \sum_k \Omega_k \exp\{i[S_a^{6j}(z_k) - S_b^{6j}(z_k) - \mu_k \pi/2]/\hbar\} \left(U_b^{0k} \tau^b(z_0)\right)^\dagger \left(U_a^{0k} \tau^a(z_0)\right)\,. \tag{6.71}$$

In the above formula, the sum is over the components of the intersection set, and z_k is a point in the kth component. Here U_a^{0k} is a rotation matrix determined from the rotation that takes z_0 to a point $z_k \in \mathcal{M}_k$ inside $\mathcal{L}_a^{6j}$, and U_b^{0k} is similarly defined. The formula (6.71) is independent of the choice of z_k, because any other choice z_k' will multiply both U_a^{0j} and U_b^{0j} by the same additional rotation matrix generated from a path from z_k to z_k', which cancel out in the product $(U_b^{0k})^\dagger U_a^{0k}$. We see that our factorization of the multicomponent wave-function leads to a simple and elegant expression for the inner product between two multicomponent wave-functions.

6.5 Derivation For the $9J$-Symbol Formula

We derive the main result (6.1) for the $9j$-symbol by using the general formula (6.71). The stationary phase approximation without the spinors in (6.70) was calculated in the semiclassical analysis of the $6j$-symbol in chapter 4. In the following, we summarize the

results of that calculation, and then evaluate the spinor inner products at the stationary phase points to derive the inner product of the two multicomponent wave-functions, as in (6.71). From this inner product, we derive the asymptotic formula for the $9j$-symbol.

6.5.1 The Relative Action at the Two Stationary Sets

Let us describe the Lagrangian manifolds and the relevant paths used to calculate their actions. The two Lagrangian manifolds $\mathcal{L}_a^{6j}$ and $\mathcal{L}_b^{6j}$ intersect at two sub-manifolds $\mathcal{M}_0$ and $\mathcal{M}_1$. The relative action $S_a^{6j}(z_1) - S_b^{6j}(z_1)$ is calculated along a loop $\gamma = \gamma_1 + \gamma_2 + \gamma_3$, as illustrated in figure 6.4. First it goes from a point z_0 in $\mathcal{M}_0$ to a point z_1 in $\mathcal{M}_1$ along a path γ_1, which is generated by the Hamiltonian flows of J_{24}^2 inside $\mathcal{L}_a^{6j}$. Then it goes back to another point in $\mathcal{M}_0$ along a path γ_2, which is generated by the Hamiltonian flows of J_{12}^2 inside $\mathcal{L}_b^{6j}$. Finally it goes back to the starting point z_0 along a path γ_3 through an overall rotation around $-\mathbf{j}_5$ by an angle equal to twice the internal dihedral angle ϕ_5 of the tetrahedron in figure 6.1, and along the flows generated by I_1, I_2, I_3, I_4. We can break this loop up into two paths $\gamma^a = \gamma_1$ and $\gamma^b = -\gamma_3 - \gamma_2$ that goes from z_0 to z_1 along the two Lagrangian manifolds.

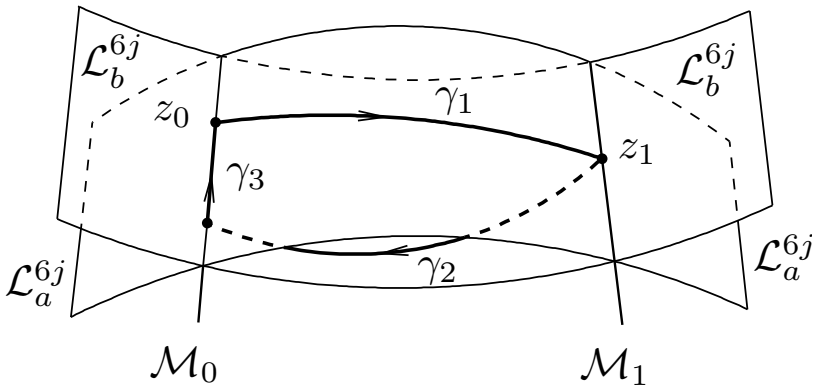

Figure 6.4: Illustration for the intersection of the two Lagrangian manifolds, and the paths γ_1, γ_2, and γ_3 on these manifolds.

By choosing z_0 as the reference point for both actions S_a^{6j} and S_b^{6j}, we have

$$S_a^{6j}(z_0) - S_b^{6j}(z_0) = 0 \tag{6.72}$$

on $\mathcal{M}_0$. From (4.53) in chapter 4, the relative action at the other stationary phase point is given by

$$S_a^{6j}(z_1) - S_b^{6j}(z_1) = -2\sum_i (j_i + 1/2)\psi_i + 2n\pi\,, \tag{6.73}$$

where ψ_i are the external dihedral angles of the tetrahedron in figure 6.1, and the sum is over $i = 1, 2, 4, 5, 12, 24$, and n is some integer that contributes to an overall phase. The

amplitudes at both stationary point are given by

$$\Omega_{0,\,1} = \frac{1}{2\sqrt{12\pi V}}\,, \tag{6.74}$$

where V is the volume of the tetrahedron in figure 6.1. Altogether, (6.71) becomes

$$\begin{aligned} & \langle B|A\rangle \\ = \;& \frac{e^{i\kappa}}{2\sqrt{12\pi V}} \Big\{ (\tau^b(z_0))^\dagger \tau^a(z_0) \\ & \qquad + \Big(U_b \tau^b(z_0)\Big)^\dagger \left(U_a \tau^a(z_0)\right) \exp\left[-2i \sum_i (j_i + 1/2)\psi_i - \frac{i\mu_1 \pi}{2} \right] \Big\}\,. \end{aligned} \tag{6.75}$$

where $e^{i\kappa}$ is some overall phase, and U_a, U_b are rotation matrices associated with γ^a and γ^b, respectively.

6.5.2 The Reference Point and the Spinor Products

We choose the vector configurations associated with z_0 to have a negative signed volume V, where $6V = \mathbf{J}_1 \cdot (\mathbf{J}_2 \times \mathbf{J}_4)$. This choice of the starting point is in agreement with the choice made in chapter 4. In addition, we choose a particular orientation for the starting point z_0, as follows. We put $\mathbf{J}_1$ along the z-axis, and $\mathbf{J}_1 \times \mathbf{J}_{24}$ along the y-axis, so that $\mathbf{J}_{24}$ and $\mathbf{J}_5$ lie inside the xz-plane, as illustrated in figure 6.5. Let the the inclination and azimuth angles (θ, ϕ) denote the direction of the vector $\mathbf{J}_4$. From figure 6.5, we see that $|\phi|$ is the angle between the $(\mathbf{J}_1, \mathbf{J}_{24})$ plane and the $(\mathbf{J}_1, \mathbf{J}_4)$ plane, so $\phi = -\phi_1$, which is defined in (6.2). Also see figure 6.2. The inclination angle is simply the angle θ between $\mathbf{J}_1$ and $\mathbf{J}_4$, so it is the same θ defined in (6.4).

The gauge choices for the spinors at the reference point are arbitrary, and they contribute only an overall phase. To be concrete, we choose the spinor τ^a at z_0 to be the standard eigenvector for S_z, that is,

$$\tau^a_\alpha(z_0) = \delta_{\alpha\mu}\,. \tag{6.76}$$

For the spinor τ^b at z_0, we choose it to be an eigenvector of $\mathbf{J}_4 \cdot \mathbf{S}$ in the north standard gauge, that is,

$$\tau^b_\alpha(z_0) = e^{-i(\alpha-\nu)\phi_1}\, d^s_{\nu\alpha}(\theta)\,. \tag{6.77}$$

Taking the spinor inner product, we obtain

$$(\tau^b(z_0))^\dagger (\tau^a(z_0)) = e^{i(\mu-\nu)\phi_1}\, d^s_{\nu\mu}(\theta)\,. \tag{6.78}$$

In order to evaluate the other spinor product in $\mathcal{M}_1$, we need to find the rotation matrices U_a and U_b, which are generated from γ_a and γ_b, respectively. The path $\gamma_a = \gamma_1$ has no flow that is generated by the total angular momentum, so

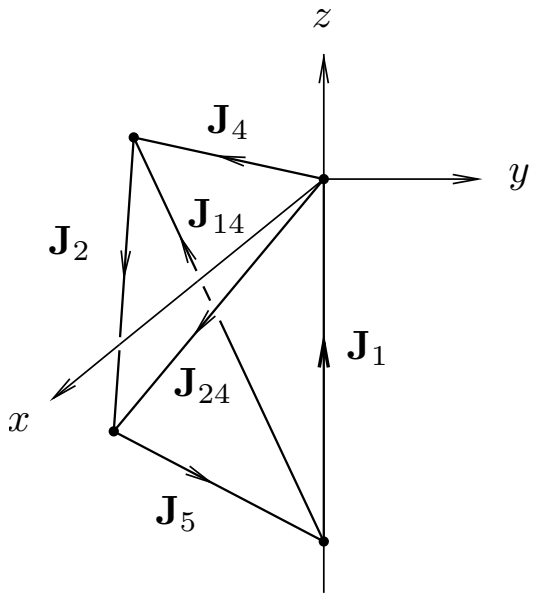

Figure 6.5: The configuration corresponding to the reference point z_0.

$$U_a = 1\,. \tag{6.79}$$

The path $\gamma_b = -\gamma_3 - \gamma_2$ contains only an overall rotation around $\mathbf{j}_5$, so

$$U_b = U(\mathbf{j}_5, 2\phi_5)\,. \tag{6.80}$$

The rotation U_b effectively moves $\mathbf{J}_4$ to its mirror image $\mathbf{J}'_4$ across the xz-plane, which has the direction given by (θ, ϕ_1). Thus $U_b\,\tau^b(z_0)$ is an eigenvector of $\mathbf{J}'_4 \cdot \mathbf{S}$, and is equal to the eigenvector of $\mathbf{J}'_4 \cdot \mathbf{S}$ in the north standard gauge up to a phase. We have

$$[U_b\,\tau^b(z_0)]_\alpha = e^{i\nu H_4}\, e^{i(\alpha-\nu)\phi_1}\, d^s_{\nu\alpha}(\theta)\,, \tag{6.81}$$

where H_4 is a holonomy phase factor that is equal to the area of a spherical triangle on a unit sphere, which is illustrated in figure 6.6.

Therefore, the spinor inner product at the intersection $\mathcal{M}_1$ is

$$\Big(U_b\tau^b(z_0)\Big)^\dagger\,(U_a\tau^a(z_0)) = e^{i\nu H_4}\, e^{-i(\mu-\nu)\phi_1}\, d^s_{\nu\mu}(\theta)\,. \tag{6.82}$$

Putting this back into (6.75), we have an asymptotic formula for the inner product

$$\langle b|a\rangle = \frac{e^{i\kappa_1}}{\sqrt{12\pi V}}\, d^s_{\nu\mu}(\theta) \cos\left[-\sum_i (j_i + 1/2)\psi_i - \frac{\mu_1\pi}{4} - \mu\phi_1 + \nu\left(\frac{H_4}{2} + \phi_1\right)\right]\,. \tag{6.83}$$

Using a different choice of the reference point and paths, we can derive an alternative expression for the inner product, and eliminate the term H_4. Let us choose a new

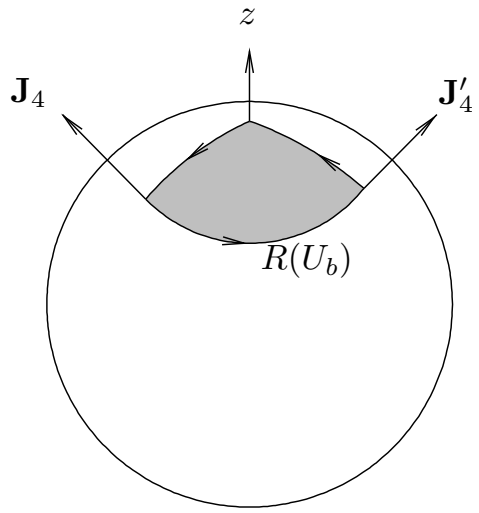

Figure 6.6: The holonomy H_4 is the area bounded by the curve that traces a great circle from $\hat{z}$ to $\hat{j}_4$, the small circle generated by the rotation $R(U_b)$ that rotates $\hat{j}_4$ to $\hat{j}'_4$ about the axis $\mathbf{j}_5$, and finally the great circle from $\hat{j}'_4$ back to $\hat{z}$.

reference point z_0 to correspond to an orientation where $\mathbf{J}_4$ is along the z-axis, and $\mathbf{J}_4 \times \mathbf{J}_{12}$ along the y-axis. For the paths, we choose $\gamma^a = \gamma_3 + \gamma_1$ and $\gamma^b = -\gamma_2$. Through essentially the same arguments, we find

$$\langle b|a\rangle = \frac{e^{i\kappa_4}}{\sqrt{12\pi V}}\, d^s_{\nu\mu}(\theta) \cos\left[-\sum_i (j_i + 1/2)\psi_i - \frac{\mu_1 \pi}{4} + \mu\left(\frac{H_1}{2} + \phi_4\right) - \nu\phi_4 \right], \qquad (6.84)$$

where H_1 is another holonomy phase factor associated with the curve traced out by $\mathbf{J}_1$ on the unit sphere.

Because the quantities $\psi_i, \phi_1, \phi_4, H_1, H_4$ depend only on the geometry of the tetrahedron, and are independent of μ and ν, we conclude that the argument in the cosine must be linear in μ and ν. Equating the two arguments of the cosine in (6.83) and (6.84), we find the linear term to be $-(\mu\phi_1 + \nu\phi_4)$. Equations (6.83) and (6.84) become

$$\langle b|a\rangle = \frac{e^{i\kappa'}}{\sqrt{12\pi V}}\, d^s_{\nu\mu}(\theta) \cos\left(\sum_i (j_i + 1/2)\psi_i + \frac{\mu_1 \pi}{4} + \mu\phi_1 + \nu\phi_4 \right). \qquad (6.85)$$

Using (A.6) and (A.6) in Appendix A for the special cases of the $9j$-symbol when $s = 0$ and $s = 1$, and through numerical experimentation, we have determined the overall phase to be

$$e^{i\kappa'} = (-1)^{j_1+j_2+j_4+j_5+2s+\nu}, \qquad (6.86)$$

where the factor $(-1)^\nu$ is necessary to make the expression (6.85) symmetrical between μ and ν, because $d^s_{\nu\mu}(\theta) = (-1)^{\mu-\nu} d^s_{\mu\nu}(\theta)$. We see that the formula (6.1) satisfies the

symmetry of the $9j$-symbol obtained from a reflection of the j's across the diagonal, which corresponds to swapping the states $|a\rangle$ and $|b\rangle$.

Again, through numerical experimentation, we found the Maslov index to be

$$\mu_1 = 1 - 4s\,. \tag{6.87}$$

Altogether, we have derived a new asymptotic formula (6.1) for the $9j$-symbol, which we repeat here:

$$\begin{Bmatrix} j_1 & j_2 & j_{12} \\ s & j_4 & j_{34} \\ j_{13} & j_{24} & j_5 \end{Bmatrix} = \frac{(-1)^{j_1+j_2+j_4+j_5+2s+\nu}}{\sqrt{(2j_{13}+1)(2j_{34}+1)\,(12\pi V)}} \cos\left(\sum_i (j_i+\frac{1}{2})\,\psi_i + \frac{\pi}{4} - s\pi + \mu\phi_1 + \nu\phi_4\right) d^s_{\nu\,\mu}(\theta)\,. \tag{6.88}$$

6.6 Plots

We illustrate the accuracy of our formula by plotting our approximation (6.88) against the exact $9j$-symbols in the classical region for the following values of the j's:

$$\begin{Bmatrix} j_1 & j_2 & j_{12} \\ s & j_4 & j_{34} \\ j_{13} & j_{24} & j_5 \end{Bmatrix} = \begin{Bmatrix} 51/2 & 53/2 & 28 \\ 1/2 & 47/2 & 24 \\ 25 & 27 & j_5 \end{Bmatrix}. \tag{6.89}$$

The result is shown in figure 6.7. We see that our approximations are in good agreement with the exact values of the $9j$-symbol in the classically allowed region, away from the caustic. However, it gets progressively worse as we come closer to the caustic, where $V = 0$ and the amplitude blows up. We can see this clearly from the error plot in part (a) of figure 6.10.

Since the asymptotic formula (6.88) should become more accurate as the values of the j's get larger, we plot the formula against the exact $9j$ for another example (6.90), which is roughly (6.89) rescaled by a factor of 4. The result in the classically allowed region away from the caustic is shown in figure 6.8, and the result in regions close to the caustic is shown in figure 6.9. The errors for this case is shown in part (b) of figure 6.10. We can see that the error also scales with the values of the j's.

$$\begin{Bmatrix} j_1 & j_2 & j_{12} \\ s & j_4 & j_{34} \\ j_{13} & j_{24} & j_5 \end{Bmatrix} = \begin{Bmatrix} 201/2 & 205/2 & 89 \\ 3/2 & 197/2 & 99 \\ 100 & 92 & j_5 \end{Bmatrix}. \tag{6.90}$$

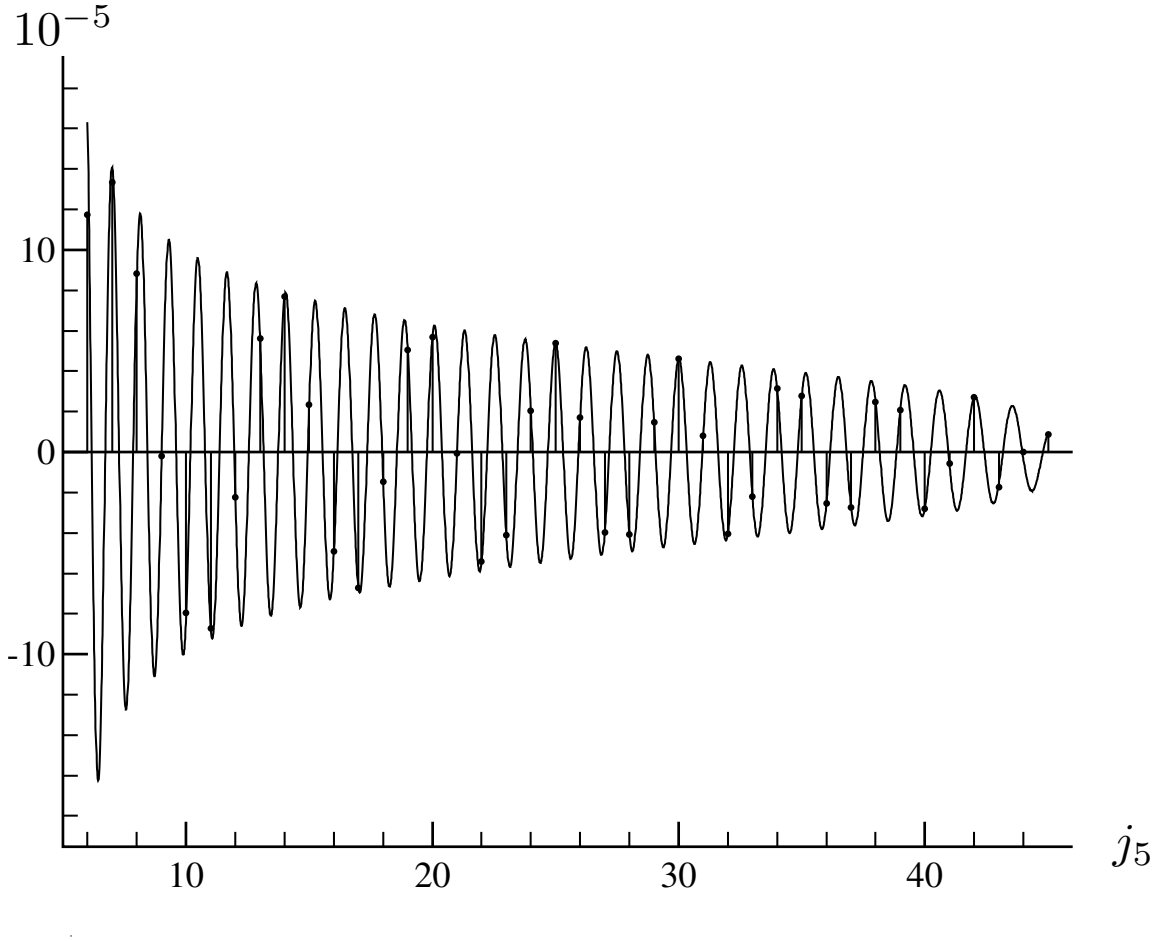

Figure 6.7: Comparison of the exact $9j$-symbol (vertical sticks and dots) and the asymptotic formula (6.88) in the classically allowed region, for the values of j's shown in (6.89).

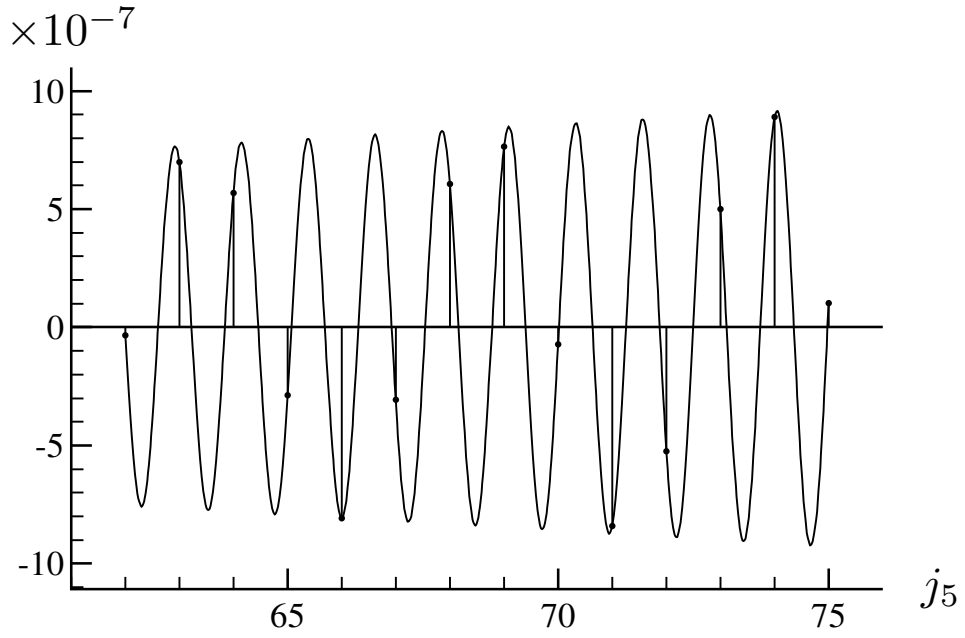

Figure 6.8: Comparison of the exact $9j$-symbol (vertical sticks and dots) and the asymptotic formula (6.88) in the classically allowed region away from the caustics, for the values of j's shown in (6.90).

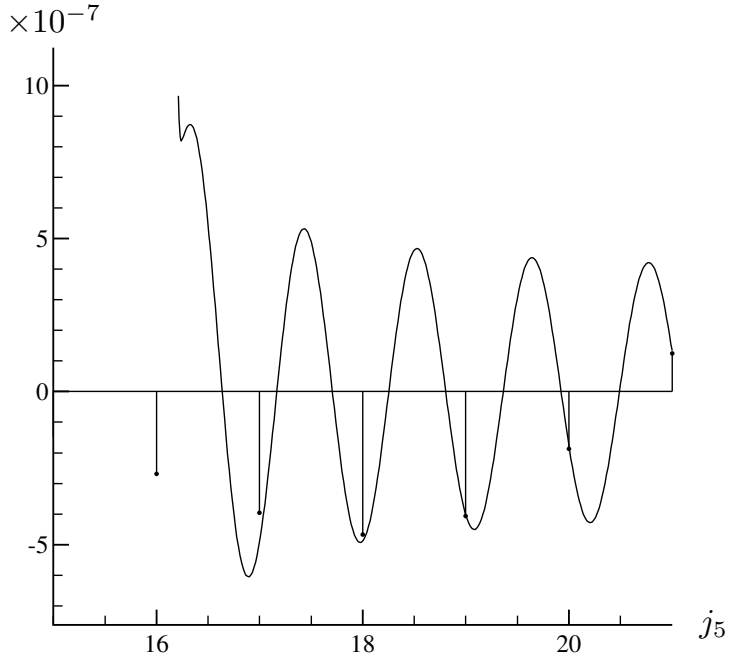

Figure 6.9: Comparison of the exact $9j$-symbol (vertical sticks and dots) and the asymptotic formula (6.88) near a caustic, for the values of j's shown in (6.90).

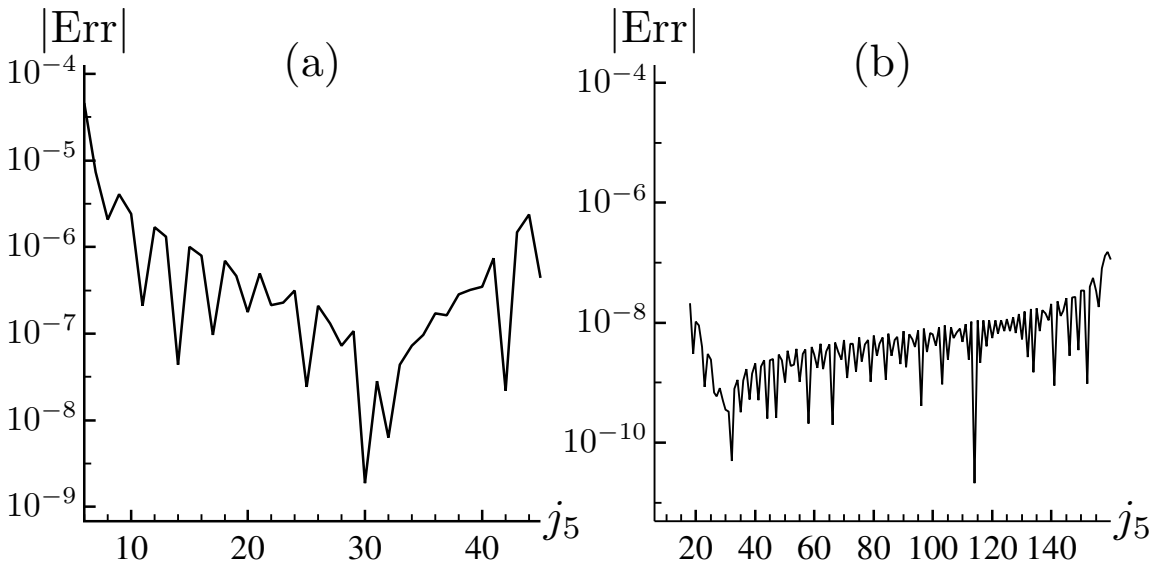

Figure 6.10: Absolute value of the error of the asymptotic formula (6.88) for (a) the case in (6.89), and (b) the case in (6.90). The error is defined as the difference between the approximate value and the exact value.

6.7 The $9J$-Symbol with Two Small Angular Momenta

We can also take the two angular momenta to be small. Let us write down the definition of the $9j$-symbol when $s_2 = j_2$ and $s_3 = j_3$ are small. It is

$$\begin{aligned} &\left\{ \begin{array}{ccc} j_1 & s_2 & j_{12} \\ s & j_4 & j_{34} \\ j_{13} & j_{24} & j_5 \end{array} \right\} \\ = \;& \frac{\langle b|a\rangle}{[(2j_{12}+1)(2j_{34}+1)(2j_{13}+1)(2j_{24}+1)]^{\frac{1}{2}}}\,, \end{aligned} \tag{6.91}$$

where

$$|a\rangle = \left| \begin{array}{ccccccccc} \hat{I}_1 & \mathbf{S}_2^2 & \mathbf{S}_3^2 & \hat{I}_4 & \hat{I}_5 & \hat{\mathbf{J}}_{13}^2 & \hat{\mathbf{J}}_{24}^2 & \hat{\mathbf{J}}_{\rm tot} \\ j_1 & s_2 & s_3 & j_4 & j_5 & j_{13} & j_{24} & \mathbf{0} \end{array} \right\rangle\,, \tag{6.92}$$

$$|b\rangle = \left| \begin{array}{ccccccccc} \hat{I}_1 & \mathbf{S}_2^2 & \mathbf{S}_3^2 & \hat{I}_4 & \hat{I}_5 & \hat{\mathbf{J}}_{12}^2 & \hat{\mathbf{J}}_{34}^2 & \hat{\mathbf{J}}_{\rm tot} \\ j_1 & s_2 & s_3 & j_4 & j_5 & j_{12} & j_{34} & \mathbf{0} \end{array} \right\rangle\,. \tag{6.93}$$

We choose the four spinors just as in the $9j$ case with one small angular momentum. Then the Hamilton-Jacobi equations for the operators $\hat{J}_{13}^2, \hat{J}_{24}^2, \hat{J}_{12}^2$, and $\hat{J}_{34}^2$, simply pick out the polarizations. The remaining Hamilton-Jacobi equations for both states after the perturbations are performed become

$$\begin{aligned} J_1 &= (j_1 + 1/2)\hbar\,, \\ J_4 &= (j_4 + 1/2)\hbar\,, \\ J_5 &= (j_5 + 1/2)\hbar\,, \\ \vec{0} &= \vec{J}_1 + \vec{J}_4 + \vec{J}_5\,. \end{aligned}$$

These equations describe a Lagrangian manifold that corresponds to a triangle having the three edge lengths J_1, J_4, J_5, illustrated in figure 6.11.

Because the two Lagrangian manifolds are identical, the inner product of the scalar part of the WKB wave-functions is unity, and only the spinor products contribute. After putting in the correct overall phase, we get

$$\begin{aligned} &\left\{ \begin{array}{ccc} j_1 & s_2 & j_{12} \\ s_3 & j_4 & j_{34} \\ j_{13} & j_{24} & j_5 \end{array} \right\} \\ = \;& \frac{(-1)^{2(j_4+j_5)+s_2+s_3+j_{12}+j_{13}}}{\sqrt{(2j_{13}+1)(2j_{24}+1)(2j_{12}+1)(2j_{34}+1)}}\, d^{(s_2)}_{j_{12}-j_1,\,j_{24}-j_4}(\theta)\, d^{(s_3)}_{j_{13}-j_1,\,j_{34}-j_4}(\theta)\,, \end{aligned} \tag{6.94}$$

where θ is the exterior angle between the vectors $\vec{J}_1$ and $\vec{J}_4$ in the triangle formed by J_1, J_4, and J_5, as illustrated in figure 6.11. The angle θ is given by

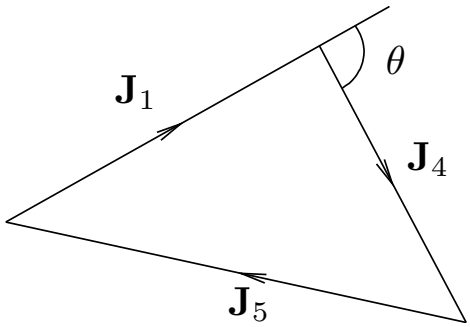

Figure 6.11: The angle θ is defined as the exterior angle between the edges J_1 and J_4 in a triangle having the three edge lengths J_1, J_4, J_5.

$$\theta = \cos^{-1}\left(\frac{\mathbf{J}_1 \cdot \mathbf{J}_4}{J_1\, J_4}\right) = \pi - \cos^{-1}\left(\frac{J_1^2 + J_4^2 - J_5^2}{2\, J_1\, J_4}\right). \tag{6.95}$$

We plot the formula (6.94) below against exact values of the $9j$-symbol in figure 6.12, for the following values of the j's:

$$\left\{ \begin{array}{ccc} j_1 & s_2 & j_{12} \\ s_3 & j_4 & j_{34} \\ j_{13} & j_{24} & j_5 \end{array} \right\} = \left\{ \begin{array}{ccc} 67 & 1/2 & 135/2 \\ 3/2 & 54 & 111/2 \\ 135/2 & 107/2 & j_5 \end{array} \right\}. \tag{6.96}$$

6.8 Conclusions

We have computed the asymptotic formula for the Wigner $9j$-symbol when some angular momenta are large while others are small. In so doing, we have formulated a gauge-invariant form of the multicomponent WKB wave-functions that appears in the definition of the $9j$-symbol. Our gauge-invariant form retains the factorization of the wavefunction into a scalar WKB part and a spinor part. Currently, there is no general theory of finding gauge-invariant multicomponent WKB wave-functions, so our formulation here provides an interesting special case for investigating when such a gauge-invariant form is possible.

There are several directions to extend the present work. A natural extension is to find the analytic continuation of our formula to the classically forbidden region where the Lagrangian manifolds do not have real intersections. While the analytic continuation of the cosine term in the $6j$-symbol into its classically forbidden region is known, it is unclear what we should do with the d-matrix and the complex argument θ in the forbidden region. This will be the subject of future research.

Another extension is to apply our technique to the $12j$-symbol with two small angular momenta, and to the $15j$-symbol with three small angular momenta. This is easy, because the same Lagrangian manifolds in this chapter, namely, those that appear in the semiclassical analysis of the $6j$-symbol in chapter 4, also appear in those cases for the $12j$- and $15j$-symbols. Since the derivations are almost identical, we will simply display these

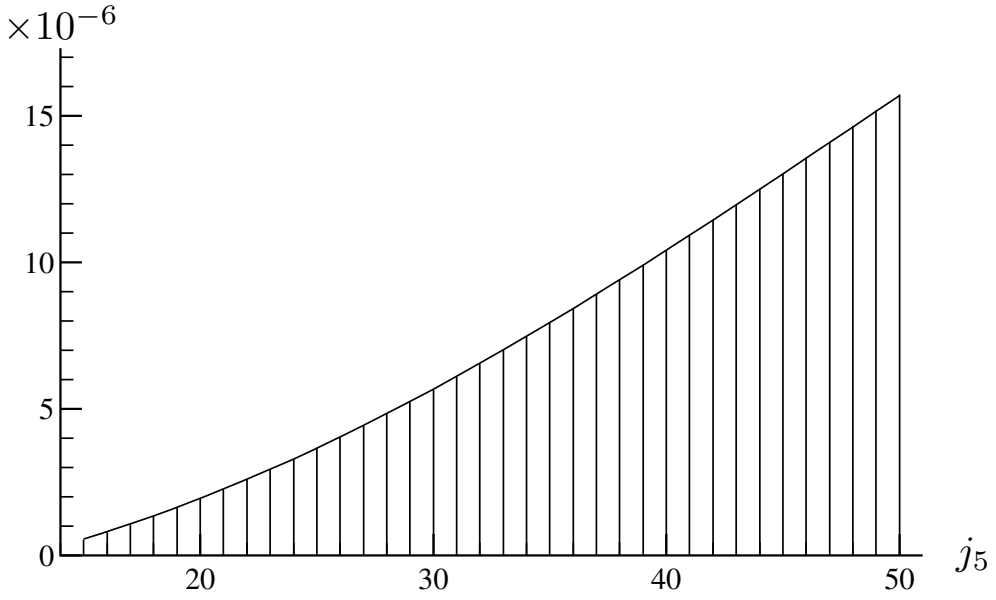

Figure 6.12: Comparison of exact $9j$-symbol (vertical sticks and dots) and the asymptotic formula (6.94), for the values of j's shown in (6.96).

results in the next two chapters, the $12j$-symbol in section 7.10, and the $15j$-symbol in section 8.3.

It is more difficult to apply our method to the case of the $12j$-symbol with one small angular momentum, or to the $15j$-symbol with two small angular momenta. The relevant Lagrangian manifolds are those that appear in the semiclassical analysis of the $9j$-symbol. We will focus on those cases in the next chapter.

One limitation of our method is that it is not applicable to cases where there are three small angular momenta in a single row or column of the $9j$-symbol. The asymptotic formula for the $(6, 3)$ case when the three small angular momenta are placed in the same row is still unknown. In such cases, the matrix operators that define the quantum states are more complicated. We expect a solution will involve a combination of the method developed in this chapter and the summation formula used in [3, 4, 86, 87]. This interplay of two very different techniques will be interesting for a future research project.

Chapter 7

The Wigner $12j$-Symbol with Small and Large Quantum Numbers

7.1 Introduction and Summary

This chapter contains new asymptotic formulas for the $12j$-symbol when some quantum numbers are large and others small. In particular, we derive in full detail an asymptotic formula for the $12j$-symbol in the limit of one small and eleven large angular momenta, as well as other results for the $12j$-symbol in the limit of two or three small quantum numbers.

Besides its definitions and symmetries, very little is known about the asymptotics of the $12j$-symbol. The $12j$-symbol was first defined in an addendum of the paper by Jahn and Hope [43]. Soon after, Ord-Smith [63] showed that the symmetry relations of the $12j$-symbol are linked to the symmetries of the Möbius strip, which in essence is the spin network for the $12j$-symbol. This spin network is illustrated in figure 7.1 below. Note that each of the twelve quantum numbers that parametrize the $12j$-symbol live either on the edge of the strip or across the center of the strip. Using the symmetry of the Möbius strip, any position in the center can be moved to any other position in the center, and any position on the edge can be moved to any other position on the edge. However, a center position cannot be move to an edge position, or vice versa. This means there are two inequivalent cases of the $12j$-symbol with one small angular momentum, corresponding to the small angular momentum being placed at the center or at the edge of the strip, respectively. In this chapter, we will focus on the case where the small angular momentum is placed at a center position. The derivation for the other case is analogous.

The main theoretical tool we use is a generalization of the Born-Oppenheimer approximation, in which the small angular momenta are the fast degrees of freedom and the large angular momenta are the slow degrees of freedom. The required generalization is described in our derivation of the asymptotic formulas for $9j$-symbol with small and large quantum numbers in chapter 6.

In this chapter, in analogy with the setup for the $9j$ problem in chapter 6, we use exact linear algebra to represent the small angular momentum, and use the Schwinger's model to represent the large angular momenta. Each wave-function consists of a spinor

factor and a factor in the form of a scalar WKB solution. In the $9j$ problem, the scalar WKB solutions are represented by Lagrangian manifolds associated with a $6j$-symbol, which has a well known action integral, namely, the Ponzano Regge phase [68]. In the problem of the $12j$-symbol with one small quantum number, the scalar WKB solutions are represented by Lagrangian manifolds associated with a $9j$-symbol. The action integral for the $9j$-symbol is only recently discovered by Haggard and Littlejohn using the Schwinger model in [42]. Although the Lagrangian manifolds that appear here are different from those in [42], the action integrals should be the same. Instead of repeating the derivation of the $9j$ action integral using a different set of Lagrangian manifolds, we will simply describe how to derive it and make use of the action integrals from [42].

We now give an outline of this chapter. In section 7.2, we display the spin network of the $12j$-symbol in the form of a Möbius strip, and decompose it into a scalar product of a bra and a ket. In section 7.3, we define the $12j$-symbol as a scalar product of two multicomponent wavefunctions, whose WKB form are derived in section 7.4. By following the procedure in chapter 6, we rewrite the multicomponent wavefunctions into their gauge-invariant forms in section 7.5. In section 7.6, we describe how one might perform a semiclassical analysis of the Lagrangian manifolds associated with the $9j$-symbol by following the calculations in chapter 4. We then summarize the asymptotic results of the $9j$-symbol from the paper [42]. Finally, we calculate the spinor inner products at the intersections of the Lagrangian manifolds in section 7.7. Putting the pieces together, we derive a new asymptotic formula for the $12j$-symbol in section 7.8, and display a plot for this formula in section 7.9. In sections 7.10 and 7.11, we summarize the results for the cases of two and three small quantum numbers, respectively. The last section contains comments and discussions.

7.2 The Spin Network of the $12j$-Symbol

The spin network [96] for the Wigner $12j$-symbol

$$\left\{ \begin{array}{cccc} j_1 & j_2 & j_{12} & j_{125} \\ j_3 & j_4 & j_{34} & j_{135} \\ j_{13} & j_{24} & j_5 & j_6 \end{array} \right\} \tag{7.1}$$

is displayed in figure 7.1 in the form of a Möbius strip with twelve edges and eight vertices.

The symmetries of the $12j$-symbol are identical to the symmetries of the Möbius strip, which is given by sliding along the Möbius strip and reflecting it about the vertical center of figure 7.1. Modulo those symmetries, there are two ways to place one small quantum number on the twelve edges. We could either place it at j_1, j_4, j_5, or j_6 across the center of the strip, or place it at $j_2, j_3, j_{12}, j_{34}, j_{13}, j_{24}, j_{125}$, or j_{135} along the edge of the strip.

One can decompose the spin network of the $12j$-symbol into two spin networks by cutting j_2, j_3 at the twist, and cutting j_1, j_4, j_5, j_6 along the center of the strip. Using this decomposition, shown in figure 7.2, the $12j$-symbol can be expressed as a scalar product between a bra and a ket, in the Hilbert space represented by the six angular momenta $j_1, \ldots, j_6$, as in (7.2) below.

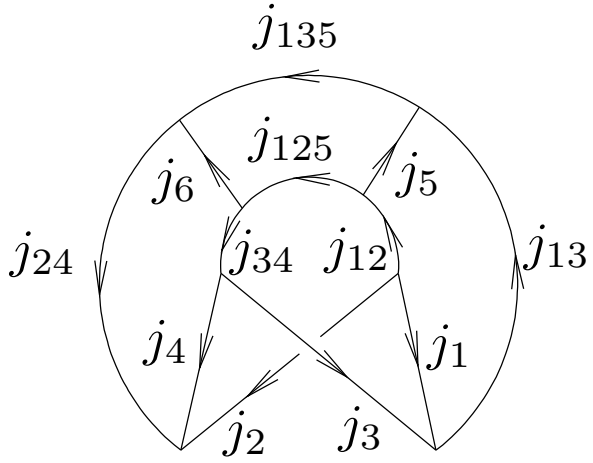

Figure 7.1: The spin network of the Wigner $12j$-symbol.

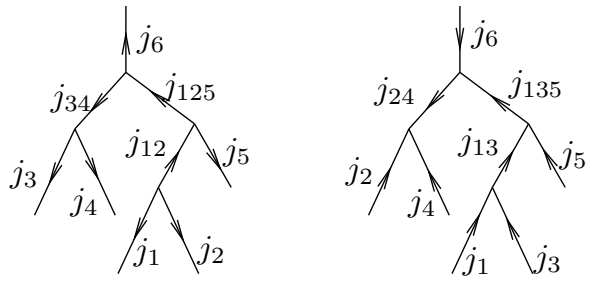

Figure 7.2: A decomposition of the spin network of the $12j$-symbol.

7.3 Defining the $12j$-Symbol

We use the decomposition of the spin network for the $12j$-symbol in figure 7.2 to write it as a scalar product. This is also equivalent to equation (A4) in [43]. The $12j$-symbol is

$$\left\{ \begin{array}{cccc} j_1 & j_2 & j_{12} & j_{125} \\ j_3 & j_4 & j_{34} & j_{135} \\ j_{13} & j_{24} & s_5 & j_6 \end{array} \right\} = \frac{\langle b|a\rangle}{\{[j_{12}][j_{34}][j_{13}][j_{24}][j_{125}][j_{135}]\}^{\frac{1}{2}}}\,, \tag{7.2}$$

where the square bracket notation $[\cdot]$ denotes $[c] = 2c+1$, and the states $|a\rangle$ and $|b\rangle$ are normalized simultaneous eigenstates of lists of operators with certain eigenvalues. We will ignore the phase conventions of $|a\rangle$ and $|b\rangle$ for now, since we did not use them to derive our formula. In our notation, the two states are

$$|a\rangle = \left| \begin{array}{cccccccccc} \hat{I}_1 & \hat{I}_2 & \hat{I}_3 & \hat{I}_4 & \mathbf{S}_5^2 & \hat{I}_6 & \hat{\mathbf{J}}_{12}^2 & \hat{\mathbf{J}}_{34}^2 & \hat{\mathbf{J}}_{125}^2 & \hat{\mathbf{J}}_{\rm tot} \\ j_1 & j_2 & j_3 & j_4 & s_5 & j_6 & j_{12} & j_{34} & j_{125} & \mathbf{0} \end{array} \right\rangle\,, \tag{7.3}$$

$$|b\rangle = \left| \begin{array}{cccccccccc} \hat{I}_1 & \hat{I}_2 & \hat{I}_3 & \hat{I}_4 & \mathbf{S}_5^2 & \hat{I}_6 & \hat{\mathbf{J}}_{13}^2 & \hat{\mathbf{J}}_{24}^2 & \hat{\mathbf{J}}_{135}^2 & \hat{\mathbf{J}}_{\rm tot} \\ j_1 & j_2 & j_3 & j_4 & s_5 & j_6 & j_{13} & j_{24} & j_{135} & \mathbf{0} \end{array} \right\rangle\,. \tag{7.4}$$

In the above notation, the large ket lists the operators on the top row, and the corresponding quantum numbers are listed on the bottom row. The hat is used to distinguish differential operators from their symbols, that is, their corresponding classical counterparts.

The states $|a\rangle$ and $|b\rangle$ live in a total Hilbert space of six angular momenta $\mathcal{H}_1 \otimes \mathcal{H}_2 \otimes \mathcal{H}_3 \otimes \mathcal{H}_4 \otimes \mathcal{H}_6 \otimes \mathcal{H}_s$. Each large angular momentum $\mathbf{J}_r$, $r = 1, 2, 3, 4, 6$, is represented by a Schwinger Hilbert space of two harmonic oscillators, namely, $\mathbf{H}_r = L^2(\mathbb{R}^2)$ [9]. The small angular momentum $\mathbf{S}$ is represented by the usual $2s+1$ dimensional representation of $SU(2)$, that is, $\mathcal{H}_s = \mathbb{C}^{2s+1}$.

Let us now define the lists of operators in (7.3) and (7.4). First we look at the operators $\hat{I}_r$, $r = 1, 2, 3, 4, 6$, and $\hat{\mathbf{J}}_{12}^2$, $\hat{\mathbf{J}}_{34}^2$, $\hat{\mathbf{J}}_{13}^2$, $\hat{\mathbf{J}}_{24}^2$, which act only on the large angular momentum spaces $\mathcal{H}_r$, each of which can be viewed as a space of wave functions $\psi(x_{r1}, x_{r2})$ for two harmonic oscillators of unit frequency and mass. Let $\hat{a}_{r\mu} = (\hat{x}_{r\mu} + i\hat{p}_{r\mu})/\sqrt{2}$, and $\hat{a}_{r\mu}^\dagger = (\hat{x}_{r\mu} - i\hat{p}_{r\mu})/\sqrt{2}$, $\mu = 1, 2$, be the usual annihilation and creation operators. The operators $\hat{I}_r$ and $\hat{J}_{ri}$ are constructed from these differential operators $\hat{a}$ and $\hat{a}^\dagger$ as follows,

$$\hat{I}_r = \frac{1}{2}\sum_\mu \hat{a}_{r\mu}^\dagger \hat{a}_{r\mu}\,, \qquad \hat{J}_{ri} = \frac{1}{2}\sum_{\mu\nu} \hat{a}_{r\mu}^\dagger (\sigma_i)_{\mu\nu} \hat{a}_{r\nu}\,, \tag{7.5}$$

where $i = 1, 2, 3$, and σ_i are the Pauli matrices. The quantum numbers j_r, $r = 1, 2, 4, 5$ specify the eigenvalues of both $\hat{I}_r$ and $\hat{\mathbf{J}}_r^2$, to be j_r and $j_r(j_r+1)$, respectively.

The operators $\hat{\mathbf{J}}_{12}^2$, $\hat{\mathbf{J}}_{34}^2$, $\hat{\mathbf{J}}_{13}^2$, $\hat{\mathbf{J}}_{24}^2$ that define the intermediate couplings of the large angular momenta are the magnitude squares of the partial sums of $\hat{\mathbf{J}}_r$,

$$\hat{\mathbf{J}}_{12} = \hat{\mathbf{J}}_1 + \hat{\mathbf{J}}_2\,, \qquad \hat{\mathbf{J}}_{34} = \hat{\mathbf{J}}_3 + \hat{\mathbf{J}}_4\,, \tag{7.6}$$

$$\hat{\mathbf{J}}_{13} = \hat{\mathbf{J}}_1 + \hat{\mathbf{J}}_3\,, \qquad \hat{\mathbf{J}}_{24} = \hat{\mathbf{J}}_2 + \hat{\mathbf{J}}_4\,. \tag{7.7}$$

See chapter 3 for more detail on the angular momentum operators in the Schwinger model.

We now turn our attention to the operator S^2 that act only on the small angular momentum space $\mathbb{C}^{2s+1}$. Let $\mathbf{S}$ be the vector of dimensionless spin operators represented by $(2s+1)\times(2s+1)$ matrices that satisfy the $SU(2)$ commutation relations

$$[S_i, S_j] = i\,\epsilon_{ijk}\,S_k\,. \tag{7.8}$$

The Casimir operator, $\mathbf{S}^2 = s(s+1)$, is proportional to the identity operator, so its eigenvalue equation is trivially satisfied.

The remaining operators $\hat{\mathbf{J}}^2_{125}$, $\hat{\mathbf{J}}^2_{135}$, and $\hat{\mathbf{J}}_{\rm tot}$ are non-diagonal matrices of differential operators. They are defined in terms of the operators $\hat{I}_r$, $\hat{\mathbf{J}}_{ri}$, and $\mathbf{S}_i$, as follows,

$$\begin{aligned}
(\hat{J}^2_{125})_{\alpha\beta} &= [\hat{J}^2_{12} + \hbar^2 s(s+1)]\delta_{\alpha\beta} + 2\hat{\mathbf{J}}_{12}\cdot\mathbf{S}_{\alpha\beta}, &(7.9)\\
(\hat{J}^2_{135})_{\alpha\beta} &= [\hat{J}^2_{13} + \hbar^2 s(s+1)]\delta_{\alpha\beta} + 2\hat{\mathbf{J}}_{13}\cdot\mathbf{S}_{\alpha\beta}, &(7.10)\\
(\hat{\mathbf{J}}_{\rm tot})_{\alpha\beta} &= (\hat{\mathbf{J}}_1 + \hat{\mathbf{J}}_2 + \hat{\mathbf{J}}_3 + \hat{\mathbf{J}}_4 + \hat{\mathbf{J}}_6)\delta_{\alpha\beta} + \hbar\,\mathbf{S}_{\alpha\beta}. &(7.11)
\end{aligned}$$

These three operators act nontrivially on both the large and small angular momentum Hilbert spaces.

7.4 Multicomponent Wave-Functions

We follow the approach used in chapter 6 to find a gauge-invariant form of the multicomponent wave-functions $\psi^a_\alpha(x) = \langle x,\alpha|a\rangle$ and $\psi^b_\alpha(x) = \langle x,\alpha|b\rangle$. Let us focus on $\psi^a_\alpha(x)$, since the treatment for ψ^b is analogous. We will drop the index a for now.

Let $\hat{D}_i$, $i = 1,\ldots,12$ denote the the operators listed in the definition of $|a\rangle$ in (7.3). We seek a unitary operator $\hat{U}$, such that $\hat{D}_i$ for all $i = 1,\ldots,12$ are diagonalized when conjugated by $\hat{U}$. In other words,

$$\hat{U}^\dagger_{\alpha\,\mu}(\hat{D}_i)_{\alpha\,\beta}\,\hat{U}_{\beta\,\nu} = (\hat{\Lambda}_i)_{\mu\,\nu}\,, \tag{7.12}$$

where $\hat{\Lambda}_i$, $i = 1,\ldots,12$ is a list of diagonal matrix operators. Let $\phi^{(\mu)}$ be the simultaneous eigenfunction for the $\mu^{\rm th}$ diagonal entries $\hat{\lambda}_i$ of the operators $\hat{\Lambda}_i$, $i = 1,\ldots,12$. Then we obtain a simultaneous eigenfunction $\psi^{(\mu)}_\alpha$ of the original list of operators $\hat{D}_i$ from

$$\psi^{(\mu)}_\alpha = \hat{U}_{\alpha\,\mu}\,\phi^{(\mu)}\,. \tag{7.13}$$

Since we are interested in ψ_α only to first order in $\hbar$, all we need are the zeroth order Weyl symbol matrix U of $\hat{U}$, and the first order symbol matrix Λ_i of $\hat{\Lambda}_i$. The resulting asymptotic form of the wave-function $\psi(x)$ is a product of a scalar WKB part Be^{iS} and a spinor part τ, that is,

$$\psi^{(\mu)}_\alpha(x) = B(x)\,e^{i\,S(x)/\hbar}\,\tau^{(\mu)}_\alpha(x,p)\,. \tag{7.14}$$

Here the action $S(x)$ and the amplitude $B(x)$ are simultaneous solutions to the Hamilton-Jacobi and the transport equations, respectively, that are associated with the Hamiltonians $\lambda^{(\mu)}_i$. The spinor τ^μ is the $\mu^{\rm th}$ column of the matrix U,

$$\tau_\alpha^{(\mu)}(x,p) = U_{\alpha\mu}(x,p)\,, \tag{7.15}$$

where $p = \partial S(x)/\partial x$.

Now let us apply the above strategy to the $12j$-symbol. The Weyl symbols of the operators $\hat{I}_r$ and $\hat{J}_{ri}$, $r = 1,2,3,4,6$, are $I_r - 1/2$ and J_{ri}, respectively, where

$$I_r = \frac{1}{2}\sum_\mu \overline{z}_{r\mu} z_{r\mu}\,, \qquad J_{ri} = \frac{1}{2}\sum_{\mu\nu} \overline{z}_{r\mu}(\sigma^i)_{\mu\nu} z_{r\nu}\,, \tag{7.16}$$

and where $z_{r\mu} = x_{r\mu} + ip_{r\mu}$ and $\overline{z}_{r\mu} = x_{r\mu} - ip_{r\mu}$ are the symbols of $\hat{a}$ and $\hat{a}^\dagger$, respectively. The symbols of the remaining operators have the same expressions as (7.6), (7.7), (7.9)-(7.11), but without the hats.

Among the operators $\hat{D}_i$, $\hat{J}^2_{125}$ and the vector of the three operators $\hat{\mathbf{J}}_{\rm tot}$ are non-diagonal. By looking at (7.9), the expression for $\hat{J}^2_{125}$, we see that the zeroth order term of the symbol matrix J^2_{125} is already proportional to the identity matrix, so the spinor τ must be an eigenvector for the first order term $\mathbf{J}_{12}\cdot\mathbf{S}$. Let $\tau^{(\mu)}(\mathbf{J}_{12})$ be the eigenvector of the matrix $\mathbf{J}_{12}\cdot\mathbf{S}$ with eigenvalue μJ_{12}, that is, it satisfies

$$(\mathbf{J}_{12}\cdot\mathbf{S})_{\alpha\beta}\,\tau_\beta^{(\mu)} = \mu J_{12}\,\tau_\beta^{(\mu)}\,, \tag{7.17}$$

where $\mu = -s, \ldots, +s$. In order to preserve the diagonal symbol matrices J_{12} through the unitary transformation, we must choose the spinor $\tau^{(\mu)}$ to depend only on the direction of $\mathbf{J}_{12}$. One possible choice of $\tau^{(\mu)}$ is the north standard gauge, (see Appendix A of [51]), in which the spinor $\delta_{\alpha\,\mu}$ is rotated along a great circle from the z-axis to the direction of $\mathbf{J}_{12}$. Explicitly,

$$\tau_\alpha^{(\mu)}(\mathbf{J}_{12}) = e^{i(\mu-\alpha)\phi_{12}}\, d^{(s)}_{\alpha\,\mu}(\theta_{12})\,, \tag{7.18}$$

where (θ_{12},ϕ_{12}) are the spherical coordinates that specify the direction of $\mathbf{J}_{12}$. Note that this is not the only choice, since (7.17) is invariant under a local $U(1)$ gauge transformations. In other words, any other spinor $\tau' = e^{ig(\mathbf{J}_{12})}\,\tau$ that is related to τ by a $U(1)$ gauge transformation satisfies (7.17). This local gauge freedom is parametrized by the vector potential,

$$\mathbf{A}_{12}^{(\mu)} = i(\tau^{(\mu)})^\dagger\,\frac{\partial\tau^{(\mu)}}{\partial\mathbf{J}_{12}}\,, \tag{7.19}$$

which transforms as $\mathbf{A}^{(\mu)'} = \mathbf{A}^{(\mu)} - \nabla_{\mathbf{J}_{12}}(g)$ under a local gauge transformation. Moreover, the gradient of the spinor can be expressed in terms of the vector potential, (Eqn (A.22) in [51]), as follows,

$$\frac{\partial\tau^{(\mu)}}{\partial\mathbf{J}_{12}} = i\left(-\mathbf{A}_{12}^{(\mu)} + \frac{\mathbf{J}_{12}\times\mathbf{S}}{J^2_{12}}\right)\tau^{(\mu)}\,. \tag{7.20}$$

Once we obtain the complete set of spinors $\tau^{(\mu)}$, $\mu = -s,\ldots,s$, we can construct the zeroth order symbol matrix U of the unitary transformation $\hat{U}$ from (7.15).

Now let us show that all the transformed symbol matrices of the operators in (7.3), namely, the Λ_i, are diagonal to first order. Let us write $\hat{\Lambda}[\hat{D}]$ to denote the operator $\hat{U}^\dagger \hat{D} \hat{U}$, and write $\Lambda[\hat{D}]$ for its Weyl symbol. First, consider the operators $\hat{I}_r$, $r = 1, 2, 3, 4, 6$, which are proportional to the identity matrix. Using the operator identity

$$[\hat{\Lambda}(\hat{I}_r)]_{\mu\nu} = \hat{U}^\dagger_{\alpha\mu}(\hat{I}_r \delta_{\alpha\beta})\hat{U}_{\beta\nu} = \hat{I}_r \delta_{\mu\nu} - \hat{U}^\dagger_{\alpha\mu}[\hat{U}_{\alpha\nu},\, \hat{I}_r]\,, \tag{7.21}$$

we find

$$[\Lambda(\hat{I}_r)]_{\mu\nu} = (I_r - 1/2)\delta_{\mu\nu} - i\hbar U^*_{0\alpha\mu}\,\{U_{0\alpha\nu},\, I_r\}\,, \tag{7.22}$$

where we have used the fact that the symbol of a commutator is a Poisson bracket. Since $U_{\alpha\mu} = \tau^{(\mu)}_\alpha$ is a function only of $\mathbf{J}_{12}$, and since the Poisson brackets $\{\mathbf{J}_{12}, I_r\} = 0$ vanish for all $r = 1, 2, 3, 4, 6$, the second term in (7.22) vanishes. We have

$$[\Lambda(\hat{I}_r)]_{\mu\nu} = (I_r - 1/2)\,\delta_{\mu\nu}\,. \tag{7.23}$$

Similarly, because $\{\mathbf{J}_{12}, J^2_{12}\} = 0$ and $\{\mathbf{J}_{12}, J^2_{34}\} = 0$, we find

$$[\Lambda(\hat{J}^2_{12})]_{\mu\nu} = J^2_{12}\,\delta_{\mu\nu}\,, \qquad [\Lambda(\hat{J}^2_{34})]_{\mu\nu} = J^2_{34}\,\delta_{\mu\nu}\,. \tag{7.24}$$

Now we find the symbol matrices $\Lambda(\hat{\mathbf{J}}_{125})$ for the vector of operators $\hat{\mathbf{J}}_{125}$, where

$$[\hat{\Lambda}(\hat{\mathbf{J}}_{125})]_{\mu\nu} = \hat{U}^\dagger_{\alpha\mu}(\hat{\mathbf{J}}_{12}\delta_{\alpha\beta})\hat{U}_{\beta\nu} + \hbar\,\hat{U}^\dagger_{\alpha\mu}\mathbf{S}_{\alpha\beta}\hat{U}_{\beta\nu}\,. \tag{7.25}$$

After converting the above operator equation to Weyl symbols, we find

$$\begin{aligned}
[\Lambda(\hat{\mathbf{J}}_{125})]_{\mu\nu} &= \mathbf{J}_{12}\delta_{\mu\nu} - i\hbar U^*_{\alpha\mu}\{U_{\alpha\mu},\, \mathbf{J}_{12}\} + \hbar\, U^*_{\alpha\mu}\mathbf{S}_{\alpha\beta}U_{\beta\nu} \\
&= \mathbf{J}_{12}\delta_{\mu\nu} - i\hbar\tau^{(\mu)*}_\alpha\{\tau^{(\nu)}_\alpha,\, \mathbf{J}_{12}\} + \hbar\,\tau^{(\mu)*}_\alpha\mathbf{S}_{\alpha\beta}\tau^{(\nu)}_\beta\,.
\end{aligned} \tag{7.26}$$

Let us denote the second term above by $T^i_{\mu\nu}$, and use (7.20), the orthogonality of τ,

$$\tau^{(\mu)*}_\alpha\,\tau^{(\nu)}_\alpha = \delta_{\mu\nu}\,, \tag{7.27}$$

to get

$$\begin{aligned}
T^i_{\mu\nu} &= -i\hbar\tau^{(\mu)*}_\alpha\{\tau^{(\nu)}_\alpha,\, J_{12i}\} \\
&= -i\hbar\tau^{(\mu)*}_\alpha[\{\tau^{(\nu)}_\alpha,\, J_{1i}\} + \{\tau^{(\nu)}_\alpha,\, J_{2i}\}] \\
&= -i\hbar\tau^{(\mu)*}_\alpha\epsilon_{kji}\left(J_{1k}\frac{\partial\tau^{(\nu)}_\alpha}{\partial J_{1j}} + J_{2k}\frac{\partial\tau^{(\nu)}_\alpha}{\partial J_{2j}}\right) \\
&= -i\hbar\tau^{(\mu)*}_\alpha\epsilon_{kji}J_{12k}\frac{\partial\tau^{(\nu)}_\alpha}{\partial J_{12j}} \\
&= \hbar(\mathbf{A}^{(\mu)}_{12}\times\mathbf{J}_{12})_i\,\delta_{\mu\nu} + \hbar\frac{\mu J_{12i}}{J_{12}}\delta_{\mu\nu} - \hbar\,\tau^{(\mu)*}_\alpha S_{\alpha\beta}\tau^{(\nu)}_\beta\,,
\end{aligned} \tag{7.28}$$

where in the third equality, we have used the reduced Lie-Poisson bracket (3.34) to evaluate the Poisson bracket $\{\tau, \mathbf{J}_1\}$ and $\{\tau, \mathbf{J}_2\}$, and in the third equality we used $\partial\tau/J_1 = \partial\tau/J_{12}$ and $\partial\tau/J_1 = \partial\tau/J_{12}$ from the chain rule, and in the fifth equality, we have used (7.20) for $\partial\tau/\partial\mathbf{J}_{12}$. Notice the term involving $\mathbf{S}$ in $T^i_{\mu\nu}$ in (7.28) cancels out the same term in $\Lambda(\hat{\mathbf{J}}_{125})$ in (7.26), leaving us with a diagonal symbol matrix

$$[\Lambda(\hat{\mathbf{J}}_{125})]_{\mu\nu} = \mathbf{J}_{12}\left[1 + \frac{\mu\hbar}{J_{12}}\right] + \hbar\,\mathbf{A}^{(\mu)}_{12} \times \mathbf{J}_{12}\,. \tag{7.29}$$

Taking the square, we obtain

$$[\Lambda(\hat{\mathbf{J}}^2_{125})]_{\mu\nu} = (J_{12} + \mu\hbar)^2\delta_{\mu\nu}\,. \tag{7.30}$$

Finally, let us look at the last three remaining operators $\hat{\mathbf{J}}_{\rm tot}$ in (7.11). Since the symbols $\mathbf{J}_r$ for $r = 3, 4, 6$ Poisson commutes with $\mathbf{J}_1$, we find $\Lambda(\hat{\mathbf{J}}_r) = \mathbf{J}_r$. Using $\Lambda(\hat{\mathbf{J}}_{125})$ from (7.29), we obtain

$$[\Lambda(\hat{\mathbf{J}}_{\rm tot})]_{\mu\nu} = \left[\mathbf{J}_{12}\left(1 + \frac{\mu\hbar}{J_{12}}\right) + \hbar\,\mathbf{A}^{(\mu)}_{12} \times \mathbf{J}_{12} + (\mathbf{J}_3 + \mathbf{J}_4 + \mathbf{J}_6)\right]\delta_{\mu\nu}\,. \tag{7.31}$$

Therefore all Λ_i, $i = 1, \ldots, 12$ are diagonal.

Not counting the trivial eigenvalue equation for S^2, we have 11 Hamilton-Jacobi equations associated with the Λ_i for each polarization μ in the 20 dimensional phase space $\mathbb{C}^{10}$. It turns out that not all of them are functionally independent. In particular, the Hamilton-Jacobi equations $\Lambda(\hat{J}^2_{12}) = J^2_{12}\hbar = (j_{12} + 1/2)\hbar$ and $\Lambda(\hat{J}^2_{125}) = (J_{12} + \mu\hbar)^2 = (j_{125} + 1/2)^2\hbar^2$ are functionally dependent. For them to be consistent, we must pick out the polarization $\mu = j_{125} - j_{12}$. This reduces the number of independent Hamilton-Jacobi equations for $S(x)$ from 11 to 10, half of dimension of the phase space $\mathbb{C}^{10}$. These 10 equations define the Lagrangian manifold associated with the action $S(x)$.

Now let us restore the index a. We express the multicomponent wave-function $\psi^a_\alpha(x)$ in the form of (7.14),

$$\psi^a_\alpha(x) = B_a(x)\, e^{iS_a(x)/\hbar}\, \tau^a_\alpha(x, p)\,. \tag{7.32}$$

Here the action $S_a(x)$ is the solution to the eight Hamilton-Jacobi equations associated with the $\mu^{\rm th}$ entries λ^a_i of 10 of the symbol matrices Λ^a_i, given by

$$\begin{aligned}
I_1 &= (j_1 + 1/2)\hbar\,, \\
I_2 &= (j_2 + 1/2)\hbar\,, \\
I_3 &= (j_3 + 1/2)\hbar\,, \\
I_4 &= (j_4 + 1/2)\hbar\,, \\
I_6 &= (j_6 + 1/2)\hbar\,, \\
J^2_{12} &= (j_{12} + 1/2)^2\hbar^2\,, \\
J^2_{34} &= (j_{34} + 1/2)^2\hbar^2\,, \\
\mathbf{J}^{(a)}_{\rm tot} &= \mathbf{J}_{12}\left[1 + \frac{\mu\hbar}{J_{12}}\right] + \hbar\,\mathbf{A}_{12} \times \mathbf{J}_{12} + (\mathbf{J}_3 + \mathbf{J}_4 + \mathbf{J}_6) = \mathbf{0}\,,
\end{aligned} \tag{7.33}$$

and $\tau^a = \tau^{(\mu)}$ with $\mu = j_{125} - j_{12}$. Note that all the Hamiltonians except the last three, $\mathbf{J}^{(a)}_{\rm tot}$, preserve the value of $\mathbf{J}_{12}$ along their Hamiltonian flows.

We carry out an analogous analysis for $\psi^b(x)$. The result is

$$\psi^b_\alpha(x) = B_b(x)\, e^{iS_b(x)/\hbar}\, \tau^b_\alpha(x,p)\,, \tag{7.34}$$

where $S_b(x)$ is the solution to the following 10 Hamilton-Jacobi equations:

$$\begin{aligned}
I_1 &= (j_1 + 1/2)\hbar\,, \\
I_2 &= (j_2 + 1/2)\hbar\,, \\
I_3 &= (j_3 + 1/2)\hbar\,, \\
I_4 &= (j_4 + 1/2)\hbar\,, \\
I_6 &= (j_6 + 1/2)\hbar\,, \\
J^2_{13} &= (j_{13} + 1/2)^2\hbar^2\,, \\
J^2_{24} &= (j_{24} + 1/2)^2\hbar^2\,, \\
\mathbf{J}^{(b)}_{\rm tot} &= \mathbf{J}_{13}\left[1 + \frac{\nu\hbar}{J_{13}}\right] + \hbar\,\mathbf{A}_{13}\times\mathbf{J}_{13} + (\mathbf{J}_2 + \mathbf{J}_4 + \mathbf{J}_6) = \mathbf{0}\,.
\end{aligned} \tag{7.35}$$

Here the spinor $\tau^b = \tau^{(\nu)}_b$ satisfies

$$(\mathbf{J}_{13}\cdot\mathbf{S})_{\alpha\beta}\,(\tau^{(\nu)}_b)_\beta = \nu J_{13}\,(\tau^{(\nu)}_b)_\beta\,, \tag{7.36}$$

where $\nu = j_{135} - j_{13}$.

The vector potential $\mathbf{A}_{13}$ is defined by

$$\mathbf{A}_{13} = i(\tau^b)^\dagger\,\frac{\partial\tau^b}{\partial\mathbf{J}_{13}}\,. \tag{7.37}$$

Again, note that all the Hamiltonians except the last three, $\mathbf{J}^{(a)}_{\rm tot}$, preserve the value of $\mathbf{J}_{13}$ along their Hamiltonian flows.

7.5 The Gauge-Invariant Form of the Wave-Functions

We follow the procedure in chapter 6 to transform the wave-functions into their gauge-invariant form. Because the arguments are identical to those presented in section 6.4, we omit the details here. We obtain a gauge-invariant representation of the wave-function,

$$\psi^a(x) = B_a(x)\, e^{iS^{9j}_a(x)/\hbar}\,\left[U_a(x)\,\tau^a(x_0)\right]\,. \tag{7.38}$$

where the action $S^{9j}_a(x)$ is the integral of $p\,dx$ starting at a point z_0, which is the lift of a reference point x_0 in the Lagrangian manifold $\mathcal{L}^{9j}_a$. The Lagrangian manifold $\mathcal{L}^{9j}_a$ is defined by the following equations:

$$\begin{aligned} I_1 &= (j_1+1/2)\hbar\,, \\ I_2 &= (j_2+1/2)\hbar\,, \\ I_3 &= (j_3+1/2)\hbar\,, \\ I_4 &= (j_4+1/2)\hbar\,, \\ I_6 &= (j_6+1/2)\hbar\,, \\ J_{12}^2 &= (j_{12}+1/2)^2\hbar^2\,, \\ J_{34}^2 &= (j_{34}+1/2)^2\hbar^2\,, \\ \mathbf{J}_{\rm tot} &= \mathbf{J}_1+\mathbf{J}_2+\mathbf{J}_3+\mathbf{J}_4+\mathbf{J}_6=\mathbf{0}\,. \end{aligned} \tag{7.39}$$

The rotation matrices $U_a(x)$ are determined by the rotation required to move the vector configuration of $\mathbf{J}_{12}, \mathbf{J}_6$ at the lift of x_0 to those at the lift of x on $\mathcal{L}_a^{9j}$.

Similarly, the multicomponent wave-function for the state $|b\rangle$ has the following form,

$$\psi^b(x) = B_b(x)\, e^{iS_b^{9j}(x)/\hbar} \left[U_b(x)\,\tau^b(x_0)\right]\,, \tag{7.40}$$

where the action $S_b^{9j}(x)$ is the integral of $p\,dx$ starting at a point that is the lift of x_0 onto the Lagrangian manifold $\mathcal{L}_b^{9j}$. The Lagrangian manifold $\mathcal{L}_b^{9j}$ is defined by the following equations:

$$\begin{aligned} I_1 &= (j_1+1/2)\hbar\,, \\ I_2 &= (j_2+1/2)\hbar\,, \\ I_3 &= (j_3+1/2)\hbar\,, \\ I_4 &= (j_4+1/2)\hbar\,, \\ I_6 &= (j_6+1/2)\hbar\,, \\ J_{13}^2 &= (j_{13}+1/2)^2\hbar^2\,, \\ J_{24}^2 &= (j_{24}+1/2)^2\hbar^2\,, \\ \mathbf{J}_{\rm tot} &= \mathbf{J}_1+\mathbf{J}_2+\mathbf{J}_3+\mathbf{J}_4+\mathbf{J}_6=\mathbf{0}\,. \end{aligned} \tag{7.41}$$

The rotation matrices $U_b(x)$ are determined by the rotation required to move the vector configuration of $\mathbf{J}_{13}, \mathbf{J}_6$ at the lift of x_0 to those at the lift of x on $\mathcal{L}_b^{9j}$.

Taking the inner product of the wave-functions, and treating the spinors as part of the slowly varying amplitudes, as we did in (6.71) for the $9j$ case, we find

$$\langle b|a\rangle = e^{i\kappa}\sum_k \Omega_k \exp\{i[S_a^{9j}(z_k) - S_b^{9j}(z_k) - \mu_k\pi/2]/\hbar\} \left(U_b^{0k}\tau^b(z_0)\right)^\dagger \left(U_a^{0k}\tau^a(z_0)\right). \tag{7.42}$$

In the above formula, the sum is over the components of the intersection set $\mathcal{M}_k$ between the two Lagrangian manifolds $\mathcal{L}_a^{9j}$ and $\mathcal{L}_b^{9j}$. The point z_k is any point in the kth component.

The amplitude Ω_k and the Maslov index μ_k are the results of doing the stationary phase approximation of the inner product without the spinors. Each rotation matrix U_a^{0k} is determined by a path $\gamma^{a(0k)}$ that goes from z_0 to z_k along $\mathcal{L}_a^{9j}$, and U_b^{0k} is similarly defined. The formula (7.42) is independent of the choice of z_k, because any other choice z_k' will multiply both U_a^{0j} and U_b^{0j} by the same additional rotation matrix which cancels out in the product $(U_b^{0k})^\dagger U_a^{0k}$.

7.6 The Lagrangian Manifolds and Actions

We now analyze the Lagrangian manifolds $\mathcal{L}_a^{9j}$ and $\mathcal{L}_b^{9j}$, defined by the Hamilton-Jacobi equations (7.39) and (7.41), respectively. We focus on $\mathcal{L}_a^{9j}$ first, since the treatment for $\mathcal{L}_b^{9j}$ is analogous. Let $\pi : \Phi_{5j} \to \Lambda_{5j}$ denote the projection of the large phase space $\Phi_{5j} = (\mathbb{C}^2)^5$ onto the angular momentum space $\Lambda_{5j} = (\mathbb{R}^3)^5$, through the functions $\mathbf{J}_{ri}$, $r = 1, 2, 3, 4, 6$. The first six equations, $I_r = j_r + 1/2$, $r = 1, 2, 3, 4, 6$ fix the lengths of the five vectors $|\mathbf{J}_r| = J_r$, $r = 1, 2, 3, 4, 6$. The three equations for the total angular momentum,

$$\mathbf{J}_{\rm tot} = \mathbf{J}_1 + \mathbf{J}_2 + \mathbf{J}_3 + \mathbf{J}_4 + \mathbf{J}_6 = \mathbf{0}\,, \tag{7.43}$$

constrains the five vectors $\mathbf{J}_i$, $i = 1, \ldots, 6$ to form a close polygon. The remaining two equations

$$J_{12}^2 = (j_{12} + 1/2)^2\hbar^2\,, \tag{7.44}$$
$$J_{34}^2 = (j_{34} + 1/2)^2\hbar^2\,, \tag{7.45}$$

put the vectors $\mathbf{J}_1, \mathbf{J}_2$ into a 1-2-12 triangle, and put the vectors $\mathbf{J}_3, \mathbf{J}_4$ into a 3-4-34 triangle. Thus, the vectors form a butterfly shape, illustrated in figure 7.3. This shape has two wings (J_1, J_2, J_{12}) and (J_3, J_4, J_{34}) that are free to rotate about the J_{12} and J_{34} edges, respectively. Moreover, the Hamilton-Jacobi equations are also invariant under an overall rotation of the vectors. Thus the projection of $\mathcal{L}_a^{9j}$ onto the angular momentum space is diffeomorphic to $U(1)^2 \times O(3)$.

The orbit of the group $U(1)^5$ generated by I_r, $r = 1, 2, 3, 4, 6$ is a 5-torus. Thus $\mathcal{L}_a^{9j}$ is a 5-torus bundle over a sub-manifold described by the butterfly configuration in figure 7.3. Altogether there is a $U(1)^7 \times SU(2)$ action on $\mathcal{L}_a^{9j}$. If we denote coordinates on $U(1)^7 \times SU(2)$ by $(\psi_1, \psi_2, \psi_3, \psi_4, \psi_6, \theta_{12}, \theta_{34}, u)$, where $u \in SU(2)$ and where the five angles are the 4π-periodic evolution variables corresponding to $(I_1, I_2, I_3, I_4, I_6, \mathbf{J}_{12}^2, \mathbf{J}_{34}^2)$, respectively, then the isotropy subgroup is generated by three elements, say $x = (2\pi, 2\pi, 2\pi, 2\pi, 2\pi, 0, 0, -1)$, $y = (0, 0, 2\pi, 2\pi, 2\pi, 2\pi, 0, -1)$, and $z = (2\pi, 2\pi, 0, 0, 2\pi, 0, 2\pi, -1)$. The isotropy subgroup itself is an Abelian group of eight elements, $(\mathbb{Z}_2)^3 = \{e, x, y, z, xy, xz, yz, xyz\}$. Thus the manifold $\mathcal{L}_a^{9j}$ is topologically $U(1)^7 \times SU(2)/(\mathbb{Z}_2)^3$. The analysis for $\mathcal{L}_b^{9j}$ is the same.

Now it is easy to find the invariant measure on $\mathcal{L}_a^{9j}$ and $\mathcal{L}_b^{9j}$. It is $d\psi_1 \wedge d\psi_2 \wedge d\psi_3 \wedge d\psi_4 \wedge d\psi_6 \wedge d\theta_{12} \wedge d\theta_{34} \wedge du$, where du is the Haar measure on $SU(2)$. The volumes V_A of $\mathcal{L}_a^{9j}$ and V_B of $\mathcal{L}_b^{9j}$ with respect to this measure are

$$V_A = V_B = \frac{1}{8}\,(4\pi)^7 \times 16\pi^2 = 2^{15}\pi^9\,, \tag{7.46}$$

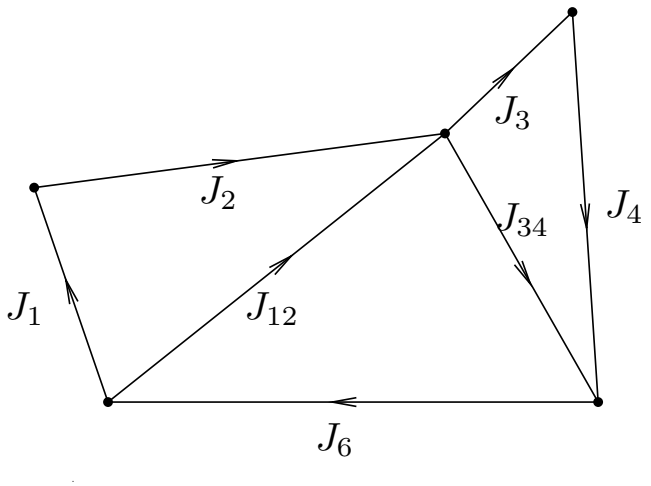

Figure 7.3: The configuration of a point on $\mathcal{L}_a^{9j}$, projected onto the angular momentum space, and viewed in a single $\mathbb{R}^3$.

where the 1/8 factor compensates for the 8-element isotropy subgroup.

We now examine the intersection of $\mathcal{L}_a^{9j}$ and $\mathcal{L}_b^{9j}$ in detail. Because the two lists of Hamilton-Jacobi equations (7.39) and (7.41) share the common equations $I_r = j_r + 1/2$, $r = 1, 2, 3, 4, 6$, the intersection in the large phase space Φ_{5j} is a 5-torus fiber bundle over the intersection of the projections in the angular momentum space Λ_{5j}. The intersections of the projections in Λ_{5j} require the five vectors $\mathbf{J}_r$, $r = 1, 2, 3, 4, 6$, to satisfy

$$\begin{aligned} |\mathbf{J}_r| = J_r\,, \qquad & \sum_r \mathbf{J}_r = \mathbf{0}\,, \\ |\mathbf{J}_1 + \mathbf{J}_2| = J_{12}\,, \qquad & |\mathbf{J}_3 + \mathbf{J}_4| = J_{34}\,, \\ |\mathbf{J}_1 + \mathbf{J}_3| = J_{13}\,, \qquad & |\mathbf{J}_2 + \mathbf{J}_4| = J_{24}\,. \end{aligned} \tag{7.47}$$

A nice way of constructing these vectors follows the procedure in section 4.4, which was generalized to apply to the $9j$ manifolds in [42]. We now describe this procedure using a different set of labeling. The method uses the Gram matrix of dot products among the vectors $\mathbf{J}_i$, $i = 1, 2, 3, 4$. Some of the dot products can be determined from the given J_i, $i = 1, 2, 3, 4, 6, 12, 34, 13, 24$. In particular, the diagonal elements are J_i^2, $i = 1, 2, 3, 4$, and

$$\mathbf{J}_1 \cdot \mathbf{J}_2 = \frac{1}{2}(J_{12}^2 - J_1^2 - J_2^2)\,, \quad \mathbf{J}_3 \cdot \mathbf{J}_4 = \frac{1}{2}(J_{34}^2 - J_3^2 - J_4^2)\,, \tag{7.48}$$

$$\mathbf{J}_1 \cdot \mathbf{J}_3 = \frac{1}{2}(J_{13}^2 - J_1^2 - J_3^2)\,, \quad \mathbf{J}_2 \cdot \mathbf{J}_4 = \frac{1}{2}(J_{24}^2 - J_2^2 - J_4^2)\,. \tag{7.49}$$

The remaining two unknown dot products, $x = \mathbf{J}_1 \cdot \mathbf{J}_4$ and $y = \mathbf{J}_2 \cdot \mathbf{J}_3$, can be solved from a system of two equations. The first equation follows from (7.43) by moving $\mathbf{J}_6$ to the other side, and taking the square,

$$\begin{aligned} J_6^2 &= (\mathbf{J}_1+\mathbf{J}_2+\mathbf{J}_3+\mathbf{J}_4)^2 \\ &= J_1^2+J_2^2+J_3^2+J_4^2+(J_{12}^2-J_1^2-J_2^2)+(J_{13}^2-J_1^2-J_3^2) \\ &\quad +(J_{24}^2-J_2^2-J_4^2)+(J_{34}^2-J_3^2-J_4^2)+2x+2y\,, \end{aligned} \tag{7.50}$$

which gives us a linear relation between x and y

$$x+y=\frac{1}{2}(J_1^2+J_2^2+J_3^2+J_4^2+J_6^2-J_{12}^2-J_{34}^2-J_{13}^2-J_{24}^2)\,. \tag{7.51}$$

The second equation comes from the fact that the Gram matrix of dot products between any four vectors in $\mathbb{R}^3$ has zero determinant, where the Gram matrix is

$$\begin{aligned} G &= \begin{pmatrix} \vec{J}_1\cdot\vec{J}_1 & \vec{J}_1\cdot\vec{J}_2 & \vec{J}_1\cdot\vec{J}_3 & \vec{J}_1\cdot\vec{J}_4 \\ \vec{J}_2\cdot\vec{J}_1 & \vec{J}_2\cdot\vec{J}_2 & \vec{J}_2\cdot\vec{J}_3 & \vec{J}_2\cdot\vec{J}_4 \\ \vec{J}_3\cdot\vec{J}_1 & \vec{J}_3\cdot\vec{J}_2 & \vec{J}_3\cdot\vec{J}_3 & \vec{J}_3\cdot\vec{J}_4 \\ \vec{J}_4\cdot\vec{J}_1 & \vec{J}_4\cdot\vec{J}_2 & \vec{J}_4\cdot\vec{J}_3 & \vec{J}_4\cdot\vec{J}_4 \end{pmatrix} \\ &= \begin{pmatrix} J_1^2 & \frac{1}{2}(J_{12}^2-J_1^2-J_2^2) & \frac{1}{2}(J_{13}^2-J_1^2-J_3^2) & x \\ \frac{1}{2}(J_{12}^2-J_1^2-J_2^2) & J_2^2 & y & \frac{1}{2}(J_{24}^2-J_2^2-J_4^2) \\ \frac{1}{2}(J_{13}^2-J_1^2-J_3^2) & y & J_3^2 & \frac{1}{2}(J_{34}^2-J_3^2-J_4^2) \\ x & \frac{1}{2}(J_{24}^2-J_2^2-J_4^2) & \frac{1}{2}(J_{34}^2-J_3^2-J_4^2) & J_4^2 \end{pmatrix}. \end{aligned} \tag{7.52}$$

Its determinant $P(x,y)\equiv|G|$ is quadratic in the variables x and y. We obtain another equation for x and y by setting

$$P(x,y)=0\,. \tag{7.53}$$

Substituting the linear relation (7.51) into (7.53) leads to a quartic equation $Q(x)=0$, which we can use to solve for x, and then use (7.51) to solve for y. In general, we find two set of real solutions of $(x,y)=(x_1,y_1)$ and $(x,y)=(x_2,y_2)$.

For each set of solutions of (x,y), if all the diagonal sub-determinant of order 3 of the Gram matrix (7.53) are positive definite, we can find the vector configurations from the Gram matrix (7.53) in two steps. Let G_3 be the first diagonal 3×3 sub-matrix of G. Then its singular decomposition gives us the vectors $\mathbf{J}_1,\mathbf{J}_2,\mathbf{J}_3$, according to the procedure in section 4.4. We can then find $\mathbf{J}_4$ from the known dot products between $\mathbf{J}_i$, $i=1,2,3$ and $\mathbf{J}_4$,

$$\mathbf{J}_1\cdot\mathbf{J}_4 = x\,, \tag{7.54}$$

$$\mathbf{J}_2\cdot\mathbf{J}_4 = \frac{1}{2}\,(J_{24}^2-J_2^2-J_4^2)\,, \tag{7.55}$$

$$\mathbf{J}_3\cdot\mathbf{J}_4 = \frac{1}{2}\,(J_{34}^2-J_3^2-J_4^2)\,, \tag{7.56}$$

to finally obtain $\mathbf{J}_6$ from

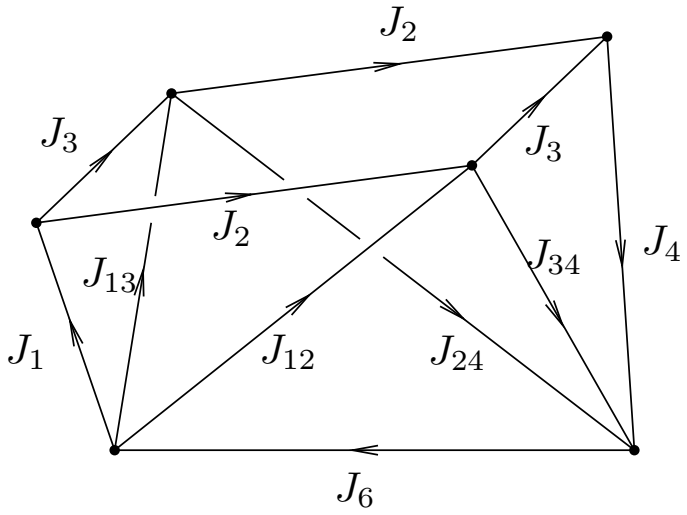

Figure 7.4: The configuration of a point in the intersection set I_{11}, projected onto the angular momentum space, and viewed in a single $\mathbb{R}^3$.

$$\mathbf{J}_6 = -(\mathbf{J}_1 + \mathbf{J}_2 + \mathbf{J}_3 + \mathbf{J}_4)\,. \tag{7.57}$$

Once we have $\mathbf{J}_i$, $i = 1, 2, 3, 4, 6$, we can find the intermediate vectors $\mathbf{J}_i$, $i = 12, 34, 13, 24$.

This method not only gives explicit solutions for all the vectors at the intersection of $\mathcal{L}_a^{9j}$ and $\mathcal{L}_b^{9j}$, the fact that we find two distinct solutions of dot products (x_1, y_1) and (x_2, y_2) shows that the solution set consist of two sets of vector configurations that are not related by an $O(3)$ symmetry. Thus the solution set of (7.47) in Λ_{5j} consists of four disconnected subsets, each diffeomorphic to $SO(3)$. These four sets can be grouped into two pairs according to the values of the dot products (x_1, y_1) and (x_2, y_2).

The intersections in Φ_{5j} are the lifts of the intersections in Λ_{5j}. Therefore, the intersection of $\mathcal{L}_a^{9j}$ consists of four disconnected subsets, where each subset is a 5-torus bundle over $SO(3)$. Let us denote the two sets corresponding to (x_1, y_1) by I_{11}, I_{12}, and denote the two sets corresponding to (x_2, y_2) by I_{21}, I_{22}. The vector configuration for a typical point in I_{11} is illustrated in figure 7.4. Each intersection set is an orbit of the group $U(1)^5 \times SU(2)$, where $U(1)^5$ represent the phases of the five spinors and $SU(2)$ is the diagonal action generated by $\mathbf{J}_{\text{tot}}$.

The isotropy subgroup of this group action is $\mathbb{Z}_2$, generated by the element $(2\pi, 2\pi, 2\pi, 2\pi, 2\pi, -1)$, in coordinates $(\psi_1, \psi_2, \psi_3, \psi_4, \psi_6, u)$ for the group $T^5 \times SU(2)$, where $u \in SU(2)$. The volume of the intersection manifold I_{11}, I_{12}, I_{21}, or I_{22}, with respect to the measure $d\psi_1 \wedge d\psi_2 \wedge d\psi_3 \wedge d\psi_4 \wedge d\psi_6 \wedge du$, is

$$V_I = \frac{1}{2}(4\pi)^5 \times 16\pi^2 = 2^{12}\pi^7\,, \tag{7.58}$$

where the 1/2 factor compensates for the two element isotropy subgroup.

The amplitude determinant is given in terms of a determinant of Poisson brackets among distrinct Hamiltonians between the two lists of Hamilton-Jacobi equations in (7.39) and (7.41). In this case, those are (J_{12}, J_{34}) from (7.39) and (J_{13}, J_{24}) from (7.41). Thus the determinant of Poisson brackets is

$$\begin{aligned} & \begin{vmatrix} \{J_{12},\, J_{13}\} & \{J_{12},\, J_{24}\} \\ \{J_{34},\, J_{13}\} & \{J_{34},\, J_{24}\} \end{vmatrix} \\ = \;& \frac{1}{J_{12}J_{23}J_{13}J_{24}} \begin{vmatrix} V_{123} & V_{214} \\ V_{341} & V_{432} \end{vmatrix} \\ = \;& \frac{1}{J_{12}J_{23}J_{13}J_{24}} |V_{123}V_{432} - V_{214}V_{341}|\,, \end{aligned} \tag{7.59}$$

where

$$V_{ijk} = \mathbf{J}_i \cdot (\mathbf{J}_j \times \mathbf{J}_k)\,. \tag{7.60}$$

The amplitude Ω_k in (7.42) is then given by the general WKB formula (3.6) in section 3.2. In the present case, each Ω_k has the same expression Ω in terms of the J_r and V_{ijk}. It is

$$\begin{aligned} \Omega \;&=\; \frac{(2\pi i)V_I}{\sqrt{V_A V_B}} \frac{\sqrt{J_{12}J_{23}J_{13}J_{24}}}{\sqrt{|V_{123}V_{432} - V_{214}V_{341}|}} \\ &=\; \frac{(2\pi i)2^{12}\pi^7}{2^{15}\pi^9} \frac{\sqrt{J_{12}J_{23}J_{13}J_{24}}}{\sqrt{|V_{123}V_{432} - V_{214}V_{341}|}} \\ &=\; \frac{i\sqrt{J_{12}J_{23}J_{13}J_{24}}}{4\pi\sqrt{|V_{123}V_{432} - V_{214}V_{341}|}}\,. \end{aligned} \tag{7.61}$$

We now determine the relative phase between the exponents $S_a(z_{12}) - S_b(z_{12})$ and $S_a(z_{11}) - S_b(z_{11})$, which can be written as an action integral

$$S^{(1)} = (S_a(z_{12}) - S_b(z_{12})) - (S_a(z_{11}) - S_b(z_{11})) = \oint p\, dx \tag{7.62}$$

around a close loop that goes from z_{11} to z_{12} along the A-manifold and then back along the B-manifold.

We shall construct the closed loop giving the relative phase $S^{(1)}$ by following the Hamiltonian flows of various observables. This loop consists of four paths, and it is illustrated in the large phase space Φ_{5j} in figure 7.5. The loop projects onto a loop in the angular momentum space Λ_{5j}, which is illustrated in figure 7.6. We take the starting point $p \in I_{11}$ of figure 7.5 to lie in the 5-torus fiber above a solution of (7.47). Its vector configuration illustrated in part (a) of figure 7.6.

First we follow the $\mathbf{J}_{12}^2$-flow and then the $\mathbf{J}_{34}^2$-flow to trace out a path that takes us along the A-manifold from a point p in I_{11} to a point q in I_{12}. Let the angles of rotations be $2\phi_{12}$ and $2\phi_{34}$, respectively, where ϕ_{12} is the angle between the triangles 1-2-12 and 12-34-6,

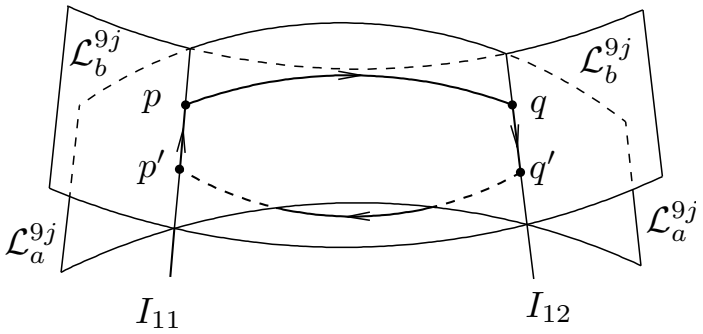

Figure 7.5: The loop from a point $p \in I_{11}$ to $q \in I_{12}$ along the A-manifold, and then to $q'' \in I_{12}$ along I_{12}, and then to $p' \in I_{11}$ along the B-manifold, and finally back to p along I_{11}.

and ϕ_{34} is the angle between the triangles 3-4-34 and 12-34-6. These rotations effectively reflect the triangles 1-2-12 and 3-4-34 across the triangle 12-34-6, as illustrated in parts (a) and (b) of figure 7.6. Thus, all five vectors $\mathbf{J}_r$, $r = 1, 2, 3, 4, 6$, are reflected across the triangle 12-34-6. In particular, the triangle 13-24-6 is also reflected across this plane.

Next, we follow the Hamiltonian flow generated by $-\mathbf{j}_6 \cdot \mathbf{J}_{\text{tot}}$ along I_{12}, which generates an overall rotation of all the vectors around $-\mathbf{j}_6$. Let the angle of rotation be $2\phi_6$, where ϕ_6 is the angle between the triangles 12-34-6 and 13-24-6. This brings the triangle 13-24-6 back to its original position. However, the triangle 12-34-6 is now rotated to the other side of triangle 13-24-6, as illustrated in part (c) of figure 7.6.

To bring the triangle 12-34-6 back to its original position, we follow the $\mathbf{J}_{13}^2$-flow by an angle $2\phi_{13}$ and follow the $\mathbf{J}_{24}^2$-flow by an angle $2\phi_{24}$, where ϕ_{13} is the angle between the triangle 1-3-13 and the triangle 13-24-6, and ϕ_{24} is the angle between the triangle 2-4-24 and the triangle 13-24-6. These rotations effectively reflect all the vectors across the triangle 13-24-6. In particular, the triangle 12-34-6 is reflected back to its original orientation. Thus we arrive at a point $p' \in I_{11}$, where the points p and p' have the same projection in Λ_{5j}, as illustrated in parts (a) and (d) of figure 7.6. This means they differ only by the phases of the five spinors, which can be restored by following the Hamiltonian flows of $(I_1, I_2, I_3, I_4, I_6)$. This constitutes the last path from p' to p.

To summarize the rotational history in the angular momentum space, we have applied the rotations

$$R_{13}(\mathbf{j}'_{13}, 2\phi_{13}) R_{24}(\mathbf{j}'_{24}, 2\phi_{24}) R(-\mathbf{j}_6, 2\phi_6) R_{34}(\mathbf{j}_{34}, 2\phi_{34}) R_{12}(\mathbf{j}_{12}, 2\phi_{12}) \,, \tag{7.63}$$

where R_{12} acts only on $\mathbf{J}_1$ and $\mathbf{J}_2$, R_{34} acts only on $\mathbf{J}_3$ and $\mathbf{J}_4$, R_{13} acts only on $\mathbf{J}_1$ and $\mathbf{J}_3$, R_{24} acts only on $\mathbf{J}_2$ and $\mathbf{J}_4$, and $R(-\mathbf{j}_6, 2\phi_6)$ acts on all five vectors. The corresponding $SU(2)$ rotations, with the same axes and angles, take us from point p in figure 7.5 to another point p' along the sequence $p \to q \to q' \to p'$.

To compute the final five phases required to close the loop, we use the Hamilton-Rodrigues formula [91], like we did in section 4.8. Let us start with vector $\mathbf{J}_1$. The action

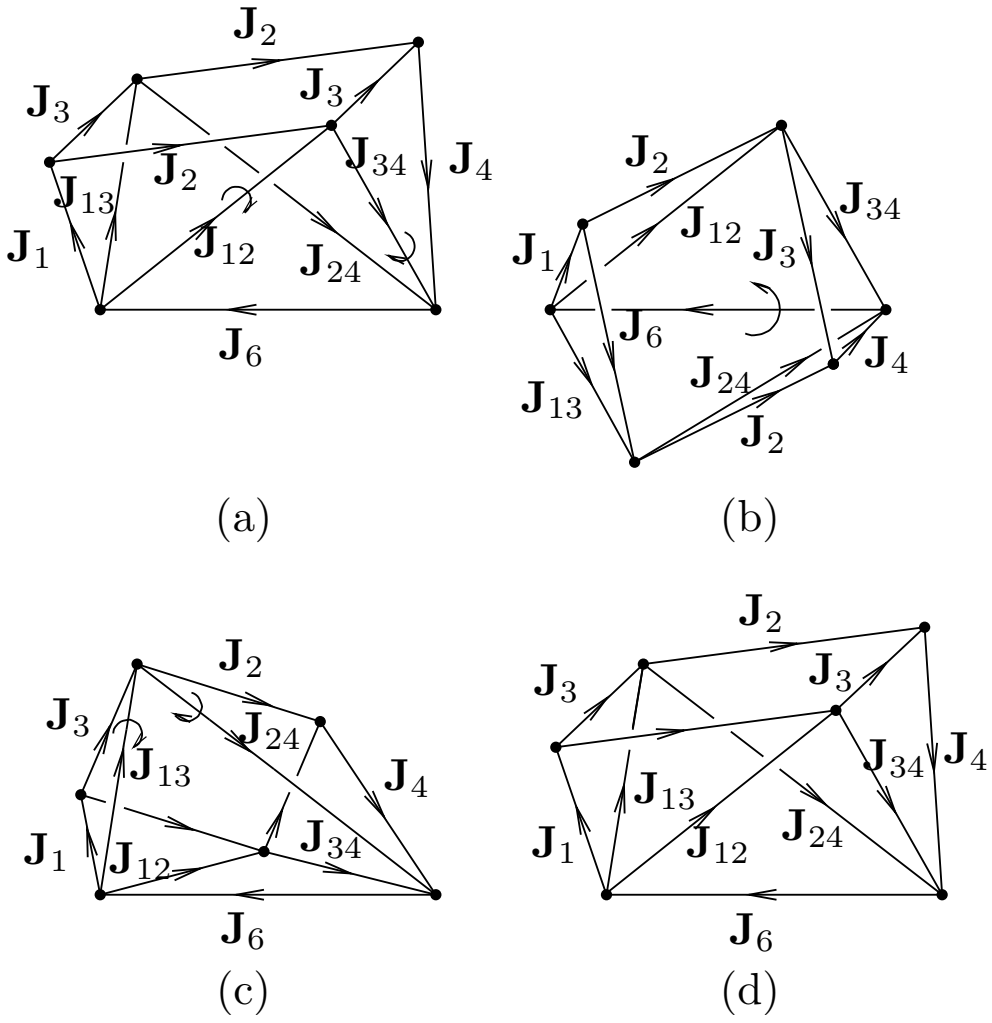

Figure 7.6: The loop from figure 7.5 projected onto a loop in the angular momentum space.

of the rotations on this vector can be written

$$R(\mathbf{j}_{13}, 2\phi_{13})R(-\mathbf{j}_6, 2\phi_6)R(\mathbf{j}_{12}, 2\phi_{12})\mathbf{J}_1 = \mathbf{J}_1\,. \tag{7.64}$$

By inserting an edge $\mathbf{J}_{16} = \mathbf{J}_1 + \mathbf{J}_6$ as in part (c) of figure 7.7, we split the angle ϕ_6 that appears in the middle rotation in (7.64) into two internal dihedral angles ϕ_{6a} and ϕ_{6b}, of the tetrahedrons in part (a) and part (b) of figure 7.7, respectively.

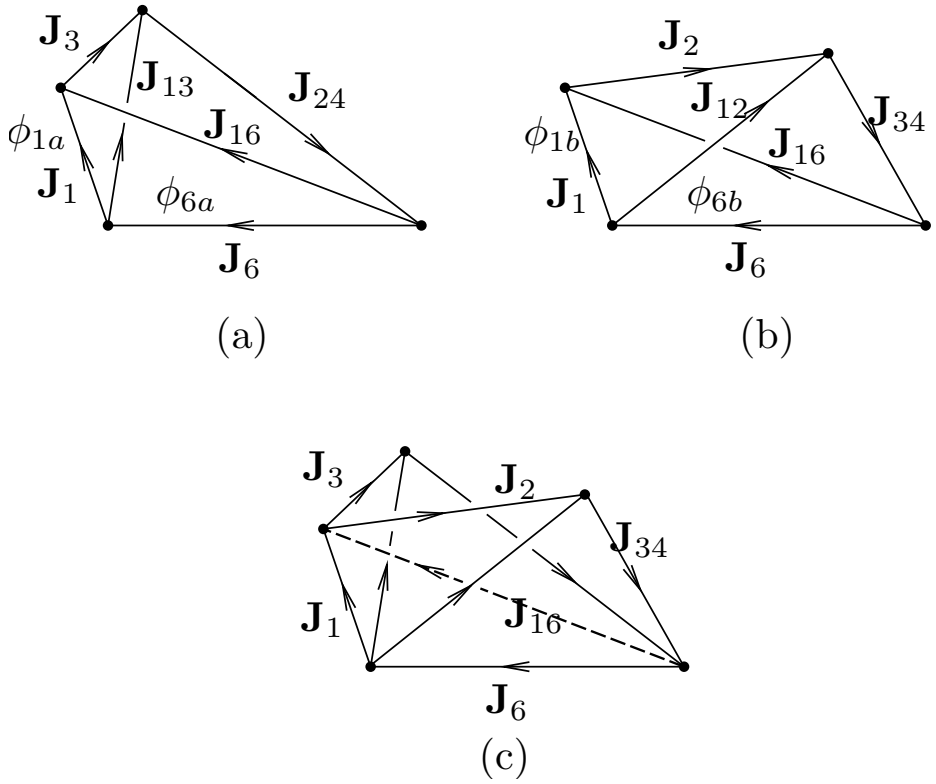

Figure 7.7: Decomposition of the angles ϕ_1 and ϕ_6 into sums of dihedral angles in two adjacent tetrahedra.

Then the rotations in (7.64) become

$$\begin{aligned} & R(\mathbf{j}_{13}, 2\phi_{13})R(-\mathbf{j}_6, 2\phi_6)R(\mathbf{j}_{12}, 2\phi_{12}) \\ = \;& [R(\mathbf{j}_{13}, 2\phi_{13})R(-\mathbf{j}_6, 2\phi_{6a})][R(-\mathbf{j}_6, 2\phi_{6b})R(\mathbf{j}_{12}, 2\phi_{12})] \\ = \;& R(\mathbf{j}_1, 2\phi_{1a})R(\mathbf{j}_1, 2\phi_{1b}) \\ = \;& R(\mathbf{j}_1, 2\phi_1)\,, \end{aligned} \tag{7.65}$$

where we have used the Hamilton-Rodrigues formula twice in the second equality. In the third equality, we used the fact that $\phi_1 = \phi_{1a} + \phi_{1b}$, where the angles ϕ_{1a} and ϕ_{1b} are internal dihedral angles for the tetrahedra in part (a) and part (b) of figure 7.7, respectively. Thus,

we find that the product of the three rotations in (7.64) is $R(\mathbf{j}_1, 2\phi_1)$, where ϕ_1 is the angle between the triangle 1-2-12 and the triangle 1-3-13. We can lift the rotation (7.65) up to $SU(2)$ with the same axis and angle. Its action on the spinor at p is a pure phase. To undo this pure phase, we follow the Hamiltonian flow of I_1 by an angle $-2\phi_1$, modulo 2π.

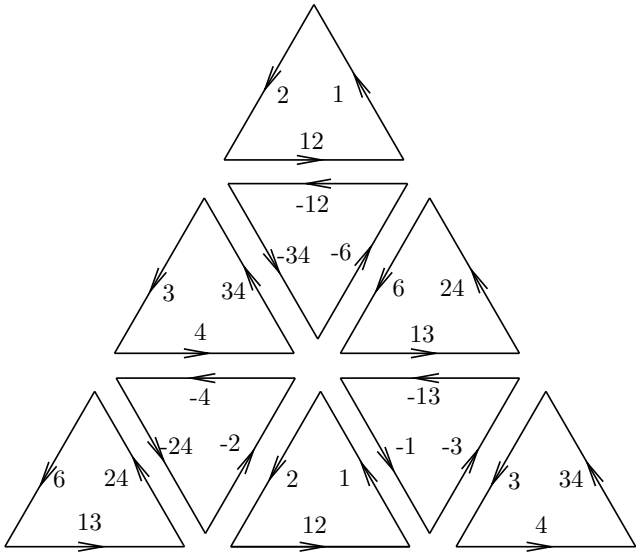

Figure 7.8: The angles ϕ_r is the angle between the normals of the adjacent triangles sharing the edge J_r, where the normals are defined by the orientation of the triangles shown.

Similarly, we can find the rotations acting on $\mathbf{J}_2, \mathbf{J}_3, \mathbf{J}_4$, and $\mathbf{J}_6$, and proceed to calculate the action integral as in section 4.8. We have not completed the calculation of the action integral, due to the asymmetric treatment of the nine j's. Fortunately, the result must be the same as the action calculated using a symmetric treatment of the $9j$-symbol, which was done in [42]. Their result is

$$S^{(1)} = 2\sum_r J_r \psi_r^{(1)}\,, \tag{7.66}$$

where $\psi_r^{(1)} = \pi - \phi_r$ is the external dihedral angle between the normals of the two triangles adjacent to J_r. The orientations of the triangles are defined in figure 7.8. the sum is over $r = 1, 2, 3, 4, 6, 12, 34, 13, 24$. The relative action integral that corresponds to the other solution (x_2, y_2) of (7.47) is

$$S^{(2)} = 2\sum_r J_r \psi_r^{(2)}\,, \tag{7.67}$$

which has the same expression as (7.66), but the angles $\psi_r^{(2)}$ are different from $\psi_r^{(1)}$, because the vector configuration has a different set of dot products. We pick $S^{(1)}$ to correspond to the root in which $-\pi \le \psi_r \le \pi$, and pick $S^{(2)}$ to correspond to the root in which $0 \le \psi_r \le \pi$.

See [42] for more details on the definitions of the action integral (7.66) and (7.67). The main result of [42] is the asymptotic formula for the $9j$-symbol when all j's are large:

$$\begin{aligned} & \left\{ \begin{array}{ccc} j_1 & j_2 & j_{12} \\ j_3 & j_4 & j_{34} \\ j_{13} & j_{24} & j_5 \end{array} \right\} \\ = & \frac{1}{4\pi\sqrt{|V^{(1)}_{123}V^{(1)}_{432} - V^{(1)}_{214}V^{(1)}_{341}|}} \cos(S^{(1)}) + \frac{1}{4\pi\sqrt{|V^{(2)}_{123}V^{(2)}_{432} - V^{(2)}_{214}V^{(2)}_{341}|}} \sin(S^{(2)}) \,. \end{aligned} \tag{7.68}$$

In [42], it was found that when the configuration goes to its time-reversed image, that is, when all the vectors reverse their directions, $S^{(1)} \to -S^{(1)}$ and $S^{(2)} \to -S^{(2)} + 2\pi(\sum_{r=1}^{9} j_r) + 9\pi$. As a result, the two terms in the $9j$ formula (7.68), $\cos(S^{(1)})$ and $\sin(S^{(2)})$, are invariant under time-reversal symmetry. In the asymptotic formula for the $12j$-symbol (7.81) that we will derive below, the additional phases generated from the spinor products break this time-reversal symmetry.

Putting these amplitudes Ω from (7.61) and the relative action integrals $S^{(1)}$ and $S^{(2)}$ into (7.42), we find

$$\begin{aligned} \langle b|a\rangle \;=\; & e^{i\kappa_1} \frac{\sqrt{J_{12}J_{34}J_{13}J_{24}}}{4\pi\sqrt{|V^{(1)}_{123}V^{(1)}_{432} - V^{(1)}_{214}V^{(1)}_{341}|}} \\ & \times \left[(\tau^b(z_{11}))^\dagger (\tau^a(z_{11})) + e^{i(S^{(1)} - \mu_1\pi/2)/\hbar} \left(U^{(1)}_b \tau^b(z_{11}) \right)^\dagger \left(U^{(1)}_a \tau^a(z_{11}) \right) \right] \\ & + e^{i\kappa_2} \frac{\sqrt{J_{12}J_{23}J_{13}J_{24}}}{4\pi\sqrt{|V^{(2)}_{123}V^{(2)}_{432} - V^{(2)}_{214}V^{(2)}_{341}|}} \\ & \times \left[(\tau^b(z_{21}))^\dagger (\tau^a(z_{21})) + e^{i(S^{(2)} - \mu_2\pi/2)/\hbar} \left(U^{(2)}_b \tau^b(z_{21}) \right)^\dagger \left(U^{(2)}_a \tau^a(z_{21}) \right) \right] , \end{aligned} \tag{7.69}$$

where the superscripts (1) and (2) distinguish the first and the second solutions to (7.47). Here we have factored out two arbitrary phases $e^{i\kappa_1}$ and $e^{i\kappa_2}$ for the two pairs of stationary phase contributions. The rotation matrices $U^{(i)}_a$, $i = 1, 2$ are determined by the paths from z_{i1} to z_{i2} along $\mathcal{L}^{9j}_a$. Similarly the rotation matrices $U^{(i)}_b$, $i = 1, 2$, are determined by the paths from z_{i1} to z_{i2} along $\mathcal{L}^{9j}_b$.

7.7 The Spinor Products

We choose the vector configurations associated with z_{11} to correspond to a particular orientation of the vectors. We put $\mathbf{J}_{12}$ along the z-axis, and put $\mathbf{J}_6$ inside the xz-plane, as illustrated in figure 7.9. Let the inclination and azimuth angles (θ, ϕ) denote the direction of the vector $\mathbf{J}_{13}$. From figure 7.9, we see that ϕ is the angle between the $(\mathbf{J}_{12}, \mathbf{J}_6)$ plane and the $(\mathbf{J}_{12}, \mathbf{J}_{13})$ plane. We denote this angle by $\phi = \phi_{12}$. The inclination angle θ is the angle between the vectors $\mathbf{J}_{12}$ and $\mathbf{J}_{13}$.

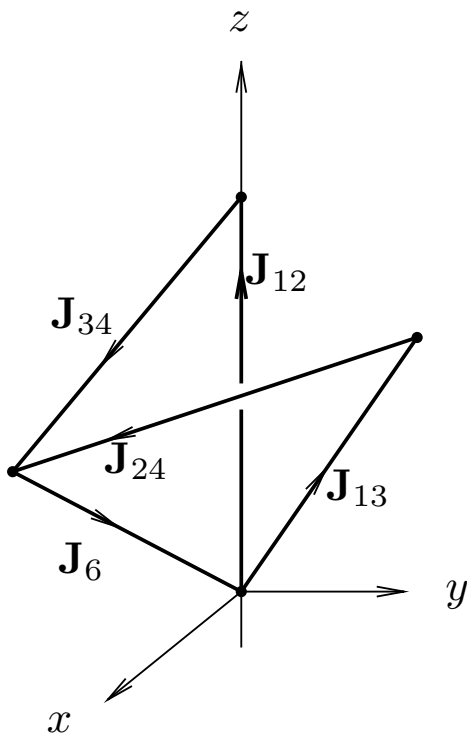

Figure 7.9: The vector configuration at the point z_{11} in I_{11}.

The gauge choices for the spinors at the reference point z_{11} are arbitrary, and they only contribute a phase that can be absorbed into $e^{i\kappa_1}$. To be concrete, since $\mathbf{J}_{12}$ points in the z direction, we choose the spinor $\tau^a(z_{11})$ to be the μ^{th} standard eigenvector for S_z, that is,

$$\tau^a_\alpha(z_{11}) = \delta_{\alpha\mu}\,. \tag{7.70}$$

For the spinor $\tau^b(z_{11})$, we choose it to be an eigenvector of $\mathbf{J}_{13}\cdot\mathbf{S}$ in the north standard gauge, that is,

$$\tau^b_\alpha(z_{11}) = e^{i(\alpha-\nu)\phi_{12}}\, d^s_{\nu\alpha}(\theta)\,. \tag{7.71}$$

Taking the spinor inner product, we obtain

$$(\tau^b(z_{11}))^\dagger(\tau^a(z_{11})) = e^{-i(\mu-\nu)\phi_{12}}\, d^s_{\nu\mu}(\theta)\,. \tag{7.72}$$

To evaluate the other spinor product at z_{12}, we need to find the rotation matrices $U^{(1)}_a$ and $U^{(1)}_b$, which are generated from paths γ_a and γ_b from z_{11} to z_{12} along $\mathcal{L}^{9j}_a$ and $\mathcal{L}^{9j}_b$, respectively.

We choose the path γ_a to be the path from p to q generated by the $\mathbf{J}^2_{12}$-flow and the $\mathbf{J}_{34}$-flow, which are illustrated in figure 7.5 in the large phase space, in part (a) of figure 7.6 in the angular momentum space. This path contains no flow generated by the total angular momentum, so

$$U^{(1)}_a = 1\,. \tag{7.73}$$

we choose the path γ_b to be the inverse of the path from q back to p along $\mathcal{L}^{9j}_b$ in figure 7.5, which contains only one overall rotation around $-\mathbf{j}_6$. Thus

$$U^{(1)}_b = U(\hat{\mathbf{j}}_6, 2\phi_6)\,. \tag{7.74}$$

The rotation associated with $U^{(1)}_b$ is illustrated in part (b) of figure 7.6. It effectively moves $\mathbf{J}_{12}$ to its mirror image $\mathbf{J}'_{13}$ across the 12-34-6 triangle in the xz-plane, which has the direction given by $(\theta, -\phi_{12})$. Thus $U_b\,\tau^b(z_{11})$ is an eigenvector of $\mathbf{J}'_{13}\cdot\mathbf{S}$, and is up to a phase equal to the eigenvector of $\mathbf{J}'_{13}\cdot\mathbf{S}$ in the north standard gauge. Thus, we have

$$[U^{(1)}_b\,\tau^b(z_{11})]_\alpha = e^{i\nu H_{13}}\, e^{-i(\alpha-\nu)\phi_{12}}\, d^s_{\nu\alpha}(\theta)\,, \tag{7.75}$$

where H_{13} is a holonomy phase factor equal to the area of a spherical triangle on a unit sphere. See figure 7.10. Therefore, the spinor product at the intersection I_{12} is

$$(U^{(1)}_b\,\tau^b(z_{11}))^\dagger(U_a\tau^a(z_{11})) = e^{i\nu H_{13}}\, e^{i(\mu-\nu)\phi_{12}}\, d^s_{\nu\mu}(\theta)\,. \tag{7.76}$$

Let us denote the first term in (7.69) by T_1. Substituting the spinor inner products (7.72) and (7.76) into (7.69), we find that T_1 is given by

$$T_1 = \frac{e^{i\kappa_1}\sqrt{J_{12}J_{34}J_{13}J_{24}}}{4\pi\sqrt{|V_{123}V_{432}-V_{214}V_{341}|}}\, d^s_{\nu\mu}(\theta)\cos\left[S^{(1)} - \frac{\mu_1\pi}{4} + \mu\phi_{12} + \nu\left(\frac{H_{13}}{2} - \phi_{12}\right)\right]\,. \tag{7.77}$$

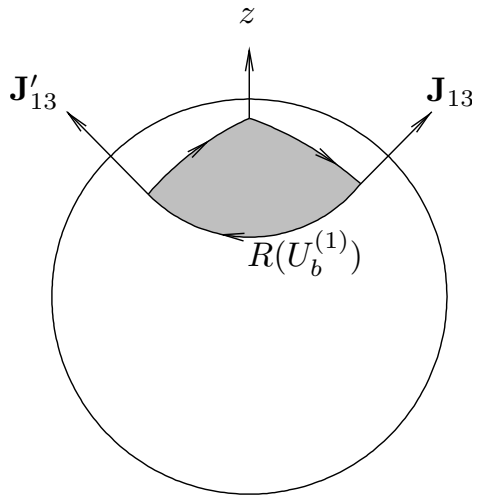

Figure 7.10: The holonomy H_4 can be expressed as an area inside a closed loop on the unit sphere.

Using a different choice of the reference point and paths, we can derive an alternative expression for the inner product, and eliminate the term H_4. Let us choose a new reference point z_{11} to correspond to an orientation in which $\mathbf{J}_{13}$ is along the z-axis, and $\mathbf{J}_6$ lies in the x-z plane. We choose the path γ_a to go from p to q' along the first two paths in figure 7.5, and we choose γ^b to be the inverse of the last two paths that goes from q' back to p in figure 7.5. Through essentially the same arguments, we find

$$T_1 = \frac{e^{i\kappa_1}\sqrt{J_{12}J_{34}J_{13}J_{24}}}{4\pi\sqrt{|V_{123}V_{432} - V_{214}V_{341}|}}\, d^s_{\nu\mu}(\theta)\, \cos\left[S^{(1)} - \frac{\mu_1\pi}{4} + \mu\left(\frac{H_{12}}{2} - \phi_{13}\right) + \nu\phi_{13})\right]. \tag{7.78}$$

Here H_{12} is another holonomy for the $\mathbf{J}_{12}$ vector, and the angle ϕ_{13} is the angle between the 1-3-13 triangle and the 13-24-6 triangle. Because the quantities $\psi_i, \phi_{12}, \phi_{13}, H_{12}, H_{13}$ depend only on the geometry of the vector configuration, and are independent of μ and ν, we conclude that the argument in the cosine must be linear in μ and ν. Equating the two arguments of the cosine in (7.77) and in (7.78), we find that this linear term is $(\mu\phi_{12}+\nu\phi_{13})$. Using the Maslov index $\mu_1 = 0$ from [42], we find

$$T_1 = \frac{e^{i\kappa_1}\sqrt{J_{12}J_{34}J_{13}J_{24}}}{4\pi\sqrt{|V^{(1)}_{123}V^{(1)}_{432} - V^{(1)}_{214}V^{(1)}_{341}|}}\, d^s_{\nu\mu}(\theta^{(1)})\, \cos\left(S^{(1)} + \mu\phi^{(1)}_{12} + \nu\phi^{(2)}_{13}\right), \tag{7.79}$$

where we have put back the superscript (1). Through an analogous calculation, we find

$$T_2 = \frac{e^{i\kappa_2}\sqrt{J_{12}J_{34}J_{13}J_{24}}}{4\pi\sqrt{|V^{(2)}_{123}V^{(2)}_{432} - V^{(2)}_{214}V^{(2)}_{341}|}}\, d^s_{\nu\mu}(\theta^{(2)})\, \sin\left(S^{(2)} + \mu\phi^{(2)}_{12} + \nu\phi^{(2)}_{13}\right). \tag{7.80}$$

7.8 An Asymptotic Formula for the $12j$-Symbol

From the definition (7.2), we see that the factor $([j_{12}][j_{34}][j_{13}][j_{24}])^{1/2}$ in the denominator of (7.2) cancels out the factor $(J_{12}J_{34}J_{13}J_{24})^{1/2}$ from T_1 and T_2 in (7.79) and (7.80). Because the $12j$-symbol is a real number, the relative phase between $e^{i\kappa_1}$ and $e^{i\kappa_2}$ must be ± 1. Through numerical experimentation, we found it to be $+1$. To determine the overall phase convention, we use the limiting case when $j_5 = s = 0$ from (A.7) in Appendix A, in which case the $12j$-symbol reduces to a $9j$-symbol. This determines most of the overall phase. The rest is determined through numerical experimentation. Putting the pieces together, we obtain an asymptotic formula for the $12j$-symbol with one small quantum number:

$$\begin{Bmatrix} j_1 & j_2 & j_{12} & j_{125} \\ j_3 & j_4 & j_{34} & j_{135} \\ j_{13} & j_{24} & s & j_6 \end{Bmatrix} = \frac{(-1)^{\mu}}{4\pi\sqrt{(2j_{125}+1)(2j_{135}+1)}} \left[\frac{d^s_{\nu\,\mu}(\theta^{(1)})}{\sqrt{|V^{(1)}_{123}V^{(1)}_{432} - V^{(1)}_{214}V^{(1)}_{341}|}} \cos(S^{(1)} + \mu\phi^{(1)}_{12} + \nu\phi^{(1)}_{13}) + \frac{d^s_{\nu\,\mu}(\theta^{(2)})}{\sqrt{|V^{(2)}_{123}V^{(2)}_{432} - V^{(2)}_{214}V^{(2)}_{341}|}} \sin(S^{(2)} + \mu\phi^{(2)}_{12} + \nu\phi^{(2)}_{13}) \right], \tag{7.81}$$

where $S^{(1)}$ and $S^{(2)}$ are evaluated at the configurations in which $V = \mathbf{J}_6 \cdot (\mathbf{J}_{12} \times \mathbf{J}_{13}) < 0$.

Here, the indices on the d-matrix are given by $\mu = j_{125} - j_{12}$ and $\nu = j_{135} - j_{13}$. They are of the same order as the small parameter s. The phases $S^{(1)}$ and $S^{(2)}$ are defined in (7.66), and the V's are defined by

$$V_{ijk} = \mathbf{J}_i \cdot (\mathbf{J}_j \times \mathbf{J}_k)\,. \tag{7.82}$$

The angle ϕ_{12} and ϕ_{13} are internal dihedral angles at the edge J_{12} and J_{13}, respectively, of a tetrahedron formed by the six vectors $\mathbf{J}_{12}, \mathbf{J}_{13}, \mathbf{J}_{24}, \mathbf{J}_{34}, \mathbf{J}_6$, and $\mathbf{J}_{2'3}$, where $\mathbf{J}_{2'3} = \mathbf{J}_3 - \mathbf{J}_2$. This tetrahedron is illustrated in figure 7.11. The angle θ is the angle between the vectors $\mathbf{J}_{12}$ and $\mathbf{J}_{13}$. The explicit expression for the angles ϕ_{12}, ϕ_{13}, and θ are given by the following equations

$$\phi_{12} = \pi - \cos^{-1}\left(\frac{(\mathbf{J}_{12} \times \mathbf{J}_{13}) \cdot (\mathbf{J}_{12} \times \mathbf{J}_6)}{|\mathbf{J}_{12} \times \mathbf{J}_{13}|\,|\mathbf{J}_{12} \times \mathbf{J}_6|} \right), \tag{7.83}$$

$$\phi_{13} = \pi - \cos^{-1}\left(\frac{(\mathbf{J}_{13} \times \mathbf{J}_{12}) \cdot (\mathbf{J}_{13} \times \mathbf{J}_6)}{|\mathbf{J}_{13} \times \mathbf{J}_{12}|\,|\mathbf{J}_{13} \times \mathbf{J}_6|} \right), \tag{7.84}$$

$$\theta = \cos^{-1}\left(\frac{\mathbf{J}_{12} \cdot \mathbf{J}_{13}}{J_{12}J_{13}} \right). \tag{7.85}$$

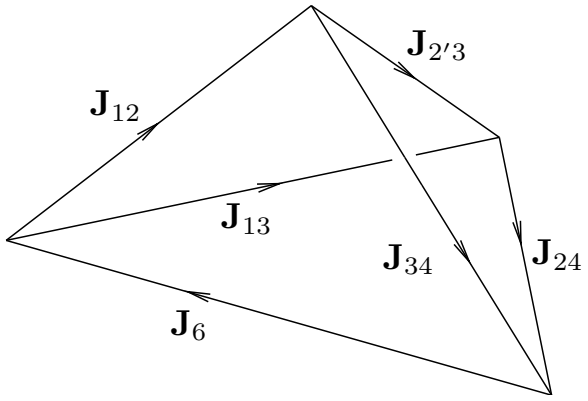

Figure 7.11: The angles ϕ_{12} and ϕ_{13} are internal dihedral angles in the tetrahedron with the six edges $\mathbf{J}_6, \mathbf{J}_{12}, \mathbf{J}_{34}, \mathbf{J}_{13}, \mathbf{J}_{24}$, and $\mathbf{J}_{2'3}$, where $\mathbf{J}_{2'3} = \mathbf{J}_3 - \mathbf{J}_2$. The angle θ is the angle between $\mathbf{J}_{12}$ and $\mathbf{J}_{13}$.

7.9 Plots

We illustrate the accuracy of the approximation (7.81) by plotting it against the exact $12j$-symbol in the classically allowed region for the following values of the j's:

$$\left\{ \begin{array}{cccc} j_1 & j_2 & j_{12} & j_{125} \\ j_3 & j_4 & j_{34} & j_{135} \\ j_{13} & j_{24} & s_5 & j_6 \end{array} \right\} = \left\{ \begin{array}{cccc} 51/2 & 59/2 & 21 & 22 \\ 55/2 & 53/2 & 27 & 26 \\ 27 & 25 & 1 & j_6 \end{array} \right\} . \tag{7.86}$$

The result is shown in figure 7.12. From the error plot in part (a) of figure 7.14, we see that the agreement is excellent.

Since the asymptotic formula (7.81) should become more accurate as the values of the j's get larger, we plot the formula against the exact $12j$-symbol for another example,

$$\left\{ \begin{array}{cccc} j_1 & j_2 & j_{12} & j_{125} \\ j_3 & j_4 & j_{34} & j_{135} \\ j_{13} & j_{24} & s_5 & j_6 \end{array} \right\} = \left\{ \begin{array}{cccc} 211/2 & 219/2 & 91 & 92 \\ 205/2 & 223/2 & 107 & 108 \\ 99 & 93 & 2 & j_6 \end{array} \right\} , \tag{7.87}$$

in the classically allowed region away from the caustic in figure 7.13. These values of the j's are roughly 4 times those in (7.86). The errors for this case is displayed in part (b) of figure 7.14. By comparing part (a) and part (b) of figure 7.14, we can conclude that the error scales with the j's.

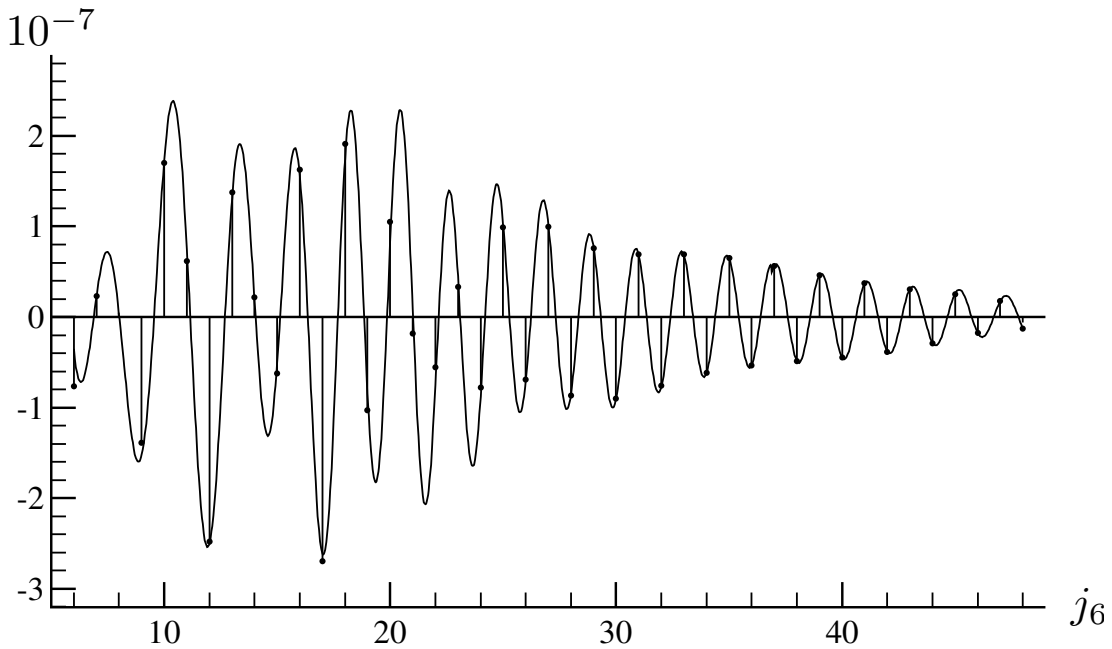

Figure 7.12: Comparison of the exact $12j$-symbol (vertical sticks and dots) and the asymptotic formula (7.81) in the classically allowed region away from the caustics, for the values of j's shown in (7.86).

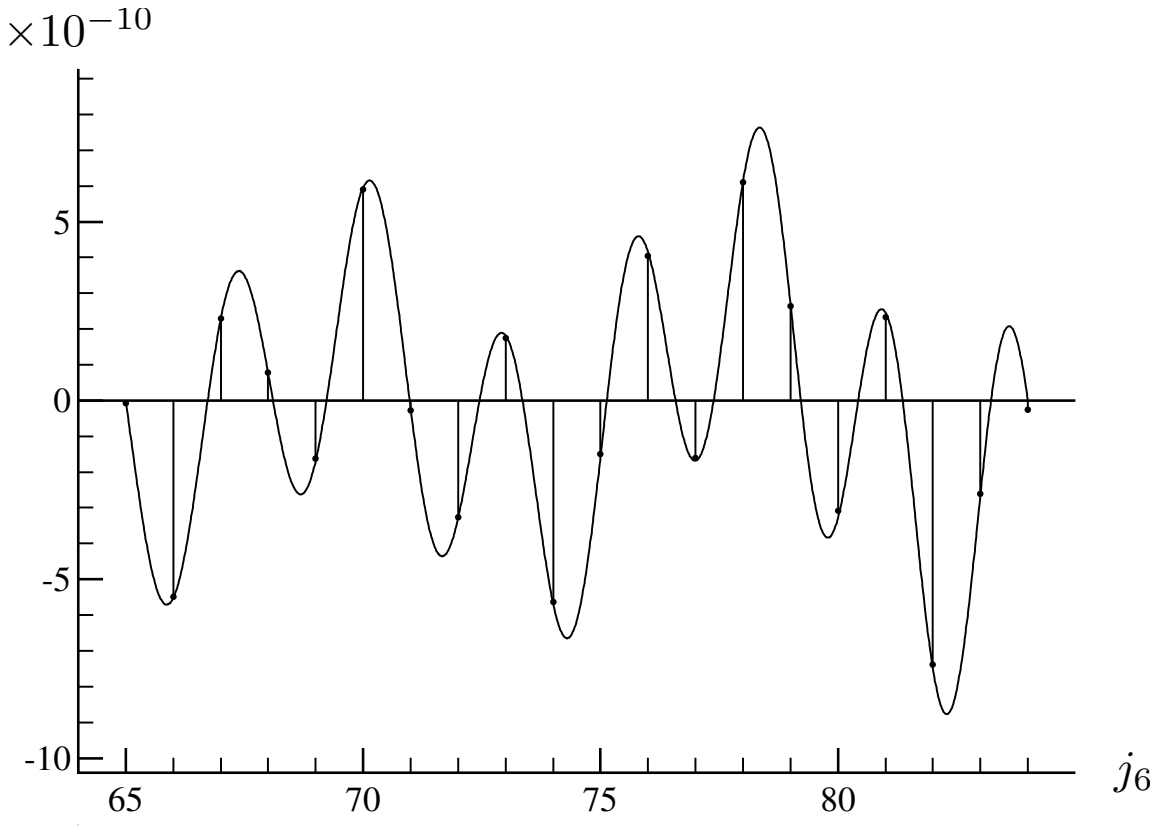

Figure 7.13: Comparison of the exact $12j$-symbol (vertical sticks and dots) and the asymptotic formula (7.81) in the classically allowed region away from the caustics, for the values of j's shown in (7.87).

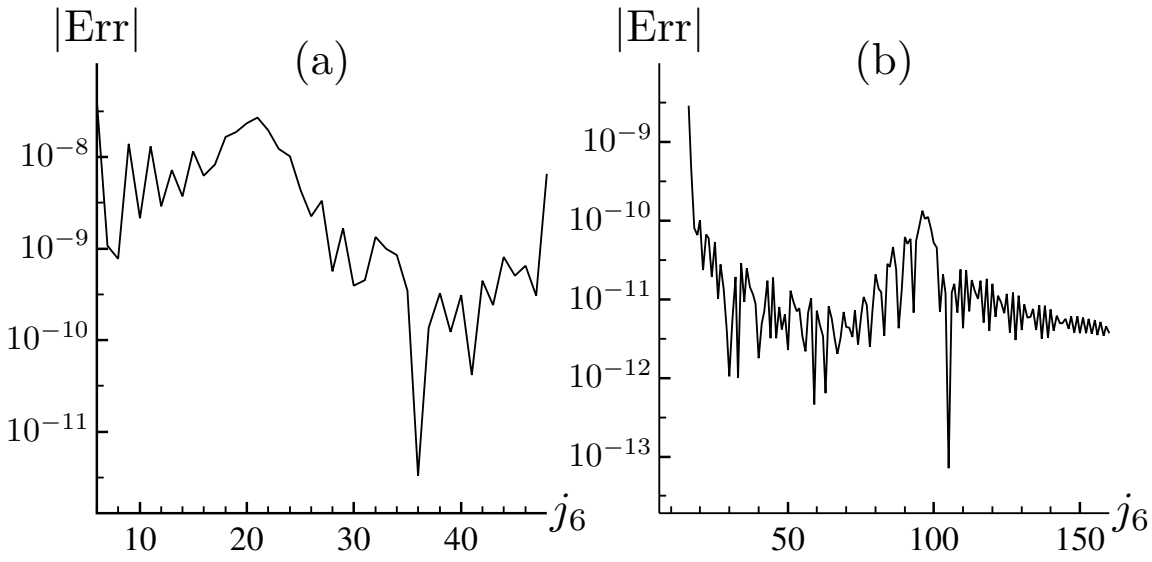

Figure 7.14: Absolute value of the error of the asymptotic formula (7.81) for (a) the case shown in (7.86), and (b) the case shown in (7.87). The error is defined as the difference between the approximate value and the exact value.

7.10 Two Small Angular Momenta

We now treat the case where two angular momenta are small. We take $j_1 = s_1$ and $j_5 = s_5$ to be small. The $12j$-symbol can again be written as a scalar product of two multicomponent wavefunctions, as follows:

$$\left\{ \begin{array}{cccc} s_1 & j_2 & j_{12} & j_{125} \\ j_3 & j_4 & j_{34} & j_{135} \\ j_{13} & j_{24} & s_5 & j_6 \end{array} \right\} = \frac{\langle b|a\rangle}{\{[j_{12}][j_{34}][j_{13}][j_{24}][j_{125}][j_{135}]\}^{\frac{1}{2}}}\,, \tag{7.88}$$

where

$$|a\rangle = \left| \begin{array}{cccccccccc} \mathbf{S}_1^2 & \hat{I}_2 & \hat{I}_3 & \hat{I}_4 & \mathbf{S}_5^2 & \hat{I}_6 & \hat{\mathbf{J}}_{12}^2 & \hat{\mathbf{J}}_{34}^2 & \hat{\mathbf{J}}_{125}^2 & \hat{\mathbf{J}}_{\rm tot} \\ s_1 & j_2 & j_3 & j_4 & s_5 & j_6 & j_{12} & j_{34} & j_{125} & \mathbf{0} \end{array} \right\rangle\,, \tag{7.89}$$

$$|b\rangle = \left| \begin{array}{cccccccccc} \mathbf{S}_1^2 & \hat{I}_2 & \hat{I}_3 & \hat{I}_4 & \mathbf{S}_5^2 & \hat{I}_6 & \hat{\mathbf{J}}_{13}^2 & \hat{\mathbf{J}}_{24}^2 & \hat{\mathbf{J}}_{135}^2 & \hat{\mathbf{J}}_{\rm tot} \\ s_1 & j_2 & j_3 & j_4 & s_5 & j_6 & j_{13} & j_{24} & j_{135} & \mathbf{0} \end{array} \right\rangle\,. \tag{7.90}$$

Using the formalism developed in chapter 6, we can now find a new asymptotic formula for the $12j$-symbol up to an overall phase. By expressing the $12j$-symbol in terms of the $9j$-symbol in the special cases $s_1 = 0$ or $s_5 = 0$ from (A.7) in Appendix A, and by using (6.1), we can determine the overall phase. The result is an asymptotic formula for the $12j$-symbol when two of the angular momenta are small:

$$\left\{ \begin{array}{cccc} s_1 & j_2 & j_{12} & j_{125} \\ j_3 & j_4 & j_{34} & j_{135} \\ j_{13} & j_{24} & s_5 & j_6 \end{array} \right\} \tag{7.91}$$

$$= (-1)^{j_{24}+j_{34}+j_{125}+j_{135}+j_1+j_5+\nu_1+\nu_5} \frac{d^{s_1}_{\nu_1\,\mu_1}(\theta)\; d^{s_5}_{\nu_5\,\mu_5}(\theta)}{\sqrt{[j_{12}][j_{125}][j_{13}][j_{135}](12\pi V)}}$$

$$\cos\left(\sum_i (j_i + \frac{1}{2})\,\psi_i + \frac{\pi}{4} - (s_1+s_5)\pi + (\mu_1+\mu_5)\phi_2 + (\nu_1+\nu_5)\phi_3\right).$$

Here $\mu_1 = j_{12} - j_2$, $\nu_1 = j_{13} - j_3$, $\mu_5 = j_{125} - j_{12}$, and $\nu_5 = j_{135} - j_{13}$. The sum in the argument of the cosine runs over the six large angular momenta $i = 2, 3, 5, 6, 24, 34$. The geometric quantities V, ψ_i, ϕ_2, ϕ_3, and θ are related to the tetrahedron in Figure 7.15, which has the six edge lengths $J_i = j_i + 1/2$, $i = 2, 3, 5, 6, 24, 34$. As before, V is the volume, and each ψ_i is the external dihedral angle at the edge J_i. The angle ϕ_2 is the angle between the plane spanned by $(\mathbf{J}_2, \mathbf{J}_3)$ and the plane spanned by $(\mathbf{J}_2, \mathbf{J}_6)$. The angle ϕ_3 is the angle between the plane defined by $(\mathbf{J}_2, \mathbf{J}_3)$ and the plane defined by $(\mathbf{J}_3, \mathbf{J}_6)$. The angle θ is the angle between $\mathbf{J}_2$ and $\mathbf{J}_3$. The explicit expression for the angles ϕ_2, ϕ_3, and θ are given by the following equations:

$$\phi_2 = \pi - \cos^{-1}\left(\frac{(\mathbf{J}_2 \times \mathbf{J}_3)\cdot(\mathbf{J}_2 \times \mathbf{J}_6)}{|\mathbf{J}_2 \times \mathbf{J}_3|\,|\mathbf{J}_2 \times \mathbf{J}_6|}\right), \tag{7.92}$$

$$\phi_3 = \pi - \cos^{-1}\left(\frac{(\mathbf{J}_3 \times \mathbf{J}_2)\cdot(\mathbf{J}_3 \times \mathbf{J}_6)}{|\mathbf{J}_3 \times \mathbf{J}_2|\,|\mathbf{J}_3 \times \mathbf{J}_6|}\right), \tag{7.93}$$

$$\theta = \cos^{-1}\left(\frac{\mathbf{J}_2 \cdot \mathbf{J}_3}{J_2 J_3}\right). \tag{7.94}$$

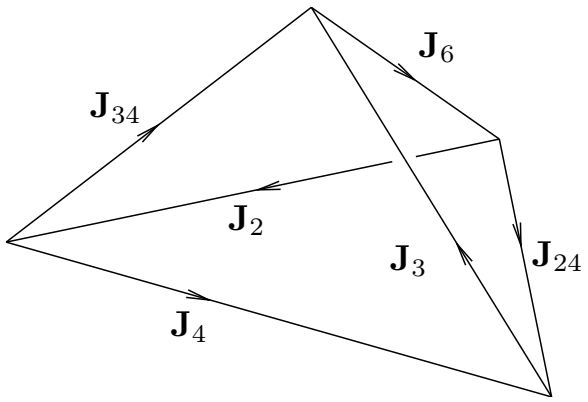

Figure 7.15: The volume V and the external dihedral angles ψ_i are defined on the tetrahedron with the six edge lengths $J_3, J_5, J_2, J_6, J_{24}, J_{34}$.

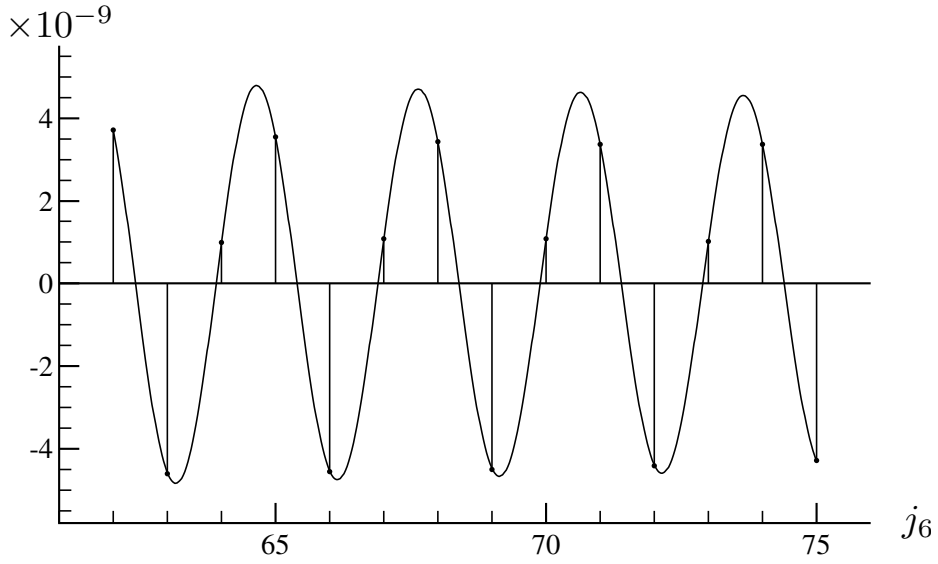

Figure 7.16: Comparison of the exact $12j$-symbol (vertical sticks and dots) and the asymptotic formula (7.91), in the classically allowed region away from the caustics. The values used are those in (7.95).

We illustrate the accuracy of the approximation (7.91) by plotting it against the exact $12j$-symbol in figure 7.16 for the following values of the j's:

$$\left\{ \begin{array}{cccc} s_1 & j_2 & j_{12} & j_{125} \\ j_3 & j_4 & j_{34} & j_{135} \\ j_{13} & j_{24} & s_5 & j_6 \end{array} \right\} = \left\{ \begin{array}{cccc} 1/2 & 201/2 & 100 & 101 \\ 213/2 & 199/2 & 117 & 105 \\ 106 & 98 & 1 & j_6 \end{array} \right\} . \tag{7.95}$$

We see that the agreement is excellent.

7.11 Three Small Angular Momenta

The last case we can cover with our method is the $12j$-symbol with three small angular momenta. This case is most similar to the $9j$-symbol with two small angular momenta, which is analyzed in section 6.7. The Lagrangian manifolds of the two states are both identical to the Wigner manifold represented by a triangle with the three sides J_2, J_3, J_6. This triangle is illustrated in figure 7.17. The Hamilton-Jacobi equations for the two Lagrangian manifolds are exactly the same, given by

$$\begin{aligned} J_2 &= (j_2 + 1/2)\hbar\,, \\ J_3 &= (j_3 + 1/2)\hbar\,, \\ J_6 &= (j_6 + 1/2)\hbar\,, \\ \vec{0} &= \vec{J}_2 + \vec{J}_3 + \vec{J}_6\,. \end{aligned} \tag{7.96}$$

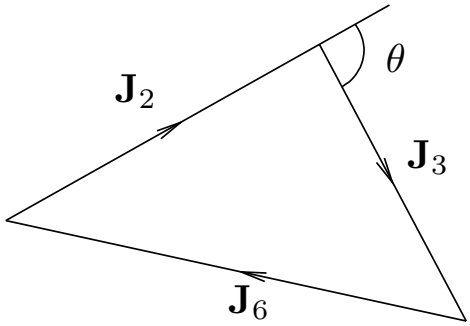

Figure 7.17: The angle θ is the exterior angle between the edges J_2 and J_3 in a triangle having the three edge lengths J_2, J_3, J_6.

Because the two Lagrangian manifolds are identical, the inner product of the two scalar part of the WKB wave-functions is unity. After putting in the correct overall phase, we find

$$\left\{ \begin{array}{cccc} s_1 & j_2 & j_{12} & j_{125} \\ j_3 & s_4 & j_{34} & j_{135} \\ j_{13} & j_{24} & s_5 & j_6 \end{array} \right\} = \frac{(-1)^{j_2+j_3+j_6+\mu_1+\mu_4+\mu_5}}{\sqrt{[j_{12}][j_{34}][j_{13}][j_{24}][j_{125}][j_{135}]}}\, d^{(s_1)}_{\nu_1\,\mu_1}(\theta)\, d^{(s_4)}_{\nu_4\,\mu_4}(\theta)\, d^{(s_5)}_{\nu_5\,\mu_5}(\theta)\,, \tag{7.97}$$

where $\mu_1 = j_{12} - j_2$, $\nu_1 = j_{13} - j_3$, $\mu_4 = j_{24} - j_2$, $\nu_4 = j_{34} - j_3$, $\mu_5 = j_{125} - j_{12}$, $\nu_5 = j_{135} - j_{13}$. The angle θ is the angle between the vectors $\mathbf{J}_2$ and $\mathbf{J}_3$. It is given by

$$\theta = \cos^{-1}\left(\frac{\mathbf{J}_2 \cdot \mathbf{J}_3}{J_2\, J_3}\right) = \pi - \cos^{-1}\left(\frac{J_2^2 + J_3^2 - J_6^2}{2\, J_2\, J_3}\right)\,. \tag{7.98}$$

We illustrate the accuracy of the approximation (7.81) by plotting it against the exact $12j$-symbol in figure 7.18, for the following values of the j's:

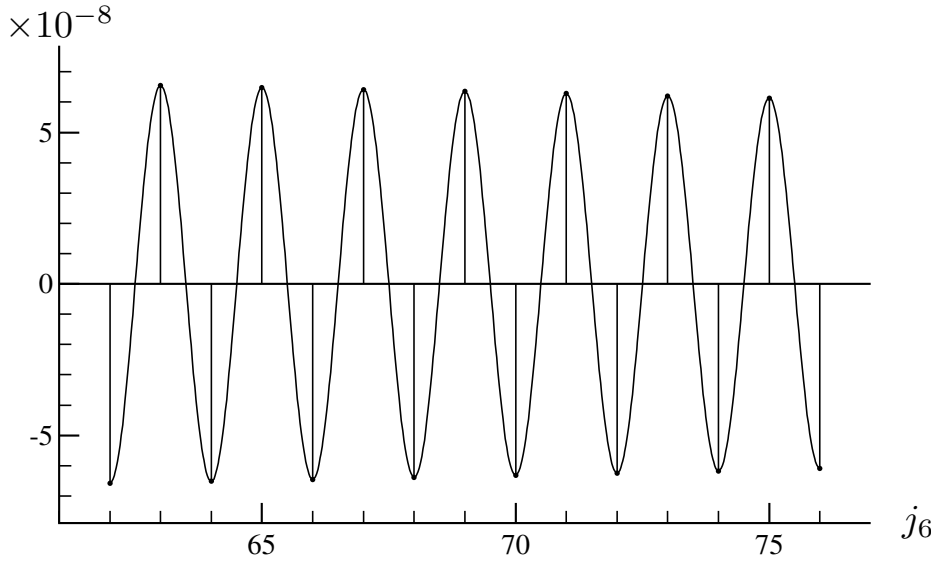

Figure 7.18: Comparison of the exact $12j$-symbol (vertical sticks and dots) and the asymptotic formula (7.97), for the values of j's shown in (7.99).

$$\left\{ \begin{array}{cccc} s_1 & j_2 & j_{12} & j_{125} \\ j_3 & s_4 & j_{34} & j_{135} \\ j_{13} & j_{24} & s_5 & j_6 \end{array} \right\} = \left\{ \begin{array}{cccc} 1/2 & 237/2 & 119 & 120 \\ 233/2 & 1/2 & 117 & 115 \\ 116 & 118 & 1 & j_6 \end{array} \right\} . \tag{7.99}$$

We see that the agreement is excellent.

7.12 Conclusions

The analysis of the $12j$-symbol in this chapter is a natural extension of the analysis of the $9j$-symbol in chapter 6. Based on the calculations in these two chapters, we can observe the general rules of finding asymptotic formulas for the $3nj$-symbols with small and large quantum numbers. First, we ignore the small quantum numbers and any of the large quantum numbers that involve the indices of the small ones. For example, if $j_3 = s_3$ is small, then we ignore both j_3, j_{23}, etc. The remaining relevant large quantum numbers determine the Lagrangian manifolds. For example, in the case of the $9j$-symbol with one small quantum number, these are $j_1, j_2, j_4, j_5, j_{12}$, and j_{24}. These determine a model for the $6j$-symbol with four angular momenta adding to zero, and specify the two intermediate angular momenta. Once we fix the Lagrangian manifolds, the scalar WKB parts of the wave-functions can be derived from a semiclassical analysis of these Lagrangian manifolds, following the procedure in chapter 3, chapter 4, and parts of this chapter. The spinor parts of the wave-functions at the intersection points of the Lagrangian manifolds are determined by the path used to calculate the action integral. Finally, taking the inner product of both

the scalar part and the spinor part of the wave-functions, we can derive asymptotic formulas for the $3nj$-symbols.

Since the semiclassical analysis for the $6j$- and $9j$-symbols are known, using our general rules, we can apply our techniques to find new asymptotic formulas for the $15j$-symbol with 2, 3, and 4 small angular momenta. We will display these results in the next chapter.

One aspect of the calculation that warrants a closer look is the breaking of the time-reversal symmetry of the $9j$-symbol formula for the large quantum numbers of the $12j$-symbol. This may give us insight into the phase space structure of the $12j$-symbol in the limit when all quantum numbers are large.

Chapter 8

The Wigner $15j$-Symbol with Small and Large Quantum Numbers

8.1 Introduction and Summary

The graphical representation of the $15j$-symbol in the quantum gravity literature has the form of a pentagon diagram, displayed in figure 8.1, where the vertices i_r, $r = 1, \ldots, 5$, represent $SO(4)$ intertwiners.

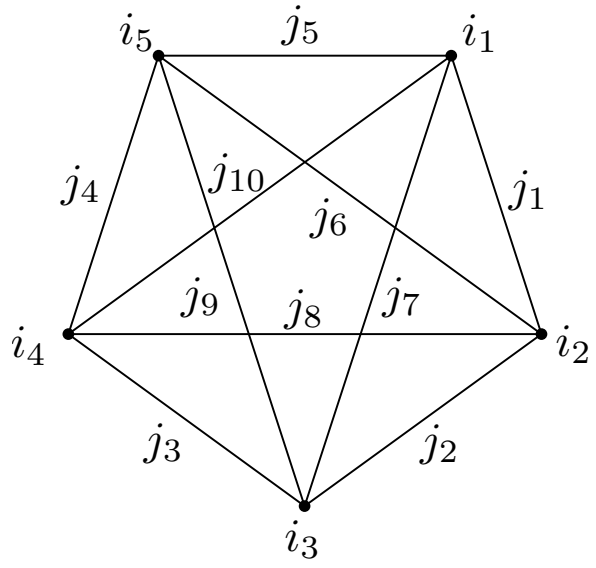

Figure 8.1: The pentagon diagram representing the 4-simplex amplitude in the spin foam models in four dimensions.

By picking a suitable basis for the intertwiners i_r, $r = 1, \ldots, 5$, in figure 8.1, we can expand the pentagon diagram in figure 8.1 into a $SU(2)$ spin network with 15 edges, which is illustrated in part (a) of figure 8.2. This spin network can be rearranged into the

form of a Möbius strip, shown in part (b) of the same figure, so it is the spin network for the Wigner $15j$-symbol of the first type. See Figure 20.2b and Figure 20.2c in the book by Yutsis [96].

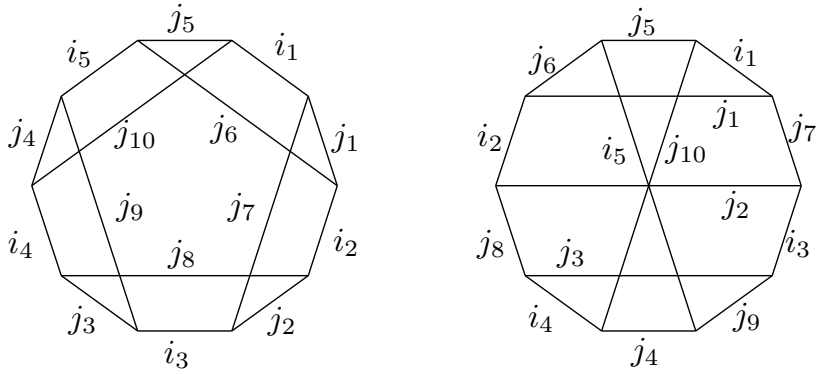

Figure 8.2: Expanding the four-valent intertwiners in the pentagon diagram to get (a) an $SU(2)$ spin network, which is equivalent to (b) a spin network in the shape of a Möbius strip.

Therefore, we can follow the procedure from chapter 6 and chapter 7 to derive asymptotic formulas for the $15j$-symbol with small and large angular momenta. Since the derivations are very similar to the those in the previous two chapters, we will omit most of the details.

The outline of this chapter is as follows: In section 8.2, we display an asymptotic formula for a case of the $15j$-symbol with two small angular momenta. In section 8.3, we treat a case with three small angular momenta. In section 8.4, we treat the case with four small angular momenta. The last section contains comments and discussions.

8.2 Two Small Angular Momenta

We take $j_5 = s_5$ and $j_6 = s_6$ to be small. Using the definition on page 66 in [96] for the $15j$-symbol of the first kind, we have

$$\begin{aligned} &\left\{ \begin{array}{ccccc} j_1 & j_2 & j_{12} & j_{125} & j_{1256} \\ j_3 & j_4 & j_{34} & j_{135} & j_{1356} \\ j_{13} & j_{24} & s_5 & s_6 & j_7 \end{array} \right\} \\ = \; &\frac{\langle b|a\rangle}{\{[j_{12}][j_{34}][j_{13}][j_{24}][j_{125}][j_{135}][j_{1256}][j_{1356}]\}^{\frac{1}{2}}}, \end{aligned} \tag{8.1}$$

where the notation $[\cdot]$ denotes $[k] = 2k + 1$, and

$$|a\rangle = \left| \begin{matrix} \hat{I}_1 \, \hat{I}_2 \, I_3 \, \hat{I}_4 \, \mathbf{S}_5^2 \, \mathbf{S}_6^2 \, \hat{I}_7 \, \hat{\mathbf{J}}_{12}^2 \, \hat{\mathbf{J}}_{34}^2 \, \hat{\mathbf{J}}_{125}^2 \, \hat{\mathbf{J}}_{1256}^2 \, \hat{\mathbf{J}}_{\rm tot} \\ j_1 \, j_2 \, j_3 \, j_4 \, \, s_5 \, \, s_6 \, j_7 \, \, j_{12} \, \, j_{34} \, \, j_{125} \, \, j_{1256} \, \, \mathbf{0} \end{matrix} \right\rangle , \tag{8.2}$$

$$|b\rangle = \left| \begin{matrix} \hat{I}_1 \, \hat{I}_2 \, I_3 \, \hat{I}_4 \, \mathbf{S}_5^2 \, \mathbf{S}_6^2 \, \hat{I}_7 \, \hat{\mathbf{J}}_{13}^2 \, \hat{\mathbf{J}}_{24}^2 \, \hat{\mathbf{J}}_{135}^2 \, \hat{\mathbf{J}}_{1356}^2 \, \hat{\mathbf{J}}_{\rm tot} \\ j_1 \, j_2 \, j_3 \, j_4 \, \, s_5 \, \, s_6 \, j_7 \, \, j_{13} \, \, j_{24} \, \, j_{135} \, \, j_{1356} \, \, \mathbf{0} \end{matrix} \right\rangle . \tag{8.3}$$

Following the derivations for the $12j$-symbol with one small quantum number in chapter 7, we find an asymptotic formula for the $15j$-symbol when two angular momenta are small. In the end, we find

$$\begin{aligned} & \left\{ \begin{matrix} j_1 & j_2 & j_{12} & j_{125} & j_{1256} \\ j_3 & j_4 & j_{34} & j_{135} & j_{1356} \\ j_{13} & j_{24} & s_5 & s_6 & j_7 \end{matrix} \right\} \\ = \; & \frac{(-1)^{\mu_5+\mu_6}}{4\pi \sqrt{(2j_{125}+1)(2j_{135}+1)(2j_{1256}+1)(2j_{1356}+1)}} \\ & \left[\frac{d^{s_5}_{\nu_5\,\mu_5}(\theta^{(1)})\, d^{s_6}_{\nu_6\,\mu_6}(\theta^{(1)})}{\sqrt{|V^{(1)}_{123}V^{(1)}_{432} - V^{(1)}_{214}V^{(1)}_{341}|}} \cos\left(S^{(1)} + (\mu_5+\mu_6)\phi^{(1)}_{12} + (\nu_5+\nu_6)\phi^{(1)}_{13} \right) \right. \\ & \left. + \frac{d^{s_5}_{\nu_5\,\mu_5}(\theta^{(2)})\, d^{s_6}_{\nu_6\,\mu_6}(\theta^{(2)})}{\sqrt{|V^{(2)}_{123}V^{(2)}_{432} - V^{(2)}_{214}V^{(2)}_{341}|}} \sin\left(S^{(2)} + (\mu_5+\mu_6)\phi^{(2)}_{12} + (\nu_5+\nu_6)\phi^{(2)}_{13} \right) \right] , \end{aligned} \tag{8.4}$$

where $S^{(1)}$ and $S^{(2)}$ are evaluated at configurations in which $V = \mathbf{J}_7 \cdot (\mathbf{J}_{12} \times \mathbf{J}_{13}) < 0$.

Here the indices on the d-matrices are $\mu_5 = j_{125} - j_{12}$, $\nu_5 = j_{135} - j_{13}$, $\mu_6 = j_{1256} - j_{125}$, and $\nu_6 = j_{1356} - j_{135}$. The phases $S^{(1)}$ and $S^{(2)}$ are actions associated with the $9j$-symbol. See section 7.6. The V's are given by

$$V_{ijk} = \mathbf{J}_i \cdot (\mathbf{J}_j \times \mathbf{J}_k) \, . \tag{8.5}$$

The angles ϕ_{12} and ϕ_{13} are internal dihedral angles at the edges J_{12} and J_{13}, respectively, of a tetrahedron formed by the six vectors $\mathbf{J}_{12}, \mathbf{J}_{13}, \mathbf{J}_{24}, \mathbf{J}_{34}, \mathbf{J}_6$, and $\mathbf{J}_{2'3}$, where $\mathbf{J}_{2'3} = \mathbf{J}_3 - \mathbf{J}_2$, and $J_i = j_i + 1/2$, $i = 1, 2, 3, 4, 6, 12, 34, 13, 24$. This tetrahedron is illustrated in figure 7.11. The angle θ is the angle between the vectors $\mathbf{J}_{12}$ and $\mathbf{J}_{13}$. Explicitly, the angles ϕ_{12}, ϕ_{13}, and θ are given by

$$\cos\phi_{12} = \pi - \frac{(\mathbf{J}_{12} \times \mathbf{J}_{13}) \cdot (\mathbf{J}_{12} \times \mathbf{J}_7)}{|\mathbf{J}_{12} \times \mathbf{J}_{13}| \, |\mathbf{J}_{12} \times \mathbf{J}_7|} \, , \tag{8.6}$$

$$\cos\phi_{13} = \pi - \frac{(\mathbf{J}_{13} \times \mathbf{J}_{12}) \cdot (\mathbf{J}_{13} \times \mathbf{J}_7)}{|\mathbf{J}_{13} \times \mathbf{J}_{12}| \, |\mathbf{J}_{13} \times \mathbf{J}_7|} \, , \tag{8.7}$$

$$\cos\theta = \frac{\mathbf{J}_{12} \cdot \mathbf{J}_{13}}{J_{12} J_{13}} \, . \tag{8.8}$$

We plot the exact values of the $15j$-symbol against our approximation (8.4) in figure 8.4 for the following values of the j's:

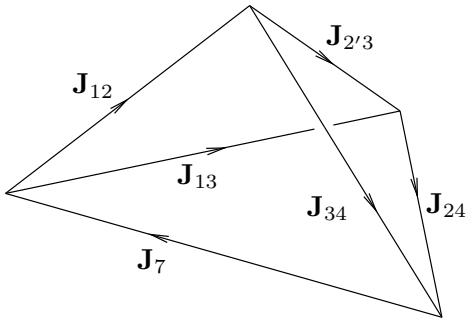

Figure 8.3: The angles ϕ_{12} and ϕ_{13} are internal dihedral angles in the tetrahedron with the six edges $\mathbf{J}_7, \mathbf{J}_{12}, \mathbf{J}_{34}, \mathbf{J}_{13}, \mathbf{J}_{24}$, and $\mathbf{J}_{2'3}$, where $\mathbf{J}_{2'3} = \mathbf{J}_3 - \mathbf{J}_2$. The angle θ is the angle between $\mathbf{J}_{12}$ and $\mathbf{J}_{13}$.

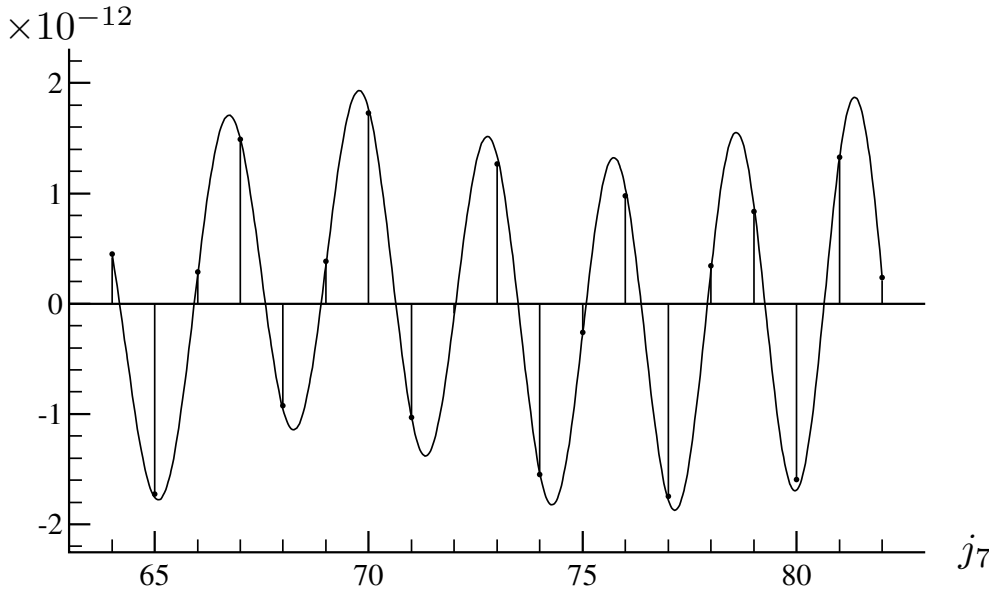

Figure 8.4: Comparison of the exact $15j$-symbol (vertical sticks and dots) and the asymptotic formula (8.4), for the values of j's shown in (8.9).

$$\left\{ \begin{array}{ccccc} j_1 & j_2 & j_{12} & j_{125} & j_{1256} \\ j_3 & j_4 & j_{34} & j_{135} & j_{1356} \\ j_{13} & j_{24} & s_5 & s_6 & j_7 \end{array} \right\} = \left\{ \begin{array}{ccccc} 197/2 & 187/2 & 74 & 75 & 74 \\ 173/2 & 205/2 & 88 & 96 & 97 \\ 95 & 90 & 1 & 1 & j_7 \end{array} \right\} . \tag{8.9}$$

The agreement is excellent.

8.3 Three Small Angular Momenta

We now treat the case where three quantum numbers are small. We take $j_3 = s_3$, $j_5 = s_5$, and $j_6 = s_6$ to be small. As before, we write the $15j$-symbol as a scalar product of two multicomponent wavefunctions,

$$\begin{aligned} & \left\{ \begin{array}{ccccc} j_1 & j_2 & j_{12} & j_{125} & j_{1256} \\ s_3 & j_4 & j_{34} & j_{135} & j_{1356} \\ j_{13} & j_{24} & s_5 & s_6 & j_7 \end{array} \right\} \\ = & \frac{\langle b|a\rangle}{\{[j_{12}][j_{34}][j_{13}][j_{24}][j_{125}][j_{135}][j_{1256}][j_{1356}]\}^{\frac{1}{2}}} , \end{aligned} \tag{8.10}$$

where

$$|a\rangle = \left| \begin{array}{cccccccccccc} \hat{I}_1 & \hat{I}_2 & \mathbf{S}_3^2 & \hat{I}_4 & \mathbf{S}_5^2 & \mathbf{S}_6^2 & \hat{I}_7 & \hat{\mathbf{J}}_{12}^2 & \hat{\mathbf{J}}_{34}^2 & \hat{\mathbf{J}}_{125}^2 & \hat{\mathbf{J}}_{1256}^2 & \hat{\mathbf{J}}_{\rm tot} \\ j_1 & j_2 & s_3 & j_4 & s_5 & s_6 & j_7 & j_{12} & j_{34} & j_{125} & j_{1256} & \mathbf{0} \end{array} \right\rangle , \tag{8.11}$$

$$|b\rangle = \left| \begin{array}{cccccccccccc} \hat{I}_1 & \hat{I}_2 & \mathbf{S}_3^2 & \hat{I}_4 & \mathbf{S}_5^2 & \mathbf{S}_6^2 & \hat{I}_7 & \hat{\mathbf{J}}_{13}^2 & \hat{\mathbf{J}}_{24}^2 & \hat{\mathbf{J}}_{135}^2 & \hat{\mathbf{J}}_{1356}^2 & \hat{\mathbf{J}}_{\rm tot} \\ j_1 & j_2 & s_3 & j_4 & s_5 & s_6 & j_7 & j_{13} & j_{24} & j_{135} & j_{1356} & \mathbf{0} \end{array} \right\rangle . \tag{8.12}$$

Following the strategy in chapter 6, we derive an asymptotic formula for the $15j$-symbol when three angular momenta are small, up to an overall phase. The result is the following formula:

$$\begin{aligned} & \left\{ \begin{array}{ccccc} j_1 & j_2 & j_{12} & j_{125} & j_{1256} \\ s_3 & j_4 & j_{34} & j_{135} & j_{1356} \\ j_{13} & j_{24} & s_5 & s_6 & j_7 \end{array} \right\} \\ = & (-1)^{j_1+j_2+j_4+j_7+2s_3+\nu_3+\mu_5+\mu_6} \frac{d^{s_3}_{\nu_3\,\mu_3}(\theta_1)\; d^{s_5}_{\nu_5\,\mu_5}(\theta_2)\; d^{s_6}_{\nu_6\,\mu_6}(\theta_2)}{\sqrt{[j_{34}][j_{13}][j_{135}][j_{1356}][j_{125}][j_{1256}](12\pi V)}} \\ & \cos\left(\sum_i (j_i + \frac{1}{2})\,\psi_i + \frac{\pi}{4} - s_3\pi + \mu_3\phi_4' + \nu_3\phi_1' - (\mu_5+\mu_6)\phi_{12} - (\nu_5+\nu_6)\phi_1 \right) . \end{aligned} \tag{8.13}$$

Here $\mu_3 = j_{34} - j_4$, $\nu_3 = j_{13} - j_1$, $\mu_5 = j_{125} - j_{12}$, $\nu_5 = j_{135} - j_{13}$, $\mu_6 = j_{1256} - j_{125}$, and $\nu_6 = j_{1356} - j_{135}$. The angles ϕ_1 and ϕ_{12} are internal dihedral angles in figure 8.5, in other words, $\phi_1 = \pi - \psi_1$ and $\phi_{12} = \pi - \psi_{12}$. Similar to the previous cases, the angle ϕ_1' is the angle between the $(\mathbf{J}_1, \mathbf{J}_4)$ plane and the $(\mathbf{J}_1, \mathbf{J}_{24})$ plane. The angle ϕ_4' is the angle between

the $(\mathbf{J}_1, \mathbf{J}_4)$ plane and the $(\mathbf{J}_4, \mathbf{J}_{12})$ plane. Here we put primes on these angles to distinguish them from the internal dihedral angles ϕ_1 and ϕ_4. The angle θ_1 is the angle between $\mathbf{J}_1$ and $\mathbf{J}_4$. The angle θ_2 is the angle between $\mathbf{J}_1$ and $\mathbf{J}_{12}$. Explicitly, the angles ϕ_1', ϕ_4', and θ are given by the following equations:

$$\phi_1' = \pi - \cos^{-1}\left(\frac{(\mathbf{J}_1 \times \mathbf{J}_4)\cdot(\mathbf{J}_1 \times \mathbf{J}_7)}{|\mathbf{J}_1 \times \mathbf{J}_4|\,|\mathbf{J}_1 \times \mathbf{J}_7|}\right), \tag{8.14}$$

$$\phi_4' = \pi - \cos^{-1}\left(\frac{(\mathbf{J}_4 \times \mathbf{J}_1)\cdot(\mathbf{J}_4 \times \mathbf{J}_7)}{|\mathbf{J}_4 \times \mathbf{J}_1|\,|\mathbf{J}_4 \times \mathbf{J}_7|}\right), \tag{8.15}$$

$$\theta = \cos^{-1}\left(\frac{\mathbf{J}_1 \cdot \mathbf{J}_4}{J_1 J_4}\right). \tag{8.16}$$

We plot the exact values of the $15j$-symbol against our approximation . (8.13) for the following values of the j's:

$$\left\{\begin{array}{ccccc} j_1 & j_2 & j_{12} & j_{125} & j_{1256} \\ s_3 & j_4 & j_{34} & j_{135} & j_{1356} \\ j_{13} & j_{24} & s_5 & s_6 & j_7 \end{array}\right\} = \left\{\begin{array}{ccccc} 203/2 & 207/2 & 96 & 97 & 98 \\ 3/2 & 199/2 & 100 & 100 & 101 \\ 101 & 108 & 1 & 1 & j_7 \end{array}\right\}. \tag{8.17}$$

Wee see that there are generally good agreements.

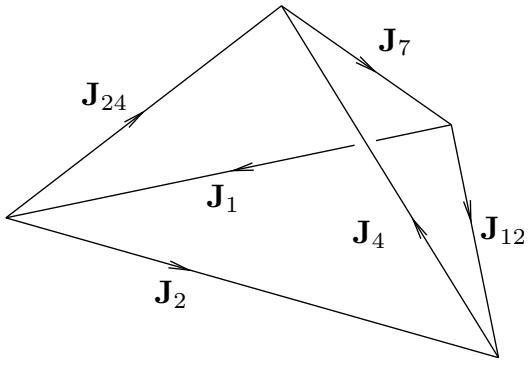

Figure 8.5: The volume V and the external dihedral angles ψ_i are defined on the tetrahedron with the six edge lengths $J_1, J_2, J_4, J_7, J_{12}, J_{24}$.

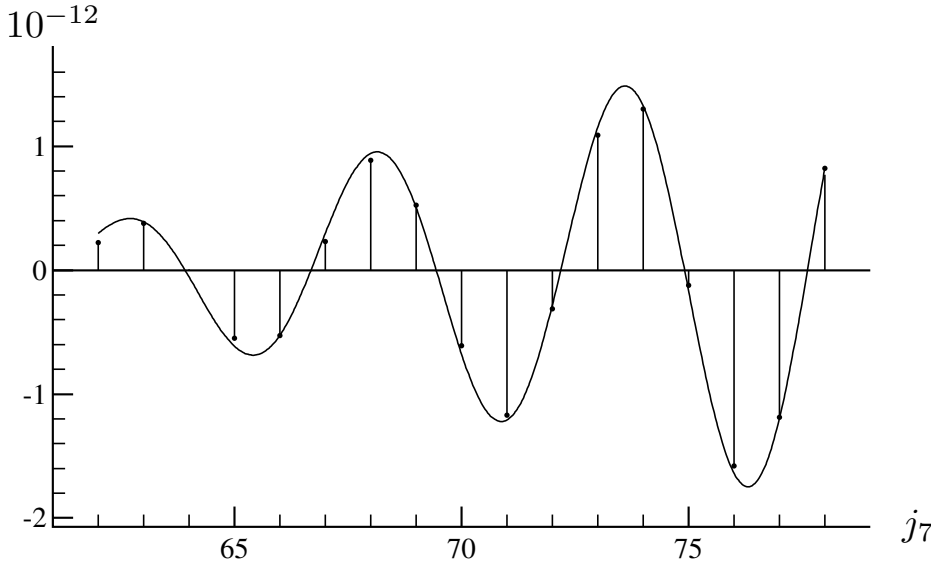

Figure 8.6: Comparison of the exact $15j$-symbol (vertical sticks and dots) and the asymptotic formula (8.13), for the values of j's shown in (8.17).

8.4 Four Small Angular Momenta

We now take four angular momenta to be small. We choose $s_1 = j_1$, $s_4 = j_4$, $s_5 = j_5$, and $s_6 = j_6$ to be small. Since the two Lagrangian manifolds are identical to the Wigner manifold represented by the triangle with the edge lengths J_2, J_3, J_7, which is illustrated in figure 8.7, the inner product of the scalar part of the WKB wave-functions is unity. Only the spinor products contribute.

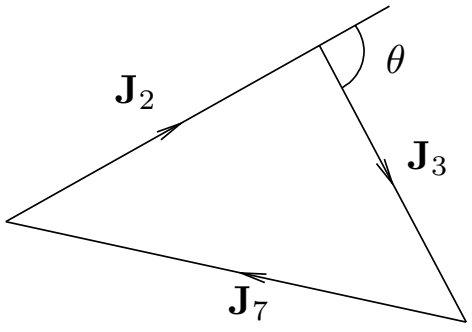

Figure 8.7: The angle θ is the exterior angle between the edges J_2 and J_3 in a triangle having the three edge lengths J_2, J_3, J_7.

In the end, we find the asymptotic formula for the $15j$-symbol with four small angular momenta is

$$\left\{ \begin{array}{ccccc} s_1 & j_2 & j_{12} & j_{125} & j_{1256} \\ j_3 & s_4 & j_{34} & j_{135} & j_{1356} \\ j_{13} & j_{24} & s_5 & s_6 & j_7 \end{array} \right\} \tag{8.18}$$
$$= \frac{(-1)^{j_2+j_3+j_7+\mu_1+\mu_4+\mu_5+\mu_6}}{\sqrt{[j_{12}][j_{34}][j_{13}][j_{24}][j_{125}][j_{135}][j_{1256}][j_{1356}]}}\, d^{(s_1)}_{\nu_1\,\mu_1}(\theta)\, d^{(s_4)}_{\nu_4\,\mu_4}(\theta)\, d^{(s_5)}_{\nu_5\,\mu_5}(\theta)\, d^{(s_6)}_{\nu_6\,\mu_6}(\theta)\,.$$

Here $\mu_1 = j_{12} - j_2$, $\nu_1 = j_{13} - j_3$, $\mu_4 = j_{24} - j_2$, $\nu_4 = j_{34} - j_3$, $\mu_5 = j_{125} - j_{12}$, $\nu_5 = j_{135} - j_{13}$, $\mu_6 = j_{1256} - j_{125}$, $\nu_6 = j_{1356} - j_{135}$, and θ is the angle between the vectors $\vec{J}_2$ and $\vec{J}_3$ in the triangle formed by J_2, J_3, and J_7, given by

$$\theta = \cos^{-1}\left(\frac{\mathbf{J}_2 \cdot \mathbf{J}_3}{J_2\, J_3}\right) = \pi - \cos^{-1}\left(\frac{J_2^2 + J_3^2 - J_7^2}{2\, J_2\, J_3}\right)\,. \tag{8.19}$$

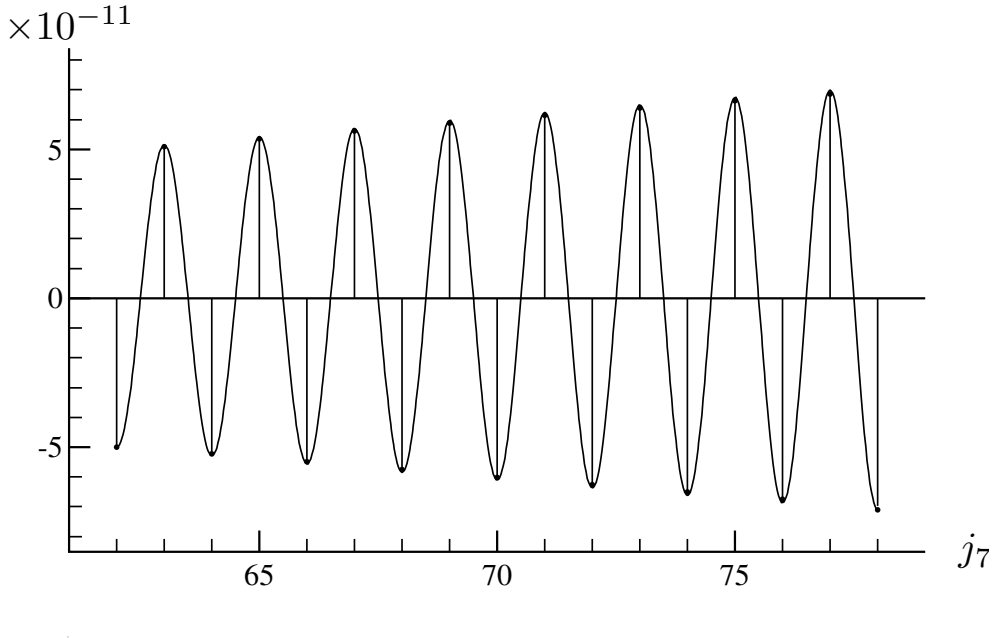

Figure 8.8: Comparison of the exact $15j$-symbol (vertical sticks and dots) and the asymptotic formula (8.18), for the values of j's shown in (8.20).

We illustrate the accuracy of the approximation (8.18) by plotting it against the exact $15j$-symbol in figure 8.8 for the following values of the j's:

$$\left\{ \begin{array}{ccccc} s_1 & j_2 & j_{12} & j_{125} & j_{1256} \\ j_3 & s_4 & j_{34} & j_{135} & j_{1356} \\ j_{13} & j_{24} & s_5 & s_6 & j_7 \end{array} \right\} = \left\{ \begin{array}{ccccc} 1/2 & 237/2 & 118 & 119 & 118 \\ 189/2 & 3/2 & 94 & 94 & 95 \\ 95 & 117 & 1 & 1 & j_7 \end{array} \right\}\,. \tag{8.20}$$

There is generally good agreement.

8.5 Conclusions

In this chapter, we have found the first few asymptotic formulas for the Wigner $15j$-symbol, in the special limit of a mixture of small and large quantum numbers. There are a few numerical results regarding the Barrett-Crane model, where the vertex amplitude is a sum of a product of two $15j$-symbols. An possible application of our results here is to provide an analytic proof of those numerical results.

Base on the general rules we have seen so far, the $15j$-symbol with one small angular momentum will depend on the Lagrangian manifolds associated with the $12j$-symbol. The semiclassical analysis of the $12j$-symbol with all quantum numbers large is an active research project in progress within our research group. Once that is available, it will be easy to obtain the asymptotic formula for the $15j$-symbol with one small quantum number.

In this chapter, we have inserted a particular set of $SU(2)$ intertwiners symmetrically into the pentagon diagram to obtain a spin network, which turns out to be a $15j$-symbol of the first kind. We can insert another set of $SU(2)$ intertwiners symmetrically into the pentagon diagram to obtain the $15j$-symbols of the fifth kind [96]. This spin network also has a representation as an inner product between two states, and we can apply our method here to find its asymptotic formulas. We will report on the results for the $15j$-symbol of the fifth kind in a future article.

Bibliography

[1] R. Abraham and J. E. Marsden. *Foundations of Mechanics*. Benjamin Cummings, New York, 1978.

[2] R. W. Anderson and V. Aquilanti. The discrete representation correspondence between quantum and classical spatial distributions of angular momentum vectors. *J. Chem. Phys.*, 124:214104, 2006.

[3] R. W. Anderson, V. Aquilanti, and C da S Ferreira. Exact computation and large angular momentum asymptotics of $3nj$ symbols: semiclassical disentangling of spin networks. *J. Chem. Phys.*, 129:161101, 2008.

[4] R. W. Anderson, V. Aquilanti, and A. Marzuoli. $3nj$ morphogenesis and semiclassical disentangling. *J. Phys. Chem. A*, 113:15106, 2009.

[5] V. Aquilanti, S. Cavalli, and C. Coletti. Angular and hyperangular momentum recoupling, harmonic superposition and racah polynomials: a recursive algorithm. *Chem. Phys. Lett.*, 344:587–600, 2001.

[6] V. Aquilanti, S. Cavalli, and D. de Fazio. Scattering of rotationally aligned oxygen molecules and the measurement of anisotropies of van der Waals forces. *Phys. Rev. Lett.*, 74:2929–2932, 1995.

[7] V. Aquilanti and C. Coletti. 3nj-symbols and harmonic superposition coefficients: an icosahedral abacus. *Chem. Phys. Lett.*, 344:601–611, 2001.

[8] V. Aquilanti, H. M. Haggard, A. Hedeman, N. Jeevanjee, R. G. Littlejohn, and L. Yu. Semiclassical mechanics of the Wigner $6j$-symbol, 2010.

[9] V. Aquilanti, H. M. Haggard, R. G. Littlejohn, and L. Yu. Semiclassical analysis of Wigner $3j$-symbol. *J. Phys. A.*, 40:5637, 2007.

[10] V. Bargmann. On a Hilbert space of holomorphic functions and an associated integral transform, part I. *Comm. Pure. Appl. Math.*, 14:187–214, 1961.

[11] V. Bargmann. On the representations of the rotation group. *Rev. Mod. Phys.*, 34:829–845, 1962.

[12] V. Bargmann. On a Hilbert space of holomorphic functions and an associated integral transform, part II. *Comm. Pure. Appl. Math.*, 20:1–101, 1967.

[13] J. W. Barrett and L. Crane. Relativistic spin networks and quantum gravity. *J. Math. Phys.*, 39:3296–3302, 1998.

[14] J. W. Barrett and L. Crane. A Lorentzian signature model for quantum general relativity. *Class. Quant. Grav.*, 17:3101–3118, 2000.

[15] M. V. Berry. Semi-classical mechanics in phase space: A study of Wigner's function. *Phil. Trans. R. Soc.*, 287:237–271, 1977.

[16] M. V. Berry and K. E. Mount. Semiclassical approximations in wave mechanics. *Rep. Prog. Phys.*, 35:315–397, 1972.

[17] M. V. Berry and M. Tabor. Closed orbits and the regular bound spectrum. *Proc. R. Soc. A*, 349:101–123, 1976.

[18] L. C. Biedenharn and J. D. Louck. *The Angular Momentum in Quantum Physics.* Addison-Wesley, Reading, MA, 1981.

[19] L. C. Biedenharn and J. D. Louck. *Angular Momentum in Quantum Physics.* Addison-Wesley, Reading, Massachusetts, 1981.

[20] M. Brack and R. K. Bhaduri. *Semiclassical Physics.* Addison-Wesley, Reading, MA, 1997.

[21] P. A. Braun, P. Gerwinski, F. Haake, and H. Schomerus. Semiclassics of rotation and torsion. *Zeit. Phys. B*, 100:115–127, 1996.

[22] M. L. Brillouin. Observations on the wave mechanics. *J. Phys. Radium Ser.*, 7:353–368, 1926.

[23] D. M. Brink and G. R. Satchler. *Angular Momentum.* Clarendon Press, Oxford, 1968.

[24] P.J. Brussaard and H. A. Tolhoek. Classical limits of Clebsch-Gordan coefficients, Racah coefficients and $d^l_{mn}(\phi, \nu, \psi)$-functions. *Physica*, 23:955–971, 1957.

[25] M. Cargo, A. Gracia-Saz, and R. G. Littlejohn. Multidimensional quantum normal forms. *arXiv.org e-Print archive*, arXiv:math-ph/0507032, 2005.

[26] M. Cargo, A. Gracia-Saz, R. G. Littlejohn, and P. de M. Rios. Quantum normal forms, Moyal star product and Bohr-Sommerfeld approximation. *J. Phys. A*, 38:1977–2004, 2005.

[27] S. Carroll. *Spacetime and Geometry: An Introduction to General Relativity.* Addison-Wesley, Reading, MA, 2004.

[28] L. Charles. On the quantization of polygon spaces. *arXiv.org e-Print archive*, arXiv:0806.1585, 2008.

[29] S. Chaturvedi and N. Mukunda. The Schwinger $su(3)$ construction i: Multiplicity problem and relation to induced representations. *J. Math. Phys.*, 43:5262–5277, 2002.

[30] J. W. Cherrington. A gauge-independent mechanism for confinement and mass gap: Part I - the general framework. *arXiv.org e-Print archive*, arXiv:hep-lat/0908.1889v1, 2009.

[31] J. W. Cherrington. A gauge-independent mechanism for confinement and mass gap: Part II - $g = su(2)$ and $d = 3$. *arXiv.org e-Print archive*, arXiv:hep-lat/0908.1893v1, 2009.

[32] L. Crane and D. Yetter. A categorical construction of 4-d TQFTs. In L. Kauffman and R. Baadhio, editors, *Quantum Topology*, Singapore, 1993. World Scientific.

[33] T. L. Curtright and C. K. Zachos. Deforming maps for quantum algebras. *Phys. Lett. B*, 243:237–244, 1990.

[34] D. de Fazio, S. Cavalli, and V. Aquilanti. Orthogonal polynomials of a discrete variable as expansion basis sets in quantum mechanics: Hyperquantization algorithm. *Int. J. of Quant. Chem.*, 93:91–111, 2003.

[35] A. R. Edmonds. *Angular Momentum in Quantum Mechanics*. Princeton University Press, Princeton, 1960.

[36] A. Einstein. On the quantum theorem of Sommerfeld and Epstein. *Verh. Dtsch. Phys. Ges.*, 19:82, 1917.

[37] E. El-Baz and B. Castel. *Graphical Methods of Spin Algebras in Atomic, Nuclear, and Particle Physics*. Marcel Dekker, New York, 1972.

[38] C. Emmrich and A. Weinstein. Geometry of the transport equation in multicomponent WKB approximations. *Comm. Math. Phys.*, 176:701, 1996.

[39] J. Engle, E. Livine, R. Pereira, and C. Rovelli. LQG vertex with finite Immirzi parameter. *Nucl. Phys. B*, 799:136–149, 2008.

[40] T. Frankel. *The Geometry of Physics: An Introduction*. Cambridge University Press, Cambridge, 1997.

[41] M. C. Gutzwiller. *Chaos in Classical and Quantum Mechanics*. Springer, New York, 1990.

[42] H. M. Haggard and R. G. Littlejohn. Asymptotics of the Wigner $9j$-symbol. *Classical and Quantum Gravity*, 27:135010, 2010.

[43] H. A. Jahn and J. Hope. Symmetry properties of the Wigner $9j$ symbol. *Phys. Rev.*, 93:318, 1954.

[44] M. Kapovich and J. J. Millson. On the moduli space of polygons in the Euclidean plane. *J. Differential Geometry*, 42:133–164, 1995.

[45] M. Kapovich and J. J. Millson. The symplectic geometry of polygons in Euclidean space. *J. Differential Geometry*, 44:479–513, 1996.

[46] J. B. Keller. Corrected Bohr-Sommerfeld quantum conditions for nonseparable systems. *Ann. of Phys.*, 4:180–188, 1958.

[47] I. Lindgren and J. Morrison. *Atomic Many-Body Theory.* Spring-Verlag, New York, 1986.

[48] R. G. Littlejohn. The semiclassical evolution of wave packets. *Phys. Rep.*, 138:193–291, 1986.

[49] R. G. Littlejohn. Semiclassical structure of trace formulas. *J. Math. Phys.*, 31:2952–2977, 1990.

[50] R. G. Littlejohn and W. G. Flynn. Geometric phases in the asymptotic theory of coupled wave equations. *Phys. Rev. A*, 44:5239, 1991.

[51] R. G. Littlejohn and W. G. Flynn. Semiclassical theory of spin-orbit coupling. *Phys. Rev. A*, 45:7697–7717, 1992.

[52] R. G. Littlejohn and L. Yu. Uniform semiclassical approximation for the Wigner $6j$-symbol in terms of rotation matrices. *J. Phys. Chem. A*, 113:14904–14922, 2009.

[53] J. E. Marsden and T. Ratiu. *Introduction to Mechanics and Symmetry.* Springer, New York, 1999.

[54] A. Marzuolia and M. Rasetti. Computing spin networks. *Ann. Phys.*, 318:345–407, 2005.

[55] C. W. Misner, K. S. Thorne, and J. A. Wheeler. *Gravitation.* W. H. Freeman, New York, 1973.

[56] S. Mizoguchi and T. Tada. 3-dimensional gravity and the Turaev-Viro invariant. *Prog. Theo. Phys. Supp.*, 110:207–226, 1992.

[57] J. E. Moyal. On the quantum correction for thermodynamic equilibrium. *Phys. Rev.*, 40:749–759, 1932.

[58] M. Nakahara. *Geometry, topology, and physics.* Institute of Physics Publishing, Bristol, 2003.

[59] A. F. Nikiforov, S. K. Suslov, and V. B. Uvarov. *Polynomials of a Discrete Variable.* Springer-Verlag, New York, 1991.

[60] H. Ooguri. Partition functions and topology-changing amplitudes in the three-dimensional lattice gravity of Ponzano and Regge. *Nucl. Phys. B*, 382:276–304, 1992.

[61] H. Ooguri. Topological lattice model in four dimensions. *Mod. Phys. Lett. A*, 7:2799–2810, 1992.

[62] H. Ooguri and N. Sasakura. Discrete and continuum approaches to three-dimensional quantum gravity. *Mod. Phys. Lett. A*, 6:3591–2600, 1991.

[63] R. J. Ord-Smith. The symmetry relations of the $12j$ symbol. *Phys. Rev.*, 94:1227–1228, 1954.

[64] D. Oriti. Spin foam models of quantum spacetime. *arXiv.org e-Print archive*, arXiv:gr-qc/0311066, 2003. Ph.D Thesis.

[65] A. Perelomov. *Generalized Coherent States and Their Applications*. Springer-Verlag, Berlin, 1986.

[66] M. E. Peskin and D. V. Schroeder. *An Introduction to Quantum Field Theory*. Basic Books, Boulder, CO, 1995.

[67] J. Polchinski. *String Theory: Vol 1-2*. Cambridge University Press, Cambridge, 1998.

[68] G. Ponzano and T. Regge. Semiclassical limit of Racah coefficients. In F. Bloch et. al., editor, *Spectroscopy and Group Theoretical Methods in Physics*, Amsterdam, 1968. North-Holland.

[69] J. M. Radcliffe. Some properties of coherent spin states. *J. Phys. A*, 4:313–323, 1971.

[70] T. Regge. General relativity without coordinates. *Nuovo Cimento*, 19:558–571, 1961.

[71] M. W. Reinsch and J. J. Morehead. Asymptotics of Clebsch-Gordan coefficients. *J. Math. Phys.*, 40:4782–4806, 1999.

[72] J. Roberts. Classical $6j$-symbols and the tetrahedron. *Geometry and Topology*, 3:21–66, 1999.

[73] C. Rovelli. *Quantum Gravity*. Cambridge University Press, Cambridge, 2004.

[74] J. J. Sakurai. *Modern Quantum Mechanics*. Addison-Wesley, New York, 1994.

[75] K. R. S. Sastry. Brahmagupta quadrilaterals. *Forum Geometricorum*, 2:167–173, 2002.

[76] K. Schulten and R. G. Gordon. Exact recursive evaluation of $3j$- and $6j$-coefficients for quantum-mechanical coupling of angular momenta. *J. Math. Phys.*, 16:1961–1970, 1975.

[77] K. Schulten and R. G. Gordon. Semiclassical approximations to $3j$- and $6j$-coefficients for quantum-mechanical coupling of angular momenta. *J. Math. Phys.*, 16:1971–1988, 1975.

[78] J. Schwinger. On angular momentum. In L. C. Biedenharn and H. van Dam, editors, *Quantum Theory of Angular Momentum*, New York, 1965. Academic Press.

[79] G. E. Stedman. *Diagram Techniques in Group Theory*. Cambridge University Press, Cambridge, 1990.

[80] Y. U. Taylor and C. T. Woodward. $6j$-symbols for $U_q(sl_2)$ and non-Euclidean tetrahedra. *Selecta Mathematica (New Series)*, 11:539–571, 2005.

[81] T. Thiemann. *Modern Canonical Quantum General Relativity.* Cambridge University Press, Cambridge, 2007.

[82] V. G. Turaev and O. Y. Viro. State sum invariants of 3-manifolds and quantum $6j$-symbols. *Topology*, 31:865–902, 1992.

[83] D. A. Varshalovich, A. N. Moskalev, and V. K. Khersonskii. *Quantum Theory of Angular Momentum.* World Scientific, Singapore, 1981.

[84] A. Voros. Asymptotic $\hbar$-expansions of stationary quantum states. *Ann. Inst. Henri. Poincaré*, 4:343–403, 1977.

[85] R. M. Wald. *General Relativity.* University of Chicago Press, Chicago, 1984.

[86] J. K. G. Watson. Comment: asymptotic approximations for certain 6-j and 9-j symbols. *J. Phys. A.*, 32:6901–6902, 1999.

[87] J. K. G. Watson. Rotation-electronic coupling in diatomic Rydberg states. In C. Sandorfy, editor, *The Role of Rydberg States in Spectroscopy and Photochemistry: Low and High rydberg States*, volume 20, page 293, Kluwer, 1999. Dordrecht.

[88] L. Wei and A. Dalgarno. Universal factorization of $3n - j$ $(j > 2)$ symbols of the first and second kinds for $su(2)$ group and their direct and exact calculation and tabulation. *J. Phys. A*, 37:3259–3269, 2004.

[89] S. Weinberg. *The Quantum Theory of Fields: Vol I – III.* Cambridge University Press, Cambridge, 2000.

[90] H. Weyl. Quantum mechanics and group theory. *Z. Phys.*, 46:1–46, 1927.

[91] E. T. Whittaker. *A Treatise on the Analytical Dynamics of Particles and Rigid Bodies.* Cambridge University Press, Cambridge, 1960.

[92] E. P. Wigner. On the quantum correction for thermodynamic equilibrium. *Phys. Rev.*, 40:749–759, 1932.

[93] E. P. Wigner. *Group Theory.* Academic, New York, 1959.

[94] N. M. J. Woodhouse. *Geometric Quantization.* Oxford University Press, Oxford, 1991.

[95] P. E. S. Wormer and J. Paldus. Angular momentum diagrams. *Adv. Quantum Chem.*, 51:59–123, 2006.

[96] A. P. Yutsis, I. B. Levinson, and V. V. Vanagas. *Mathematical Apparatus of the Theory of Angular Momentum.* Israel Program for Scientific Translations, Jerusalem, 1962.

Appendix A

Exact Formulas for the Wigner $3nj$-Symbols

The exact $6j$-symbol can be calculated using (6.2.3) in Edmonds [35]. The formula is

$$\left\{ \begin{array}{ccc} j_1 & j_2 & j_3 \\ j_4 & j_5 & j_6 \end{array} \right\} = \left(\prod_{r=1}^{6} (-1)^{2j_r} \sqrt{2j_r+1} \right) \sum_{\text{all } m\text{'s}} \times \left(\begin{array}{ccc} j_1 & j_2 & j_3 \\ m_1 & m_2 & m_3 \end{array} \right) \left(\begin{array}{ccc} j_1 & j_5 & j_6 \\ m_1' & m_5' & m_6 \end{array} \right) \left(\begin{array}{ccc} j_2 & j_6 & j_4 \\ m_2' & m_6' & m_4 \end{array} \right) \left(\begin{array}{ccc} j_3 & j_4 & j_5 \\ m_3' & m_4' & m_5 \end{array} \right) \times \left(\begin{array}{cc} j_1 & j_1 \\ m_1 & m_1' \end{array} \right) \cdots \left(\begin{array}{cc} j_6 & j_6 \\ m_6 & m_6' \end{array} \right) . \tag{A.1}$$

The exact $9j$-symbol can be computed from a single sum formula, (6.4.3) in Edmonds [35], involving products of three $6j$-symbols,

$$\begin{aligned} & \left\{ \begin{array}{ccc} j_1 & j_2 & j_{12} \\ j_3 & j_4 & j_{34} \\ j_{13} & j_{24} & j_5 \end{array} \right\} \\ = \; & (-1)^R \sum_x (-1)^{2x} (2x+1) \left\{ \begin{array}{ccc} j_1 & j_3 & j_{13} \\ j_{24} & j_5 & x \end{array} \right\} \left\{ \begin{array}{ccc} j_2 & j_4 & j_{24} \\ j_3 & x & j_{34} \end{array} \right\} \left\{ \begin{array}{ccc} j_{12} & j_{34} & j_5 \\ x & j_1 & j_2 \end{array} \right\} , \end{aligned} \tag{A.2}$$

where R is the sum of all 9 of the j's.

The exact $12j$-symbol [43, 63, 88] can be expressed as a single sum of products of four $6j$-symbols, given by the formula

$$\begin{Bmatrix} j_1 & j_2 & j_{12} & j_{125} \\ j_3 & j_4 & j_{34} & j_{135} \\ j_{13} & j_{24} & j_5 & j_6 \end{Bmatrix} \tag{A.3}$$
$$= (-1)^R \sum_x (-1)^{-x}(2x+1) \begin{Bmatrix} j_{125} & j_{135} & x \\ j_{13} & j_{12} & j_5 \end{Bmatrix} \begin{Bmatrix} j_{12} & j_{13} & x \\ j_4 & j_2 & j_1 \end{Bmatrix} \begin{Bmatrix} j_2 & j_3 & x \\ j_{34} & j_{24} & j_4 \end{Bmatrix} \begin{Bmatrix} j_{24} & j_{34} & x \\ j_{125} & j_{135} & j_6 \end{Bmatrix},$$

where R is the sum of all 12 of the j's.

The exact $15j$-symbol [96, 88] can be expressed as a single sum of products of five $6j$-symbols,

$$\begin{Bmatrix} j_1 & j_2 & j_{12} & j_{125} & j_{1256} \\ j_3 & j_4 & j_{34} & j_{135} & j_{1356} \\ j_{13} & j_{24} & j_5 & j_6 & j_7 \end{Bmatrix} \tag{A.4}$$
$$= (-1)^R \sum_x (-1)^{4x}(2x+1) \begin{Bmatrix} j_{1256} & j_{1356} & x \\ j_{135} & j_{125} & j_6 \end{Bmatrix} \begin{Bmatrix} j_{125} & j_{135} & x \\ j_{13} & j_{12} & j_5 \end{Bmatrix} \begin{Bmatrix} j_{12} & j_{13} & x \\ j_4 & j_2 & j_1 \end{Bmatrix} \begin{Bmatrix} j_2 & j_3 & x \\ j_{34} & j_{24} & j_4 \end{Bmatrix} \begin{Bmatrix} j_{24} & j_{34} & x \\ j_{1256} & j_{1356} & j_7 \end{Bmatrix},$$

where R is the sum of all $15j$'s.

In the special case where one of the j is equal to 0 or 1, the $9j$-symbol is proportional to a $6j$-symbol. From (10.9.2) in [83], we have

$$\begin{Bmatrix} j_1 & j_2 & j_{12} \\ 0 & j_4 & j_{34} \\ j_{13} & j_{24} & j_5 \end{Bmatrix} = \frac{(-1)^{j_1+j_2+j_4+j_5}}{\sqrt{(2j_{13}+1)(2j_{34}+1)}} \begin{Bmatrix} j_1 & j_2 & j_{12} \\ j_4 & j_5 & j_{24} \end{Bmatrix}. \tag{A.5}$$

From (10.9.6) in [83], we have

$$\begin{Bmatrix} j_1 & j_2 & j_{12} \\ 1 & j_4 & j_4 \\ j_1 & j_{24} & j_5 \end{Bmatrix} = \frac{(-1)^{j_1+j_2+j_4+j_5+1}}{\sqrt{(2j_1+1)(2j_4+1)}} \times \frac{[(j_5-j_{12})(j_5+j_{12}+1)-(j_{24}-j_2)(j_{24}+j_2+1)]}{2\sqrt{j_1(j_1+1)j_4(j_4+1)}} \begin{Bmatrix} j_1 & j_2 & j_{12} \\ j_4 & j_5 & j_{24} \end{Bmatrix}. \tag{A.6}$$

In the special case where one of the j is equal to 0 or 1, the $12j$-symbol is proportional to a $9j$-symbol. Using formulas (A9) in [43], we have

$$\left\{ \begin{array}{cccc} j_1 & j_2 & j_{12} & j_{12} \\ j_3 & j_4 & j_{34} & j_{13} \\ j_{13} & j_{24} & 0 & j_6 \end{array} \right\} = \frac{(-1)^{2R_9}}{\sqrt{(2j_{12}+1)(2j_{13}+1)}} \left\{ \begin{array}{ccc} j_1 & j_2 & j_{12} \\ j_3 & j_4 & j_{34} \\ j_{13} & j_{24} & j_6 \end{array} \right\}, \tag{A.7}$$

where R_9 is the sum of all 9 j's on the right hand side.